Investigating the role of lipid mobilisation and metabolism in the rice blast fungus *Magnaporthe oryzae*

Submitted by Mohd. Termizi bin Yusof

to the University of Exeter as a thesis for the degree of Doctor of Philosophy,
Biological Sciences,
May 2012.

I certify that all material in this thesis which is not my own work has been identified and that no material has been previously submitted and approved for the award of a degree by this or any other University.

Mohd. Termizi bin Yusof

Abstract

The rice blast fungus *Magnaporthe oryzae* infects plants by developing a specialised infection structure known as an appressorium. In *M. oryzae* the appressorium is a melanin-pigmented cell with a reinforced cell wall, allowing the cell to generate enormous internal turgor to enable penetration of the plant tissue by a narrow penetration hypha. Previously it has been shown that mobilisation of lipid droplets to the nascent appressorium is essential for successful plant infection. In this thesis, I describe a series of studies that have identified and characterised genes associated with infection-associated lipid metabolism in *M. oryzae*, including the role of fatty acid β-oxidation, acetyl-CoA transport and metabolism and regulation of lipid body breakdown. First, I report identification of *FAR1* and *FAR2*, which encode putative Zn2-Cys6 binuclear proteins that appear to act as transcriptional regulators of lipid metabolism. Deletion mutants of *M. oryzae FAR1* and *FAR2* were deficient in growth on long chain fatty acids. In addition Δ*far1* mutants were unable to grow on acetate as a sole carbon source. *FAR1* and *FAR2* affect the expression of genes involved in fatty acid β-oxidation, acetyl-CoA translocation, peroxisomal biogenesis, the glyoxylate cycle and acetyl-CoA synthesis. Next, I functionally characterized the *CAR1*, *CAR2*, *CAR3* and *CAR4* genes, which encode enzymes involved in carnitine biosynthesis, which is required for translocation of acetyl-CoA between mitochondria, peroxisomes and the cytoplasm. Only a sub-set of carnitine biosynthetic enzymes was necessary for growth on fatty acids and lipids by *M. oryzae*, but redundancy was also apparent in carnitine biosynthesis, because *CAR1, CAR2, CAR3* and *CAR4* were dispensable for pathogenicity, while the carnitine acetyltranferase, *PTH2*, is essential for rice blast disease. To investigate the role of the appressorium acetyl-CoA pool in more detail, I functionally characterized the acetyl-CoA synthetase gene, *ACS2* and *ACS3*, and *CRC1*, which encodes the mitochondrial carnitine carrier, both of which are highly expressed during appressorium development and appear to play a role in appressorium physiology. Finally, to understand the onset of lipid droplet degradation in more detail, I characterised a putative perilipin, encoded by *CAP20*, which localizes specifically to the periphery of lipid droplets. Perilipins are known to play roles in lipid droplet mobilisation and lipase accessibility. Consistent with this idea, *M.* oryzae mutants lacking *CAP20*, were severely affected in fungal virulence due to impaired appressorium function. When considered together, the results presented in this thesis suggest that lipid body mobilisation and acetyl-CoA metabolism are fundamental processes required for appressoria to function correctly and cause rice blast disease.

Table of contents

List of Figures

List of Tables

List of *Magnaporthe oryzae* strains utilized in this study

Strains	**Reference**
Guy11	Leung et al., 1990
Δ*ku70*	Kershaw and Talbot, 2009
Δ*far1*	This study
Δ*far2*	This study
Δ*far1*Δ*far2*	This study
Far1:GFP	This study
Far2:GFP	This study
Δ*cap20*	This study
H1:RFP::Guy11	Saunders et al., 2010
Cap20:mRFP	This study
H1:RFP:: Δ*cap20*	This study
Δ*car1*	This study
Δ*car2*	This study
Δ*car3*	This study
Δ*car4*	This study
Δ*acs2*	This study
Δ*acs3*	This study
Δ*crc1*	This study
Lifeact:RFP:: Δ*pth2*	This study
GFP:Atg8::Δ*pth2*	This study
GFP:Atg8::Guy11	Kershaw and Talbot, 2009

Acknowledgements

First of all, I would like to thank my supervisor, Professor Nick Talbot of the School of Biological Sciences for all his help, guidance and advice which makes it possible for me to complete my study here in the University of Exeter. I would also like to thank Malaysia Ministry of Higher Education and Universiti Putra Malaysia for financial assistance as well as providing me with the opportunity to study abroad.

My utmost appreciation to the technical staff from the School of Biological Sciences for their technical support throughout my study. I would like to especially thank Michael Kershaw, Ana Lillia Martinez-Rocha, Darren Soanes and Nick Tongue without whom this study could not have been completed. Also special thanks to Tina Penn for her help in this thesis writing.

Members of the Talbot Group, Muhammad Badaruddin, Muhammad Sougatul Islam, Yasin Fatih Dagdas, Romain Huguet, Thomas Mentlak, Min He, Lauren Hobbs, Magdalena Basiewicz, Yogesh Gupta, Miriam Oses-Ruiz and Kae Yoshino thanks for all the advice and making my time during this PhD so enjoyable.

Finally, I would like to thank my family for all their love and support which gives me the strength to keep on going and complete my study, but most importantly my wife, Ina Salwany, and my daughter, Hana Adelya, for bringing joy and happiness to my life.

Abbreviations

AMP	adenosine monophosphate
ATP	adenosine-5'- triphosphate
bp	basepair
CACT	carnitine/acylcarnitine translocase
cAMP	cyclic 3', 5' adenosine monophosphate
CAT	carnitine acetyltransferase
cDNA	complementary DNA
CM	complete medium
CTAB	cetyltrimethylamonium bromide
dATP	2'-deoxyadenosine triphosphate
DMSO	dimethyl sulfoxide
DEPC	diethylpyrocabonate
EDTA	ethylenediaminetetracetic acid
°C	degree Celcius
DNA	deoxyribonucleic acid
g	grams
g	relative centrifugal force
g/L	grams per litre
GFP	green fluorescent protein
h	hour
kb	kilobase
LB	lysogeny broth
µg	microgram
µL	microlitre
mg	milligram
min	minute
mL	millilitre
mm	millimetre
mM	millimolar
M	molar
MAPK	mitogen-activated protein kinase
MM	minimal medium
NADPH	nicotinamide adenine dinucleotide phosphate
ng	nanogram
PCR	polymerase chain reaction
PKA	protein kinase A
%	percentage
% w/v	percentage weight by volume
% v/v	percentage volume by volume
RFP	red fluorescent protein

RNA	ribonucleic acid
RNase	ribonuclease
rpm	revolutions per minute
SDS	sodium dodecyl sulphate
sec	second
Tris	tris(hydroxymethyl)methylamine
TBE	Tris-borate EDTA buffer
UV	ultraviolet
wt	wild type
X-gal	5-bromo-4-chloro-3-indolyl-β-D-galactosidase

1.0 Introduction

1.1 Challenges in global food security

Global demand for food is increasing and will continue for decades to come, with an anticipated 2.3 billion increase in the global human population projected by the middle of the century (Tilman et al., 2011). Increased agricultural production will need to occur both as a result of extending current areas under agricultural production, altering natural ecosystems to food production, and sustainable intensification, whereby more food is produced per unit area on land already used for agriculture (Gregory and Ingram, 2000). Without improved agricultural technologies, ensuring global food security will necessitate another 350 million hectares, an area the size of India, to be cropped to fulfil the rising food demand (Krattinger, 1998). In China alone, the area of cultivated cereals will need to increase three-fold, which may lead to destruction of many ecosystems (Flood, 2010). With demand rising and the amount of land limited, fertile areas such as, Sub-Saharan Africa, will need to be utilised for agriculture to help increase production where it is most needed.

Increased production of agricultural crops is therefore inevitable. However, the impact of such activity on the environment is still unclear. Land clearing, fragmentation and fertiliser usage have been shown to threaten biodiversity (Dirzo and Raven, 2003), increase global greenhouse gas production (Burney et al., 2010) and to be harmful to marine, freshwater and terrestrial ecosystems (Tilman et al., 2011). This suggests the need for better policies to be implemented and better agricultural technologies to be applied in order to fulfil demand, while also minimising damage to the environment.

1.2 Phytopathogens and food security

One important means by which food security could be enhanced is to control the threat posed by pests and disease to crop production. No one knows exactly how much food is lost in farms due to these problems (Pinstrup-Anderson, 2000) and most of the information on crop losses is estimated based on only limited data (Flood, 2010). Every year, however, it is estimated that at least 10% of the world's total crops are lost due to pests and diseases (Strange and Scott, 2005). (Bentley et al., 2009) estimated the world could be losing a third of potential harvests due to plant disease. For example, in 2003, economic losses in cassava production due to cassava brown streak virus totalled more than $10 million per year (Pennisi, 2010). A disease outbreak caused by the Southern corn leaf blight fungus, *Cochliobolus heterostrophus*, struck maize grown in the US in 1970-1971 and was estimated to have destroyed more than 15% of the US maize crop, resulting in loss of $5 million worth of maize (Strange and Scott, 2005). Another serious disease that still threatens food security is Black Sigatoka, caused by *Mycospaerella fijiensis*, which is considered to be the most damaging and costly disease of banana and plantain (Jacome and Schuh, 1992). It has been estimated that Sigatoka disease causes greater than 38% yield losses on plantain and even greater losses may occur on export-quality bananas when control measures fail (Marín et al., 2003). Another example of a serious threat to food security is Fusarium head blight, a fungal disease that affects wheat, barley, and other small grains and which caused direct economic losses estimated at $870 million from 1998 to 2000 for US wheat and barley producers, and up to $2.7 billion when direct and secondary economic losses for all crops were combined (Nganje et al., 2004).

Among all microorganisms that infect plants and cause diseases, fungi are responsible for the majority of serious plant diseases and include all white and true rusts, smuts,

needle casts, leaf curls, mildew, sooty molds, and anthracnoses; most leaf, fruit, and flower spots; cankers; blights; scabs, root, stem, fruit, and wood rots; wilts; leaf, shoot, and bud galls; and many others. All economically important plants are attacked by one or more fungal species and often many different fungi can cause disease in a single plant species. For instance, in North America *Solanum tuberosum* (potato) is exposed to many fungal diseases in both field and storage components such as silver scurf (*Helminthosporium solani*), dry rot (*Fusarium sambucinum*), verticillium wilt (*Verticillium dahliae* and *Verticillium albo-atrum*), black scurf (*Rhizoctonia solani*), and early blight (*Alternaria solani*) (Secor and Gudmestad, 1999).

1.3 Rice blast disease

Rice blast disease is one of the most devastating of all cereal diseases worldwide. Cultivated rice is a staple food for more than a third of the global population and, as such, more than 3 billion people consume rice as their major calorie intake (Goff, 1999). It is estimated that each year rice blast causes harvest losses of 10-30% of the global rice yield (Talbot, 2003). The fungus that causes blast disease is a filamentous ascomycete called *Magnaporthe oryzae* Couch (formerly *M. grisea* Cav.) part of the Magnaporthe species complex (Couch and Kohn, 2002). *Pyricularia oryzae* is the anamorph name for the fungus as it is found in the field. *M. oryzae* is a heterothallic, filamentous fungus that can also infect other agriculturally important crops including wheat (*Triticum aestivum*), barley (*Hordeum vulgare*), maize (*Zea mays*), oats (*Avena sativa*), rye (*Secale cereal*), perennial ryegrass (*lolium perenne*) and millet (*Eleusine coracana*) (Igarashi *et al.*, 1986; Dean *et al.*, 2005; Skamnioti and Gurr, 2009). However, the main reason that *M. oryzae* is so widely studied is because of the threat it poses to rice as the causal agent of rice blast disease. *M. oryzae* infection results in two

major symptoms on rice plants, the first being a leaf spot disease that is characterised by large ellipsoid lesions on the surface of rice leaves (Talbot, 1995). The second type of disease symptoms can be seen in older rice plants, where the fungus spreads into the stem and panicle causing neck blast panicle blast symptoms (Wilson and Talbot, 2009). Rice blast epidemics have led to serious economical harvest losses. For instance, a serious outbreak of rice blast occurred in Bhutan in 1995 destroyed more than 700 hectares of cultivated land and resulted in the loss of 1 090 tonnes of rice (Talbot, 2003). In China, it was reported that between 2001 and 2005, 5.7 million hectares of rice were destroyed as a result of a rice blast outbreak (Wilson and Talbot, 2009).

M. oryzae has emerged as a model organism for the study of host-pathogen interactions (Ebbole, 2007). This is due to its economic significance and also to its experimental amenability. Both the *M. oryzae* genome and rice genome have been completely sequenced and are publicly available, providing a significant advantage in using *M. oryzae* as a model organism (Goff *et al.*, 2002; Yu *et al.*, 2002; Dean *et al.*, 2005). Other advantages include the ability to culture the fungus axenically away from its host in standard growth medium, possession of a sexual stage which leads to molecular genetic tractability, and an efficient transformation system (Talbot, 2003). Targeted gene deletion is routinely carried out using homologous recombination to facilitate the study of gene function and when combined with an efficient transformation method, as well as the availability of fluorescent markers, a number of strains have been developed and can be used by the scientific community worldwide. Cell biology can also be carried out using glass cover-slips which mimic the surface of a rice leaf. This will induce the entire pre-penetration phase development which can be further analysed by microscopy.

1.4 The life cycle of *Magnaporthe oryzae*

Magnaporthe oryzae reproduces both sexually and asexually. However, only asexual spores are involved in rice blast disease development. Sexual reproduction only occurs under suitable environmental conditions, producing a fruiting body called a perithecium which carries numerous eight spored asci (Valent et al., 1991).

Rice blast infection is initiated when three-celled, tear drop shaped conidia land on the hydrophobic surface of a rice leaf. Upon landing, conidia attach to the surface of the rice leaf by producing an adhesive material at the apex of the conidium (Hamer et al., 1988). Only in the presence of water, will conidia germinate. This process occurs rapidly and within 2 h of landing on the leaf surface, a polarized germ tube is formed (Talbot, 2003). The germ tube extends for a short distance (15-30 µm) before swelling at its tip and changing direction, while becoming flattened against the leaf surface in a process called hooking (Bourett and Howard, 1990). Hooking marks the beginning of the differentiation of a specialised dome-shaped structure called the appressorium (Bourett and Howard, 1990). Several cues are involved prior to appressorium differentiation, including leaf surface topography and the absence of exogenous nutrients (Dean, 1997). Some chemicals such as soluble cutin or lipid monomers can also be used to induce appressorium differentiation on a hydrophilic surface (Gilbert et al., 1996). The cell wall of an appressorium is rich in chitin and contains a layer of melanin on the inside (Bourett and Howard, 1990). The melanin layer is important for the fungus to withstand the physical force produced by the appressorium in order to penetrate the plant cuticle and to retard the efflux of glycerol from the cell (de Jong et al., 1997). It has been shown that pressure of up to 8.0 MPa is generated by the appressorium (de Jong et al., 1997).

Nuclear division takes place in the germ tube during appressorium differentiation. The *M. oryzae* conidium contains three nuclei, one in each cell. Between 4 and 6 h after inoculation, one of the nuclei migrates to the germ tube and differentiates into two daughter nuclei by a single mitotic division (Veneault-Fourrey et al., 2006). One of the two daughter nuclei migrates into the appressorium while the other returns to the conidium. After 12 to 15 h, the three nuclei in the conidium start to degrade and only the nucleus in the appressorium remains (Veneault-Fourrey et al., 2006). Nutrient mobilisation from the conidium into the appressorium occurs at the same time as mitotic division. After mitotic division is complete and all the cytoplasm has moved into the appressorium, a specialised septum develops, separating the appressorium and the collapsing conidium. The conidium then undergoes autophagic cell death leaving the appressorium intact on the plant leaf (Kershaw and Talbot, 2009).

Once the leaf cuticle is ruptured, the fungus starts to form a penetration peg which swells into a primary infection hypha. Penetration hyphae differentiate into a series of branched and bulbous invasive hyphae (Talbot, 2003). After colonising the initial epidermal cell, invasive hyphae start to invade adjacent cells and colonise host plant tissue (Valent *et al.*, 1991; Talbot *et al.*, 1993). After 4 days, disease lesions are produced on the surface of the leaf, leading to release of very large numbers of conidia into the atmosphere under high humidity conditions, thereby restarting the infection cycle (Wilson and Talbot, 2009). Figure 1.1 summarizes the infection cycle of *M. oryzae*.

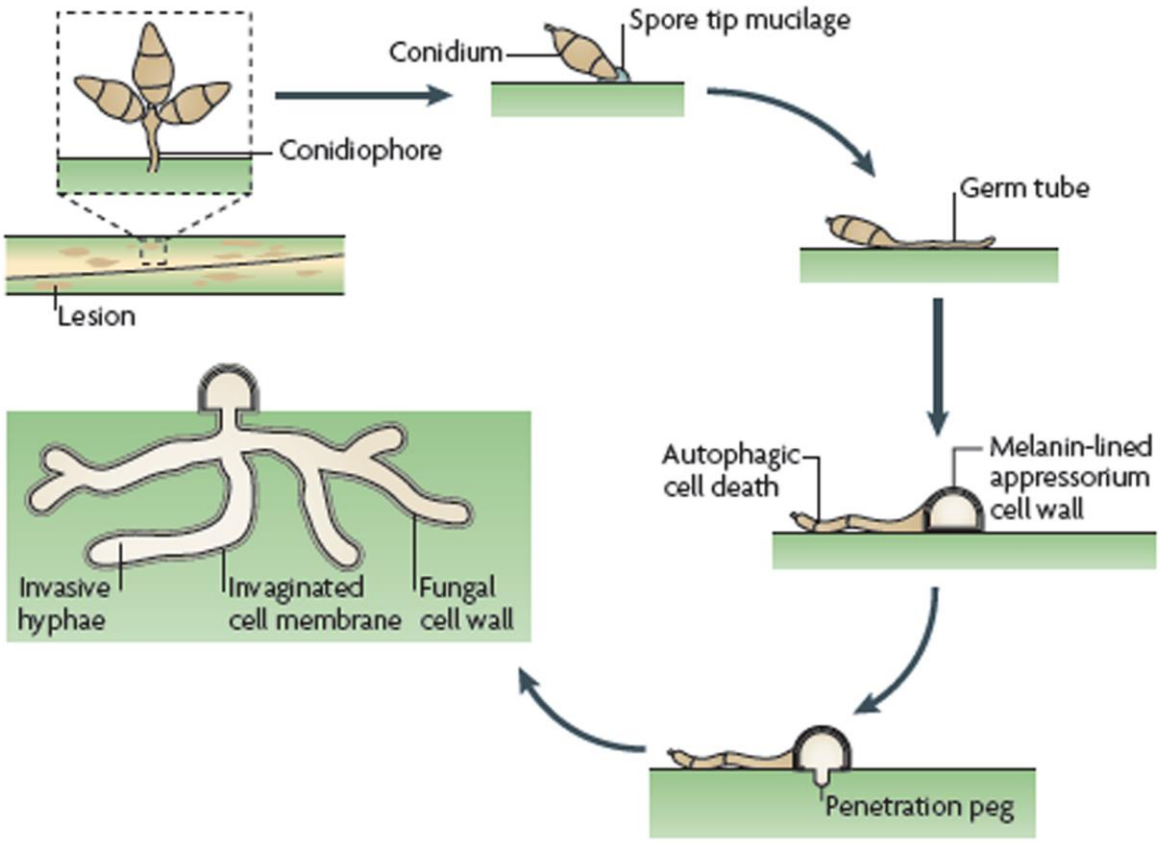

Figure 1.1 Life cycle of the rice blast fungus, *Magnaporthe oryzae*.

A three-celled, pyriform conidium attaches to the rice leaf surface and produces a germ tube that differentiates into a dome shaped appressorium. The appressorium penetrates the plant surface and produces invasive hyphae that invade and colonise rice tissue. Under appropriate conditions, hyphae within disease lesions sporulate and restart the cycle again (taken from Wilson and Talbot, 2009).

1.5 Cell signalling in *Magnaporthe oryzae*

In many fungi-plant interactions, physical properties of the plant surface, including hydrophobicity and surface topography, are sufficient to initiate fungal recognition (Tucker and Talbot, 2001). Environmental signals, which are likely to be transmitted through the cell to the nucleus via signal transduction pathways or cascades, lead to new gene expression, triggering a series of morphological changes in the germinating fungal spore that ultimately results in attachment to, and penetration of, the plant surface by the appressorium (Dean, 1997). Three signalling pathways have been shown to play an important role in plant infection development; the cyclic AMP signalling pathway, the Pmk1 MAPK signalling pathway and the Mps1 MAPK signalling pathway (Lee and Dean, 1993; Xu and Hamer, 1996; Xu et al., 1998).

1.5.1 Cyclic AMP signalling

The cyclic AMP signalling pathway has been shown to play an important role in appressorium differentiation in *M. oryzae* (Lee and Dean, 1993). It is involved in surface recognition and triggering of appressorium formation. Cyclic AMP levels are regulated by membrane-associated adenylate cyclase (*MAC1*) for synthesis and a cAMP-specific phosphodiesterase for degradation (Choi and Dean, 1997). The central components of the cAMP signalling pathway in *M. oryzae* have also been characterised including a Gα sub-unit protein encoded by *mag*B, adenylate cyclase encoded by *MAC1* and the catalytic and regulatory subunits of PKA encoded by *CpkA* and *Sum1* respectively (Lee et al., 2003) (Figure 1.2).

There are three genes that encode Gα protein in *M. oryzae* - *mag*A, *mag*B and *mag*C (Liu and Dean, 1997) and they are negatively regulated by the Rgs1 protein (Liu et al., 2007). However, only *mag*B has been shown to play an important role in plant

infection. A Δ*magB* mutant showed a reduction in vegetative growth, conidiation, appressorium formation and was reduced in ability to infect rice plants (Liu and Dean, 1997). A connection with cAMP signaling was established through the demonstration that appressorium formation could be restored to the Δ*magB* mutant by the addition of cAMP.

Choi and Dean have described the importance of *MAC1* in *M. oryzae* in order to infect plants. A Δ*mac1* mutant displayed reduction in vegetative growth, as well as defects in conidiation and germination. The Δ*mac1* mutant was also unable to form an appressorium on a hydrophobic surface and was unable to penetrate rice leaves. However, appressorium formation was restored in the presence of exogenous cAMP (Choi and Dean, 1997). (Adachi and Hamer, 1998), have generated a Δ*mac1 sum1-99* mutant, which has a single base change in the cAMP-binding domain of the regulatory subunit of PKA. In Δ*mac-1 sum 1-99* mutants, there is no requirement for cAMP to bind to the regulatory unit of PKA and hence overcoming the loss of *MAC1*. This restores the wild type growth, morphology and appressorium formation of Δ*mac1* mutant. However, the suppression of the Δ*mac1* phenotype was not complete because the Δ*mac-1 sum 1-99* still causes impaired disease symptoms suggesting that there are divergent cAMP signalling pathways for growth and pathogenesis (Adachi and Hamer, 1998).

The role of the PKA catalytic subunit in *M. oryzae* pathogenesis has been studied by analysis of a Δ*cpkA* mutant (Mitchell and Dean, 1995). The Δ*cpkA* mutant revealed a slightly different phenotype from that of the Δ*magB* and Δ*mac1* mutants, displaying normal vegetative growth and conidiation but delayed appressorium formation and a reduction in plant virulence (Mitchell and Dean, 1995). Appressoria of the Δ*cpkA* mutant are smaller than that of the wild type and although fully melanized, are unable to facilitate plant penetration. However, virulence was recovered when the Δ*cpkA* mutant

was inoculated into a wounded leaf. As the fungus is able to proliferate once inside the leaf cells, this suggests that the primary pathogenicity defect is the inability of the mutant to generate sufficient turgor to penetrate the leaf cuticle due to size of the appressorium.

1.5.2 Mitogen-activated protein kinase (MAPK) pathways in *M. oryzae* and pathogenesis

To date, three mitogen-activated protein kinase (MAPK) pathways have been characterised in *M. oryzae*; the Pmk1 MAPK pathway (involved in appressorium formation and penetration), the Mps1 MAPK pathway (involved in conidiation and penetration) and the Osm1 MAPK pathway (involved in osmoregulation). However, only the *PMK1* and *MPS1* genes are involved in plant virulence (Xu and Hamer, 1996; Xu *et al.*, 1998; Dixon *et al.*, 1999).

PMK1 was the first MAP kinase gene to be characterised and is a functional homologue of *S. cerevisiae FUS3*/*KSS1* (Xu and Hamer, 1996) (Figure 1.2). The Δ*pmk1* mutant is able to grow and produce conidia normally, and therefore is not essential for vegetative growth or sexual and asexual reproduction. However, deletion of the *PMK1* gene affects the ability of the fungus to infect plants (Xu and Hamer, 1996). The Δ*pmk1* mutant failed to cause blast lesions even when injected into wound sites suggesting that it is unable to grow invasively in plant cells and is completely non-pathogenic (Xu and Hamer, 1996). The Δ*pmk1* mutant has the capacity to recognize, attach to and germinate on an artificial surface, but is unable to initiate appressorium differentiation. Several upstream components of the *PMK1* pathway in *M. oryzae* have been characterised including Mst11 and Mst7, which are functional homologues of *S. cerevisiae* Ste11 and Ste7, respectively, and Mst50, which is a homologue of Ste50 (Park et al., 2006; Rispail

et al., 2009). Mst50 interacts with both Mst11 and Mst7 and may function as the adaptor (or scaffold) protein for the Pmk1 MAP kinase pathway. The Gβ subunit Mgb1, a Cdc42 homologue, and Ras proteins Ras1 and Ras2, all directly interact with Mst50 (Liu and Dean, 1997; Nishimura *et al.*, 2003; Liu *et al.*, 2007). These proteins are responsible for transducing upstream signals to activate the Mst11-Mst7-Pmk1 cascade to regulate different plant infection processes.

The second MAP kinase gene identified in *M. oryzae* was *MPS1* (Figure 1.2) (Xu et al., 1998). *MPS1* is a functional homologue of the *S. cerevisiae SLT2* which is required for cell wall integrity (Xu et al., 1998). The Δ*mps1* mutant showed normal vegetative growth, but conidial production and aerial hyphae development were severely reduced. The central part of the Δ*mps1* mutant colony was shown to undergo autolysis under normal incubation conditions (Xu et al., 1998). The cell wall of the Δ*mps1* mutant appears much weaker than that of the wild type and mycelium harvested from a liquid culture is hypersensitive to cell wall degrading enzyme (Xu et al., 1998). The Δ*mps1* mutant was able to germinate normally and form appressoria, however, the appressoria failed to penetrate the plant cuticle (Xu et al., 1998) and were unable to cause plant infection although virulence was restored when the fungus was inoculated directly into wound sites. This means the mutant can still grow invasively inside plant cells. An upstream component of *MPS1* pathway, *MCK1*, which is a functional homologue of *S. cerevisiae BCK1*, has been characterised (Jeon et al., 2008). As seen in the Δ*mps1* mutant, Δ*mck1* mutant also showed hypersensitivity to cell wall degrading enzyme, undergoes autolysis, is reduced in conidiation and is unable to cause plant infection (Jeon et al., 2008). Even though Δ*mck1* mutant was able to form an appressorium, the appressorium formed is slightly retarded in its development compared to the wild type and was shown not to generate sufficient turgor to penetrate the rice cuticle (Jeon et al.,

2008). However, upon inoculation of Δ*mck1* mutant spores to wounded leaves, the mutant remains non-pathogenic, suggesting that *MCK1* is also required for invasive growth in the plant cells (Jeon et al., 2008).

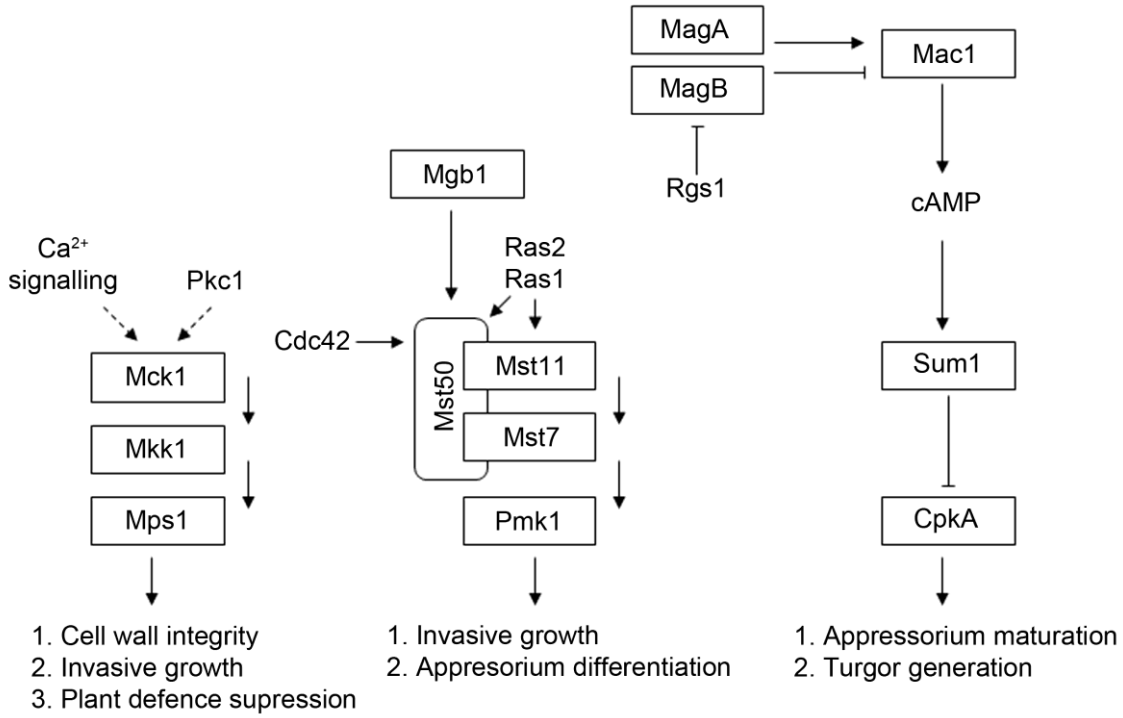

Figure 1.2 MAP kinase pathways (Pmk1 and Mps1) and cyclic AMP signalling pathway which play a crucial role in plant-infection development in *Magnaporthe oryzae*.

Mps1 is necessary for penetration peg formation and invasive growth development. Activation of Mps1 occurs through calcium signalling or protein kinase C. Pmk1 is required for appressorium formation and plant tissue colonization. Activation of Pmk1 involves the Ras proteins (Ras1 and Ras2), Cdc 42 and the Gβ-subunit protein, Mgb1. The cyclic AMP signalling pathway is required for appressorium maturation and turgor generation. Regulation of the cyclic AMP pathway involves the G proteins, MagA and MagB. Adenylate cyclase (Mac1) causes the accumulation of cAMP which binds to the regulatory subunit of protein kinase A (Sum1) and releasing the catalytic subunit, CpkA. Solid lines denote physical interactions supported by experimental evidence while dotted lines denote predicted interactions that require further experimental evidence. Adapted from Wilson and Talbot, 2009.

1.6 Autophagy in *Magnaporthe oryzae*

Autophagy is a catabolic process whereby the cell degrades its own components through the vacuolar or lysosomal machinery. Autophagy helps maintain the balance between synthesis, degradation and recycling of cellular products. It also re-allocates nutrients in starving cells from unnecessary processes to essential cellular processes. Autophagy research has increased significantly in the last ten years due in part to its association with a number of diseases, including cancer and neurodegenerative diseases, and to various human developmental processes (Klionsky et al., 2007).

In fungi, autophagy appears to be involved in nutrient recycling during starvation and normal developmental processes. Genetic analysis in *S. cerevisiae* has revealed a family of thirty *ATG* genes which encode proteins necessary for autophagy (Cao et al., 2008). The term autophagy can describe a number of phenomena including macroautophagy; the non-specific engulfment of cytosolic components by double membrane vesicles, which subsequently fuse with the vacuole or lysosome where the contents are degraded, microautophagy (direct invagination of cytosolic material into the vacuole or lysosome), pexophagy (degradation of the targeted peroxisomes in the vacuole or lysosome) and chaperone-mediated autophagy (degradation of specific cytosolic proteins with assistance from chaperone molecules) (for review, see (Pollack et al., 2009).

A simple autophagy model has been described by (Klionsky and Emr, 2000), and is shown in Figure 1.3. This model involves four sequential steps; induction, formation of autophagosomes and sequestration of cytoplasm and organelles, docking of autophagosome and fusion with a vacuole and breakdown of autophagic bodies in the vacuole. In this model autophagic degradation is both developmentally and nutritionally regulated. Autophagy is, for instance, inhibited in a nutrient-rich environment and induced during starvation (Klionsky and Emr, 2000). Once induced, the activity of Tor

kinase is inhibited, thus activating the autophagy pathway. In yeast, an Atg1 complex was shown to be essential for autophagy induction and consists of Atg1, Atg13 and Atg17 (Kamada et al., 2000), all of which are highly conserved in filamentous fungi (Meijer et al., 2007). Following induction, the next step is formation of the autophagosome, which begins with vesicle nucleation involving Atg18, Atg20, Atg21, Atg24 and Atg29. The vesicle then expands forming a fully developed autophagosome. This process involves Atg3, Atg4, Atg5, Atg7, Atg8, Atg10, Atg12 and Atg16 (Klionsky, 2005). The third step is docking and fusion of the autophagosome to the vacuole. In yeast, it has been shown that proteins involved in this stage are also implicated in membrane fusion and include the soluble N-ethylmaleimide-sensitive factor activating protein receptor (SNARE) proteins and Rab proteins (Klionsky, 2005). Finally, autophagic bodies are degraded in the vacuole and recycling of cellular macromolecules occurs (Klionsky, 2005).

Autophagy has been shown to play an important role in pathogenicity of phytopathogens. In *M. oryzae*, deletion of a series of genes that are involved in non-selective autophagy (*MoATG1*, *MoATG2*, *MoATG3*, *MoATG4*, *MoATG5*, *MoATG6*, *MoATG7*, *MoATG8*, *MoATG9*, *MoATG10*, *MoATG12*, *MoATG13*, *MoATG15*, *MoATG16*, *MoATG17* and *MoATG18*) has shown them to be vital to virulence (Kershaw and Talbot, 2009). Mutant strains were able to form appressoria normally, but were unable to penetrate the leaf cuticle. Direct inoculation of the conidia into wounded sites did not restore fungal virulence, suggesting involvement of autophagy in invasive growth in plant cells. Furthermore, conidial collapse was prevented in the mutant strains (Kershaw and Talbot, 2009).

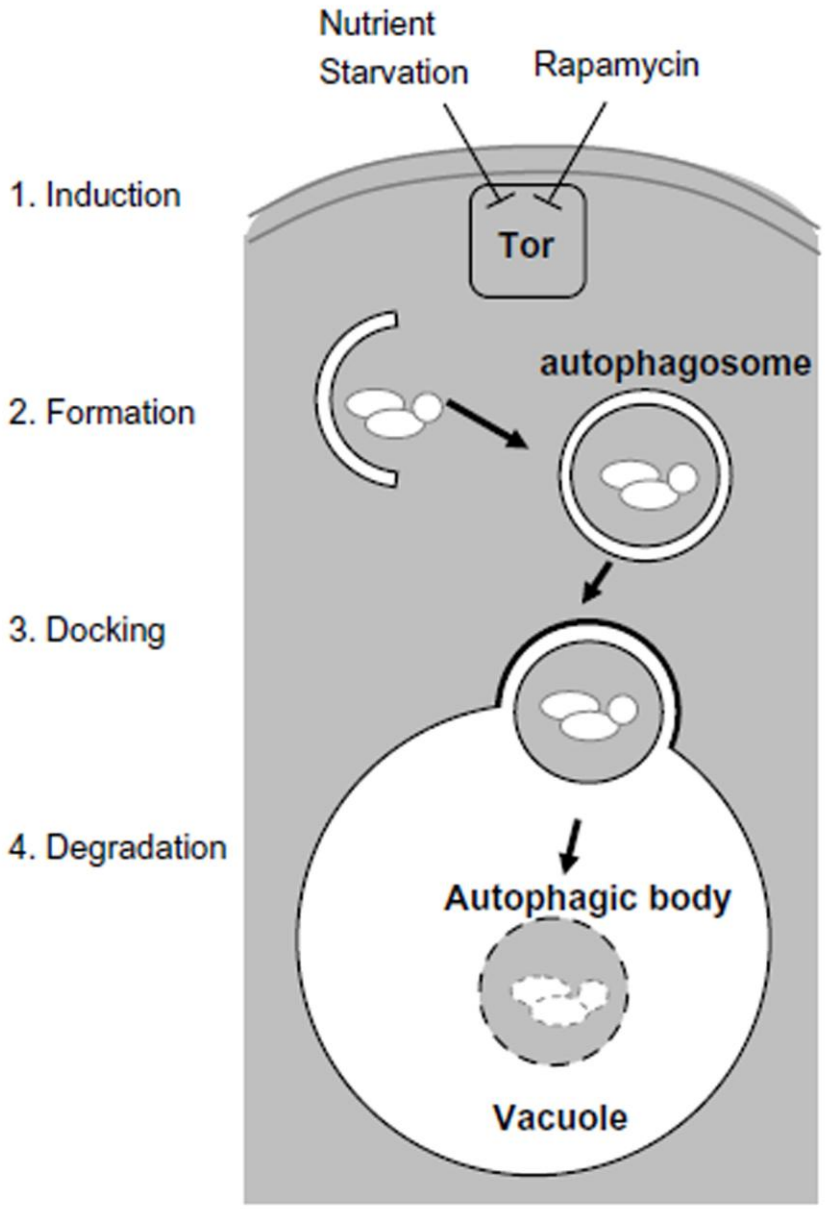

Figure 1.3 Simple model of autophagy based on observations in *S. cerevisiae*.

Autophagy involves four sequential steps; (1) Induction by nutrient starvation or rapamycin treatment. This step requires a complex consisting of Atg1, Atg3 and Atg17, which is known as the Atg1 complex. (2) Formation of autophagosomes involves vesicle nucleation and expansion to form a fully developed autophagosome. (3) Docking of the autophagosome and (4) fusion with vacuole followe by autophagic body degradation by hydrolytic enzymes (see Klionsky and Emr, 2000). See text for details.

1.7 Turgor and metabolism in *M. oryzae*

Magnaporthe oryzae infects rice plants by forming a melanin-pigmented appressorium, which enables the fungus to apply turgor pressure to penetrate the plant cuticle, producing a narrow penetration hypha from the base of the appressorium (Henson et al., 1999). It was shown using an incipient cytorrhysis assay that the turgor developed by *M. oryzae* appressorium to penetrate the rice leaf cuticle was as high as 8 MPa (Howard *et al.*, 1991; de Jong *et al.*, 1997). Melanin biosynthesis has been shown to be essential for plant-infection development with melanin-deficient mutants (Δ*alb1*, Δ*buf1* and Δ*rsy1*) unable to breach the plant cuticle (Chumley and Valent, 1990). Melanin-deficient mutants were unable to generate sufficient turgor to breach the plant cuticle which suggested that melanin might provide an impermeable layer to prevent leakage of an osmotically active metabolite responsible for turgor generation in the fungus (Howard et al., 1991).

Besides melanin biosynthesis, glycerol accumulation inside the appressorium is essential for the fungus to be able to generate sufficient turgor to penetrate the plant cuticle. It was shown that accumulation of compatible solutes, mainly glycerol, inside the appressorium draws free water from the outside of the appressorium by osmosis, hence generating hydrostatic turgor (de Jong et al., 1997). Melanin-deficient mutants also accumulated a lower concentration of glycerol as compared to the wild type, which explains why they were unable to generate sufficient turgor to penetrate the plant cuticle. *M. oryzae* accumulates as much as 3.2 M of glycerol during turgor generation (de Jong et al., 1997).

1.8 Major metabolic changes during appressorium-mediated plant infection by *Magnaporthe oryzae*

As discussed previously, infection-related development in *M. oryzae* involves a series of morphogenetic events including conidial germination, appressorium differentiation, turgor generation and invasive hyphae development. Since the environment surrounding the conidium is lacking in nutrients, the fungus must instead utilise nutrients available in the conidium in order to undergo development to infect plants. Trehalose, glycogen and lipids are among the most abundant storage components in the conidium (Thines et al., 2000). Here I have reviewed the major metabolic changes associated with appressorium-mediated plant infection.

The non-reducing disaccharide trehalose (α-D-glucopyranosyl-α-D-glucopyranoside) is a common storage product within living cells including bacteria, plants, insects, invertebrates and fungi (Wang et al., 2005; Wilson et al., 2007). The major role of trehalose is to protect the integrity of cells against various environmental injuries and nutritional limitations (Argüelles, 2000). Trehalose metabolism has been described in detail in *S. cerevisiae* (Argüelles, 2000). Trehalose is synthesised by a multienzyme complex containing trehalose-6-phosphate synthase, (T6PS) encoded by *TPS1*, trehalose-6-phosphatase encoded by *TPS2*, and two regulatory subunits encoded by the *TSL1* and *TPS3* (Vuorio et al., 1993). The first step in trehalose biosynthesis is the transfer of a glucosyl unit from UDP-glucose to glucose 6-phosphate, producing trehalose 6-phosphate. This reaction is catalyzed by trehalose-6-phosphate synthase. The second step is dephosphorylation of trehalose 6-phosphate by trehalose 6-phosphatase leading to the formation of free trehalose (Argüelles, 2000).

Trehalose hydrolysis is carried out by trehalase which cleaves its substrate with strict specificity, producing two molecules of glucose (Argüelles, 2000). Three distinct

trehalases have been described in *S. cerevisiae*, *ATH1*, *NTH1* and *NTH2* (Foster et al., 2003; Wilson et al., 2007). *ATH1* encodes an acidic trehalase which is involved in utilisation of trehalose as a carbon source while both *NTH1* and *NTH2* code for a cytoplasmic neutral trehalase, which is involved in mobilisation of intracellular trehalose (Mittenbühler and Holzer, 1988; Nwaka and Holzer, 1998).

In *M. oryzae*, it was shown that trehalose synthesis is essential for appressorium-mediated plant infection while mobilisation of stored trehalose is only critical after cuticle penetration (Foster et al., 2003). *TPS1* encodes trehalose-6-phosphate synthase and has been shown to be essential for fungal virulence. A Δ*tps1* mutant was non-pathogenic because turgor generation was severely impaired, thus affecting the ability of the fungus to breach the plant cuticle (Foster et al., 2003). The Δ*tps1* mutant was also unable to utilise glucose, lipid or acetate as a sole carbon source. However, addition of an alternative carbon source or complex nitrogen sources, such as yeast extract or peptone, restores the ability of the fungus to utilise glucose. It was suggested that *TPS1* might be involved in regulation of gluconeogenesis because the Δ*tps1* mutant was unable to grow on lipid or acetate (Foster et al., 2003).

Recent studies on *TPS1* have revealed that the Tps1 protein itself is required for fungal virulence, rather than trehalose synthesis (Wilson et al., 2007; Wilson et al., 2010). *TPS1* was shown to regulate the pentose phosphate pathway which leads to maintaining the cellular NADPH pool and regulation of nitrate reductase (Wilson et al., 2007). *TPS1* was shown to bind NADPH directly and to regulate a set of related transcriptional corepressors, comprising three proteins, Nmr1, Nmr2 and Nmr3, each of which can bind NADP (Wilson et al., 2010). Deletion of any of the Nmr-encoding genes in Δ*tps1* mutant partially restored the pathogenicity (Wilson et al., 2010). Based on these observations, it was suggested that initiation of rice blast disease by *M. oryzae* requires

a regulatory mechanism involving an NADPH sensor protein, Tps1, a set of NADP-dependent transcriptional co-repressors, and the maintained balance of NADPH and NADP that acts as a signal transducer (Foster et al., 2003; Wilson et al., 2007; Wilson et al., 2010).

Two genes which code for trehalase have also been characterised in *M. oryzae*, *NTH1* and *TRE1*. *NTH1* is essential for invasive growth in plant cells and has been shown to be highly expressed during conidiogenesis and spore germination while *TRE1* is required for trehalose mobilisation during conidia germination (Foster et al., 2003). An Δ*nth1* mutant was reduced in pathogenicity due to its decreased ability to perform invasive growth in plant cells. In contrast to the Δ*nth1* mutant, a Δ*tre1* mutant was found to be dispensable for fungal virulence (Foster et al., 2003).

Glycogen is one of the most abundant storage components present in the cytoplasm of conidia besides trehalose and lipid (Bourett and Howard, 1990). Glycogen is a major intracellular reserve polymer consisting of α-1,4-linked glucose subunits with α-1,6-linked glucose at the branching points. In *S. cerevisiae*, glycogen is formed upon limitation of carbon, nitrogen, phosphorus or sulphur (Lillie and Pringle, 1980). Glycogen synthesis requires glycogenin, a self-glucosylating initiator protein, glycogen synthase which catalyzes bulk synthesis and the branching ezymes which are involved in introducing the branches characteristic of the mature polysaccharide (Farkas et al., 1991; Rowen et al., 1992). The first step of glycogen synthesis requires UDP-glucose (UDPG) as a glucose donor. Glycogenin attaches a glucose residue from UDPG to a tyrosine residue within its own sequence. Glycogenin then adds additional glucose residues, in an α-1,4-glycosidic linkage, forming a short oligosaccharide. This oligosaccharide serves as a primer for glycogen synthase, which catalyzes bulk glycogen synthesis by processively adding additional glucose residues in α-1,4-

glycosidic linkage. The branching enzyme introduces the α-1,6-branch points characteristic of glycogen (Wilson et al., 2010). In *S. cerevisiae*, two isoforms of glycogenin exist, *GLG1* and *GLG2* (Cheng et al., 1995). Glycogen synthase is responsible for synthesis of α-1,4 linkages and is encoded by *GSY1* and *GSY2* (Farkas et al., 1991) while α-1,6 linkages are catalyzed by a branching enzyme encoded by *GLC3* (Rowen et al., 1992).

In *S. cerevisiae*, glycogen degradation occurs via two pathways. The first pathway for glycogen degradation involves glycogen phosphorylase, encoded by *GPH1*, which releases glucose in the form of glucose-1-phosphate from the non-reducing ends of α-1,4 linked chains (Hwang et al., 1989) and a debranching enzyme, encoded by *GDB1*, which is involved in hydrolysing the α-1,6 linkages (Teste et al., 2000). The second pathway for glycogen degradation is via hydrolysis which is catalyzed by a vacuolar glucoamylase, encoded by *SGA1* (Pugh et al., 1989).

Little is known of the importance of glycogen in *M. oryzae*. Thines *et al.*, (2000) have shown that glycogen is present in abundance in the conidia. However, during germination, glycogen is deposited within the appressorium and is rapidly degraded at the onset of appressorium maturation. Deng and Naqvi (2010) have reported that vacuolar breakdown of glycogen, catalyzed by Sga1, following the delivery of cytosolic glycogen via the autophagic machinery, is crucial for conidiation in *M. oryzae*. In an Δ*atg8* mutant, expression of *GPH1* appeared to be induced to maintain the supply of glucose for conidiation from the cytoplasm (Deng et al., 2009). Since *GPH1* is negatively regulated by glucose-6-phosphate, a product of glycogen autophagy, it was not able to produce sufficient glucose in the cytoplasm to maintain the requirement for condiation in Δ*atg8* mutant (Deng and Naqvi, 2010). Both *GPH1* and *SGA1* have been shown to be involved in conidiation. Deletion of *GPH1* in an autophagy mutant (Δ*atg8*

mutant) restored conidiation (Deng et al., 2009) while deletion of *SGA1* significantly reduced the number of conidia produced by the fungus (Deng and Naqvi, 2010). Both Δ*gph1* and Δ*sga1* mutants were still able to cause plant infection despite their role in asexual development (Deng *et al.*, 2009; Deng and Naqvi, 2010).

1.9 Lipid metabolism

The main focus of this study is to understand how lipid metabolism is regulated and to determine its contribution to infection-related development in *M. oryzae*. Lipids are hydrophobic or amphiphilic molecules and can be divided into eight categories; fatty acids, glycerolipids, glycerophospholipids, sphingolipids, sterol lipids, prenol lipids, saccharolipids and polyketides (Fahy et al., 2005). Lipids form a vital component of cell membranes and play indispensable roles in a range of biological functions including energy storage, as a precursor for hormone synthesis and by acting as signalling molecules (Sul and Wang, 1998; Bozza *et al.*, 2007). Lipid biosynthesis occurs through a process known as lipogenesis which takes place in the cytoplasm with acetyl-CoA as the precursor (Kersten, 2001). Lipid metabolism is tightly connected to carbohydrate metabolism since this is also a source of acetyl-CoA which can be used for lipogenesis. The first step of triacylglycerol degradation is hydrolysis in a reaction catalyzed by triacylglycerol lipases producing glycerol and fatty acids. This is followed by oxidation of fatty acids to acetyl-CoA through a process called β-oxidation.

1.9.1 Hydrolysis of triglycerides by triacylglycerol lipases (lipolysis)

Lipases are required for hydrolyzing triacylglycerol and cholesteryl esters stored in lipid droplets. Hormone sensitive lipase (HSL) is the most extensively characterised and was shown to be highly expressed in adipocytes and at lower levels in other cells and tissues

(Holm et al., 1987; Holm et al., 1988). An increase in lipid hydrolysis can occur primarily in response to hormones such as epinephrine and glucagon (Leboeuf *et al.*, 1959; Hagen, 1961). These trigger the G protein-coupled receptor to activate adenylate cyclase resulted in increased of cAMP production. Cyclic AMP activates protein kinase A (PKA) which subsequently phosphorylates HSL and perilipin A (Kawamura *et al.*, 1981; Londos *et al.*, 1999; Brasaemle *et al.*, 2009). Phosphorylation of HSL leads to translocation of HSL from the cytosol to the surface of lipid droplet (Clifford et al., 2001). Phosphorylation of perilipin A which resides on the lipid droplet surface, results in a major physical alteration of the lipid droplet surface releasing and allowing hydrolysis of triacylglycerol by lipases (Brasaemle et al., 2009).

Besides HSL, there were reports of the identification of a new cytosolic triacylglycerol lipase that has been named adipose triglyceride lipase (ATGL) (Jenkins et al., 2004; Villena et al., 2004; Zimmermann et al., 2004). ATGL is highly expressed in adipose tissue of mice and humans, slightly less expression was observed in heart, muscle, testis, adrenal gland and colon and very low but detectable expression in most other tissues (Villena *et al.*, 2004; Zimmermann *et al.*, 2004; Lake *et al.*, 2005; Kershaw *et al.*, 2006). It was shown that intact cultured cells overexpressing ATGL, mammalian cell extracts containing ectopic ATGL or purified recombinant ATGL have demonstrated triacylglycerol lipase activity (Jenkins *et al.*, 2004; Villena *et al.*, 2004; Zimmermann *et al.*, 2004; Lake *et al.*, 2005; Kershaw *et al.*, 2006; Smirnova *et al.*, 2006).

1.9.2 Fatty acid β-oxidation

Fatty acid β-oxidation is the process of breaking down a long chain acyl-CoA molecule to acetyl-CoA molecules. The first step involves activation of fatty acids by fatty acyl-CoA synthetase to the corresponding acyl-CoA (Black and DiRusso, 2003). This is followed by oxidation of β carbon which involves a set of four consecutive reactions catalyzed by four major enzymes; acyl-CoA oxidase/dehydrogenase, 2-enoyl-CoA hydratase, 3-hydroxyacyl-CoA dehydrogenase and 3-ketoacyl-CoA thiolase (Figure 1.4). Through this process, acetyl-CoA is produced, as well as an acyl-CoA shortened by two carbons, which will undergo additional cycles of β-oxidation. Studies in mammals and the filamentous fungus *Aspergillus nidulans* have shown that β-oxidation occurs in both mitochondria and peroxisomes (Eaton *et al.*, 1996; Wanders *et al.*, 2001; Maggio-Hall and Keller, 2004). However, in yeasts such as *S. cerevisiae*, *Yarrowia lipolytica* and *Candida tropicalis*, β-oxidation has been shown to occur exclusively in peroxisomes (Kurihara *et al.*, 1992; Smith *et al.*, 2000; Hiltunen *et al.*, 2003).

In *M. oryzae*, fatty acid β-oxidation has been shown to play a role in appressorium physiology (Wang et al., 2007). *MFP1*, which encodes multifunctional β-oxidation protein in *M. oryzae*, has been deleted and the Δ*mfp1* mutant was shown to have a significant reduction in rice blast disease. In *Candida albicans*, it was shown that peroxisomal β-oxidation is not required for virulence. However, it is required for a functional glyoxylate cycle (Piekarska *et al.*, 2006; Piekarska *et al.*, 2008).

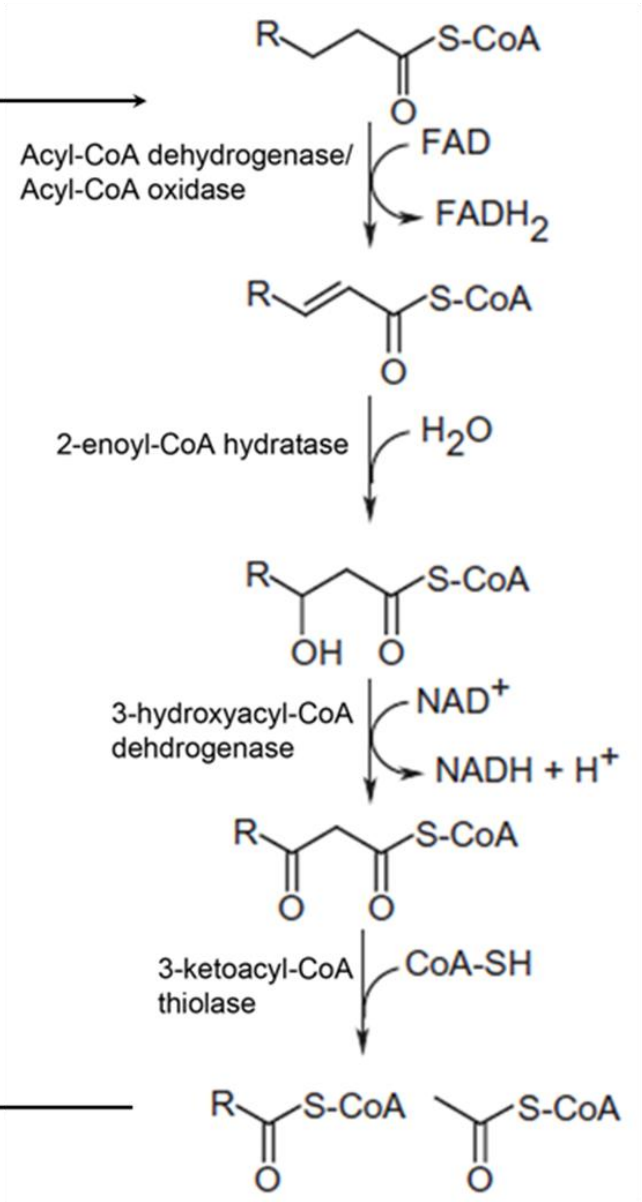

Figure 1.4 β-oxidation of fatty acids.

The first step involves the dehydrogenation of acyl-CoA in a reaction catalyzed by acyl-CoA dehydrogenase (mitochondria) or acyl-CoA oxidase (peroxisomes). The second step is generation of 3-hydroxyacyl-CoA in a reaction catalyzed by 2-enoyl-CoA hydratase. The third step requires dehydrogenation of 3-hydroxyacyl-CoA catalyzed by 3-hydroxyacyl-CoA dehydrogenase. The fourth step is the release of shortened acyl-CoA which will undergo additional cycles of β-oxidation, and acetyl-CoA in a reaction catalyzed by 3-ketoacyl-thiolase (Maggio-Hall and Keller, 2004).

1.9.3 The glyoxylate cycle

The glyoxylate cycle was first described as a modified tricarboxylic acid (TCA) cycle (Kornberg and Madsen, 1958). It involves conversion of C_2-units to C_4-precursors for biosynthesis, allowing growth on fatty acids and C_2-compounds. The glyoxylate and TCA cycles share some common reactions; conversion of malate into oxaloacetate, oxaloacetate to citrate and citrate to isocitrate in reactions catalyzed by malate dehydrogenase, citrate synthase and aconitase respectively (Figure 1.5). Instead of the two decarboxylation steps of the TCA cycle, isocitrate lyase and acetyl-CoA were converted to succinate and malate in reactions catalyzed by isocitrate lyase and malate synthase. Isocitrate lyase splits the C_6-unit of isocitrate lyase into succinate and glyoxylate, which in turn is condensed by malate synthase with acetyl-CoA, generating free CoA and malate (Lorenz and Fink, 2001). Malate is then used by malate dehydrogenase to continue the cycle and succinate is released as a net product into the TCA cycle (Kunze et al., 2006).

The glyoxylate cycle takes place both inside and outside of peroxisomes, and transport of several glyoxylate cycle intermediates across the peroxisomal membrane is therefore important (Kunze et al., 2006). In bacteria, the glyoxylate cycle proceeds in the cytosol, while early studies on eukaryotes have suggested that all the glyoxylate cycle enzymes are located in the peroxisomes (Breidenbach and Beevers, 1967). More recent studies have shown that none of the various plant aconitase enzyme variants are actually peroxisomal (Courtois-Verniquet and Douce, 1993) and yeast aconitase has been reported to be localised in the mitochondria and cytoplasm (Regev-Rudzki et al., 2005). A fraction of aconitase is exported from the mitochondria to the cytosol where it participates in the glyoxylate cycle (Regev-Rudzki et al., 2005).

There are reports showing that the glyoxylate cycle is required for microbial virulence (Lorenz and Fink, 2001). A mutant strain of the bacterium *Rhodococcus fascians* lacking malate synthase has also been characterized. The mutant was able to persist on plant tissues but unable to cause disease (Vereecke et al., 2002). A mutant strain which lacks isocitrate lyase has been generated in *Leptosphaeria maculans*, an ascomycetous fungus that causes blackleg disease of canola. The mutant was shown to have slower lesion development than the wild type (Idnurm and Howlett, 2002). In *M. oryzae*, deletion of the *ICL1* gene which encodes isocitrate lyase, has been shown to result in a delay in the development of symptoms (Wang et al., 2003).

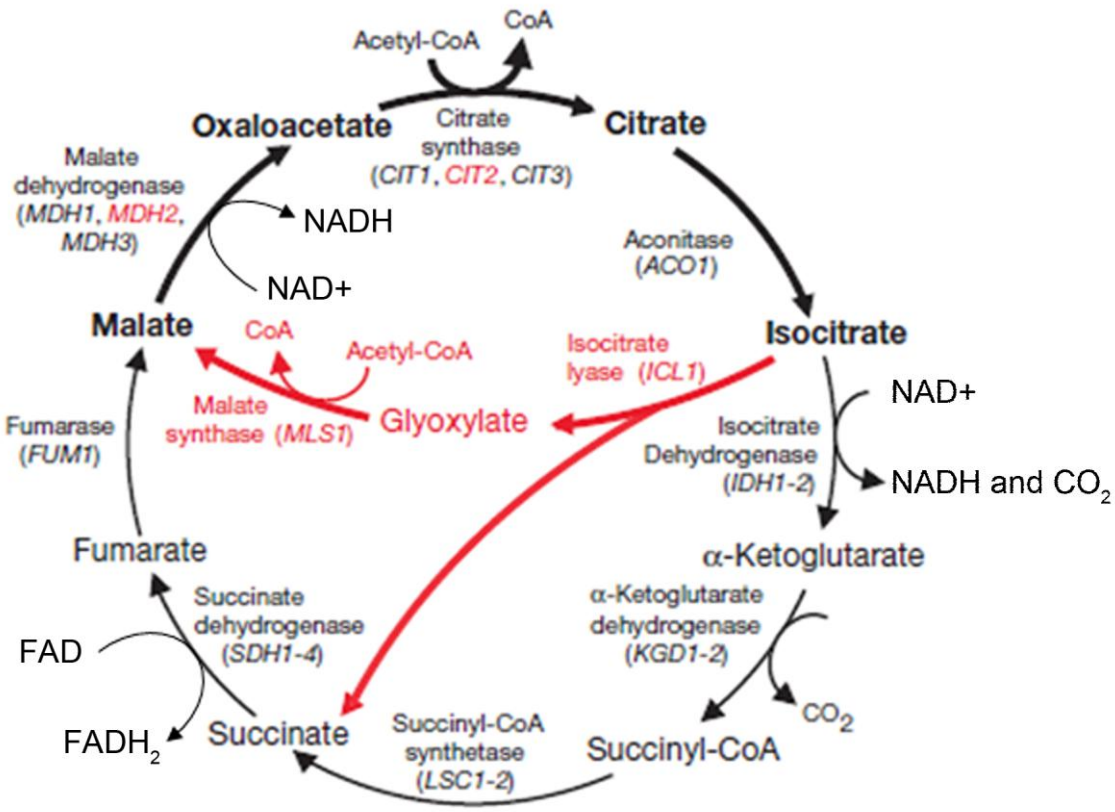

Figure 1.5 Schematic drawing of glyoxlate and TCA cycles.

Black lines represent basic enzymatic steps in TCA cycle; bold lines represent enzymatic steps shared by both TCA and glyoxylate cycle; red lines represent glyoxylate-specific enzymatic steps (as shown by Lorenz and Fink, 2001).

1.10 Aim of this study

This study is based on two important aspects involved in fungal growth and infection-related development; lipid metabolism and acetyl-CoA translocation. Further understanding of lipid metabolism and acetyl-CoA translocation may provide key elements regarding the regulation of infection-related development in *M. oryzae*, which could then be used to devise new means of efficiently controlling the rice blast disease. In order to do this, three objectives were addressed.

The first objective was to identify key transcriptional regulators involved in lipid metabolism in *M. oryzae*. Two transcriptional regulators were selected, *FAR1* and *FAR2*, based on their predicted functions as transcriptional regulators in lipid metabolism of other fungi (Hynes *et al.*, 2006; Poopanitpan *et al.*, 2010; Rocha *et al.*, 2008). In order to determine the function of *FAR1* and *FAR2* in *M. oryzae*:

1. The *FAR1* and *FAR2* genes have been GFP-tagged to establish the cellular localisation as well as spatial and temporal expression of the gene products.
2. Targeted gene deletion of *FAR1* and *FAR2* has been carried out to investigate their biological functions.
3. Lipid body mobilisation has been observed in Δ*far1* and Δ*far2* mutants.
4. The ability of Δ*far1* and Δ*far2* mutants to utilise carbon sources has been observed and gene expression during growth on various carbon sources has been measured.
5. Plant infection assays have been carried out on Δ*far1* and Δ*far2* mutants.

The second objective was to investigate the relationship between lipid storage and infection-related development. I identified a gene, *CAP20*, which encodes a perilipin in *M. oryzae* and is involved in lipid body development and storage. To determine the role of the *CAP20* perilipin in infection-related development:

1. A *CAP20-RFP* gene fusion was generated to determine the cellular localisation of perilipin.
2. Targeted deletion of *CAP20* was carried out has been carried out to investigate its biological functions.
3. The role of *CAP20* in lipid mobilisation and nuclear division was determined during conidial germination.
4. Plant infection assays were carried out on a Δ*cap20* mutant.

The third objective of this project was to investigate the importance of regulating the acetyl-CoA pool and determining the role of acetyl-CoA translocation in *M. oryzae*. Based on sequence homology and HT-superSAGE data (Soanes *et al.*, 2012), I selected genes which are involved in acetyl-CoA translocation and are also highly expressed during appressorium development including the genes involved in carnitine biosynthesis pathway (*CAR1*, *CAR2*, *CAR3*, *CAR4*), genes that encode for acetyl-CoA synthetase (*ACS1*, *ACS2*, *ACS3*) and a gene that encodes a mitochondrial carnitine carrier (*CRC1*). In order to determine the functions of each of these genes in *M. oryzae*:

1. Targeted deletion of each of the eight genes was carried out to investigate their biological functions.
2. The ability of each mutant strain to utilise distinct carbon sources was assayed.
3. Appressorium differentiation was observed in each mutant.
4. Plant infection assay were carried in each mutant.

Based on this analysis, I was able to demonstrate clear roles for lipid degradation, fatty acid β-oxidation and acetyl-CoA synthesis and turnover in the process of appressorium-mediated plant infection by *M. oryzae*.

2.0 Materials & Methods

2.1 Growth and maintenance of fungus stocks

The fungus was grown in Complete Medium (CM) (Talbot et al., 1993) supplemented with the appropriate antibiotics (usually 100 µg/mL of penicillin and streptomycin). For a 1 L preparation, the medium consisted of 10 g glucose, 2 g peptone, 1 g yeast extract (BD Biosciences), 1 g casamino acids, 50 mL 20X nitrate salt solution, 1 mL 1000X trace elements solution and 1 mL vitamin supplement solution. The chemicals were mixed and the pH adjusted to 6.5. For solid medium, 15 g of agar was added to the mixture.

20 X nitrate solution was prepared by mixing 120 g $NaNO_3$, 10.4 g KCl, 10.4 g $MgSO_4.7H_2O$, 30.4 g KH_2PO_4 in a total volume of 1 L deionized distilled water. The solution was then autoclaved and stored at 4 ºC until required. 1000 X trace elements solution consisted of 2.2 g $ZnSO_4.7H_2O$, 1.1 g H_3BO_3, 0.5 g $MnCl_2.4H_2O$, 0.5 g $FeSO_4.7H_2O$, 0.17 g $CoCl_2.6H_2O$, 0.16 g $CuSO_4.5H_2O$, 0.15 g $Na_2MoO_4.2H_2O$ and 5 g EDTA. The chemicals were mixed, boiled and cooled to 60 °C before pH to 6.5 with 10 M NaOH and diluted to 100 mL with deionized distilled water and stored at 4°C. Vitamin supplement solution was prepared by mixing 0.01 g biotin, 0.01 g pyridoxin, 0.01 g thiamine, 0.01 g riboflavin, 0.01 g p-aminobenzoic acid, 0.01 g nicotinic acid and brought up to 100 mL with deionized distilled water. The solution was kept in a dark bottle at stored at 4 °C. All the chemicals used were obtained from Sigma unless otherwise stated.

All isolates of *Magnaporthe oryzae* used in this study are stored in the laboratory of N. J. Talbot (University of Exeter). For long term storage, the isolates were grown through filter paper discs (3 mm, Whatman International) and desiccated for at least 48 hours

before being stored at -20 °C. The fungus was routinely incubated in a controlled temperature room at 24 °C with 12 hour light and dark cycles.

2.2 Fungal genomic DNA extraction

The CTAB (Hexadecyltrimethylammonium bromide) extraction method was routinely used for genomic DNA extraction. CTAB extraction solution consists of 33 mM CTAB, 0.1 M Tris (Tris (hydroxymethyl)aminomethane), 7.8 mM EDTA and 0.7 M NaCl. The fungal isolates were first grown through a layer of cellophane on a CM plate for 10-12 days at 24 °C. Then, the cellophane layer was placed into a mortar containing liquid nitrogen and ground to a fine powder. The powder was transferred into a sterile 1.5 mL eppendorf tube until almost full. 500 µL of CTAB extraction solution prehaeated to 65 °C was added into the eppendorf tube. The mixture was mixed and incubated at 65 °C for 30 min with occasional shaking. An equal volume (500 µL) of chloroform:pentanol (CIA)(24:1) was added and the tubes shaken vigorously for 30 min at room temperature. Following centrifugation at 13 000 × *g* for 10 min at 4 °C using Beckman J2-MC high speed centrifuge, top aqueous phase was transferred into another eppendorf tube and the CIA extraction step was repeated. The upper aqueous phase was transferred into a new eppendorf tube to which 1 mL propan-2-ol was added and incubated on ice. After 5 min, the tube was centrifuged at 13 000 × *g* for 10 min at 4 °C. The supernatant was discarded leaving the pellet at the bottom of the tube. The tube was inverted on a paper towel and allowed to drain for 5 min. The nucleic acid pellet was resuspended in 500 µL sterile milliQ water and precipitated by adding 0.1 volume of 3 M sodium acetate (pH 5.2) and 2 volumes of ice cold 100% ethanol and incubated at -20 °C for 10 min or overnight for a higher yield. The purified nucleic acids were recovered by centrifugation at 13 000 × *g* for 20 min at 4 °C and then washed with 70% ice cold

ethanol. The supernatant was discarded and the nucleic acid pellet dried using a centrifugal evaporator for 20-30 min. The pellet was then resuspended in 30 to 100 µL of sterile milliQ water + 10 µg/mL RNase A. Genomic DNA samples were routinely stored at -20 °C.

2.3 Digestion of genomic or plasmid DNA with restriction enzymes

Restriction endonucleases were routinely obtained from Promega UK Ltd. (Southampton, UK) or New England Biolabs (Hitchin, UK). DNA digestion was carried out using buffer solutions provided by the manufacturer in a total volume of 30 µL with 2 µg of plasmid DNA or 10 µg of genomic DNA and 5-10 units of enzyme.

2.4 DNA gel electrophoresis

Digested DNA was fractionated by gel electrophoresis in 0.8% (w/v) agarose gel matrices using 1X Tris-borate-EDTA (TBE) buffer (90 mM Tris-borate, 2 mM EDTA) or 1X Tris-acetate-EDTA (TAE) buffer. Ethidium bromide was added into the agarose gel solution (0.5 µg/mL) to visualise DNA fragments and a 1 kb plus (invitrogen) size marker was used to determine the length of DNA fragments. DNA fragments were visualised using a gel documentation system (Image Master® VDS with a Fujifilm Thermal Imaging system FTI-500, Pharmacia Biotech).

2.5 The polymerase chain reaction (PCR)

The polymerase chain reaction (PCR) was performed using an Applied Biosystems GeneAmp® PCR system 2400 cycler. The PCR reactions consist of 2.5 units GoTaq® Flexi DNA polymerase (Promega), GoTaq® Flexi DNA polymerase 5X reaction buffer, 10 nM $MgCl_2$, 100 nM of each dNTP, 1 µL of 10 pM stock solution of each primer, 50

ng of genomic DNA or 30 ng of plasmid DNA as template and deionized distilled water to a final volume of 25 µL.

PCR was routinely carried out according to the following conditions: initial denaturation step at 94 °C for 10 min followed by 35 cycles of PCR cycling parameters of: 94 °C for 30 sec, 56-64 °C for 30 sec and 72 °C for 1 min/kb target length, followed by a final extension at 72 °C for 10 min.

2.6 Gel purification of DNA fragments

DNA fragments were recovered from agarose gels using a commercial kit (Wizard® SV Gel and PCR Clean-Up System, (Promega) (Cat. # A9282) according to the manufacturer's instructions. Fragments were excised from the gel using a razor blade and placed in a pre-weighed eppendorf tube. The mass of agarose removed from the gel was measured and Membrane Binding Solution (4.5 M guanidine isothiocyanate and 0.5 M potassium acetate, pH 5.0) was added to the gel slice in a microfuge tube at a ratio of 1 µL per 1 mg. Samples were incubated at 65 °C and mixed by vortexing every 2-3 min until the gel slice had dissolved. The dissolved gel mixture was transferred to an SV Minicolumn and Collection tube and incubated at room temperature for 1 min. After centrifugation for 1 min in an IEC, Micromax at 13 000 × *g*, the flow-through was discarded and the column replaced in the collection tube. To wash the column, 700 µL of Membrane Wash Solution (ethanol-based) was added and centrifugation carried out for 1 min at 13 000 × *g*. The flow-through was discarded and the column processed by centrifugation for an additional minute at top speed with a further wash of 500 µL Membrane Wash Solution. The SV Minicolumn was placed in a clean microfuge tube, 50 µL of Nuclease-Free Water added and after 1 min DNA was recovered by

centrifugation for 1 min at 13 000 × *g*. The DNA was quantified using a Nano-drop (company) and stored at -20 °C.

2.7 Bacterial plasmid DNA preparations

2.7.1 Alkaline lysis plasmid mini preparations

Single bacterial colonies were picked and used as inoculum in 5 mL Luria-Bertani broth (LB) containing an appropriate antiobiotic in a universal bottle. LB medium consists of 10 g/L tryptone, 5 g/L yeast extract, 86 mM NaCl, adjusted pH to 7.5. Cultures were grown overnight with vigorous shaking (300 rpm) in a rotary incubator (Innova 4000, New Brunswick Scientific). For long term storage, a fraction of the bacterial culture was used to prepare a 20% glycerol stock. The bacterial glycerol stock was vortexed rapidly and stored at -80 °C. The remainder of the culture was transferred to a fresh eppendorf tube and pelleted by centrifugation (IEC, Micromax) at 13 000 × *g* for 2 min. The supernatant was discarded and the bacterial pellet was resuspended in 200 µL of ice cold resuspension solution (Solution I) (50 mM glucose, 25 mM Tris-HCl [pH 8.0], 10 mM EDTA [pH 8.0]) by vortexing using whirlmixer (Fisher Scientific). 400 µL of freshly prepared lysis solution (Solution II) (0.2 M NaOH, 1% SDS) was added to the cell suspension. The contents were mixed by inversion, ensuring the entire surface of the tube came into contact with Solution II, before placing on ice for 5 min. A 300 µL aliquot of ice cold neutralisation solution (Soution III) (5 M potassium acetate, 11.5% [v/v] glacial acetic acid) was added and the contents mixed rapidly by vortexing. The tube was placed on ice for 3 to 5 min before centrifugation at 12 000 × *g* for 5 min at 4 °C. A 600 µL aliquot of the supernatant was transferred to a fresh eppendorf tube and DNA was precipitated using an equal volume of propan-2-ol at room temperature for 2 min. The DNA was recovered by centrifugation at 12 000 × *g* for 5 min at 4 °C. The

supernatant was discarded and the tube inverted on a paper towel to dry. The pellet was washed with 70% (v/v) ice cold ethanol and dried using a rotary evaporator. The pellet was resuspended in 50 µL of sterile milliQ water containing DNAase free pancreatic RNAase (20 µg/mL), vortexed briefly and incubated at 37 °C for 20 min. The plasmid DNA was stored at -20 °C prior to use.

2.7.2 High quality plasmid DNA preparations

High quality plasmid DNA for sequencing was prepared using a commercially available kit (Promega PureYield™ Plasmid Midiprep System) (Cat. #A2492) according to the manufacturer's instructions. A 50-100 mL aliquot of bacterial culture was grown overnight and bacterial cells harvested by centrifugation for 10 min at 10 000 × *g*. The resulting pellet was resuspended in 3 mL of cell resuspension solution (50 mM Tris [pH 7.5], 10 mM EDTA, 100 µg/mL RNase A). 3 mL of cell lysis solution (0.2 M NaOH, 1% SDS) was added to the mixture and the tubes inverted 3-5 times. Following incubation at room temperature for 3 min, 5 mL of neutralization solution (4.09 M guanidine hydrochloride, 0.759 M potassium acetate, 2.12 M glacial acetic acid, [final pH 4.2]) was added. The cell lysate was mixed well by inverting 5-10 times and centrifuged for 15 min at 15 000 × *g* at room temperature. A column stack was then assembled by placing a PureYield™ Clearing Column on top of a PureYield™ Binding Column. The column stack was placed onto a vacuum manifold and the bacterial lysate poured into the column. A vacuum was applied to the column stack until the liquid had passed through both the clearing and binding columns. The vacuum was slowly released before the clearing column was discarded. A 5 mL aliquot of endotoxin removal wash solution was added to the binding column and a vacuum applied. After the solution had been drawn through the column, 20 mL of column wash solution was added. A vacuum

was then applied to draw the solution through the column. A vacuum was applied for a further 30-60 sec to remove excess ethanol from the DNA binding membrane. The binding column was removed from the vacuum manifold and transferred to a 50 mL plastic tube before 600 μL of nuclease free water was added to the binding column and left for 1 min at room temperature. Centrifugation was then carried out for 5 min at 1 500-2 000 × *g*. The DNA was transferred to an eppendorf tube and stored at -20 °C for further analysis.

2.8 DNA ligation and selection of recombinant clones

For routine cloning into standard vectors (pGEM® series [Promega] and TOPO TA Cloning® [Invitrogen]) recombinant clones were selected using α-complementation of *lacZ* (Sambrook et al., 1989). To a 40 μL restriction digest, 4 μL of NEBuffer (New England Biolabs) or 10X Buffer (Promega), 1 μL of restriction enzyme for a single digest and 2 μL for a double digest and nuclease free water to give a total volume of 30 μL. This reaction mix was then incubated at 37 °C for overnight. The digested DNA was gel purified and ligation reactions prepared. DNA fragments amplified by the polymerase chain reaction (PCR) were routinely cloned by ligation into pGEM-T (Promega) or TOPO TA Cloning (Invitrogen) which allows T:A cloning of PCR fragments generated by certain thermostable DNA polymerases such as *Taq* polymerase (Mead et al., 1991). Ligation reactions with pGEM-T were performed at 4 °C (Sambrook et al., 1989) overnight. For efficient cloning of weakly amplified PCR products, the TOPO TA cloning® kit (Invitrogen) was used according to the manufacturer's instructions. Approximately 0.5-4 μL of insert DNA was added to a ligation mix containing 10 ng of pCR® 2.1-TOPO vector (Invitrogen) and salt solution (1.2 M NaCl; 0.06 M $MgCl_2$) in a total volume of 6 μL. The reaction was gently

mixed and incubated at room temperature for 5 min. An aliquot of 2 μL of the ligation mix was added to a vial of One Shot® chemically competent *E. coli*, (TOP10 F^- *mcr*A Δ(*mrr-hsd*RMS-*mcr*BC) ϕ80*lac*ZΔM15 Δ*lac*X74 *rec*A1 *ara*D139 ΔD139 Δ(*ara-leu*)7697 *gal*U *gal*K *rps*L (Str^r) *end*A1 *nup*G) mixed, and placed on ice for 5 min. The cells were then heat-shocked for 30 seconds at 42°C and kept on ice for 2 min before 250 μL of room temperature S.O.C. (Invitrogen) was added. Following incubation at 37°C (200 rpm) for 1 hour, 50 μL of the transformation mix was plated onto LB agar plates with ampicillin (50μg/ml) and 5-bromo-4-chloro-3-indolyl-β-D-galactopyranoside (X-gal, 0.8 mg/mL per plate) (Calbiochem (VWR International Ltd.)). Plates were inverted and incubated at 37°C overnight.

2.9 Preparation of competent cells

Stocks of laboratory-prepared transformation-competent cells were generated using a protocol adapted from (Sambrook et al., 1989). Single bacterial colonies were obtained by streaking bacterial cells across a plate of LB containing the appropriate antibiotic and incubating at 37 °C for 16 h. A single colony was used to generate an overnight culture in 10 mL LB broth (37 °C, 200 rpm). A 2.5 mL aliquot of this culture was inoculated into 250 mL of SOC (20 g/L tryptone, 5 g/L yeast extract, 8.6 mM NaCl, 10 mM $MgSO_4$, 10 mM $MgCl_2$) and this was allowed to grow until an OD_{600}= 0.6 had been reached (Sambrook et al., 1989). The culture was then transferred to a 50 mL Oakridge tube and incubated on ice for 10 min. Cells were recovered by centrifugation at 2,510 × *g* (Beckman J2-MC, JS13.1 rotor) for 10 min at 4 °C. To each tube, 15 mL filter-sterilised FSB (10 mM potassium acetate [pH 7.5], 45 mM $MnCl_2{\cdot}4H_2O$, 10 mM $CaCl_2{\cdot}2H_2O$, 100 mM KCl, 3 mM hexamine-cobalt chloride, 10% glycerol [pH 6.4]) was added and the cells re-suspended by gentle pipetting. Samples were incubated on

ice for 10 min and the centrifugation step repeated once. The cells were then resuspended in 4 mL FSB and DMSO (dimethyl sulfoxide, Sigma) was added to a final concentration of 3.4% (v/v). The mixture was incubated on ice for 15 min. A further volume of DMSO was added such that the final concentration was 6.5% DMSO (v/v). The cells were then dispensed into 100 µL aliquots in prechilled microfuge tubes. Samples were immediately frozen by immersion in liquid nitrogen and stored at -80 °C.

2.10 Transformation of bacterial hosts

Bacterial transformation was carried out using *Escherichia coli* strain XL1 Blue (Stratagene). XL1 – Blue has genotype *sup*E44 *hsd*R17 *rec*A1 *end*A1 *gyr*A46 *thi rel*A1 *lac*$^-$ [F′ *pro* AB$^+$ *lac*I^q *lac*ZΔM15 *Tn*10 (*tet* ^{r})] and competent *E. coli* JM109 cells (Promega, *rec*A1 *sup*E44 *end*A1 *hsd*R17 (r_k^- m_k^+) *gyr*A96 *rel*A1 *thi* Δ(*lac-pro*AB) [F′ *tra*D36 *pro*AB$^+$ *lac*I^q *lac*ZΔM15]). JM109 is a recombination-deficient strain that will support growth of vectors carrying amber mutations and will modify but not restrict transfected DNA (Sambrook et al., 1989). A 200 µL aliquot of competent cells was thawed at room temperature and immediately transferred into a pre-chilled 15 mL tube (Falcon 2059, BD Biosciences). 1 to 5 µL of DNA was added to the tube and the mixture was placed on ice for 30 min. Cells were heat shocked at 42 °C for 45 sec and placed on ice for 2 min. After that, 800 µL of SOC medium was added to the tube and the recovering cells were incubated at 37 °C for 1 h with vigorous shaking. Aliquots were plated on LB agar with the appropriate antibiotic. Where α-complementation selection was available (Sambrook et al., 1989) the agar contained isopropyl-thiogalactoside (IPTG, 0.8 mg/mL per plate) (Calbiochem [VWR International Ltd.]) and 5-bromo-4-chloro-3-indolyl-β-D-galactopyranoside (X-gal, 0.8 mg/mL per plate)

(Calbiochem [VWR International Ltd.]). Plates were inverted and incubated at 37 ^{o}C overnight.

2.11 Targeted gene deletion using split marker strategy

A PCR based split marker strategy was used to carry out genes deletion and involved multiple PCR rounds of amplification and no cloning steps (Figure 2.1). Gene specific primers were designed to allow amplification of 1-1.5 kb fragments from the flanking sequence of the open reading frame of the gene of interest. The primers for the 5' and 3' inner flanks were each designed to include an extension complementary to the ends of the selectable marker (Catlett et al., 2003).

The first round of PCR involved the amplification of the 5' and 3' flanks and the overlapping fragments of the selectable marker. The PCR was carried out as described in Section 2.5. In a second round of PCR the amplified flanks were fused with the overlapping fragments of the selectable marker using one primer from the flanking region and a second specific to the selectable marker. The conditions were set out as described in Section 2.5. The resulting products, each contained a flanking sequence of the target gene and an overlapping region of the selectable marker gene, following analysis by gel electrophoresis and gel purification were transformed into the fungus. Homologous recombination between the flanking regions and chromosomal DNA and between the overlapping fragments of the selectable marker should result in a targeted deletion (Catlett et al., 2003).

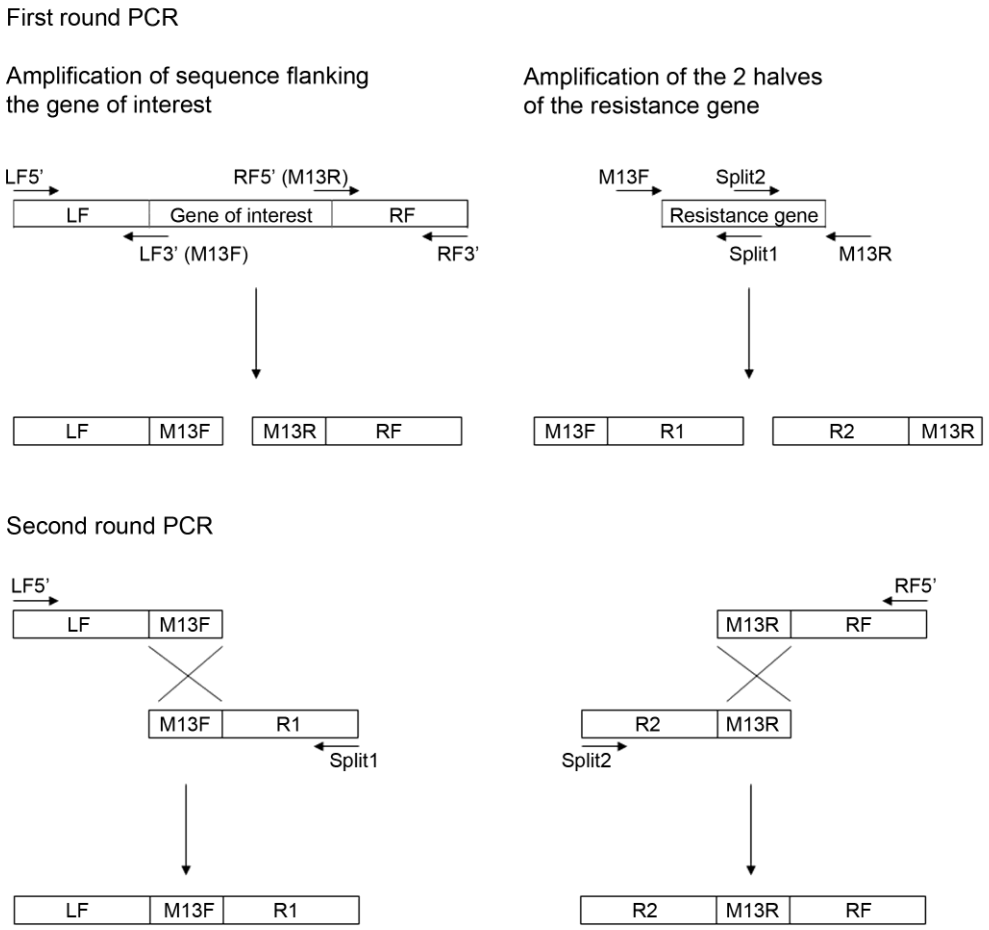

Figure 2.1 Split marker strategy for targeted gene deletion in *M. oryzae*.

In the first round of PCR reactions flanking sequence from each side of the gene are amplified using primers LF5'/LF3' (M13F) and RF5' (M13R)/RF3'. In the parallel PCR reaction, resistance gene is amplified in two unequal halves using primers M13F/Split1 and Split2/M13R. Primers LF3' (M13F) and RF5' (M13R) contain complementary sequences at 5´ end corresponds to M13F and M13R respectively. In the second round of PCR reaction, primers LF5'/Split1 and Split2/RF5' are used to fuse each half of resistance gene with flanking products; left flank (LF) with the first half of the resistance gene (R1) and right flank (RF) with the second half of the resistance gene (R2). The products from the second round PCR are used for fungal transformation. Homologous recombination facilitates the replacement of the targeted sequence with the resistance gene. Schematic diagram is not drawn to scale.

2.12 Fungal transformation

A 2.5 cm^2 section of *M. oryzae* mycelium was removed from a CM plate culture, blended in 150 mL complete medium incubated at 24 °C with shaking at 125 rpm in an orbital incubator for 48 hours. The mycelium was harvested by filtration through sterile Miracloth (Calbiochem) and washed with sterile distilled water. The mycelium was transferred to a 50 mL Falcon tube (Becton Dickinson) containing 40 mL of filter sterilised OM buffer (1.2 M $MgSO_4$, 10 mM $NaPO_4$ [pH 5.8]) and 5% glucanex (Novo Industries, Copenhagen) and shaken gently at 75 rpm for 2 to 3 hours at 30 °C in an orbital incubator. The resulting protoplasts were transferred to a sterile polycarbonate or polysulfonate Oakridge tube and overlaid with an equal volume of freshly prepared sterile cold ST buffer (0.6 M sucrose, 0.1 M Tris-HCl pH 7). The tube was centrifuged at 5000 × *g* for 15 min at 4 °C in a swinging bucket rotor (Beckman JS-13.1) in a Beckman J2.MC centrifuge. The protoplasts were recovered from the OM/ST interface and transferred into another sterile Oakridge tube. The tube was then filled with freshly prepared sterile cold STC buffer (1.2 M sucrose, 10 mM Tris-HCl pH 7.5, 10 mM $CaCl_2$). Protoplasts were pelleted at 3 000 × *g* for 10 min at 4 °C using a swinging bucket rotor. The washes were repeated twice more with 10 mL STC buffer, with complete resuspension each time. The protoplasts were resuspended in 1 mL of STC buffer and the concentration of the protoplasts was determined by counting using a haemocytometer.

DNA mediated transformation was undertaken in 1.5 mL microfuge tubes by combining an aliquot of purified protoplasts (10^6 to 10^7 per mL) with DNA (5-10 μg) in a total volume of 150 μL of STC buffer. The mixture was incubated at room temperature for 15-25 min and 1 mL of sterile PTC (60% PEG 400, 10 mM Tris-HCl pH 7.5, 10 mM $CaCl_2$) was added (in 2-3 aliquots with gentle mixing after each addition). The mixture

was incubated at room temperature for 15-20 min then added to 150 mL molten (45 °C) 1.5% agar/OCM (CM osmotically stabilised with 0.8M sucrose), mixed gently and poured into 5 sterile Petri dishes (approximately 30 mL/plate). For selection of transformants on Hygromycin B (Calbiochem), plate cultures were incubated in the dark for at least 16 hours at 24 °C and then overlaid with approximately 15 mL OCM/1% agar containing 200 μg/mL hygromycin B freshly added to the medium from a stock solution of 50 mg/mL. For selection of sulfonylurea resistant transformants, hygromycin B was replaced with chlorimuron ethyl (AppliChem) and for selection of bialophos resistant transformants, it was replaced with glufosinate ammonium (Fluka). BDCM medium was used instead of OCM (Sweigard et al., 1997).

2.13 Southern blot analysis

Blotting of agarose DNA gels was performed according to an adaptation of the method from (Southern, 1975). The gel was submerged in 0.25 N HCl for 15 min with gentle shaking to depurinate the fractionated DNA and then denatured by soaking in gel blotting solution (0.4 N NaOH, 0.6 M NaCl) for 30 min. The gel was transferred to neutralization solution (1.5 M NaCl, 0.5 M Tris-HCl pH 7.5) for 30 min before capillary blotting onto Hybond-N (GE Healthcare). Gel blots were performed by placing the inverted gel onto a sheet of filter paper wick, which was supported on a perspex sheet with each end of the wick submerged in 20X SSPE solution (3.6 M NaCl, 200 mM NaH_2PO_4, 22 mM EDTA). Hybond-N membrane was then placed onto the gel and overlaid with five layers of wet Whatman 3 mm paper and five layers of dry Whatman 3 mm paper onto which a 10 cm high stack of paper towels was placed (Kimberley Clark Corporation). Finally, a 500 g weight was placed on the stack and the blot was left to stand at room temperature overnight. The transferred DNA was UV cross-linked to the

membrane using a BLX crosslinker (Bio-link®) and either probed immediately or wrapped in Saran wrap for storage.

2.14 Radio-labelled DNA probe construction

DNA hybridisation probes were labelled by the random primer method (Feinberg and Vogelstein, 1983) using a Ready-To-Go kit (GE Healthcare) according to the manufacturer's instructions. A 25-50 ng aliquot of DNA was made to a final volume of 47 μL in water. The sample was boiled for 5 min to denature the DNA and put on ice for 2 min. The sample was centrifuged briefly and the contents were added to a Ready-To-Go reaction mix bead containing buffer, dATP, dGTP, dTTP, FLPC*pure*™ Klenow polymerase (7-12 units) and random oligonucleotides, primarily 9-mers. The reagents were mixed by gently pipetting and 1 μL of [α-^{32}P]dCTP (3,000 Ci/mmol) added. The labelling reaction was then incubated at 37 °C for 10 min. The reaction was stopped by adding 100 μL of labelling stop dye (0.1% SDS, 0.06 M EDTA, 0.5% bromophenol blue, 1.5% blue dextran). The labelling reaction was passed through a Biogel P60 (Bio-Rad) column to remove the unincorporated isotope with collection of the dextran blue labelled fraction. The probe was denatured by heating at 100 °C for 5 min and quenched on ice for 2 min before adding to the hybridisation mixture.

2.15 DNA gel blot hybridisations

DNA gel blot hybridisations were performed using standard procedures (Sambrook et al., 1989). Membrane were incubated in a hybridisation bottle (Hybaid Ltd.) in a hybridisation oven (Hybaid) for at least 4 hours at 65 °C in 25-30 mL of pre-hybridisation solution, (6 x SSPE (diluted from a 20 X stock prepared by dissolving 175.3 g of NaCl, 27.6 g of NaH_2PO_4 and 7.4 g of EDTA in 800 mL of ddH_2O, adjusting

the pH to 7.4 with NaOH and making up to 1 litre with ddH_2O), 5 X Denhardt's solution (diluted from a 50 X stock prepared with 5 g Ficoll [type 400, Pharmacia], 5 g polyvinylpyrrolidone in 500 mL ddH_20, 0.5 % SDS), with 100 μL denatured herring sperm DNA (1% [w/v] in 0.1 M NaCl) (Sigma) added. A denatured radio-labelled probe was then added and the mixture incubated overnight at 65 ^oC.

Following hybridisation, the blot was washed at high stringency. The pre-hybridisation solution was discarded along with any unbound probe and 25-30 mL of 2 X SSPE wash (0.1% SDS, 0.1% sodium pyrophosphate [PPi], 2X SSPE (diluted from the 20 X SSPE stock) [pH 7.4]) was added with incubation at 65 °C for 30 min. The wash solution was discarded and 25-30 mL of 0.2 X SSPE wash (0.1% SDS, 0.1% sodium pyrophosphate [PPi], 0.2 X SSPE, [pH 7.4]) was added with incubation at 65 °C for a further 30 min. The 0.2 X SSPE wash was repeated and the membrane left to dry.

Autoradiography was carried out by exposure of membranes to X-ray film (Fuji medical X-ray film, Fuji Photo Film (U.K.) Ltd.) at -70 °C in the presence of an intensifying screen (Amersham). X-ray films were developed using Kodak chemicals.

2.16 Extraction of total *M. oryzae* RNA

2 cm^2 plug of *M. oryzae* mycelium from a CM agar plate was blended with 150 mL of liquid CM and grown for 48 hour, with 150 rpm aeration at 24 °C in an orbital incubator. The mycelium was harvested by filtering through sterile Miracloth, washed with sterile distilled water before being transferred into minimal medium supplemented with various carbon sources (glucose, acetate, olive oil, oleic acid, triolein) and grown for another 24 hour. Once again the mycelium was harvested, washed and blotted dry with paper towel and ready for RNA extraction by the lithium chloride method. The mycelium was ground to a fine powder in liquid nitrogen and transferred into eppendorf

tube containing equal volume (400 µL) of extraction buffer (0.1 M LiCl, 0.1 M Tris [pH 8.0], 10 mM EDTA, 1% SDS) and phenol. The tube was inverted for 1 min, 0.5 vol (400 µL) of chloroform was added and mixed by inverting the tube for 30 sec before centrifuged at 13 000 × *g* for 30 min at 4 °C. The aqueous phase was transferred into a fresh eppendorf tube and an equal volume of 4 M LiCl was added before incubating the sample in ice at 4 °C overnight. After that, the sample was centrifuged at 13 000 × *g* for 20 min at 4 °C and the pellet washed with 70% (v/v) ethanol before resuspended in 500 µL of DEPC treated water. An equal volume of phenol:CIA was added into the tube and the sample was inverted for 30 sec before centrifugation at 13 000 × *g* for 10 min at 4 °C. The aqueous phase was transferred into a fresh eppendorf tube and RNA precipitated by adding 0.1 vol of 3 M sodium acetate (pH 5.2) and 2 vol of ethanol and incubated at-20 °C overnight. The RNA was recovered by centrifugation at 13 000 × *g* for 20 min at 4 °C. The pellet was washed with 70% (v/v) ethanol, air dried and resuspended in 100 µL DEPC water and stored at -80 °C.

2.17 Plant infection assays

Dwarf Indica rice (*Oryza sativa*) cultivar, CO-39, which is susceptible to rice blast (Valent et al., 1991), was used for rice infections. *M. oryzae* was grown on CM agar for 11 days before harvesting the conidia in 5 mL of 0.2% gelatine (BDH). The suspension was diluted to 1×10^5 conidia per mL for plant infections and spray-inoculated using an artist's airbrush (Badger Airbrush, Franklin Park, Illinois, USA). Rice plants were grown in pots (15 plants per pot) and were inoculated when 16 days old (2-3 leaf stage). Following spray-inoculation, plants were wrapped in polythene bags and incubated in a controlled environment chamber (Sanyo Versatile Environmental test chamber) at 24 °C with a 12 hours light-12 hours dark photo-phase and 90% relative humidity according to

(Valent et al., 1991). After 48 hours, the polythene bags were removed and the plants were incubated for a further 2-3 days. Lesion formation was monitored 3 days post-inoculation and lesion density was recorded 4-5 days after inoculation.

2.18 Microscopy and live cell imaging

2.18.1 Microscopy using the Zeiss Axioskop 2 epifluorescence microscope

Experiments throughout this project required quantification following microscopic analysis. The Zeiss Axioskop 2 compound epifluorescence microscope was used for all general microscopic quantification. Several images were captured from the Zeiss Axioskop 2 microscope using an AxioCam HR digital camera (Zeiss) and figures were subsequently prepared from digitised images in Adobe Photoshop 7.0 (Adobe Systems Inc.).

2.18.2 Microscopy analysis using the Olympus IX81 microscope

Epifluorescence microscopy to visualize GFP, RFP and BODIPY-stained samples was routinely performed using an IX81 motorized inverted microscope (Olympus) equipped with a UPlanSApo 100X/1.40 Oil objective (Olympus). Excitation of fluorescently-labeled proteins and lipid droplets were carried out using a VS-LMS4 Laser-Merge-System with solid state lasers (488 nm/50 mW). The laser intensity was controlled by a VS-AOTF100 System and coupled into the light path using a VS-20 Laser-Lens-System (Visitron System). Images were captured using a Charged-Coupled Device camera (Photometric CoolSNAP HQ2, Roper Scientific). All parts of the system were under the control of the software package MetaMorph (Molecular Devices).

3.0 Regulation of lipid metabolism in *Magnaporthe oryzae* by *FAR1* and *FAR2*

3.1 Introduction

Appressorium formation in *Magnaporthe oryzae* occurs in the absence of available nutrients and the fungus must therefore mobilise nutrient sources from the conidium in order to generate turgor and fuel the initial stages of plant infection (Wilson and Talbot, 2009). Trehalose, glycogen and lipids are the major storage reserves in the conidium. Trehalose and glycogen degradation occurs rapidly during conidium germination and appressorium development (Thines et al., 2000; Wang et al., 2005). Lipid mobilization occurs from the conidium to the germ tube apex and then into the nascent appressorium, where lipid droplets coalesce and are taken up by the central vacuole before lipolysis (Weber et al., 2001).

In the appressorium, catabolism of lipids yields both glycerol and fatty acids and is catalyzed by triacylglycerol lipases. Triacylglycerol lipase activity is highly induced during the onset of appressorium formation and remains high throughout maturation and generation of turgor (Thines et al., 2000). Genomic analysis has shown that *M. oryzae* possesses 19 genes that encode intracellular lipases, which may be used for degradation of substrates containing lipid as well as utilization of intracellular lipid stores. Deletion of any one of these genes individually does not, however, significantly affect plant infection by *M. oryzae* (Wang et al., 2007), suggesting that the orchestrated breakdown of lipid involves the coordinated action of more than one lipase. The liberation of fatty acids during spore germination also suggests the need for fatty acid β-oxidation during appressorium-mediated infection by the fungus. The four-step pathway results in the release of a 2 carbon unit from each fatty acid in the form of acetyl-CoA and the whole process occurs in a peroxisome like body or glyoxysome (Wang et al., 2007). Genomic

analysis identified a set of genes predicted to encode enzymes involved in fatty acid β-oxidation in *M. oryzae* (Dean et al., 2005) and showed that deletion of the peroxisomal localised *MFP1*, which encodes a multifunctional β-oxidation protein, is important for appressorium function and virulence (Wang et al., 2007).

Acetyl-CoA is a metabolic intermediate that feeds both the glyoxylate and TCA cycles, but is also essential for synthesis of melanin, isoprenoids, amino acids, and a number of secondary metabolites. The glyoxylate cycle has been shown be important in the virulence of the human pathogenic fungus *Candida albicans* (Lorenz and Fink, 2001) and the bacterial pathogen *Mycobacterium tuberculosis* (McKinney et al., 2000). The glyoxylate cycle was also shown to be important during infection in *M. oryzae*. Mutants lacking *ICL1*, which encodes isocitrate lyase, showed a delay in generation of symptoms of rice blast disease (Wang et al., 2003).

Consistent with the requirement for both peroxisomal fatty acid β-oxidation and the glyoxylate cycle, deletion of *PTH2*, which encodes a peroxisomal carnitine acetyl transferase (CAT), has also been shown to affect virulence of *M. oryzae* (Bhambra et al., 2006). CAT is an enzyme required to transport acetyl-CoA from peroxisomes to other cellular compartments. In addition, the deletion of *PEX6* which encodes a peroxin protein, essential for peroxisomal biogenesis, caused defects in appressorium function and a loss of pathogenicity (Wang et al., 2007). It is apparent therefore that peroxisomal biogenesis and metabolism are essential processes required for the formation of an effective appressorium and subsequent plant infection.

It has therefore become clear that the breakdown of lipids and subsequently fatty acids are important in the development and pathogenicty in *M. oryzae*. Enzymes involved in fatty acid catabolism are up-regulated during infection (Soanes et al., 2012). Microarray analysis of gene expression of *Candida albicans* infecting macrophages, for instance,

showed increased expression of genes involved in fatty acid utilisation (Lorenz et al., 2004). In *Aspergillus nidulans*, two genes, FarA and FarB, have been identified and shown to regulate the induction of many genes involved in fatty acid β-oxidation, the glyoxylate cycle and peroxisomal biogenesis (Hynes et al., 2006). FarA and FarB encode transcriptional regulators which appear to control the expression of genes involved in fatty acid beta oxidation and lipid metabolism. Consistent with this, specific cis-acting elements have been identified in the upstream promoter sequences of many of these genes (Hynes et al., 2006). *Fusarium oxysporum* and the human pathogen *Candida albicans* also possess homologues of the Far proteins and these have been show also to be involved in regulating lipid metabolism (Rocha *et al.*, 2008; Ramirez and Lorenz, 2009).

In this chapter I report a series of experiments to identify and characterize M. oryzae orthologues of FarA and FarB and to investigate whether these putative transcriptional regulators also control the expression of genes required for lipid metabolism. In order to do this, targeted gene deletion experiments were initially carried out to produce mutants lacking each putative transcriptional regulator. I subsequently characterised each mutant to define the affect on carbon source utilisation as well as infection-related development, lipid mobilisation and pathogenicity.

3.2 Materials and methods

3.2.1 Targeted deletion of genes that encodes *MoFAR1*, *MoFAR2* and *MoFAR1*/*MoFAR2*

The split marker strategy was used for the targeted deletion of *FAR1* and *FAR2* as described in Section 2.11 (Catlett et al., 2003). Hygromycin B was used as a selectable marker and the primers used are listed in Table 3.1. The first round PCR involved the amplification of sequences flanking the gene of interest and the hygromycin B resistance gene cassette. The left flanks of *FAR1* and *FAR2* were amplified using the following primers; FarA50.1/FarA.M13F and FarB50.1/FarB.M13F respectively. Amplification of the right flanks was carried out using primers FarA30.1/FarA.M13R and FarB30.2/FarB.M13R respectively. The HY half of the hygromycin B resistance gene cassette was amplified using M13F and HY split primers while the YG half of hygromycin was amplified using YG split and M13R primers.

Table 3.1 Primers used in this study to carry out targeted gene deletion of *FAR1* and *FAR2* in Δ*ku70*.

Primer	Sequence 5'-3'
FarA50.1	ACATTCAGGTAGGGAGGACACAAA
FarA.M13F	GTCGTGACTGGGAAAACCCTGGCGCGTCTGCTCCTTCGCGCCATTGTT
FarA30.1	TCCTGTGTGAAATTGTTATCCGCTACAGAGGAGGACTTCAACGAGGAC
FarA.M13R	CTGGGAATAGTTGATCGGGCTGAA
FarB50.1	CATAACCTGTCTTTCTGCCTACCT
FarB.M13F	GTCGTGACTGGGAAAACCCTGGCGCCGCTCGTCGTTTTGTGATCTTGG
FarB30.2	TCCTGTGTGAAATTGTTATCCGCTGTAGCACAAACATGGCTCCTCGTA
FarB.M13R	GGTTTGGTCCTCAGGCTCACTTTC
pFarB.F1	GTGGGAATTGCCGTTGGGA
pFarB.R1	CTCGGATCGGTAATTCGCC
M13F	GTCGTGACTGGGAAAACCCTGGCG
HY split	GGATGCCTCCGCTCGAAGTA
YG split	CGTTGCAAGACCTGCCTGAA
M13R	TCCTGTGTGAAATTGTTATCCGCT

In a second round of PCR, the amplified flanks were fused with the two halves of the hygromycin B resistance cassette with PCR using one primer from the flanking region and a second from the HYGR cassette. The products were then transformed into an appropriate background strain using the fungal transformation protocol as described in Section 2.12. Putative transformants were selected for their resistance to hygromycin B and DNA was extracted as described in Section 2.2 and mutants confirmed by Southern blot analysis.

Double deletion of *FAR1* and *FAR2* was also carried out. The Δ*far1* mutant strain was used as the recipient strain for targeted deletion of *FAR2*. Glufosinate (BASTA) was used as selectable marker. The BA half of BASTA resistance cassette was amplified using M13F and BA split primers while the AR half of BASTA resistance cassette was amplified using AR split and M13R primers. Putative transformants were selected for their resistance to BASTA and confirmed by Southern blot analysis.

3.2.2 Lipid staining

Lipid droplets in germinating conidia and appressoria were visualized by staining with BODIPY® (493/503) (Invitrogen). Conidia were harvested by from plate cultures with a glass rod in sterile distilled water, followed by centrifugation at 5 000 x *g* for 5 min, two washes and resuspended in distilled water. Conidia were then inoculated onto glass cover slips at a concentration of 2×10^5 spores/mL in a moist chamber at 24 °C and observed at intervals for appressorium formation and lipid mobilization, by mounting directly in fresh BODIPY® (493/503) solution for 15 min.

3.2.3 Construction of *FAR1:GFP:trpC* and *FAR2:GFP:trpC.*

The *MoFAR1:GFP* gene fusion construct was made by amplifying a 5.0 kb fragment of *MoFAR1* containing 1.4 kb of upstream promoter sequence using the primers listed in Table 3.2, generating *Spe*I and *Eco*RI sites at the end of the fragment. The fragment was then cloned into plasmid vector pGEM-T (Promega) to create pGEM-1. *GFP-trpC* was amplified using the two sets of primers listed in Table 3.2 and cloned into pGEM-T, to create pGEM-1G, which has *Eco*RI and *Xho*I restriction sites at the end of the GFP fragment. The *FAR1* fragment was cleaved from pGEM-1 by digesting with *Spe*I and *Eco*RI and cloned into pGEM-1G which was also digested with *Spe*I and *Eco*RI generating pGEM-A. pGEM-A was digested with *Spe*I and *Xho*I to release the *FAR1* and *GFP-trpC* fusion and cloned into pCB1532, which carries a selectable marker bestowing resistance to sulfonyl urea (Sweigard et al., 1997) to create *MoFAR1:GFP*.

Table 3.2 Primers used in this study to carry out GFP tagged *FAR1* and *FAR2*

Primer	Sequence 5'-3'
FarA.SpeI.F3	CGACTAGTTGGACTGATACTTGGCGTGG
Far A.EcoRI.R2	CGGAATTCAACAAGTGCAGAAAAGTCGATAT
GFP.TrpC.EcoRI.F1	CGGAATTCATGGTGAGCAAGGGCGAGG
TrpC.XhoI.R	ATCTCGAGGTGGAGATGTGGAGTGGGCGC
SUR.F	AACTGTTGGGAAGGGCGATCGGTGCGGGCCGTCGACGTGCCAACGCCA
SUR.R	GTCGACGTGAGAGCATGCA
ProFarB.F1	GATTATTGCACGGGAATTGCATGCTCTCACTACCTACCTACCTAATACTCC
FarB.R4	GGTGAACAGCTCCTCGCCCTTGCTCACCATAGACGATACAGCCACCTGC
GFP.F1	AATAACGCACAGCAGGTGGCTGTATCGTCTATGGTGAGCAAGGGCGAGG
TrpC.R1	TTCACACAGGAAACAGCTATGACCATGATTAGTGGAGATGTGGAGTGGG

The *MoFAR:GFP* gene fusion construct was made using recombination-mediated, PCR-directed plasmid construction *in vivo* in yeast (Oldenburg et al., 1997). In this technique, the pNEB-Nat-Yeast1284 cloning vector was used which contains the *URA3* gene, allowing uracil synthesis and therefore complementation of uracil (-) auxotrophy.

The sulfonylurea resistance gene, *FAR2* open reading frame including promoter, and *GFP-trpC* were amplified separately using primers listed in Table 3.2. SUR.F and SUR.R were used to amplify the sulfonylurea resistance gene, ProFarB.F1 and FarB.R4 were used to amplify the *FAR2* open reading frame including the promoter and GFP.F1 and TrpC.R1 were used to amplify the *GFP-trpC* fragment. 1284 pNEB-Nat-Yeast cloning vector was linearised using *Hin*dIII and *Sac*I and transformed into a yeast uracil auxotrophic *ura3* (-) strain. Primers used to amplify the PCR fragments were designed to incorporate overhangs corresponding to the adjacent PCR fragments or to the yeast plasmid. The linearized vector and PCR fragments (400 ng each) were combined together along with 32 µL of 1 M lithium acetate and 240 µL of 50% (w/v) PEG 4000 and incubated at 30 °C for 30 min before being heat shocked at 45 °C for 15 min. Homologous recombination results in assembly of the fragments in the correct orientation to generate the gene fusion construct. To screen for correct clones, yeast colonies were grown on selected MM plates. For large scale production of the plasmid, the plasmid was transformed into *E. coli* (Promega JM109 *end*A1, *rec*A1, *gyr*A96, *thi*, *hsd*R17 (rk–, mk+), *rel*A1, *sup*E44, Δ(*lac-pro*AB), [F´ *tra*D36, *pro*AB, *laq*IqZΔM15) since yeast plasmid isolation is inefficient and a large quantity of the plasmid DNA (4 µg) is required for fungal transformation.

3.2.4 Quantitative Real Time PCR (QPCR) analysis

M. oryzae wild type strain Guy11, the Δ*ku70* mutant (Kershaw and Talbot, 2009) and the Δ*far1*, Δ*far2* and Δ*far1*Δ*far2* mutants were grown in liquid CM for 48 h, followed by transfer to minimal medium supplemented with 50 mM of oleic acid or triolein for a further 24 h. Minimal medium consists of 10 g/L glucose, 6 g/L $NaNO_3$, 0.5 g/L KCl, 0.5 g/L $MgSO_4$, 1.5 g/L KH_2PO_4 (pH 6.5), 0.1% (v/v) trace elements, 0.01% thiamine

and 0.00025% biotin. The mycelium was harvested and RNA was extracted using LiCl extraction method as described in Section 2.16. The RNA was treated with DNAaseI (Invitrogen) according to the manufacturer's instructions and cDNA was synthesised using the AffinityScript cDNA master mix (Agilent Technologies). The DNAase treated RNA was incubated with oligonucleotide primers and AffinityScript RT/RNase Block enzyme in the provided buffer using the following reaction conditions; 25 °C for 5 min, 42 °C for 15 min and 95 °C for 5 min. The synthesised cDNA was diluted to 5 ng/µL before qPCR was performed using Brilliant SYBR green QPCR master mix according to the manufacturer's protocol. The Brilliant SYBR green QPCR master mix contains SureStart Taq DNA polymerase, which is a modified version of Taq2000 DNA polymerase with hot start capability, and SYBR® Green 1, a dye that binds non-specifically with double stranded DNA with fluorescence increasing 1 000 fold in the bound state compared to the unbound state and the optimised buffer for the PCR reaction. cDNA was mixed with SYBR Green Master Mix along with the upstream and downstream primers of the gene of interest listed in Table 3.3. Gene expression was routinely compared to that of the β-tubulin-encoding gene, *TUB2*, which is constantly expressed in all growth stages of *M. oryzae* as a normalisation control. The Δ*ku70* mutant, grown in oleic acid or triolein, was used as the calibrator control. The PCR was carried out in a Stratagene Mx3005P QPCR System using the following conditions; an initial denaturation step at 95 °C for 5 min, followed by 40 cycles of PCR cycling parameters, 95 °C for 30 sec, 60 °C for 1 min and 72 °C for 30 sec.

Table 3.3 Primers used for expression profiling using QPCR

Primer	Sequence 5'-3'
Fq.PEX6	AAATTCACACTCCACCCTTCA
Rq.PEX6	GGCACTCACACTGGGAATC
Fq.PTH	CGAGTACATCACAGCCGCT
Rq. PTH	CGATGTTGAAGTTGATGCTGT
Fq.MFP1	TGTCTATGAGGGAGCCGAG
Rq.MFP1	ACCCCCTCAGGAAGATGCT
Fq.ICL1	GTGTACCCCGAGCAAAAACT
Rq.ICL1	ACCCGTCACCATCTTCTGC
B-tub.F	CGCGGCCTCAAGATGTCGT
B-tub.R	GCCTCCTCCTCGTACTCCTCTTCC

3.3 Results

3.3.1 Identification of gene that codes for *FAR1* and *FAR2* in *M. oryzae*

Identification of the *FAR1* and *FAR2* genes was carried out using the BLAST programme provided by the Magnaporthe genome database (http://www.broadinstitute.org/). The amino acid sequences of *A. nidulans* FarA and FarB were used as query sequences. MGG_01836.6 (*FAR1*) and MGG_08199.6 (*FAR2*) were identified as having highest similarity to FarA and FarB, respectively. The predicted *MoFAR1* protein is 941 amino acids in length and shows 58% amino acid identity to FarA (Figure 3.1) while the predicted *MoFAR2* protein is 1009 amino acids and shows 42% identity to FarB (Figure 3.2). Both *MoFAR1* and *MoFAR2* proteins possess two domains; a fungal Zn_2-Cys_6 binuclear cluster domain (*FAR1*, amino acids 66-106; *FAR2*, amino acids 85-124) and a fungal transcription factor domain (*FAR1*, amino acids 265-509; *FAR2*, amino acids 320-594) (Figure 3.3). These domains have been shown to be highly conserved in filamentous euascomycetes (Hynes et al., 2006).

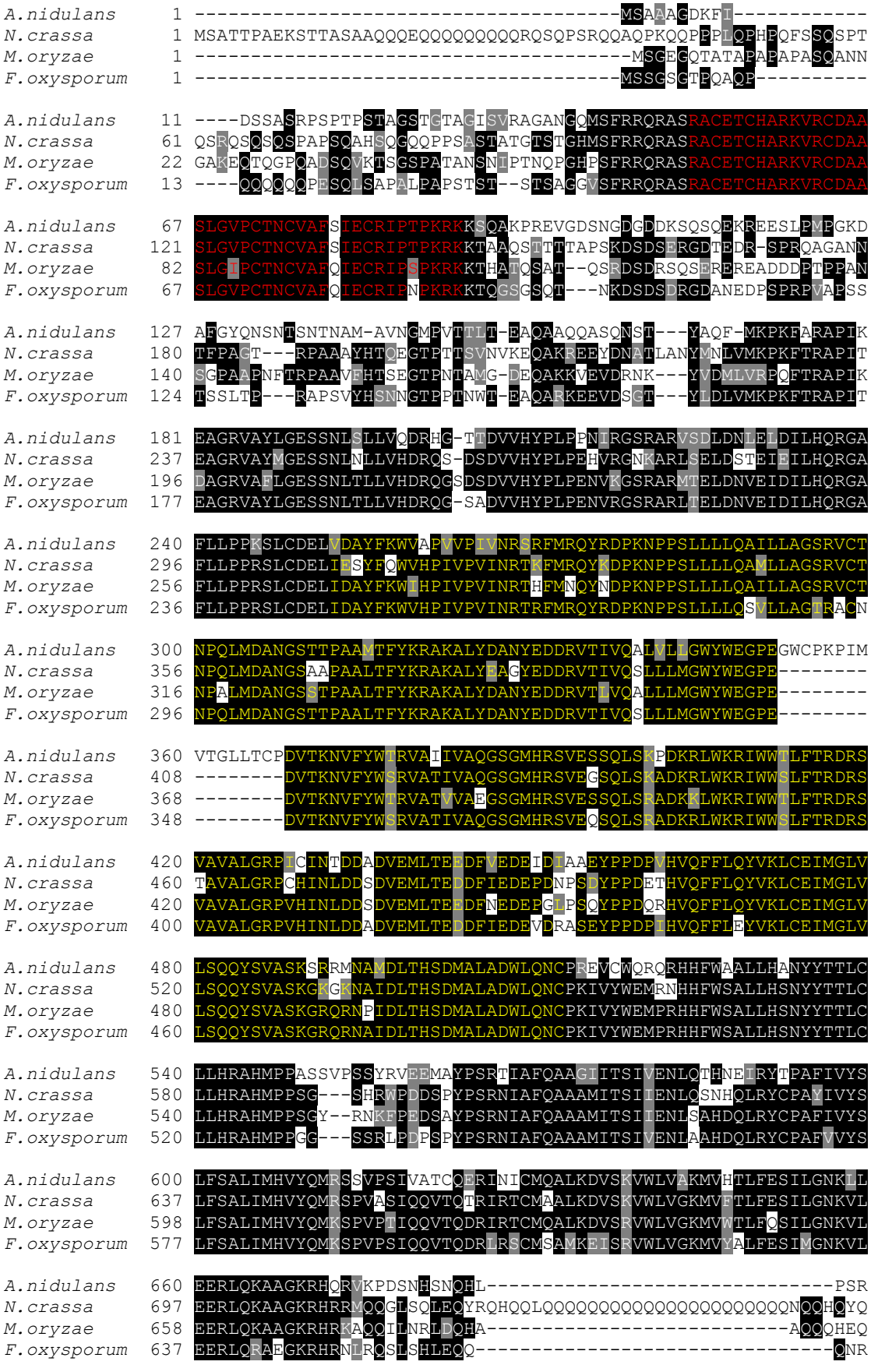
A.nidulans
N.crassa
M.oryzae
F.oxysporum

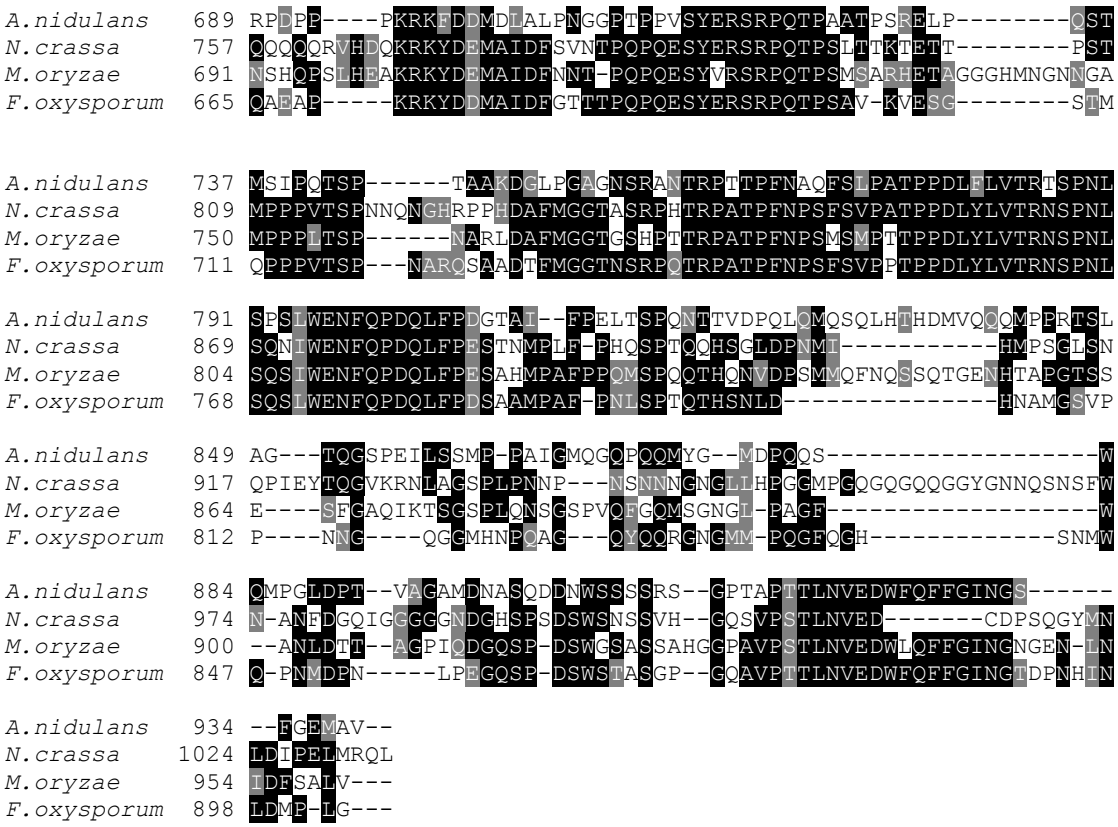

Figure 3.1 Predicted amino acid sequence of the *FAR1* gene product.

Sequences were aligned using the program CLUSTALW (Thompson et al., 1994). Identical amino acids are highlighted on a black background and similar amino acids on a light grey background. Gaps in the alignment are indicated by dashes. Sequences aligned were the predicted products of *FAR1* (MGG_01836.6), *A. nidulans* FarA (AN7050.2), *N. crassa* cutinase transcription factor alpha (NCU08000.5) and *F.oxysporum* Ctf1 (FOXG_04196.2). Sequences in red show the Zn_2-Cys_6 binuclear cluster domain while sequences in yellow show the fungal specific transcription factor domain.

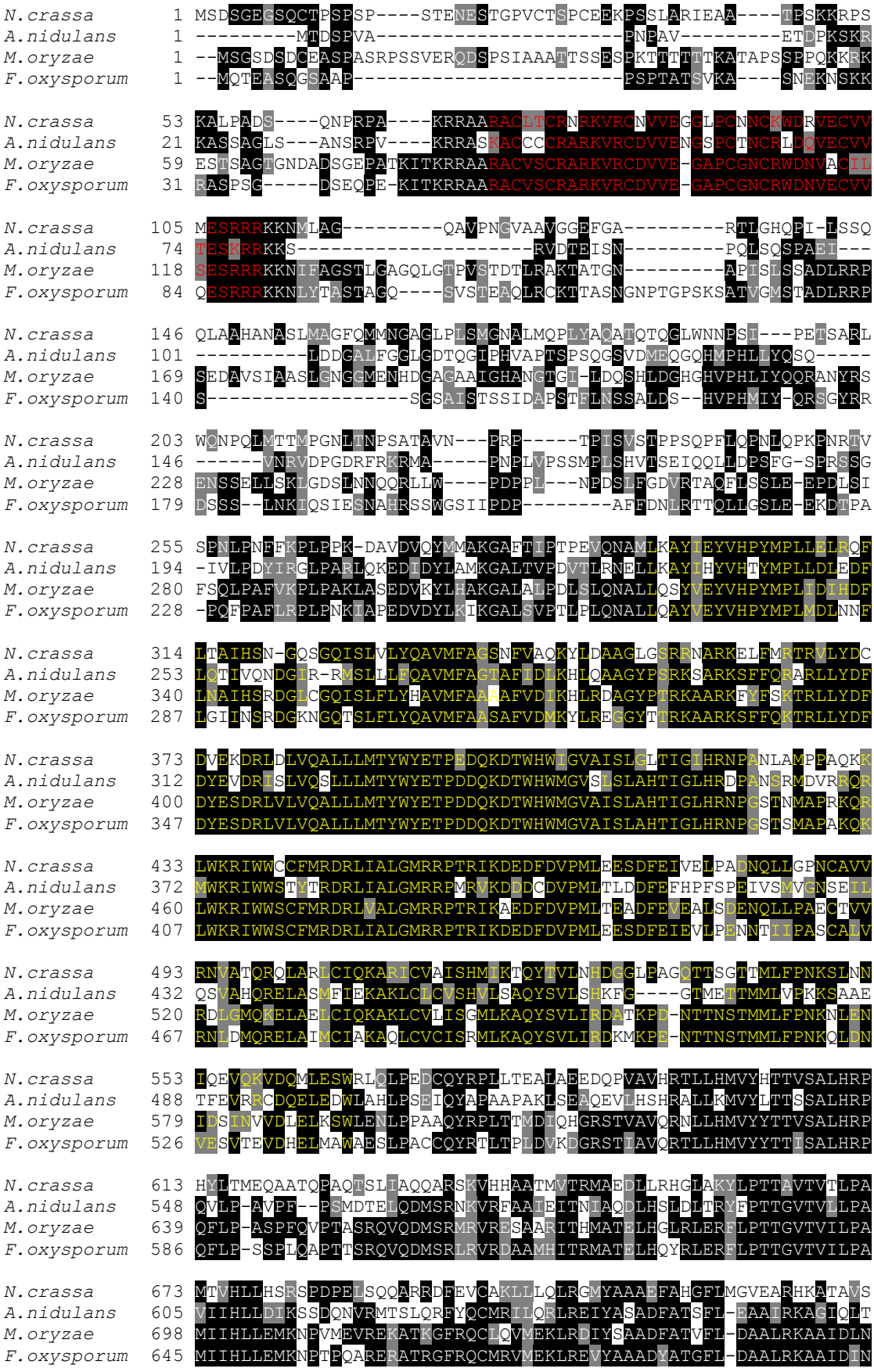
N.crassa
A.nidulans
M.oryzae
F.oxysporum

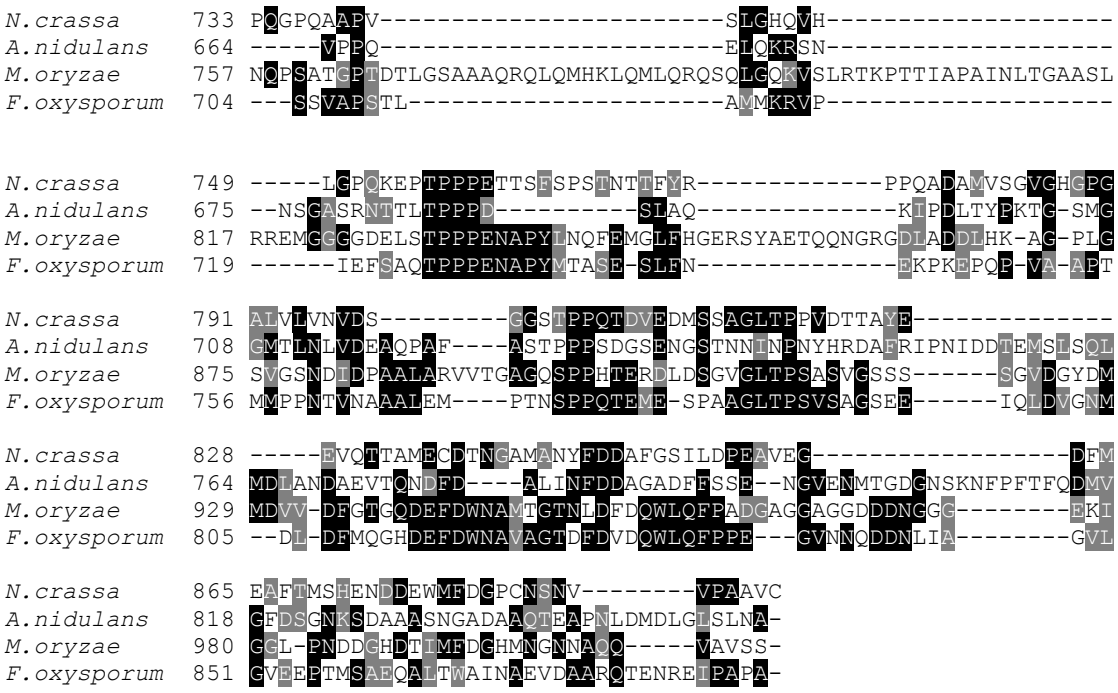

Figure 3.2 Predicted amino acid sequence of the *FAR2* gene product.

Sequences were aligned using the program CLUSTALW (Thompson et al., 1994). Identical amino acids are highlighted on a black background and similar amino acids on a light grey background. Gaps in the alignment are indicated by dashes. Sequences aligned were the predicted products of *FAR2* (MGG_08199.6), *A. nidulans* FarB (AN1425.2), *N. crassa* cutinase transcription factor beta (NCU03643.5) and *F.oxysporum* cutinase transcription factor 1 beta (FOXG_01610.2). Sequences in red show the Zn_2-Cys_6 binuclear cluster domain while sequences in yellow show the fungal specific transcription factor domain.

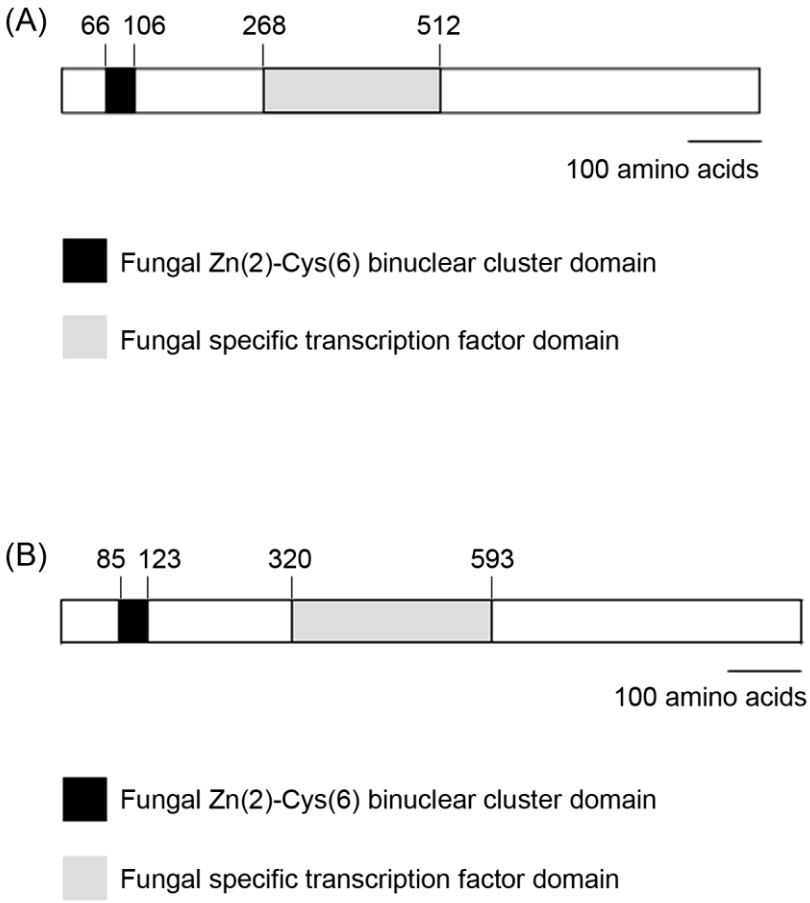

Figure 3.3 Schematic representations of functional domains in *FAR1* and *FAR2*.

(A) The putative *FAR1* gene product showing the positions of fungal Zn(2)-Cys(6) binuclear cluster domain (black box) and fungal-specific transcription factor domain (grey box). (B) The putative *FAR2* gene product showing the positions of fungal Zn(2)-Cys(6) binuclear cluster domain (black box) and fungal-specific transcription factor domain (grey box).

3.3.2 Targeted gene deletion of *FAR1* and *FAR2*

For further analysis of the function of *FAR1* and *FAR2* during plant infection development, targeted gene deletion of each locus was carried out (Catlett et al., 2003). These constructs were then transformed into the Δ*ku70* background (Kershaw and Talbot, 2009) and transformants selected based on resistance to hygromycin B. Genomic DNA of the putative transformants were extracted and digested with either *Mfe*I (*FAR1*) or *Bam*HI (*FAR2*) before being fractionated by gel electrophoresis. The fractionated DNA was then transferred to Hybond-N. In the case of *FAR1* transformants, DNA was probed with a 1.5 kb fragment upstream of the targeted gene locus, previously generated for the gene deletion construct. Following replacement of the native coding sequence with the hygromycin resistance gene cassette, a size difference in the locus was generated. Figure 3.4 shows the size of the hybridizing restriction fragment observed in the wild type, Δ*ku70* (3.5 kb) and in the putative *FAR1* mutants (5.1 kb). Multiple fragments were observed in lanes 2, 4 and 5 suggesting ectopic integration of the hygromycin resistance gene cassette in these transformants. The presence of the 5.1 kb fragments in lanes 1, 3, 6 and 7 confirmed the targeted deletion of *FAR1* and the positive Δ*far1* transformants were selected for further analysis.

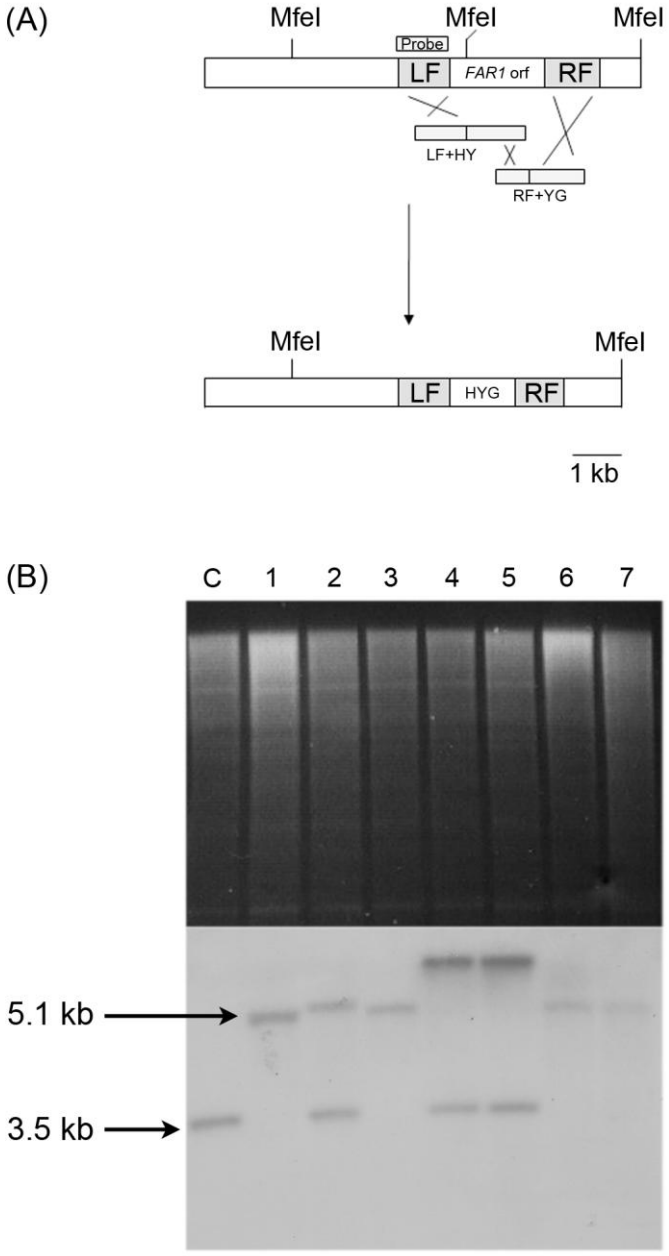

Figure 3.4 Targeted gene deletion of *FAR1* in *M. oryzae* Δ*ku70* background.

(A) Diagram describing the targeted locus of *FAR1*. (B) DNA was isolated and digested with *Mfe*I before being fractionated in 0.8% agarose gel. The gel was then processed by Southern analysis and probed with a 1.5 kb genomic fragment upstream of the *FAR1* coding region. The putative transformants in lanes 1, 3, 6 and 7 were confirmed as Δ*far1* mutants.

FAR2 putative transformants were probed with a 1 kb open reading frame fragment generated by PCR using primers pFarB.F1 and pFarB.R1. After digestion with *Bam*HI a 6.4 kb fragment was predicted to be present in the wild type and no hybridising fragment was expected to be present in the corresponding null mutant. The results for Southern blot analysis for *FAR2* (Figure 3.5) show that the 6.4 kb fragment was absent from all the putative transformants of *FAR2* and present only in the wild type Δ*ku70* strain. This confirmed the targeted deletion of *FAR2* and positive Δ*far2* transformants were selected for further analysis.

A double mutant of *FAR1* and *FAR2* was also generated to determine the phenotypic characteristics of a mutant strain lacking both putative regulatory genes. The gene deletion construct of *FAR2* was transformed into a Δ*far1* mutant background and transformants selected based on resistance to BASTA. Genomic DNA of the putative transformants was digested with *Bam*HI and probed with the same probe used for *FAR2* mutants screening. The results for Southern blot analysis for the double deletion (Figure 3.5) show that the 6.4 kb fragment was absent from samples in lanes 4, 5 and 7 and this confirmed the targeted deletion of *FAR2* in the Δ*far1* mutant background. The presence of restricted fragment in lane 6 suggested an ectopic integration of the BASTA resistance gene cassette in this transformant. Positive Δ*far1*Δ*far2* transformants were selected for further analysis.

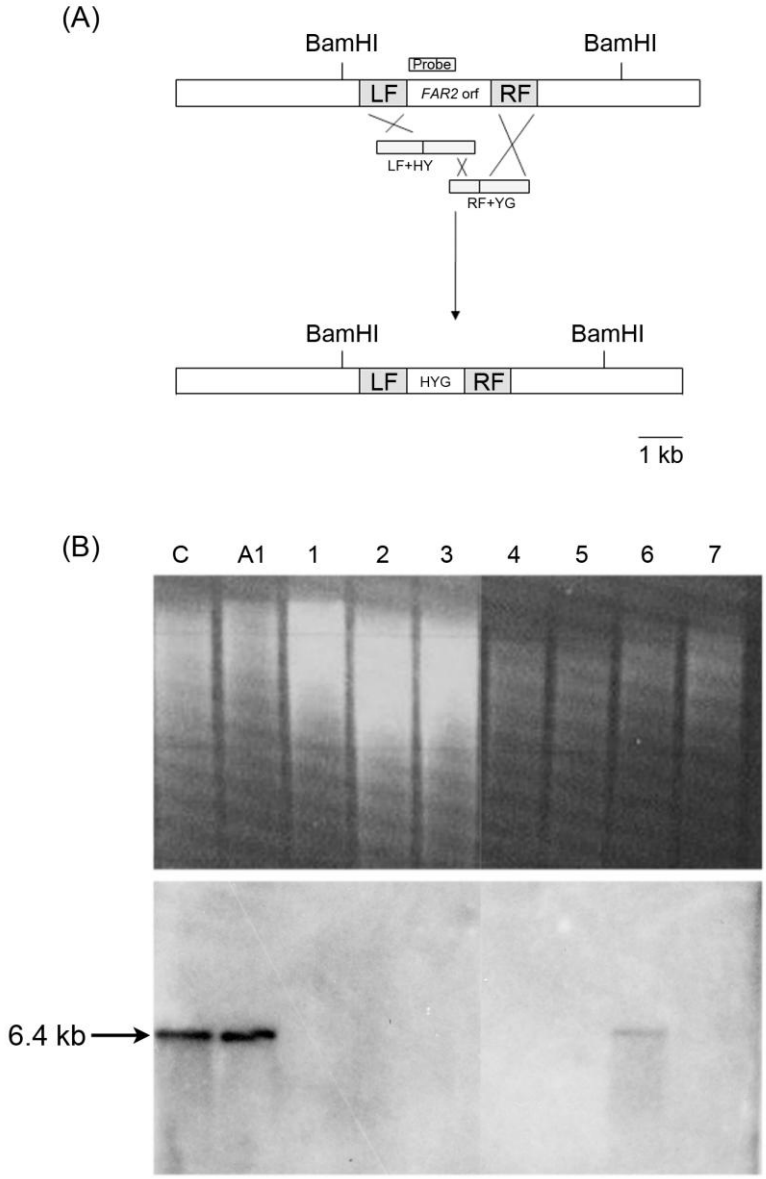

Figure 3.5 Targeted gene deletion of *FAR2* in *M. oryzae* Δ*ku70* and Δ*far1* mutant background.

(A) Diagram describing the targeted locus of *FAR2*. (B) DNA was isolated and digested with *Bam*HI before being fractionated in 0.8% agarose gel. The gel was then processed by Southern analysis and probed with a 1 kb genomic fragment from the *FAR2* locus. Lanes C and A1 are controls, Δ*ku70* and Δ*far1* mutant, respectively. The putative transformants in lanes 1, 2 and 3 are confirmed as Δ*far2* mutants. The putative transformants in lanes 4, 5 and 7 are confirmed as the Δ*far1*Δ*far2* mutants.

3.3.3 Expression profile of *FAR1* and *FAR2* and lipid utilisation of Δ*far1*, Δ*far2* and Δ*far1*Δ*far2* mutants

For further analysis, the expression profiles of *FAR1* and *FAR2* throughout appressorium development were obtained from the HT-superSAGE analysis (Soanes et al., 2012) (Figure 3.6). Both *FAR1* and *FAR2* genes were over expressed throughout appressorium development when compared to the Guy11 mycelium grown on CM. The results suggest a peak of expression between 4 to 6 h, corresponding to the appressorium development and maturation.

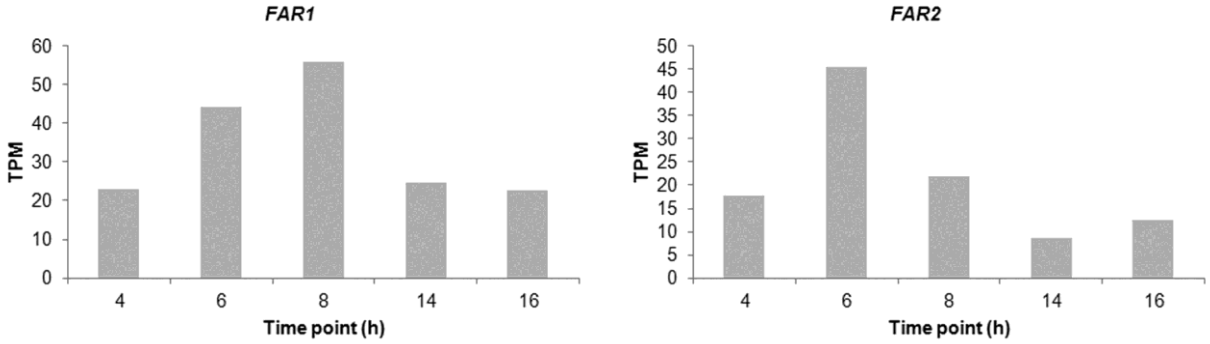

Figure 3.6 Expression profile produced from HT-SuperSAGE analysis of the wild type Guy11.

The graph describes the relative expression profile of *FAR1* and *FAR2* throughout appressorium development as compared to Guy11 mycelium grown in CM. The result is based on pooled data from two biological replicates.

The Δ*far1*, Δ*far2* and Δ*far1*Δ*far2* mutants were next grown on minimal medium supplemented with three different lipid sources (olive oil, oleic acid or triolein), as sole carbon source. Our results showed that the growth of both Δ*far1* and Δ*far2* mutants on olive oil, oleic acid or triolein were severely reduced, and the fungus grew very sparsely, compared to the isogenic wild type strain (Figure 3.7). The double mutant Δ*far1*Δ*far2* demonstrated growth defects similar to the single deletion mutants when grown on these different lipid sources. This suggests that, even though *FAR1* and *FAR2* have similar functions, they are both independently required for growth on lipids, and the double mutant is therefore indistinguishable from the single mutants when these lipids are the only carbon source. The inability of Δ*far2* to utilise olive oil, oleic acid and triolein is distinct from that observed with its *A. nidulans* homologue. The Δ*farB* mutant was capable of grow on long chain fatty acids including oleic acid whereas the Δ*farA* mutant was unable to grow (Hynes et al., 2006).

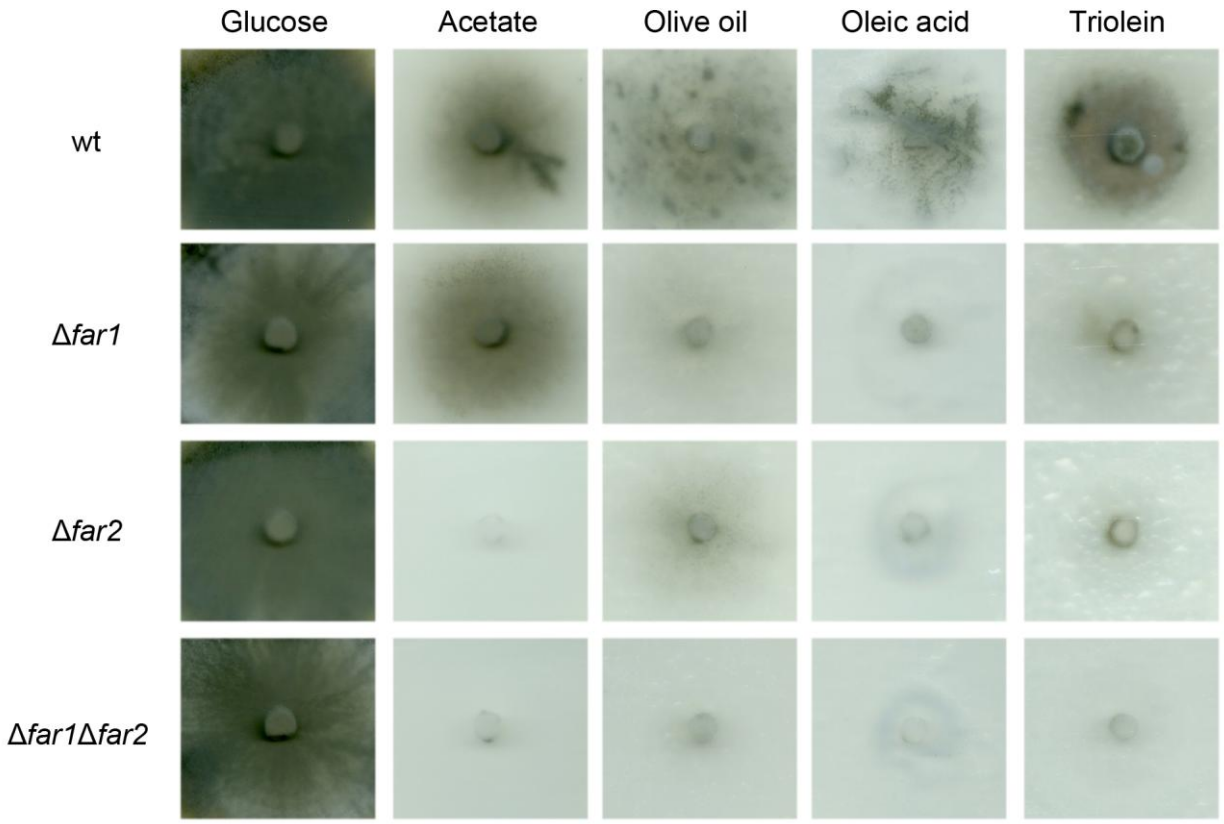

Figure 3.7 Vegetative growth of the wild type, Δ*ku70* and Δ*far1*, Δ*far2*, Δ*far1*Δ*far2* mutants on a range of different carbon sources.

The fungal strains were inoculated onto minimal medium supplemented with glucose, acetate, olive oil, oleic acid or triolein and incubated at 24 °C for 14 days. All the mutants showed reduced growth on minimal medium supplemented with lipid (olive oil, oleic acid and triolein). Only the Δ*far2* mutant and the double mutant showed reduced growth on minimal medium supplemented with acetate.

3.3.4 Expression profiling of genes involved in lipid metabolism in Δ*far1*, Δ*far2* and Δ*far1*Δ*far2* mutants

The Δ*far1*, Δ*far2* and Δ*far1*Δ*far2* mutants revealed severe growth defects on minimal medium supplemented with lipids. I therefore carried out expression profiling of genes involved in lipid metabolism in both wild type and mutant backgrounds in order to determine whether there was an obvious regulatory role for the *FAR1* and *FAR2* genes. Total RNA was extracted from Δ*far1*, Δ*far2*, Δ*far1*Δ*far2* mutants and the wild type, Δ*ku70,* grown for 24 h in oleic acid or triolein. Expression profiles of *MFP1, PEX6, PTH2* and *ICL1*, (see Section 3.1) were determined using QRT-PCR, as described in Section 3.2.4. The expression profiles are shown in Figure 3.8. Overall there was an observed reduction in the expression of each gene analysed in the Δ*far1*, Δ*far2* and Δ*far1*Δ*far2* mutant backgrounds compared to the wild type, when grown on either triolein or oleic acid. When grown on oleic acid a significant lowering in expression was observed for *PTH2* (70%) and *MFP1* (60-70%) in all mutant backgrounds. Expression of *ICL1* was also lowered on oleic acid but slight variations were recorded with a 70% reduction in the Δ*far1*Δ*far2* mutant and 60% and 45% reduction in for Δ*far1* and Δ*far2* mutants respectively. *PEX6* expression was lowered by about 60% in both in Δ*far2* and Δ*far1*Δ*far2* mutants, however there was only a 20% reduction in *PEX6* expression in the Δ*far1* mutant compared to that of the wild type, suggesting that *FAR2* may have a more significant role in regulating peroxisome function. However, the expression of levels of *PEX6* when grown on triolein does not fully support this. The reduction of expression *PEX6* was similar at about 40% for Δ*far1* and Δ*far2* and only slightly lower (50%) for the double mutant. Expression of *PTH2* was reduced in all backgrounds when grown on triolein with a 50% lowering in Δ*far2* and lower again in Δ*far1* and Δ*far1*Δ*far2* strain (70%). The expression levels of *MFP1* were reduced in

similarly Δ*far1* and Δ*far2* (70%) but a greater reduction in the Δ*far1*Δ*far2* was observed (90%). The same was also the case with *ICL1* with a notable reduction of expression in the Δ*far1*Δ*far2* mutant, compared to the Δ*far1* and Δ*far2* single mutants which were both reduced compared to the wild type although not to the same degree (45% and 65% respectively). Therefore with *MFP1* and *ICL1* which are involved in the generation of acetyl-CoA and its utilisation through the glyoxylate shunt into gluconeogenesis there was an indication of a cumulative effect on expression levels in Δ*far1*Δ*far2* on triolein and oleic acid although the difference was less apparent in the latter. Taken together, these results indicate a role for *FAR1* and *FAR2* in the regulation of genes associated with the breakdown and utilisation of lipid reserves.

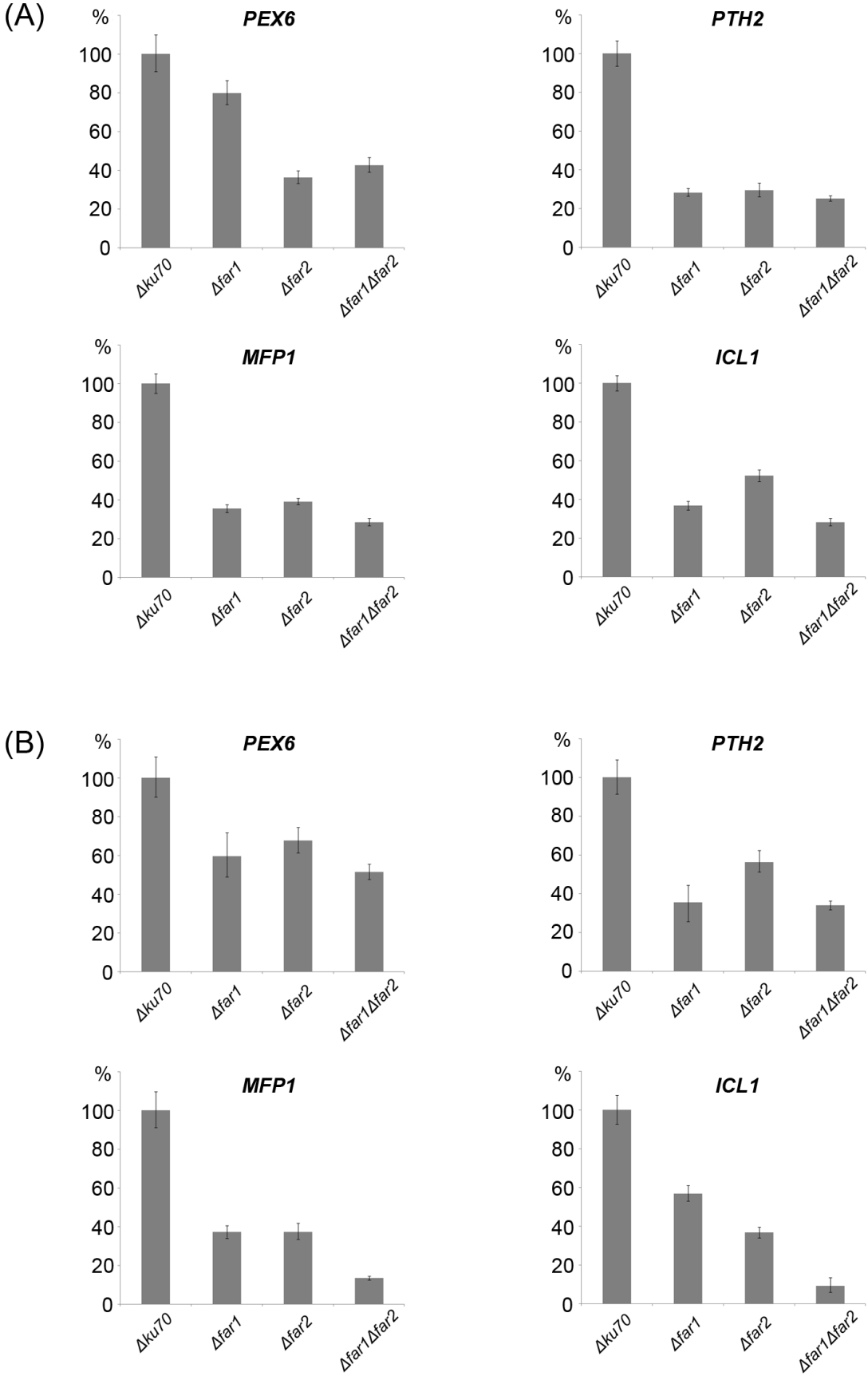
(A)
PEX6
PTH2
MFP1
ICL1
(B)
PEX6
PTH2
MFP1
ICL1
%
100
80
60
40
20
0
Δku70
Δfar1
Δfar2
Δfar1Δfar2

Figure 3.8 Expression profile of *PEX6*, *PTH2*, *MFP1* and *ICL1* in mutants grown in oleic acid (A) or triolein (B) as sole carbon source.

Total RNA was extracted from the *M. oryzae* grown on oleic acid or triolein for 24 h. Expression profiling of genes involved in lipid metabolism was compared using QRT-PCR; *PEX6* (peroxisomal biogenesis), *MFP1* (fatty acid β-oxidation), *PTH2* (acetyl-CoA translocation), *ICL1* (glyoxylate cycle) were investigated and a 20% to 80% reduction in gene expression was observed in the mutant strains compared to the isogenic wild type, Δ*ku70*. This shows that *FAR1* and *FAR2* are required for *PEX6*, *MFP1*, *PTH2* and *ICL1* expression in the presence of lipid source. Wild type (wt): Δ*ku70*.

3.3.5 Acetate utilisation in Δ*far1*, Δ*far2* and Δ*far1*Δ*far2* mutants

I also tested the ability of the Δ*far1*, Δ*far2* and Δ*far1*Δ*far2* mutants to utilise acetate as the sole carbon source. The results show that whilst the Δ*far1* mutant is capable of growth on acetate we showed that the Δ*far2* mutant and also the Δ*far1*Δ*far2* double mutant were unable to grow on minimal medium supplemented with acetate as sole carbon source (Figure 3.7). This suggests that *FAR2* also plays an important role in acetate utilisation, but once again distinguishes the *M. oryzae FAR2* from its *A. nidulans* homologue *farB,* which was able to grow on acetate (Hynes et al., 2006).

Acetate is converted into acetyl-CoA through a reaction catalyzed by the enzyme acetyl-CoA synthetase in a process which takes place in the cytoplasm. Under conditions where ethanol or acetate is the only available nutrients expression levels of these genes required for utilisation of should be upregulated (Sandeman and Hynes, 1989; Kratzer and Schüller, 1995). I therefore decided to determine whether the expression levels of genes encoding acetyl-CoA sythetases were affected in a Δ*far1* able to utilise acetate and Δ*far2* mutant which is unable to. The genes that encode this enzyme in *M. oryzae* were identified by homology to *A. nidulans facA.* The *ACS2* and *ACS3* genes, and their relative expression was determined by a comparative analysis using the wild type Δ*ku70*. Total RNA was extracted from Δ*far1* and Δ*far2* mutants and the wild type (Δ*ku70*) grown in minimal medium with acetate or glucose as sole carbon source for 24 h, and the expression profiles of *ACS2* and *ACS3* determined using QRT-PCR as described in Section 3.2.4. In the wild type strain both the *ACS2* and *ACS3* were highly upregulated on acetate. *ACS2* expression was completely repressed on glucose, and whilst some expression of *ACS3* was seen on glucose its expression was significantly higher on acetate. The results for the Δ*far1* mutant were similar to those seen in the wild type. However in the Δ*far2* mutant no significant induction of *ACS2*

was seen on acetate and the expression of *ACS3* on acetate was greatly reduced compared with the wild type (Figure 3.9). This is consistent with the finding that Δ*far2* mutant cannot utilise acetate and indicates that *FAR2* also plays a significant role in acetate utilisation.

3.3.6 Localisation of *FAR1* and *FAR2*

FAR1 and *FAR2* genes were expressed throughout appressorium development as compared to the wild type mycelium grown on CM, as shown in Figure 3.6. The results suggest a peak of expression between 4 to 6 h, corresponding to the appressorium development and maturation. To confirm the sub-cellular localisation of *FAR1* and *FAR2*, I constructed C-terminal GFP gene fusions of *FAR1* and *FAR2*, under the control of their native promoters. *FAR1:GFP* and *FAR2:GFP* expression was observed throughout germination and development of the appressorium. The signal was specific to one point in the each cell of the conidia and the appressorium corresponding with localisation observed with H1-RFP (Figure 3.10). The localisation of Far1-GFP and Far2-GFP are to the nucleus, is consistent with their proposed role as transcription factors.

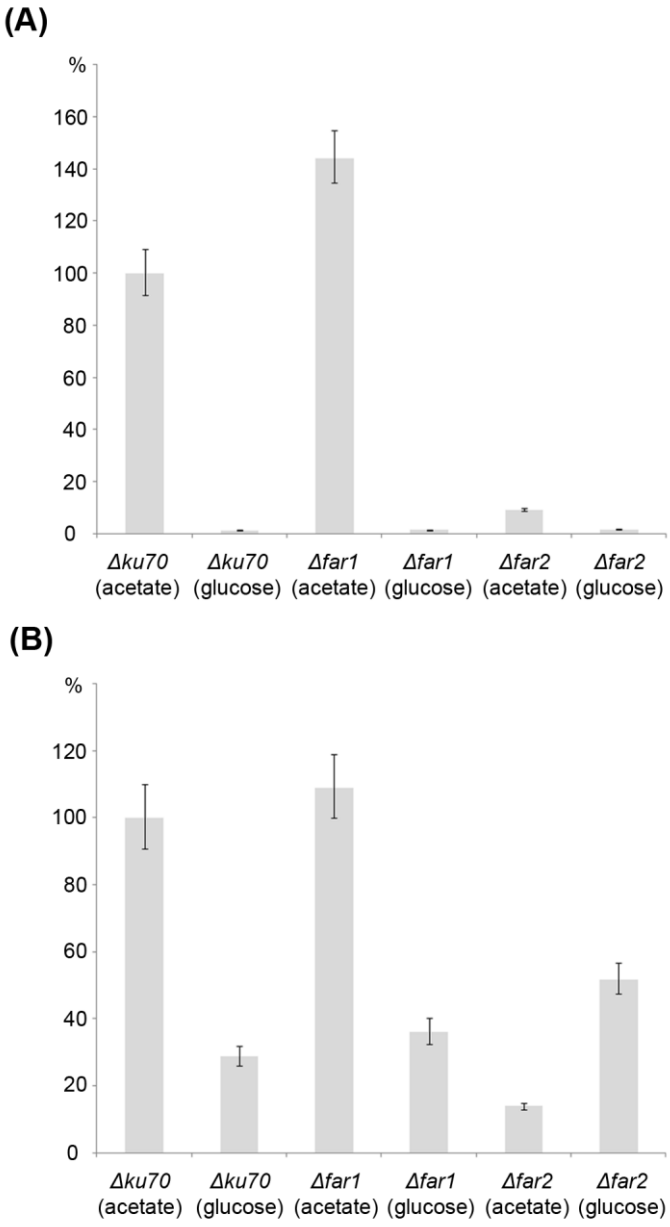

Figure 3.9 Bar charts to show expression profile of *ACS2* (A) and *ACS3* (B) in the wild type (Δ*ku70*), Δ*far1* and Δ*far2* mutants, as determined by QRT-PCR analysis.

Total RNA was extracted from *M. oryzae* mycelium grown on minimal medium containing acetate or glucose as sole carbon source for 24 h. Expression profiles for *ACS2* and *ACS3* were determined using QRT-PCR as described in section 3.2.4.

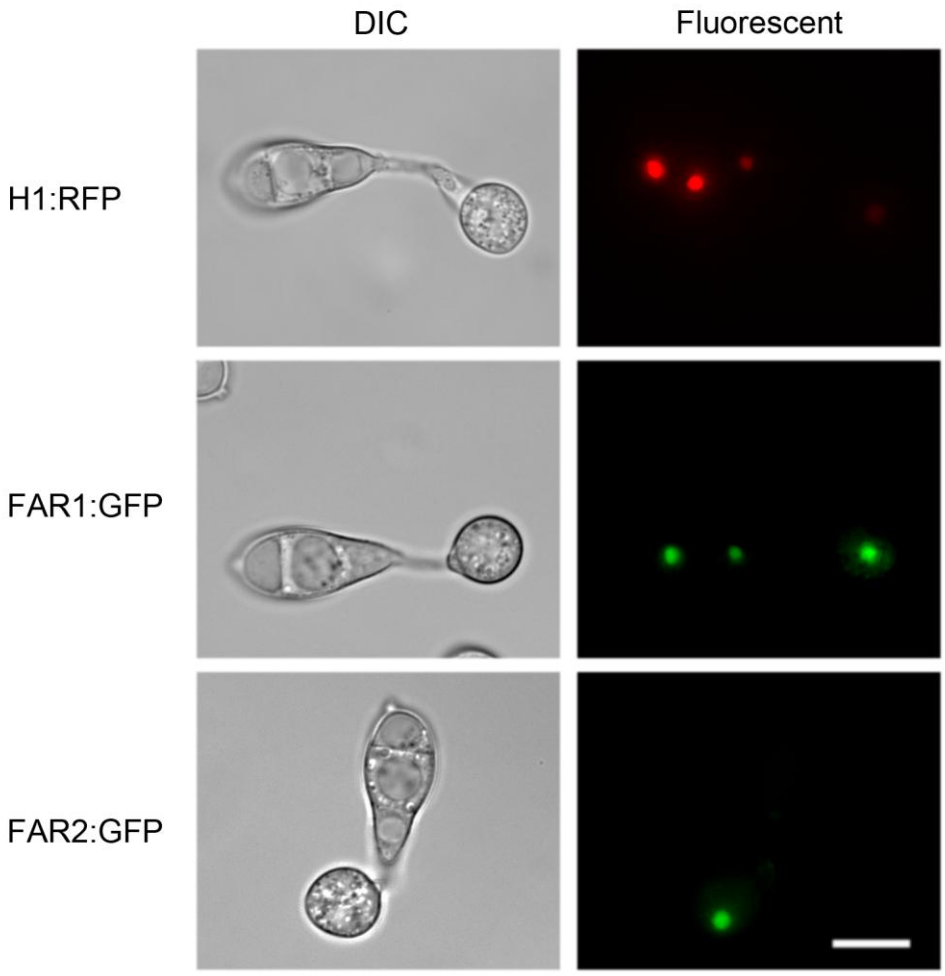

Figure 3.10 Localisation of *FAR1* and *FAR2* after 4 h of appressorium development.

The signal was specific to one point in each cell of the conidia and the appressorium corresponding with localisation observed with H1-RFP. The localisation of *FAR1* and *FAR2* are to the nucleus, is consistent with their proposed role as transcription factors. (Scale bar = 10 µm).

3.3.7 Appressorium development and lipid mobilisation in Δ*far1*, Δ*far2* and Δ*far1*Δ*far2* mutants

To determine the potential function of Far1 and Far2 in lipid droplet mobilisation during appressorium formation, live cell imaging was carried out by epifluorescence microscopy using BODIPY lipid staining (Figure 3.11, Figure 3.12, Figure 3.13). Typically in both wild type and Δ*far1*, Δ*far2* and Δ*far1*Δ*far2* mutants, germ tube emergence was observed soon after conidial germination and appressorium development was observed by 4 h and after 8 h appressoria were fully melanised. After 24 h conidia had already undergone cell collapse (Veneault-Fourrey et al., 2006). Lipid mobilisation is an essential process necessary to enable the fungus to develop functional appressoria and therefore cause plant infection (for review see (Wilson and Talbot, 2009). In Guy11, lipid mobilisation occurs as soon as conidia adhere to the surface of the rice leaf. As shown in Figure 3.11, lipid droplets start to accumulate at the apex of the germ tube as soon as it emerges. By 6 h, more lipid droplets are seen to accumulate in greater numbers in the appressorium as compared with the conidium. By 8 h, almost all lipid droplets have mobilised into the appressorium where lipid degradation occurs. In the Δ*far1* and Δ*far2* mutants, the temporal dynamics of lipid mobilisation are similar to the wild type (Figure 3.11). The proportion of lipid droplets observed in the conidium, germ tube and appressorium of the Δ*far1*, Δ*far2* and Δ*far1*Δ*far2* mutants corresponded to that observed in the wild type over the course of germination and appressorium development (Figure 3.12). These observations were confirmed by quantitative analysis based upon lipid body distribution during appressorium development (Figure 3.14).

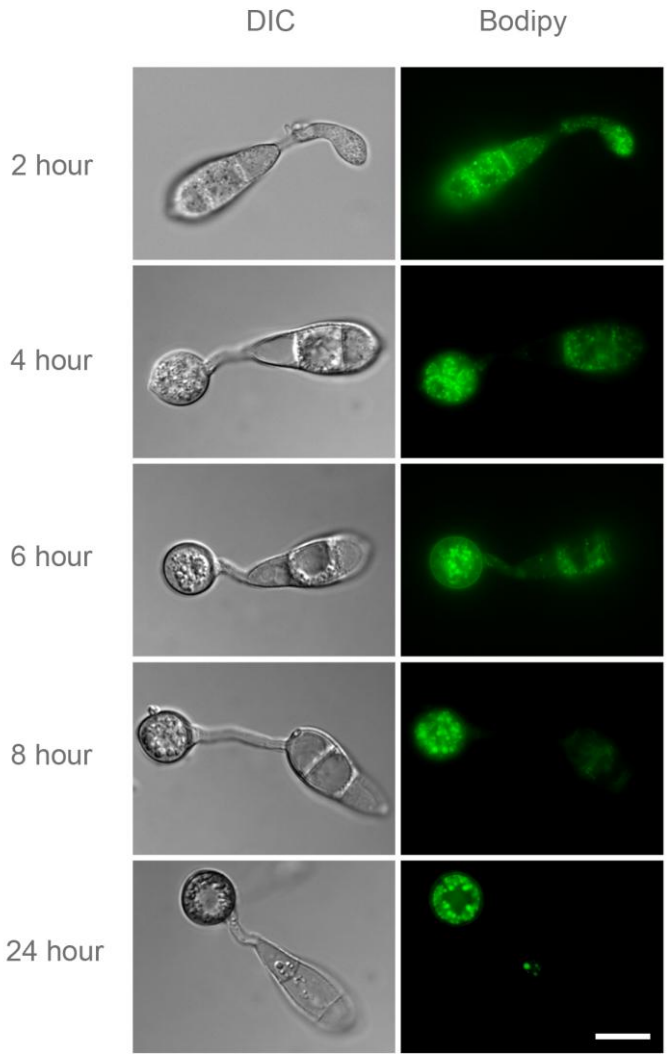

Figure 3.11 Cellular distribution of lipid droplets during appressoria morphogenesis by *M. oryzae*.

Conidial suspension was inoculated onto glass cover slips and incubated for 24 h. Samples were taken at various time points and stained with BODIPY® (493/503) to observe lipid droplets. Lipid droplets start to accumulate at the apex of the germ tube as soon as it emerges. By 6 h, more lipid droplets are seen to accumulate in greater numbers in the appressorium as compared with the conidium. By 8 h, almost all lipid droplets have mobilised into the appressorium where lipid degradation occurs. (Scale bar = 10 µm).

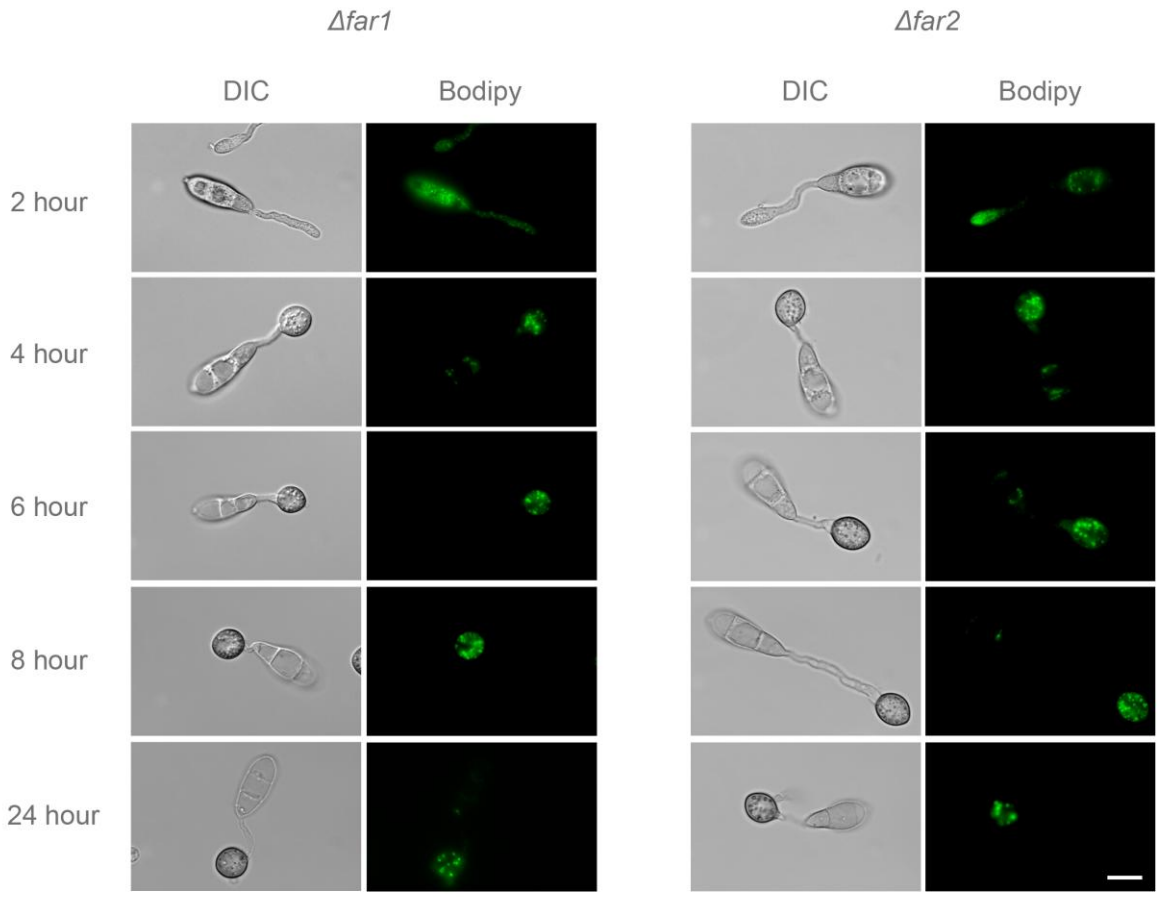

Figure 3.12 Cellular distribution of lipid droplets during appressoria morphogenesis in Δ*far1* and Δ*far2* mutants.

Conidial suspension was inoculated onto glass cover slips and incubated for 24 h. Samples were taken at various time points and stained with BODIPY® (493/503) to observe lipid droplets. There were no differences revealed by the mutants compared to the wild type (Figure 3.11). (Scale bar = 10 µm).

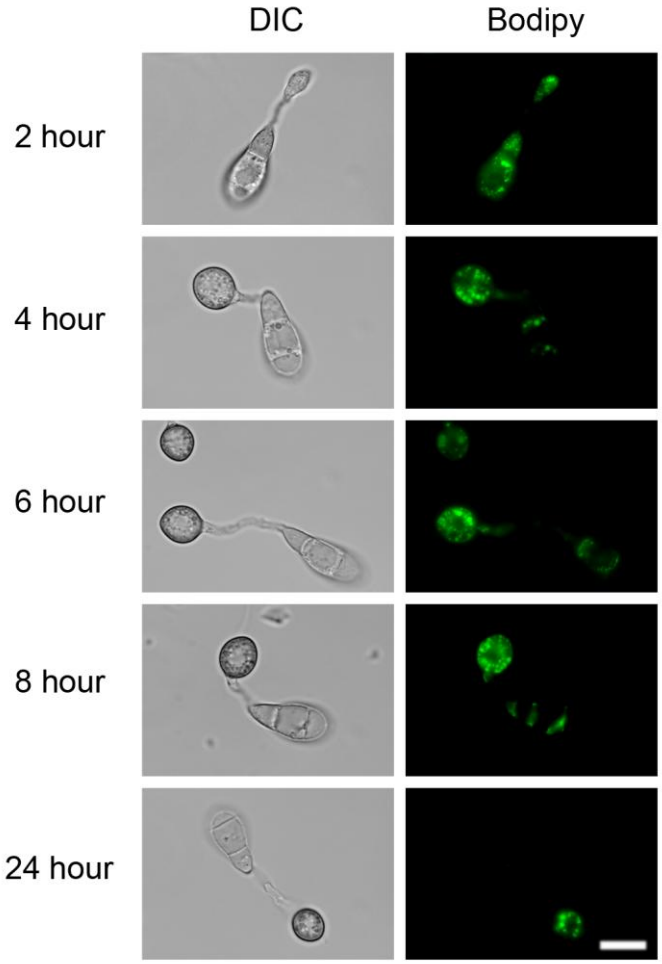

Figure 3.13 Cellular distribution of lipid droplets during appressoria morphogenesis in a Δ*far1*Δ*far2* mutant.

Conidial suspension was inoculated onto glass cover slips and incubated for 24 h. Samples were taken at various time points and stained with BODIPY® (493/503) to observe lipid droplets. There were no differences revealed by the mutants compared to the wild type (Figure 3.11). (Scale bar = 10 µm).

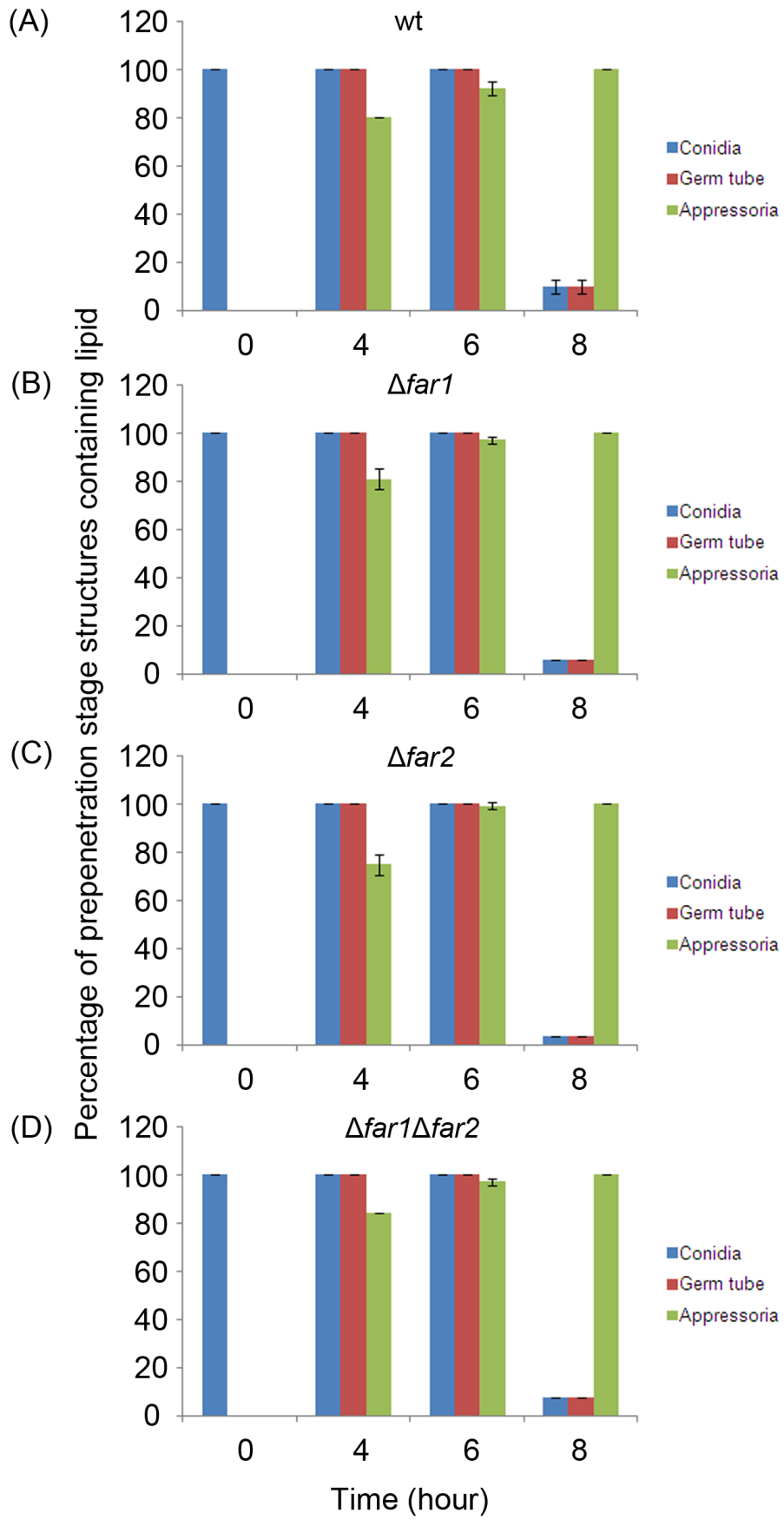
(A)
wt
(B)
Δfar1
(C)
Δfar2
(D)
Δfar1Δfar2
120
100
80
60
40
20
0
0
4
6
8
Conidia
Germ tube
Appressoria
Percentage of prepenetration stage structures containing lipid
Time (hour)

Figure 3.14 Quantitative analysis of lipid distribution during infection related development by *M. oryzae*.

Conidia were allowed to germinate in water drops on the surface of cover slips and to undergo infection related development. Samples were removed at intervals over an 8 h period and stained for the presence of triacylglycerol by using Bodipy stain. The percentage of fungal structures that contained lipid bodies at a given time was recorded from a sample of 100 germinated conidia. The bar charts show the mean and standard deviation from 2 independent replications of the experiment. (A) Wild type strain, Δ*ku70*; (B) Δ*far1* mutant; (C) Δ*far2* mutant; (D) Δ*far1*Δ*far2* mutant.

3.3.8 Plant infection analysis of Δ*far1*, Δ*far2* and Δ*far1*Δ*far2* mutants

Targeted deletion of *FAR1* and *FAR2* did not cause any significant observable effects on mycelial growth or appressorium development. However, there was a significant reduction in conidiogenesis in Δ*far1*, Δ*far2* mutants ($P < 0.01$) and the double mutant when compared to the wild type (Figure 3.15). In Δ*far1* mutants, a 40% reduction in conidiation was observed while in Δ*far2* mutants and Δ*far1*Δ*far2* mutant, a 60% reduction was seen when compared to the wild type.

To assess the ability of Δ*far1*, Δ*far2* mutants and the Δ*far1*Δ*far2* mutant to cause rice blast disease, conidial suspensions of uniform concentration were sprayed onto seedlings of a susceptible rice cultivar, CO-39, and the seedlings allowed to develop blast symptoms for 5 to 7 days. All the mutant strains were still able to infect plants and produced disease lesions on the leaf surface after 96-144 hours (Figure 3.15). There was no delay in infection and no significant observable effects could be seen on lesion number. I conclude that *FAR1* and *FAR2* are not required for the ability of *M. oryzae* to cause rice blast disease.

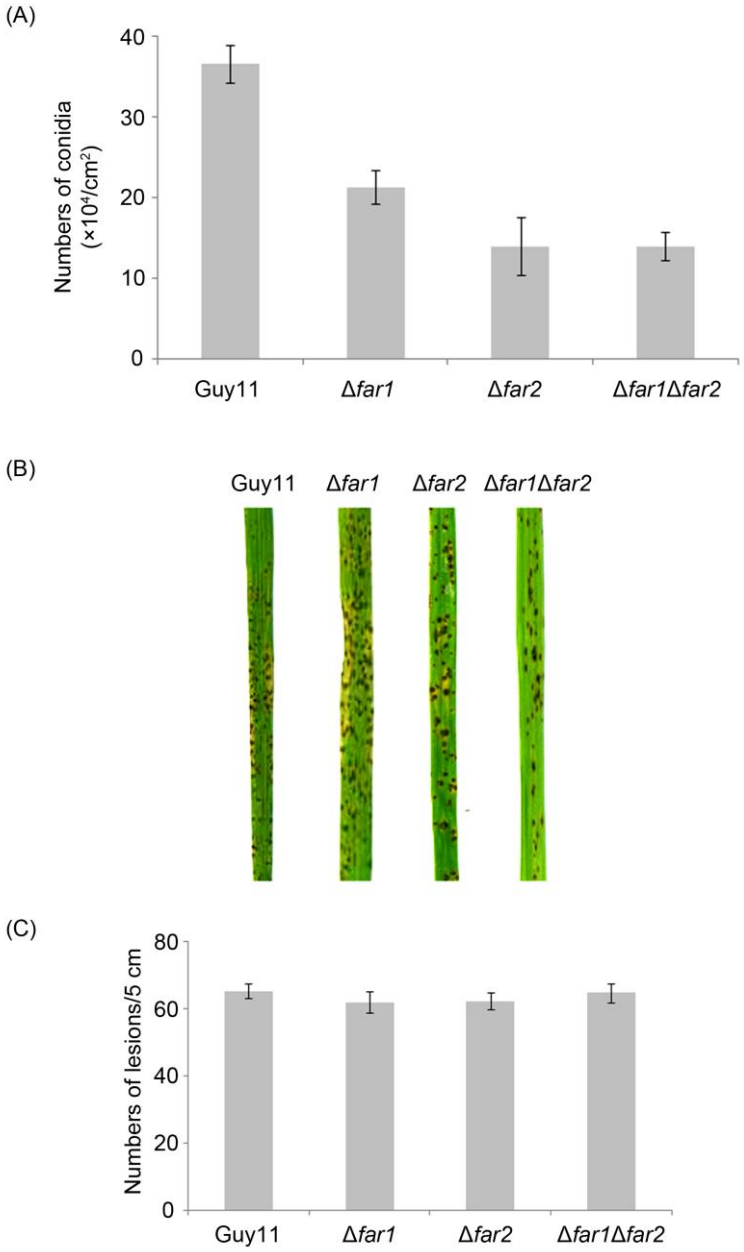

Figure 3.15 Comparison of conidiation between Δ*ku70* and Δ*far1*, Δ*far2*, Δ*far1*Δ*far2* mutants and plant pathogenicity assay on rice cultivar CO-39.

(A) Numbers of condia are reduced in Δ*far1*, Δ*far2* and Δ*far1*Δ*far2* mutants by 40% to 50% compared to the wild type (Δ*ku70*). (B) Rice blast symptoms produced by Δ*far1*, Δ*far2* and Δ*far1*Δ*far2* mutants after 5 days of inoculation are similar to the wild type. (C) Statistical analysis showed no significant difference between the disease symptoms of each mutant strain and the Δ*ku70* isolate (P >0.01).

3.4 Discussion

Previous work in *M. oryzae* established that lipid mobilisation is important for the ability of the fungus to cause rice blast disease. Degradation of lipids occurs rapidly following conidial germination and has the capacity to produce glycerol directly which has been shown to be the major compatible solute accumulating in an appressorium (de Jong et al., 1997; Thines et al., 2000). Mobilization of lipid bodies during spore germination has been shown to be regulated by the *PMK1* MAP kinase (Thines et al., 2000) and lipid droplets are, for instance, unable to move in a Δ*pmk1* mutant during appressorial development. By the time the appressorium is fully developed, lipid droplets accumulate inside the appressorium, coalesce with the vacuole, and undergo lipolysis during the onset of turgor generation (Weber et al., 2001).

Triacylglycerol lipase is the major enzyme involved in breakdown of triglycerides within cells. Previous work has established that *M. oryzae* possesses multiple copies of genes encoding triacylglycerol lipases and significant enzyme activity is present in appressoria (Thines et al., 2000). Triacylglycerol lipase activity is cAMP regulated and in Δ*cpkA* mutants, which lack the catalytic subunit of PKA, appressorium development and lipid mobilization are delayed with lipid droplets in the mutant being unable to coalesce, which leads to failure of lipid degradation (Thines et al., 2000).

In this study, I set out to explore how lipid body mobilisation, intracellular lipolysis and fatty acid β-oxidation might be regulated. In this way, I reasoned that it would be possible to overcome the inherent redundancy in lipid metabolic genes that preclude the generation of clear mutant phenotypes. In previous studies it has become obvious that many lipase-encoding genes probably contribute to appressorium turgor generation (Wang et al., 2007). Moreover, fatty acid β-oxidation and glyoxylate function also appear to contribute to virulence of *M. oryzae*, but no single gene involved in either of

these processes is absolutely indispensable for fungal pathogenicity. The purpose of this study was to define potential wide domain regulators of lipid metabolism and then see if they were necessary for rice blast disease to progress. In this way, I reasoned that it would be possible to evaluate the overall contribution of lipid metabolic processes to appressorium function in *M. oryzae.* The first clues to potential regulators of lipid metabolism came from a report in the model ascomycete fungus *A. nidulans,* where it has been reported that two genes, *farA* and *farB,* encode putative transcriptional regulators that control genes associated with fatty acid metabolism and peroxisomal function (Hynes et al., 2006). I therefore identified *FAR1* and *FAR2* in *M. oryzae,* which are these nearest equivalents of these *A. nidulans* genes.

Interestingly, both Δ*far1* and Δ*far2* mutants of *M. oryzae* were impaired in growth on a variety of lipids (Figure 3.7). This is consistent with their role as regulators of lipid metabolism and also confirmed that both putative transcription factors independently fulfil such a role. There were, for instance, no additive phenotypes associated with deletion of both *FAR1* and *FAR2* genes (Figure 3.7). I also showed that expression of genes involved in fatty acid β-oxidation (*MFP1*), acetyl-CoA translocation (*PTH2*), peroxisomal biogenesis (*PEX6*) and the glyoxylate cycle (*ICL1*) were all affected by loss of both *FAR1* and *FAR2* (Figure 3.8). Interestingly, I did demonstrate an additional new function for *M. oryzae FAR2* because the gene is required for growth on acetate in the rice blast fungus (Figure 3.7). Consistent with this, the two acetyl-CoA synthetase-encoding genes *ACS2* and *ACS3,* appear to be regulated in response to the presence of Far2. Acetate, which is present in the fungal cytoplasm, is a notable source for acetyl-CoA production which plays a pivotal role in plant infection by *M. oryzae*. Acetyl-CoA translocation, catalysed by the *PTH2* encoded carnitine acetyl transferase is necessary for pathogenicity (Bhambra et al., 2006).

When considered together, the results reported in this chapter suggest that *M. oryzae* possesses two wide domain regulators, Far1 and Far2, that are important in regulation of genes associated with lipid utilization and metabolism. They appear similar in function to the previously reported FarA and FarB regulators in *A. nidulans*, but in addition, Far2, likely regulates additional genes associated with acetate utilization. Strikingly, although both regulators are essential for utilization of exogenous lipids, being necessary to support fungal growth on these diverse substrates, they do not appear to regulate the mobilisation of intracellular stores of lipids. Lipid body distribution was not, for example, affected at all by the absence of either Far1 or Far2. Furthermore, the temporal dynamics of lipid body mobilisation during conidial germination and appressorium development does not appear to be regulated by Far1 or Far2. Consistent with this, neither regulator is essential for pathogenicity of *M. oryzae*, whereas impairment of lipid body mobilization to the appressorium, which occurs in Δ*cpkA* mutants (Thines et al., 2000) and strains of the fungus that are unable to undergo macroautophagy (Kershaw and Talbot, 2009) renders the fungus unable to infect plants. Based on the results reported here, I therefore propose that *M. oryzae* has an independent mechanism for regulating intracellular lipid body movement and subsequent lipolysis which operates separately from the regulation of lipid utilization by Far1 and Far2. The best evidence to date is that such a mechanism probably requires the cAMP-dependent protein kinase A signalling pathway and associated downstream transcription factors.

4.0 *Magnaporthe oryzae* perilipin homologue *CAP20* and its role in appressorial development and plant virulence

4.1 Introduction

In organisms as diverse as fungi, plants, insects, and mammals, lipid droplets were stored inside cells for later use as metabolic fuel, membrane components, post-translational protein modifications, and as signaling molecules (Murphy, 2001). Consistent with lipid droplets being metabolically active, the membranes encasing them contain proteins with wide-ranging biochemical activities including perilipin, adipophilin, TIP47, S3-12 and OXPAT (oxidative tissue-enriched PAT protein). These proteins are collectively referred to as the PAT family proteins, named after perilipin, adipophilin and TIP47 (Brasaemle, 2007).

Perilipin has been studied extensively in mammals (Martinez-Botas *et al.*, 2000; Tansey *et al.*, 2001; Tansey *et al.*, 2004; Brasaemle, 2007). In humans and mice, a single perilipin gene gives rise to at least 3 protein isoforms (perilipin A, B and C) that have a common N-terminal region, but differ in their C-terminal domains (Lu et al., 2001). Perilipin A is found in both adipocytes and steroidogenic cells. Perilipin B is primarily found in adipocytes, while perilipin C is unique to steroidogenic cells (Brasaemle et al., 2000). Perilipin A is the longest isoform with a unique C-terminal sequence of 112 amino acids and is the most abundant lipid droplet-associated protein in adipocytes (Brasaemle et al., 2009). All 3 perilipin isoforms have 3 of the 6 recognized protein kinase A (PKA) phosphorylation sites, a stretch of 16 aspartate and glutamate residues (the acidic loop region) and 2 of the 3 hydrophobic regions (H1, H2 and H3) that target the proteins to lipid droplets (Subramanian et al., 2004). These regions have been hypothesised to act as hydrophobic fingers that dip into the non-polar core of the lipid droplet (Garcia et al., 2003).

Perilipin forms a barrier surrounding lipid droplets, protecting them from cytosolic lipases. During starvation, perilipin is phosphorylated by protein kinase A, impairing the barrier function of perilipin allowing lipid degradation (Marcinkiewicz et al., 2006). In comparison with normal mice, perilipin-deficient mice have less fat, more muscle, a higher metabolic rate and are resistant to diet-induced and genetic obesity (Martinez-Botas *et al.*, 2000; Tansey *et al.*, 2001; Tansey *et al.*, 2004). This is consistent with evidence from studies conducted in the fruit fly *Drosophila melanogaster*, where mutants which lack perilipin have less fat compared to the wild type (Teixeira et al., 2003). Human perilipin variants have also been shown to associate with either obesity or leanness (Qi et al., 2004).

Recently, a gene called *MPL1*, which has structural similarity to the mammalian perilipins, has been described in the entomopathogenic fungus *Metarhizium anisopliae* (Wang and St. Leger, 2007). Even though *MPL1* is only 35% of the size of mouse perilipin, it contains several conserved regions such as the N-terminal β-strands, 3 hydrophobic regions (H1, H2 and H3), the acidic loop region and multiple phosphorylation sites, including a consensus cAMP-dependent protein kinase phosphorylation site (Wang and St. Leger, 2007). In *M. anisopliae*, *MPL1* has been shown to encode a protein involved in lipid metabolism. Expression of *MPL1* is induced when cells accumulate lipid droplets and a *MPL1-GFP* fusion protein co-localised with lipid droplets. *MPL1* promotes lipid storage, by protecting the lipid from instantly being degraded by lipases. This was shown by ectopically-expressing *MPL1-GFP* in *S. cerevisiae*. The *MPL1-GFP* fusion protein was shown to localise at lipid droplets and may interfere with the lipid breakdown under starvation conditions in *S. cerevisiae* (Wang and St. Leger, 2007). *MPL1* also acts as a virulence factor by playing an important role in appressorium turgor generation and host penetration in the insect

pathogenic fungus. *MPL1* mutants have been shown to have fewer lipid droplets and their ability to infect the insect host was impaired (Wang and St. Leger, 2007). However, upon direct injection of spores into the insect haemolymph, the ability of the fungus to infect insects was restored and the speed of kill was similar for both wild type and mutant (Wang and St. Leger, 2007). This suggests that the *MPL1* mutant was unable to generate sufficient turgor pressure to infect insects since the amount of lipid stored in the mutant was reduced compared to the wild type (Wang and St. Leger, 2007).

Perilipin homologues are found only in pezizomycotinal filamentous ascomycetes and occur as a single copy gene and many of these fungi are economically and medically important fungi (Wang and St. Leger, 2007). In *M. oryzae*, lipid is one of the prominent nutrient sources present in conidia. Degradation of lipid is important because it can produce glycerol which is responsible for generating high turgor pressure, thus enabling the fungus to penetrate the plant cuticle (de Jong et al., 1997), as well as fuelling other metabolic pathways.

In this chapter, I aimed to identify and characterise a gene that encodes a perilipin in *Magnaporthe oryzae*. Targeted gene deletion was carried out in order to investigate the importance of perilipin in relation to carbon utilisation, appressorium differentiation, lipid mobilisation, appressorium maturation and plant pathogenicity.

4.2 Materials and methods

4.2.1 Targeted deletion of gene that encodes perilipin (*CAP20*) in *M. oryzae*

To investigate the function of perilipin in appressorium function of *M. oryzae*, a Δ*cap20* mutant was generated using the split marker strategy, described in Section 2.11 (Catlett et al., 2003). Hygromycin B was used as a selectable marker and the primers used are listed in Table 4.1. The left flank of *CAP20* was amplified using CAP20.F1 and CAP20.R1 primers while the primers used to amplify the right flank were CAP20.F2 and CAP20.R2. The HY half of the hygromycin resistance cassette was amplified using M13F and HY split primers while the YG half was amplified using YG split and M13R primers.

Table 4.1 Primers used in this study to carry out targeted gene deletion of *CAP20* in Guy11

Primer	Sequence 5'-3'
CAP20.F1	CTGACCCCGTAGGAGTTTG
CAP20.R1	GTCGTGACTGGGAAAACCCTGGCGATGTGCTTTGCCTCGCTGG
CAP20.F2	TCCTGTGTGAAATTGTTATCCGCTAGTTAGCCGTCAAGCCGCA
CAP20.R2	TTGAGGTGGGTTGGCAGGT
pCAP20.F1	GGCACAATGGCTTCACCT C
pCAP20 R1	GGACCGCCAGCAGTTTGAA
M13F	GTCGTGACTGGGAAAACCCTGGCG
HY split	GGATGCCTCCGCTCGAAGTA
YG split	CGTTGCAAGACCTGCCTGAA
M13R	TCCTGTGTGAAATTGTTATCCGCT

The amplified flanks were fused with the overlapping fragments of the hygromycin B resistance cassette in a second round of PCR by using one primer from the flanking region and a second from HYGR cassette. The PCR products were transformed into the wild type, Guy11 strain (Leung et al., 1988). Putative transformants were selected for

resistance to hygromycin B before the DNA was extracted, followed by confirmation of mutants by Southern blot analysis.

4.2.2 Lipid staining

Lipid droplets in germinating conidia and appressoria were visualized by staining with BODIPY® (493/503) (Invitrogen). Conidia were harvested by scraping sporulating plate cultures of *M. oryzae* with a glass rod in sterile distilled water, followed by centrifugation at 5 000 × *g* for 5 min, two washes and resuspension in distilled water to a concentration of 2×10^5 spores/mL. Conidia were inoculated onto plastic cover slips in a moist chamber at 24 °C and observed for appressorium formation and lipid mobilization at intervals by mounting directly in fresh BODIPY® (493/503) solution for 15 min.

4.2.3 Construction of RFP-tagged *CAP20* for localisation analysis

The plasmid *CAP20:mRFP:trpC* was made using recombination-mediated PCR directed plasmid construction *in vivo* in yeast (Oldenburg et al., 1997). In this technique, the 1284 pNEB-Nat-Yeast cloning vector was used which contains the *URA3* gene, that allows uracil synthesis and complementation of uracil (-) auxotrophy. The vector was linearized with *Hin*dIII and *Spe*I before the PCR products were transformed directly into a yeast uracil auxotrophic *ura3* (-) strain. The primers used to amplify the PCR fragments have overhangs corresponding to the adjacent PCR fragments or with the yeast plasmid. Once the linearized vector and the PCR fragments were mixed together (400 ng of each), in appropriate conditions, homologous recombination takes place and joins the PCR fragments with the vector in the correct orientation to generate the plasmid. To screen for the correct clones, yeast was grown on selected MM plates. For

large scale production of the plasmid, the plasmid was transformed into *E. coli* (Promega JM109 *end*A1, *rec*A1, *gyr*A96, *thi*, *hsd*R17 (rk–, mk+), *rel*A1, *sup*E44, Δ(*lac-pro*AB), [F´ *tra*D36, *pro*AB, *laq*IqZΔM15) since yeast plasmid isolation is inefficient and a large quantity of plasmid DNA (4 µg) is required for fungal transformation. 3 pairs of primers (Table 4.2) were used to generate the *CAP20:mRFP:trpC* construct. The first pair for the amplification of the selectable marker, in this case sulfonylurea (Sweigard et al., 1997), the second pair to amplify the *CAP20* open reading frame, including the promoter and the third pair for *mRFP* gene amplification.

Table 4.2 Primers used in this study to carry the *mRFP* tagging of *CAP20* gene

Primer	Sequence 5'-3'
gCAP20.F1	GATTATTGCACGGGAATTGCATGCTCTCACGCCTACCTTCCAAACGACG
rCAP20.R1	CTCCTTGATGACGTCCTCGGAGGAGGCCATATTGCTGTTGTTGTTGTTGTTG
SUR.F	AACTGTTGGGAAGGGCGATCGGTGCGGGCCGTCGACGTGCCAACGCCA
SUR.R	GTGAGAGCATGCAATTCCCG
mRFP.F	ATGGCCTCCTCCGAGGACGTCAT
mRFP.R	GATCCCCCGGGCTGCAGCCGGGCGGCCGCTTTAGGCGCCGGTGGAGTGGCG
TrpC.F	AGCGGCCGCCCGGCTGCA
TrpC.R	TTCACACAGGAAACAGCTATGACCATGATTGTGGAGATGTGGAGTGGGC

4.2.4 Yeast transformation

A single *S. cerevisiae* colony was picked and used as inoculum in 10 mL YPD medium and grown overnight at 30 °C with continuous shaking at 230 rpm. YPD medium consists of 10 g/L yeast extract, 20 g/L peptone and 20 g/L glucose. A 2 mL aliquot of the overnight culture was then inoculated into 50 mL YPD medium in a 250 mL flask and incubated at 30 °C for 5 h with continuous shaking at 230 rpm. Following

centrifugation at 2 200 × *g* for 5 min, the supernatant was discarded and the pellet was resuspended in 10 mL distilled water before being centrifuged at 2 200 × *g* for 5 min. The supernatant was discarded and the pellet was resuspended in 300 µL distilled water. A 50 µL aliquot of the yeast cells, 50 µL of 2 µg/µL salmon sperm DNA (denatured at 95 °C and cooled on ice for 2 min), linearized vector and PCR products were combined in a fresh eppendorf tube. 32 µL of 1 M lithium acetate and 240 µL of 50% PEG 4 000 were added to the mixture and the tube was incubated at 30 °C for 30 min. Following heat shock at 45 °C for 15 min, the tube was centrifuged at 2 000 × *g* for 2 min. The supernatant was removed by pipetting and the pellet was resuspended in 200 µL distilled water. A 10X dilution of the 200 µL suspension was made and both were plated on YPD plates and incubated at 30 °C. Transformants usually appeared after 2-3 days of incubation.

4.2.5 Yeast plasmid extraction

A 10 mL yeast culture was grown for 48 h in yeast synthetic drop out media at 30 °C with continuous shaking at 120 rpm. Yeast synthetic drop out medium consists of 1.7 g/L yeast nitrogen base (without amino acids) (Fluka), 5 g/L ammonium sulfate, 5 g/L casein hydrolysate (Fluka), 0.02 g/L adenine (Sigma), 0.02 g/L tryptophan (Fluka) and 20 g/L glucose. The cells were centrifuged for 5 min at 1 500 × *g* and the pellet was resuspended in 0.5 mL sterile distilled water and transferred to an eppendorf tube. Once again the cells were centrifuged for 5 sec at 13 000 × *g*, the supernatant was discarded and the pellet was vortexed and resuspended in the residual water. 200 µL of yeast lysis buffer [2% (v/v) triton X-100 (Sigma), 1% SDS, 0.1 M NaCl, 1 mM EDTA, 10 mM Tris], 200 µL phenol:chloroform:isoamylalcohol (25:24:1) and 0.3 g of acid washed glass beads (425-600 µm) were added into the tube. The tube was vortexed for 10 min

and 200 µL of TE (pH 8.0) was added. The tube was centrifuged for 5 min at 13 000 × *g* and the aqueous phase was transferred to a fresh eppendorf tube, to which 0.1 volume of 3 M sodium acetate (pH 5.5) and 2 vol of 96% ethanol were added. Following incubation at -20 °C for 15 min, the tube was centrifuged at 13 000 × *g* for 20 min and the resulting pellet was resuspended in 400 µL of TE treated with 4 µL of RNase A (10 mg/mL) and incubated at 37 °C until the pellet dissolved. Following the addition of 10 µL of 4 M ammonium acetate and 1 mL of 96% ethanol the tube was centrifuged at 13 000 × *g* for 20 min. The supernatant was discarded and the pellet was washed with 500 µL of 70% ethanol before being air dried and resuspended in 20 µL of distilled water. To increase the DNA yield for fungal transformation, the plasmid was transformed into *E. coli* as described in Section 2.10.

4.3 Results

4.3.1 Identification of gene that codes for perilipin in *M. oryzae*

The first fungal perilipin was described in the fungus *Colletotrichum gloeosporioides*, where the *CAP20* gene was identified (Hwang et al., 1995) and more recently in *Metarhizium anisopliae*, *Mpl1*, (Wang and St. Leger, 2007). Identification of a gene that codes for perilipin in Magnaporthe was carried out by using the BLAST programme provided by the Magnaporthe genome database (http://www.broadinstitute.org/). The sequence of *M. anisopliae* perilipin, *Mpl1*, and *C. gloeosporioides*, *CAP20*, were obtained and used as query sequence. Only 1 hit was obtained for both searches, MGG_11916.6.

The coding sequence of MGG_11916.6 predicts a protein of 187 amino acids and it has 48% identity to *MPL1* and 43% identity to cap20 (Figure 4.1 A). It was also suggested that MGG_11916.6 is the most likely candidate as the *MPL1* homologue (Wang and St. Leger, 2007). MGG_11916.6 has a similar overall structure and several conserved regions when compared to the perilipin in *M. anisopliae* and mammalian cells, in particular the N-terminal β-strand, three hydrophobic regions (H1, H2, H3) and multiple phosphorylation sites (Figure 4.1 B).

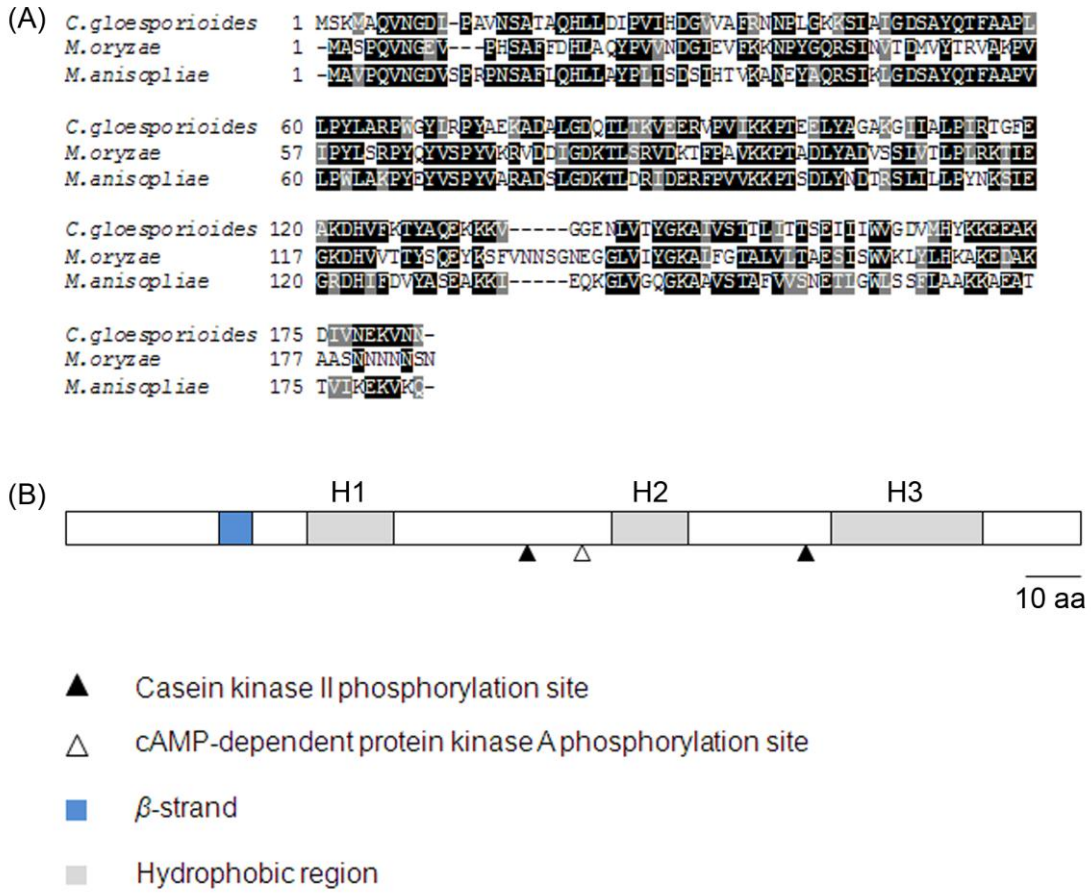

Figure 4.1 Alignment of the predicted amino acid sequence of *CAP20* with fungal *CAP20*-encoding genes and the structural motifs of the protein.

(A) The predicted amino acid sequence of *M. oryzae CAP20* was aligned with *M. anisopliae MPL1* (ADH51538.1) and *C. gloesporioides CAP20* (AAA77678.1) using the program CLUSTALW (Thompson et al., 1994). *MoCAP20* shows 48% amino acid identity to *MaMPL1* and 43% amino acid identity to *CgCAP20*. Identical amino acids are highlighted on a black background and similar amino acids on a grey background. (B) Structural motifs in *MoCAP20* including the N-terminal *β*-strand and hydrophobic regions (H1, H2 and H3). (Scale bar = 10 amino acids).

4.3.2 Targeted gene deletion of *CAP20*

For further analysis of the function of perilipin in plant infection, deletion of *CAP20* was carried out using targeted gene deletion (Catlett et al., 2003). These constructs were transformed into Guy11 and transformants selected based on resistance to hygromycin B. The DNA of the putative transformants were extracted and digested with either *Xho*I or *Hin*dIII before being fractionated by gel electrophoresis. The fractionated DNA was then transferred onto Hybond-N and probed with either 1 kb of the open reading frame fragment generated by PCR using primers pCAP20.F1 and pCAP20.R1 (digested with *Xho*I) or 1.5 kb of upstream flanking region of the targeted genes locus (digested with *Hin*dIII).

In the case of a successful targeted homologous recombination, using the open reading frame fragment as a probe, a 10.6 kb hybridizing restriction fragment was expected to be present in the wild type, but absent in the null mutant. Figure 4.2 shows the result of the Southern blot hybridization analysis. The absence of a 10.6 kb hybridizing restriction fragment in lanes 1, 2, 4, 5 and 6 is consistent with successful targeted replacement of *CAP20*. The presence of the 10.6 kb hybridizing restriction fragment in lane three indicated an ectopic integration of the hygromycin B resistance gene cassette. To confirm the successful targeted gene deletion, a 1.5 kb genomic fragment upstream of the *CAP20* coding region was used to probe a blot generated following genomic DNA digestion with *Hin*dIII. A size difference was expected in the event of successful replacement of the native *CAP20* locus with the hygromycin resistance gene cassette. Figure 4.2 shows the size of the hybridizing restriction fragments observed in the wild type and the ectopic transformants (6.5 kb) and putative Δ*cap20* mutants (4.3 kb). This result confirms targeted gene deletion in transformants 1, 4 and 5. The transformant in

lane 1 was selected for further phenotypic analysis and is hereafter referred to as the Δ*cap20* mutant.

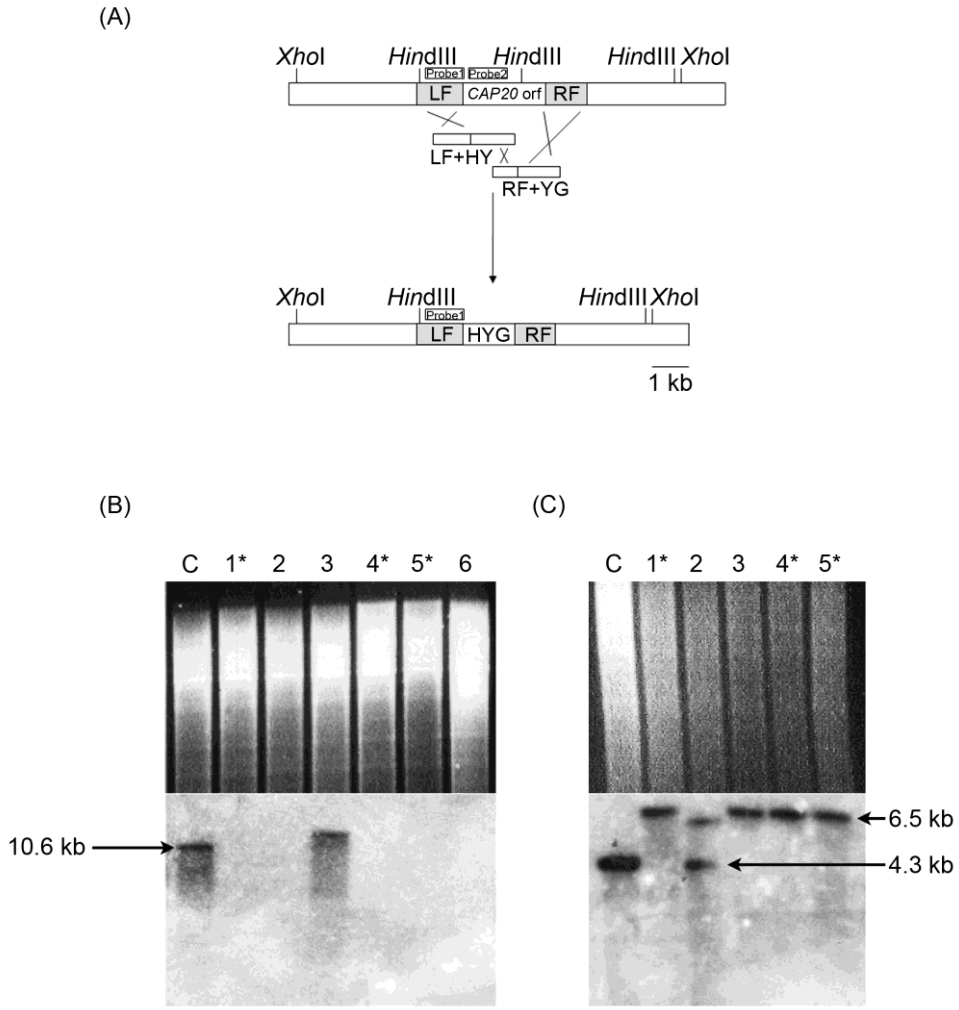

Figure 4.2 A schematic representation of the targeted deletion of *CAP20* by the split-marker deletion method.

(A) Diagram describing the targeted gene deletion of *CAP20*. (B) Genomic DNA was restriction digested with *Xho*I, fractionated by gel electrophoresis and transferred to Hybond-N. The Southern blot was subsequently probed with a 1 kb fragment from the *CAP20* locus. The absence of the hybridising fragment reveals a correctly targeted deletion. (C) Genomic DNA was restriction digested with *Hin*dIII, and the Southern blot was probed with a 1.5 kb genomic fragment upstream of the *CAP20* coding region. The probe hybridised to a 4.3 kb fragment from *Hin*dIII digested Guy11 and to a 6.5 kb fragment from Δ*cap20* mutants. The putative transformants in lanes 1, 4 and 5 were confirmed as Δ*cap20* mutants. C: wild type control, Guy11.

4.3.3 Localisation of perilipin

In order to investigate the localisation and identity of *CAP20*, a *CAP20:mRFP*-expressing plasmid was transformed into Guy11. Perilipin is a protein that functions as a shield preventing lipid from instantly being degraded by cytosolic lipases (Brasaemle et al., 2000). It localises exclusively to the periphery of lipid droplets and is found in no other cellular compartments (Blanchette-Mackie et al., 1995).

To analyse the localisation of the Cap20 protein in *M. oryzae*, conidia from *MoCAP20:mRFP* were harvested, stained with Bodipy lipid stain, inoculated onto hydrophobic glass coverslips and incubated in a moist chamber at 24 °C. The transformants were then analysed at certain time intervals (4, 6, 8 and 24 h) for mRFP and Bodipy signals using epifluorescence microscopy. I observed that *MoCAP20* co-localised with lipid droplets specifically at the periphery of the lipid droplets (Figures 4.3 A and 4.3 B). This is consistent with the predicted identity of *CAP20* encoding a perilipin involved in lipid storage.

4.3.4 Appressorium development and lipid mobilisation in Δ*cap20* mutant

Appressorium development and lipid mobilisation were observed in the mutants (Figure 4.4). There were significant differences observed in appressorium development between Guy11 and Δ*cap20* mutant. The differences could be seen clearly after 4 h when a mixture of phenotypes was observed. Some of the Δ*cap20* mutant conidia were able to germinate normally and form appressoria while others produced a very long germ tube which sometimes resulted in appressoria being formed and sometimes in continued elongation. Our results showed that even after 48 h, only 60% of germinating conidia were able to produce appressoria when compared to the wild type (Student's t-test $P < 0.01$). I also carried out a single spore isolation to confirm that the presence of the

mixed phenotype was not caused by generation of a heterokaryon. All 20 single spores isolated and observed, showed a similar phenotypes.

Even though appressorium development was severely impaired, lipid mobilisation was unaffected. In the case of normal germinating conidia from the mutant, lipid mobilisation occurred as seen in the wild type. Lipid droplets started to mobilise as soon as the germ tube emerged and after 2 h, lipid droplets were seen to accumulate at the tip of the germ tube (Figure 4.4). After 4 h, appressoria started to form and lipid droplets were seen to accumulate in appressoria. After 6 h, more lipid droplets were observed in appressoria, compared to conidia and after 8 h, almost all the lipid droplets were within appressoria. In the case of abnormal germinating conidia, lipid droplets can be seen moving and accumulating at the tip of the elongated germ tube. If the elongated germ tube is able to form an appressorium, then lipid droplets could be seen accumulating in the appressorium. This suggests that even though appressorium development was severely compromised, lipid mobilisation still occurred normally.

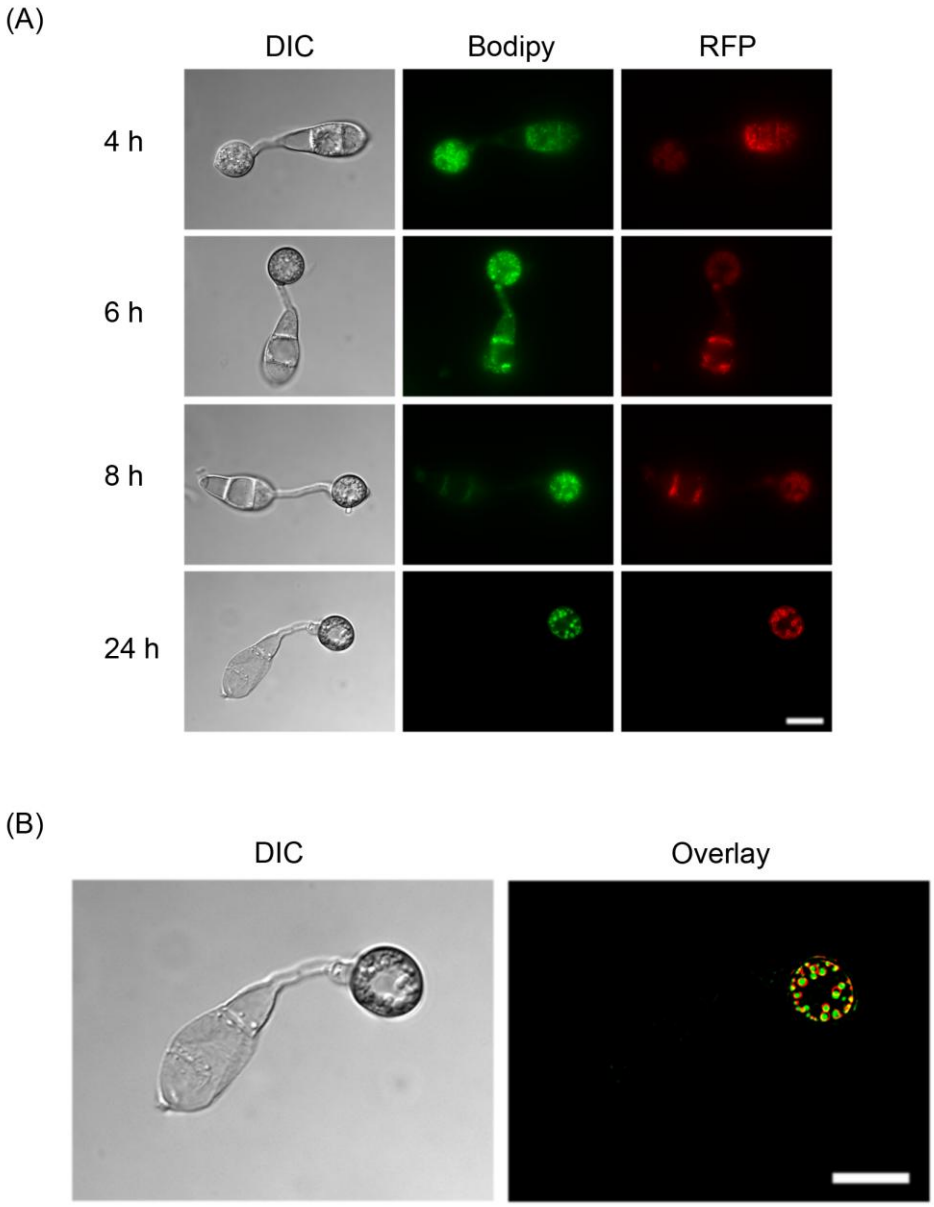

Figure 4.3 Epifluorescence microscopy of lipid body distribution of *CAP20-mRFP* and Cap20 localisation in *M. oryzae*.

(A) Conidia expressing *CAP20:mRFP* and stained with Bodipy were incubated on an unyielding surface (glass coverslip) and examined by epifluorescence microscopy at 4 , 6, 8 and 24 hpi. Representative bright-field (differential interference contrast (DIC)) and fluorescence images at each time point are shown. (B) Overlay of the mRFP signal and Bodipy stain revealed that *CAP20* is localised at the periphery of lipid droplets. Scale bar = 10 µm.

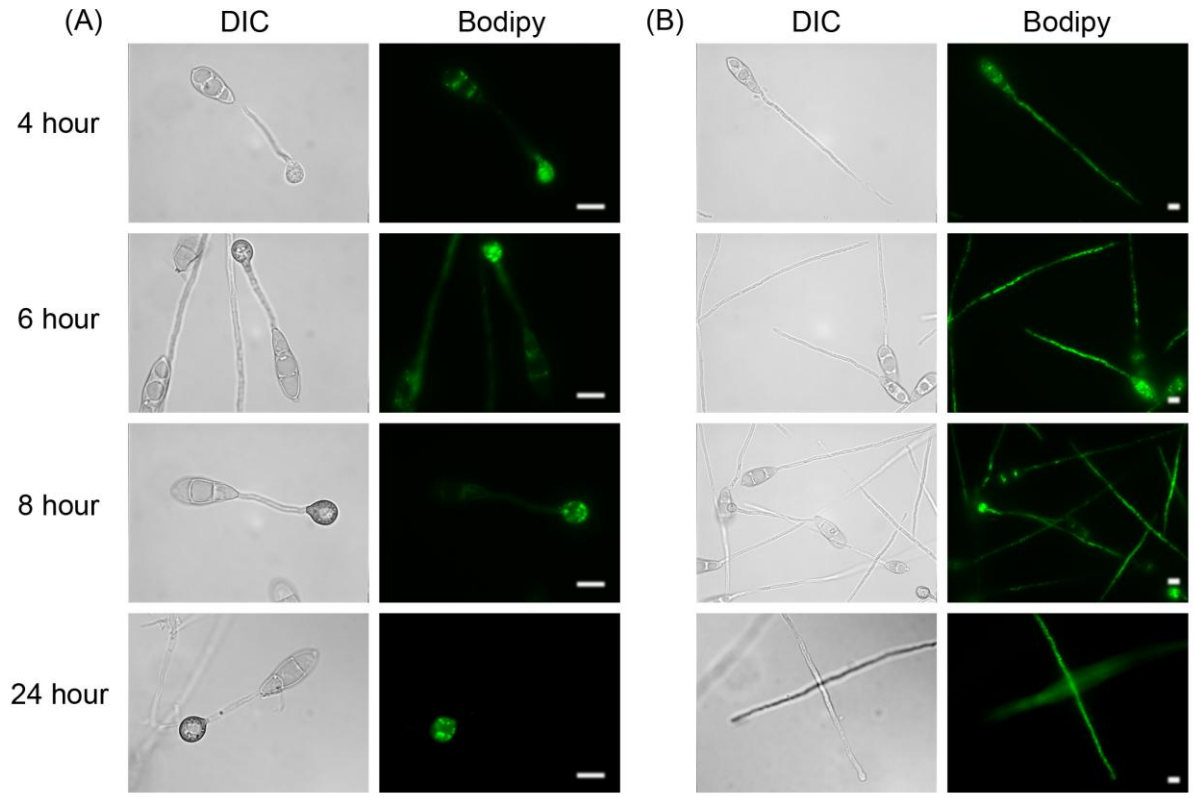

Figure 4.4 Appressorium development and lipid mobilisation in a *M. oryzae* Δ*cap20* mutant.

(A) When a conidium was able to form an appressorium, lipid mobilisation occurred normally in the Δ*cap20* mutant. Lipid droplets were mobilised on emergence of the germ tube and accumulated at the tips of germ tubes and subsequently in the appressorium. (B) When appressorium development was impaired, lipid mobilisation was unaffected. Scale bar = 10 µm.

4.3.5 The effect of *CAP20* deletion on nuclear division in *M. oryzae*

Since deletion of *CAP20* affects appressorium development severely, studies on nuclear division were carried out to investigate whether there is a relationship between the presence of *CAP20* and the onset and pattern of nuclear division. In order to do this, I obtained a nuclear marker construct (Saunders et al., 2010), *H1:RFP*, and transformed it into a Δ*cap20* mutant background. The live cell imaging analysis was carried out using epifluorescence microscopy and the results were shown in Figure 4.6.

In the case of conidia that can germinate and form appressoria, nuclear division was shown to occur normally. By 4 h, the time point at which nuclear division should have occurred, four nuclei could be seen, three in the conidia and one in the appressoria. By 24 h, the three nuclei in the conidia had been degraded leaving one nucleus remaining inside the appressorium. In the case of conidia with elongated germ tubes, I observed that nuclear division was constantly occurring until the formation of appressoria. As a result, multiple nuclei can be seen in the germ tube.

4.3.6 Carbon utilisation and plant pathogenicity in Δ*cap20* mutants

Further characterisation of *M. oryzae* Δ*cap20* mutants was carried out by investigating their carbon utilisation ability. Mutants were grown on minimal medium supplemented with different carbon sources (50 mM glucose, 50 mM acetate, 50 mM oleic acid and 50 mM triolein) and the growth of the mutants was observed after 14 days (Figure 4.7). The results showed that mutants were able to grow on acetate and lipid suggesting *CAP20* is not required for carbon utilisation.

To investigate the role of *CAP20* in causing blast disease, conidia from a Δ*cap20* mutant along with Guy11, were harvested and spray inoculated onto 3 week old seedlings of blast susceptible rice cultivar CO-39. We observed that a Δ*cap20* mutant

was still able to cause rice blast infection. However, there was a reduction in the symptoms. This was confirmed by quantitative analysis (Figure 4.8) showing that the number of necrotic lesions produced by the mutant was 50% reduced compared to the wild type, Guy11 (Student's t-test $P < 0.01$).

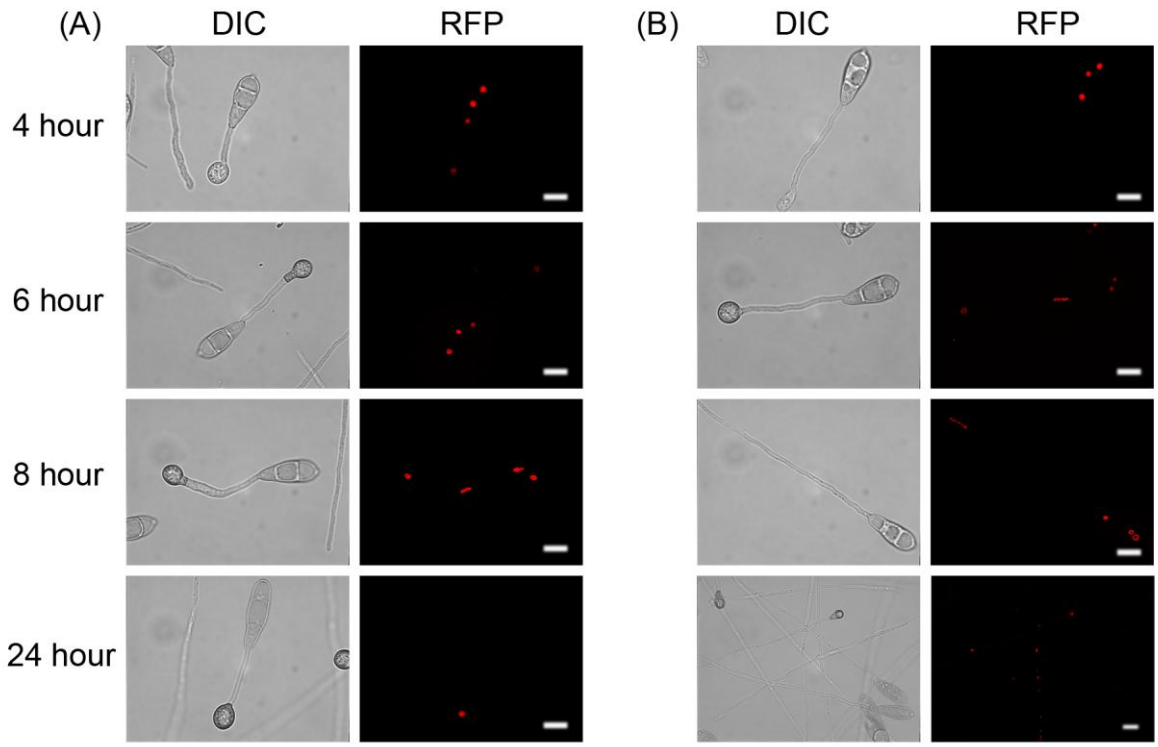

Figure 4.5 Analysis of the nuclear division pattern of the Δ*cap20* mutant.

Conidia of the Δ*cap20* mutant expressing RFP-tagged histone H1 (*H1:RFP*) were examined by epifluorescence microscopy for analysis of the nuclear division pattern. (A) When formation of an appressorium occurred, normal nuclear division was observed. After 24 h, a single nucleus remained in the appressorium, while the nuclei in the conidium had been degraded. (B) When appressorium development was impaired, nuclear division occurred constantly, resulting in multiple nuclei in the germ tube. Scale bar = 10 µm.

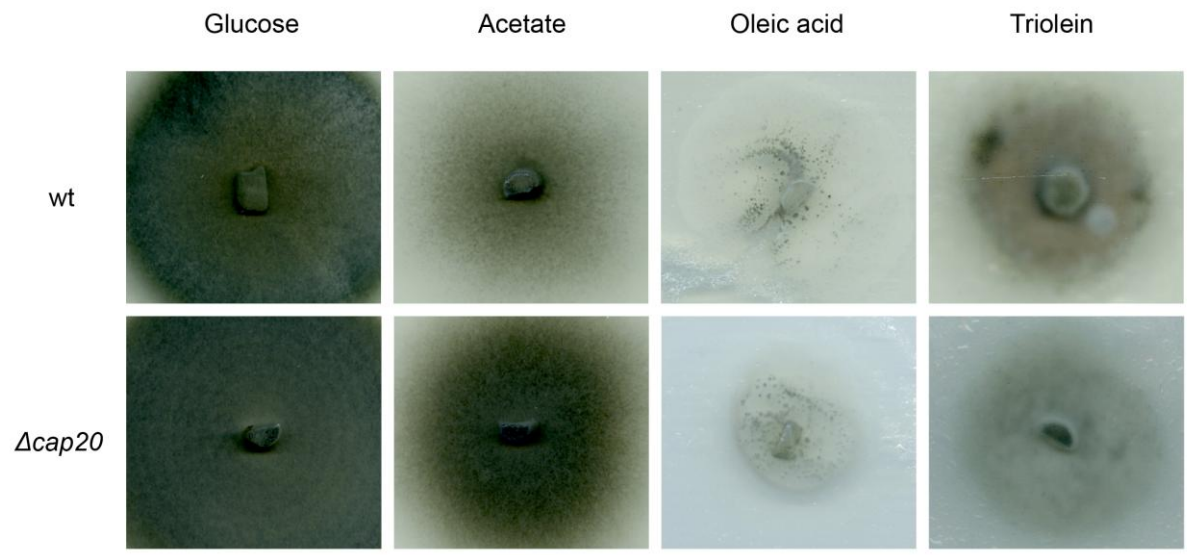

Figure 4.6 Vegetative growth of the wild type, Guy11 and Δ*cap20* mutant on a range of different carbon sources.

The fungal strains were inoculated onto minimal medium supplemented with glucose, acetate, oleic acid or triolein and incubated at 24 °C for 14 days. No difference was observed between the Δ*cap20* mutant and wild type, Guy11, which suggests *CAP20* is not required for carbon utilisation.

Figure 4.7 Plant pathogenicity assay on rice cultivar CO-39.

Conidial suspension from the wild type (wt), Guy11 and the Δ*cap20* mutant were spray inoculated onto 3 week old rice seedlings of rice cultivar CO-39. The plants were incubated at 24 °C with high light and 90% relative humidity for 5 days. (A) The Δ*cap20* mutant was able to cause blast symptoms on rice plants. (B) Statistical analysis revealed the number of necrotic lesions produced by the mutant was 50% reduced compared to the wild type, Guy11 (Student's t-test $P < 0.01$).

4.4 Discussion

Perilipin is a protein that is involved in lipid storage by protecting the lipid from being degraded by cytosolic lipases. As previously mentioned, in mammalian cells perilipin has been shown to localise to the periphery of lipid droplets (Blanchette-Mackie et al., 1995). In results reported in this chapter, I identified and characterised a gene that encodes perilipin, MGG_11916.6, in *M. oryzae*. The gene was subsequently named *CAP20*. Perilipin has been studied extensively in mammalian systems. In fungi, the most recent report on perilipin was in *M. anisopliae, Mpl1* (Wang and St. Leger, 2007). It was suggested that MGG_11916.6 is the most likely to be the homolog of *Mpl1* in *M. oryzae* (Wang and St. Leger, 2007).

To further confirm the identity of MGG_11916.6, the C-terminal mRFP construct of *CAP20* was generated and transformed into Guy11. The transformant was stained with Bodipy and analysed using epifluorescence microscopy. Based on the observation, it was confirmed that *CAP20* was localised to the periphery of lipid droplets. This is consistent with what has been shown by the mammalian and *M. anisopliae* perilipin (Blanchette-Mackie et al., 1995; Wang and St. Leger, 2007). This further supports the identity of *CAP20* as a homologue of *Mpl1*.

In order to investigate the role of *CAP20* in *M. oryzae*, targeted gene deletion was carried out and null mutants confirmed through Southern blot analysis. Observation of appressorium development of Δ*cap20* mutant quickly revealed that there was a difference with the wild type, Guy11. Δ*cap20* mutants were unable to germinate and form appressoria normally. A mixture of phenotypes was observed (Figure 4.4) where some of the germinating conidia produced a very long germ tube and only 60% of them were able to form an appressorium (Student's t-test $P < 0.01$) (Figure 4.5). Up to this point, it was clear that *CAP20* plays an important role in conidia germination and

appressorium formation. This is different from observations in Δ*mpl1* mutants which also showed appressorium development defects. The Δ*mpl1* mutants can however still germinate but the germ tube was narrower compared to the wild type and they were still able to form an appressorium (Wang and St. Leger, 2007). However, the appressorium formed was not fully functional because it was not able to generate turgor (Wang and St. Leger, 2007). Lipid mobilisation was also observed in a Δ*cap20* mutant (Figure 4.4). Even though appressorium development was severely impaired, lipid mobilisation still occurs normally. Lipid droplets were seen to mobilise once the germ tube emerged and accumulate at the tip of the germ tube. When appressorium formation occurred, lipid droplets were seen accumulating in the appressorium which is also seen normally in the wild type. This observation suggests that *CAP20* plays an important role in appressorium development, but is dispensable for lipid mobilisation. This also suggests that appressorium development and lipid mobilisation occur independently of each other.

To further understand the role of *CAP20* in *M. oryzae*, nuclear division was observed because appressorium differentiation normally occurs following nuclear division (Saunders et al., 2010). A Δ*cap20* mutant expressing *H1:RFP* construct was generated and analysed using epifluorescence microscopy throughout appressorium development. The results revealed that nuclear division was severely impaired (Figure 4.6). It was shown that nuclear division occurs repeatedly, especially in conidia with elongated germ tubes. As a consequence, after 24 h, multiple nuclei were seen in the germ tube rather than just a single nucleus in the appressorium. In the case of the *M. anisopliae* Δ*mpl1* mutant, it was shown that the mutant lacked a septum that separates the germ tube and appressorium, which in turn affected turgor pressure generated by the appressorium (Wang and St. Leger, 2007).

An investigation of the role of *CAP20* in carbon utilisation was then carried out. The *M. oryzae* Δ*cap20* mutant was grown on minimal medium supplemented with various carbon sources (glucose, acetate, oleic acid and triolein), incubated at 24 °C. After 14 days, results showed that there was no significant difference seen between Guy11 and Δ*cap20* mutants (Figure 4.7). This suggests that *CAP20* is not involved in ability of *M. oryzae* to utilise different carbon sources.

The role of *CAP20* in plant pathogenicity was also investigated. In the *M. anisopliae* Δ*mpl1* mutant, it was shown that ability of the fungus to infect insect was reduced (Wang and St. Leger, 2007). However, the ability of the fungus to infect insects was restored when spores were injected directly in the haemocoel of the insect. This suggests that the appressorium formed was not fully functional, which reduced its turgor pressure (Wang and St. Leger, 2007). The *M. oryzae* Δ*cap20* mutant showed a reduction in blast symptoms (Figure 4.8). Statistical analysis showed that the Δ*cap20* mutant produced 50% less necrotic lesions compared to the wild type, Guy11 (Student's t-test $P < 0.01$) (Figure 4.8). This is consistent with the impaired ability of Δ*cap20* mutant to produce an appressorium. Only 50% of Δ*cap20* mutant were able to form appressoria (Student's t-test $P < 0.01$) (Figure 4.5).

Based on all these observations, it is clear that perilipin plays an important role not only in lipid storage and metabolism, but also in appressorium differentiation and nuclear division in *M. oryzae*. This in turn affects the ability of the fungus to infect rice plants. In order to fully understand the role of perilipin in plant infection development in *M. oryzae*, more analysis needs to be done to study the relationship of perilipin, lipid metabolism, appressorium differentiation and nuclear division. The amount of lipid stored in the Δ*cap20* mutant conidia needs to be measured and compared with the wild type to determine whether there is any significant reduction of lipid storage. It is also

worth measuring the amount of lipid in Δ*cap20* and Δ*cpkA* mutants after 24 h of inoculation to determine whether there is any difference between the mutants since protein kinase A is known to be involved in perilipin phosphorylation during starvation, allowing lipid degradation to take place (Marcinkiewicz et al., 2006). Actin and septin distribution also need to be observed in Δ*cap20* mutant to understand the role of perilipin in appressorium differentiation. Studies regarding the relationship between perilipin and autophagy will also need to be carried out because it is known that autophagy plays an important role in lipid metabolism (Singh et al., 2009) and is pivotal to appressorium function in *M. oryzae* (Kershaw and Talbot, 2009).

5.0 Acetyl-CoA metabolism and translocation in *M. oryzae*

5.1 Introduction

Acetyl-CoA is an essential metabolite with notable roles in carbon and energy metabolism (Strijbis and Distel, 2010). Acetyl-CoA is mainly generated from two sources. The first source is through the glycolytic pathway leading to the generation of pyruvate. Acetyl-CoA can be generated from pyruvate through pyruvate dehydrogenase in the matrix of mitochondria or pyruvate carboxylase in the cytoplasm (Strijbis and Distel, 2010). The second source is lipid degradation through fatty acid β-oxidation which occurs in peroxisomes or mitochondria. Since essential metabolic pathways, such as the tricarboxylic acid (TCA) cycle, glyoxylate cycle, gluconeogenesis and fatty acid β-oxidation take place in different cellular compartments, translocation of acetyl-CoA is important for fungal growth and survival on different carbon sources (Strijbis et al., 2010). However, acetyl-CoA has a bulky structure and is amphiphilic in nature and because of these characteristics, it cannot freely cross biological membranes (Rottensteiner and Theodoulou, 2006).

Two systems for translocation of acetyl-CoA have been identified in fungal species; a carnitine-dependent pathway and a peroxisomal citrate synthase-dependent pathway (van Roermund et al., 1995). The importance of each system is distinct in different species. Some species, especially plants, rely predominantly, or exclusively, on peroxisomal citrate synthase pathway for acetyl-CoA transport (Pracharoenwattana et al., 2005), while most fungal species rely solely on the carnitine-dependent pathway. However, the budding yeast *Saccharomyces cerevisiae* is an exception because it uses both systems for acetyl-CoA translocation (Thewes et al., 2007).

Other non-fermentable carbon sources that can be utilised by fungi to produce acetyl-CoA are ethanol and acetate (Strijbis et al., 2008). Ethanol and acetate are converted

into acetyl-CoA in the cytoplasm by the action of acetyl-CoA synthetase (Strijbis and Distel, 2010). Cytoplasmic acetyl-CoA can also be used in the TCA and glyoxylate cycles and therefore needs to be transported from the cytoplasm into the appropriate sub-cellular compartments to participate in the appropriate metabolic pathways. It has been shown that growth of *Candida albicans* on ethanol and acetate as sole carbon source is dependent on the glyoxylate cycle (McKinney *et al.*, 2000; Lorenz and Fink, 2001) as well as translocation of acetyl units between compartments (Zhou and Lorenz, 2008; Strijbis *et al.*, 2010). A model for acetyl-CoA transport between peroxisomal, cytosolic and mitochondrial compartments in *C. albicans* is shown in Figure 5.1.

5.1.1 Carnitine acetyltransferase (CAT)

Shuttling of acetyl units between cellular compartments is clearly a crucial factor in the growth of fungi on different sources of acetyl-CoA. The key enzymes for this process are carnitine acetyltransferases (CATs) which convert acetyl-CoA to acetylcarnitine before it can be transported (Kohlhaw and Tan-Wilson, 1977). CATs are a member of the carnitine acyltransferase family that also comprises the carnitine palmitoyltransferases and carnitine octanoyltransferases and are highly conserved throughout eukaryotes (Schulz, 1991).

Saccharomyces cerevisiae possesses three genes that encode carnitine acetyltransferase; Cat2, Yat1 and Yat2. Yat1 is localised at the mitochondrial outer membrane (Schmalix and Bandlow, 1993) and Yat2 is localised in the cytoplasm (Jaco et al., 2008). Cat2 is localised in both peroxisomes and mitochondria and possesses two in-frame start codons that are regulated by carbon source-dependent transcription initiation (Elgersma et al., 1995). The longer transcript encodes a protein containing an N-terminal mitochondrial targeting signal (MTS) and thus its translation product is targeted to

mitochondria. The protein encoded by the shorter transcript lacks the *MTS* and is targeted instead to peroxisomes via its C-terminal peroxisomal targeting signal (*PTS1*). In *Candida albicans*, CATs are encoded by *CTN2*, *CTN1* and *CTN3* (Prigneau et al., 2004) and it has been shown that *C. albicans* is completely dependent on CAT activity for acetyl-CoA transport (Strijbis et al., 2008; Zhou and Lorenz, 2008). *CTN2* is a homologue of *CIT2* (Cat2) while *CTN1* and *CTN3* are homologues of *YAT1* and *YAT2* respectively. The presence of both mitochondrial and peroxisomal targeting signals in *C. albicans* Cat2 (*CTN2*) suggests that the mechanism of dual localisation of Cat2 is conserved between these two yeasts.

In the peroxisome, Cat2, catalyzes conversion of acetyl-CoA to acetyl-carnitine, which can then be transported across the peroxisomal membrane. Acetyl-carnitine can also be transported into mitochondria where the acetyl unit is released from acetyl-carnitine through a reaction which is catalyzed by the mitochondrial Cat2. In *C. albicans*, deletion of *CAT2* resulted in loss of both mitochondrial and peroxisomal CAT activities and the mutant could not grow on alternative carbon sources (Strijbis et al., 2008). However, it was shown that peroxisomal Cat2 is not essential for fatty acid β-oxidation because a strain lacking peroxisomal Cat2 was still able to transport acetyl units across the peroxisomal membrane and enter the mitochondrial TCA cycle (Strijbis et al., 2010). This shows that whilst mitochondrial CAT activity is essential for growth on alternative carbon sources, peroxisomal CAT activity is dispensible.

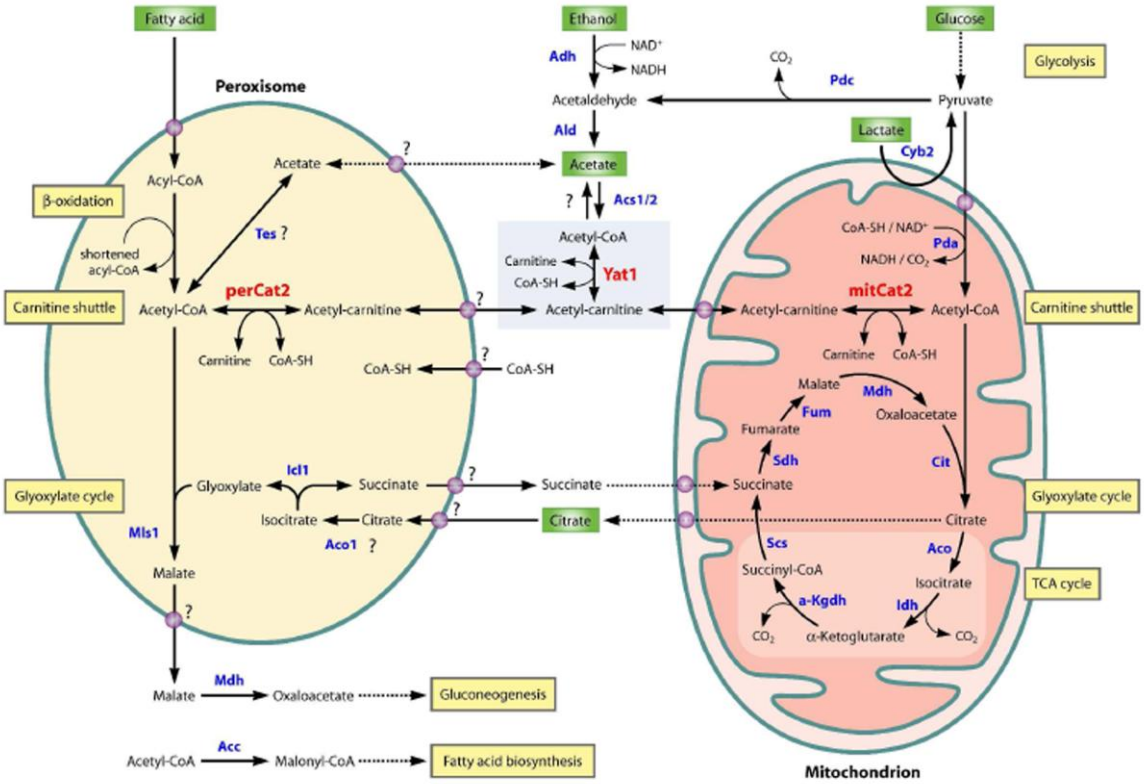

Figure 5.1 Model for acetyl-CoA transport between peroxisomal, cytosolic and mitochondrial compartments in *C. albicans* (adapted from (Strijbis and Distel, 2010).

Biochemical pathways are shown for fatty acid β-oxidation, the carnitine shuttle, the glyoxylate cycle, TCA cycle, glycolysis, gluconeogenesis and fatty acid biosynthesis. Abbreviations used: Acc: acetyl-CoA carboxylase, Aco: aconitase, Acs1/2: acetyl-CoA synthase, Adh: alcohol dehydrogenase, Ald: acetaldehyde dehydrogenase, α-Kgdh: α-ketogluterate dehydrogenase, Cit: citrate synthase, Cyb2: L-lactate dehydrogenase, Fum: Fumarase, Icl1: isocitrate lyase, Idh: isocitrate dyhydrogenase, Mdh: malate dehydrogenase, mitCat2: mitochondrial Cat2, Mls1: malate synthase, Pda: pyruvate dehydrogenase complex, 16 Pdc: pyruvate decarboxylase, perCat2: peroxisomal Cat2, Scs: succinyl-CoA synthetase, Sdh: succinate dehydrogenase, Tes: thioesterase, Yat1: carnitine acetyl-transferase. Question marks indicate uncertainties regarding conversions or means of transport.

In *Magnaporthe oryzae*, the major CAT is encoded by *PTH2* (Bhambra et al., 2006). *PTH2* was shown to be highly expressed in the presence of acetate and lipid and is regulated by the cyclic AMP response pathway. Deletion of *PTH2* greatly affected the ability of the fungus to grow on acetate and lipid as well as the loss of plant virulence. A *GFP-PTH2* gene fusion was found to be peroxisomally localised (Bhambra et al., 2006).

5.1.2 Carnitine biosynthesis

Carnitine is an essential metabolite, which has a number of indispensible roles in intermediary metabolism. In fungi, the most important role of carnitine is the transfer of products of peroxisomal β-oxidation, including acetyl-CoA, to other cellular compartments. Other functions of carnitine include modulation of the acyl-CoA/CoA ratio (Carter et al., 1995), storage of energy in the form of acetylcarnitine (Bremer, 1983) and the modulation of toxic effects of poorly metabolised acyl groups by excreting them as carnitine esters (Duran et al., 1990).

In mammalian species, carnitine is primarily obtained from the diet, in particular meat and dairy products which contain high levels of carnitine compared to foods derived from plants (Rebouche and Engel, 1984). However, most mammalian species have the capability to synthesise carnitine endogenously (Bremer, 1962; Tanphaichitr and Broquist, 1973). Carnitine biosynthesis has also been described in *Neurospora crassa* (Kaufman and Broquist, 1977) and *C. albicans* (Strijbis et al., 2009). Carnitine is synthesised from the amino acids lysine and methionine. Lysine provides the carbon backbone of carnitine (Tanphaichitr and Broquist, 1973) and the 4-*N*-methyl groups originate from methionine (Tanphaichitr et al., 1971). Proteins, such as calmodulin, myosin, actin, cytochrome *c* and histones contain lysine residues that are *N*-methylated,

a post-translational modification catalyzed by specific methyltransferases that use *S*-adenosylmethionine as a methyl donor (Paik and Kim, 1971). Lysosomal degradation of such proteins produces 6-N-trimethyllysine (TML), which is the first metabolite in carnitine biosynthesis. TML is first hydroxylated at carbon 3 by TML dioxygenase (TMLD) to yield 3-hydroxy-TML (HTML). Aldolytic cleavage of HTML between carbon 2 and 3 will generate 4-trimethylaminobutyraldehyde (TMABA) and glycine, a reaction catalyzed by pyridoxal 5'-phosphate (PLP)-dependant aldolase (HTMLA). The next step is dehydrogenation of TMABA by TMABA dehydrogenase (TMABADH) resulting the formation of γ-butyrobetaine (γ-BB). The final step is hydroxylation of γ-BB at the 3-position by γ-BB dioxygenase (BBD) producing carnitine (Vaz and Wanders, 2002; Strijbis *et al.*, 2009). Figure 5.2 describes the carnitine biosynthesis pathway.

5.1.3 Carnitine carrier

Mitochondrial membranes are impermeable to acyl-CoAs of any chain length (Palmieri et al., 1999). In order to be transported across the mitochondrial inner membrane, acyl-CoAs need to be transferred to carnitine in a reaction that is catalyzed by specific CATs. In mammalian mitochondria, the carnitine/acylcarnitine translocase (CACT) catalyzes the transport of acylcarnitines of various lengths the mitochondria in exchange for free carnitine (Indiveri et al., 1990). In *S. cerevisiae*, *CRC1* has been shown to be the homologue of CACT (Palmieri et al., 1999). *CRC1* has 29% identity to CACT and is the only gene in *S. cerevisiae* encoding a member of the mitochondrial carrier family that has a promoter region containing an oleate responsive element (ORE) and whose transcription has been shown to be induced by oleate (Palmieri et al., 2000). It was also shown that *CRC1* transported carnitine, acetylcarnitine and propionylcarnitine (Palmieri

et al., 1999). It was suggested that the main physiological function of the yeast Crc protein is to import acetylcarnitine, generated in the peroxisome by Cat2, into the mitochondria, which is consistent with co-regulation of *CRC1* and Cat2 by oleate (Karpichev and Small, 1998).

Crc1 may also be involved in oxidation of other non-fermentable carbon sources such as ethanol and acetate which are found in the cytoplasm. Ethanol is converted to acetate which is in turn converted to acetyl-CoA. Conversion of acetate to acetyl-CoA is catalyzed by an enzyme called acetyl-CoA synthetase. Acetyl-CoA will then be transferred to carnitine to form acetylcarnitine which is transported across the mitochondria inner membrane with the help of Crc1 releasing acetyl-CoA and carnitine (Strijbis and Distel, 2010).

In this Chapter, I describe the identification and characterisation of genes that encode enzymes involved in carnitine biosynthesis and acetyl-CoA translocation in *Magnaporthe oryzae*. Targeted gene deletion was carried out in order to investigate the importance of these enzymes in order to determine the role of acetyl-CoA and its translocation in virulence of *M. oryzae*. Further analysis was carried out to investigate their role in lipid metabolism as well as infection-related development.

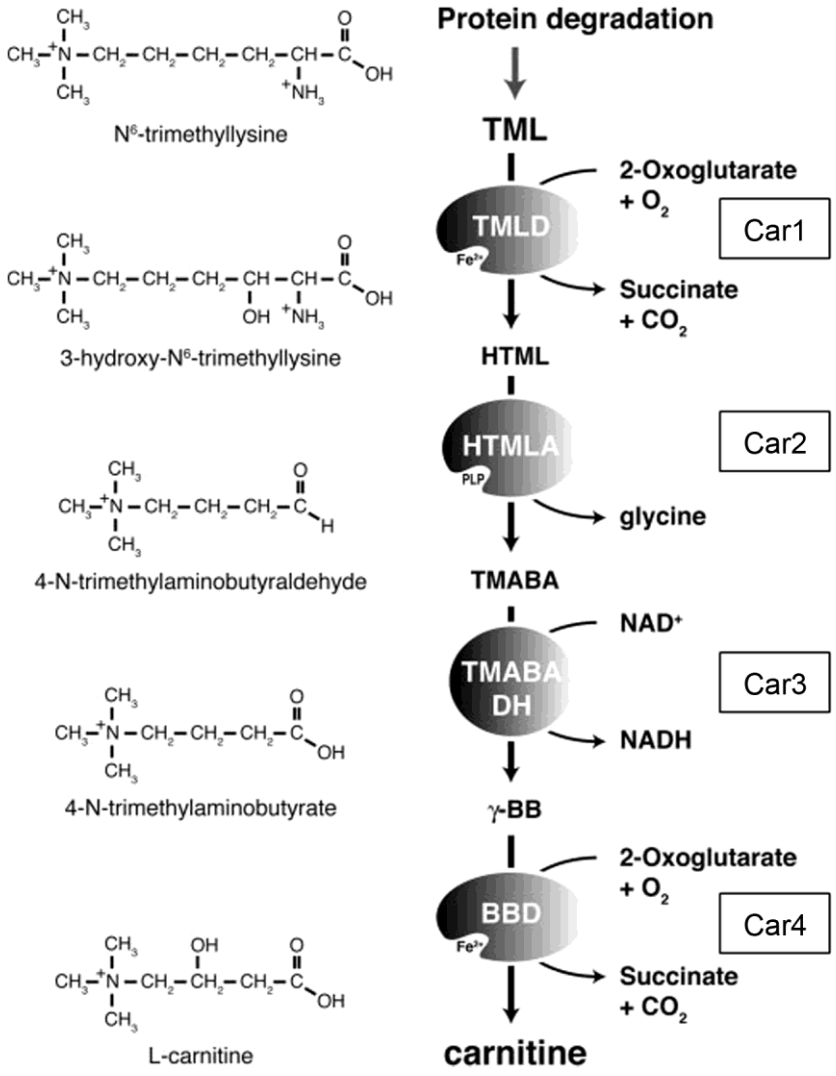

Figure 5.2 Schematic diagram describing the carnitine biosynthesis pathway (Vaz and Wanders, 2002).

6-N-trimethyllysine (TML) is released during lysosomal protein degradation. TML is then hydroxylated by TML dioxygenase (TMLD) to form 3-hydroxy-TML (HTML), which in turn is cleaved by pyridoxal 5'-phosphate (PLP)-dependant aldolase (HTMLA) into 4-trimethylaminobutyraldehyde (TMABA) and glycine. After that, TMABA is converted into γ-butyrobetaine (γ-BB) by TMABA dehydrogenase (TMABADH) followed by hydroxylation of γ-BB by γ-BB dioxygenase (BBD) to form carnitine.

5.2 Materials and Methods

5.2.1 Targeted deletion of genes involved in carnitine biosynthesis (*CAR1, CAR2, CAR3, CAR4*) and cytoplasmic acetyl-CoA translocation (*ACS1, ACS2, ACS3, CRC1*) in *M. oryzae*

The split marker strategy was used to delete each *M. oryzae* gene (Catlett et al., 2003). The hygromycin phosphotransferase-encoding gene was used as a selectable marker gene and the primers used are listed in Table 5.1. The first round of PCR involved amplification of sequences that flank the gene of interest and the hygromycin B cassette (Catlett et al., 2003). The left flanks of *CAR1*, *CAR2*, *CAR3*, *CAR4*, *ACS1*, *ACS2*, *ACS3* and *CRC1* were amplified using the following primers; TMLD.F1/TMLD.R1 for *CAR1*, HTMLA.F1/HTMLA.R1 for *CAR2*, TMABADH.F1/TMABADH.R1 for *CAR3*, BBD.F1/BBD.R1 for *CAR4*, ACS1.F1/ACS1.R1 for *ACS1*, ACS2.F1/ACS2.R1 for *ACS2*, ACS3.F1/ACS3.R1 for *ACS3* and CRC.F1/CRC.R1 for *CRC*. For amplifying the right flanks, the primers used were; TMLD.F2/TMLD.R2 for *CAR1*, HTMLA.F2/HTMLA.R2 for *CAR2*, TMABADH.F2/TMABADH.R2 for *CAR3*, BBD.F2/BBD.R2 for *CAR4*, ACS1.F2/ACS1.R2 for *ACS1*, ACS2.F2.2/ACS2.R2.2 for *ACS2*, ACS3.F2/ACS3.R2 for *ACS3* and CRC.F2/CRC.R2 for *CRC*. The hygromycin resistant cassette was amplified in two parts using M13F and HY split primers to amplify 1.2 kb of the 5' region of the gene including the trpC promoter whilst a 800 bp of 3' region of the gene was amplified using YG split and M13R primers.

The amplified flanks were then fused with the two halves of the hygromycin B resistance gene cassette by PCR, using one primer from the flanking region and a second from the HYGR cassette (2nd round PCR) as previously described (Kershaw and Talbot, 2009). The products of the 2nd round PCR were then transformed into an appropriate background strain. Putative transformants were selected for resistance to

hygromycin B and DNA extracted, as described in Section 2.2. Mutants were all confirmed by Southern blot analysis.

5.2.2 Lipid staining

Lipid droplets in germinating conidia and appressoria were visualized by staining with BODIPY® (493/503) (Invitrogen). Conidia were harvested by scraping sporulating plate cultures with a glass rod in sterile distilled water, followed by centrifugation at 5,000 × *g* for 5 min, two washes and resuspension in distilled water to a concentration of 2×10^5 spores/mL. Conidia were inoculated on plastic cover slips (Menzel-Gläser) in a moist chamber at 24 °C and observed for appressorium formation and lipid droplets mobilization at intervals, by mounting directly in fresh BODIPY® (493/503) solution for 15 min. The stain was removed and replaced with water before observation.

Table 5.1 Primers used in this study to carry out targeted gene deletion of *CAR1, CAR2, CAR3, CAR4, ACS1, ACS2, ACS3* and *CRC* in Guy11

Primer	Sequence
BBD.F1	5’ AAAAGGGAGGCAGTGGTGG 3’
BBD.R1	5’ GTCGTGACTGGGAAAACCCTGGCGGGCGGTGTACTTTTCGGCA 3’
BBD.F2	5’ TCCTGTGTGAAATTGTTATCCGCTGGGTTAGAGACAGTCGGCA 3’
BBD.R2	5’ GGCTGTGGCTGTTAGTTGG 3’
HTMLA.F1	5’ ATGGCGAGGGGTACTACGA 3’
HTMLA.R1	5’ GTCGTGACTGGGAAAACCCTGGCGGGCAGGTAAGGTAGGTAGG 3’
HTMLA.F2	5’ TCCTGTGTGAAATTGTTATCCGCTACTTGGCGGTCCCTAATCG 3’
HTMLA.R2	5’ CAGGATGATGACGGGGAAC 3’
TMABADH.F1	5’ GAGGACTGTATGGGAGAGG 3’
TMABADH.R1	5’ GTCGTGACTGGGAAAACCCTGGCGTGGTGGACTGCCGACTCTT 3’
TMABADH.F2	5’ TCCTGTGTGAAATTGTTATCCGCTATTGGCTCTGGGGTGCGTT 3’
TMABADH.R2	5’ GTTGACCGACTACCGAAGC 3’
TMLD.F1	5’ AACAAAGCGACTGCCCAGG 3’
TMLD.R1	5’ GTCGTGACTGGGAAAACCCTGGCGCTGGCGTTCCGAATACCGA 3’
TMLD.F2	5’ TCCTGTGTGAAATTGTTATCCGCTTACTGCTGCGGGTGCTCTT 3’
TMLD.R2	5’ CTCGGTGTTGATGTAGCCC 3’
ACS1.F1	5’ TCAGCGGTAGGAAGGGAGT 3’
ACS1.R1	5’ GTCGTGACTGGGAAAACCCTGGCGCCGAGTGTAATCCCGTTCC 3’
ACS1.F2	5’ TCCTGTGTGAAATTGTTATCCGCTTAGTCTGAATGGGTTGTGGG 3’
ACS1.R2	5’ CTTTCTGCCATTCACCCGC 3’
ACS2.F1	5’ TGCGACTTACCTTGCCCCT 3’
ACS2.R1	5’ GTCGTGACTGGGAAAACCCTGGCGGGCTGAGGGAGACCGTTTA 3’
ACS2.F2.2	5’ TCCTGTGTGAAATTGTTATCCGCTGCTGGCGACCCTCAAGATA 3’
ACS2.R2.2	5’ AATGGCAGCAGGTGGTCAG 3’
ACS3.F1	5’ GGGAAGCCAGCCAGGATTA 3’
ACS3.R1	5’ GTCGTGACTGGGAAAACCCTGGCGGTAAGCCAGGTAGGGTAGG 3’
ACS3.F2	5’ TCCTGTGTGAAATTGTTATCCGCTCAGCACACAGCAATGACCG 3’
ACS3.R2	5’ GCTGGTCTCTCTCTCTCTC 3’
CRC.F1	5’ GACCGCCCTGACCTACTAT 3’
CRC.R1	5’ GTCGTGACTGGGAAAACCCTGGCGTGGGTTCGGGACAATGGAG 3’
CRC.F2	5’ TCCTGTGTGAAATTGTTATCCGCTGGCATCGTAGTAATCGGGC 3’
CRC.R2	5’ CACAGTCAGGCAGCAATGG 3’
M13F	5’ CGCCAGGGTTTTCCCAGTCACGAC 3’
M13R	5’ AGCGGATAACAATTTCACACAGGA 3’
HY Split	5’ GGATGCCTCCGCTCGAAGTA 3’
YG Split	5’ CGTTGCAAGACCTGCCTGAA 3’

Table 5.1 Primers used in this study to carry out targeted gene deletion of *CAR1, CAR2, CAR3, CAR4, ACS1, ACS2, ACS3* and *CRC* in Guy11

Primer	Sequence
BBD.F1	5’ AAAAGGGAGGCAGTGGTGG 3’
pTMLD.F1	5’ CAGTCCTGTCAAGCCACCT 3’
pTMLD.R1	5’ AGTGTGTATTGCGGATTGGG 3’
pTMABADH.F1	5’ TCAACTTTCCGCCCCCAAC 3’
pTMABADH.R1	5’ AGGACCTTTTCGTACTGTGC 3’
pACS2.F1	5’ CCCCGATGGAGACTCTGAA 3’
pACS2.R1	5’ GAGTTCCTACGGGCTTTCC 3’
pCRC.F1	5’ CAGCATCTTCGCAACAGGG 3’
pCRC.R1	5’ CACCCAAAAACGTCGCAGC 3’

5.3 Results

5.3.1 Importance of carnitine acetyl transferases (CATs) in plant infection development

Previous studies have shown that CATs play an important role in infection-related development of *M. oryzae* (Bhambra et al., 2006). *MoPTH2* was shown to be localised to the peroxisome and Δ*pth2* mutants were reduced in conidiation, able to generate turgor and penetrate the plant cuticle but unable to cause rice blast disease (Bhambra et al., 2006). The authors showed that even though Δ*pth2* mutants are able to penetrate the leaf cuticle, the growth of penetration hyphae is impaired, such that the mutant cannot penetrate neighbouring rice cells. They reasoned that this is due to deficiency of chitin in the fungal cell wall, as chitin synthesis requires acetyl-CoA (Bhambra et al., 2006). Deletion of *PTH2* clearly disrupts the acetyl-CoA pool and its distribution in the fungus, may affect chitin synthesis.

In order to provide more insight into the role of *PTH2* during infection-related development, I decided to investigate further the relationship between CAT activity and the ability of the fungus to cause disease. To do this, I focused on two processes that have been shown to be necessary for successful infection. Autophagy is a catabolic process where cells degrade their own components through the vacuolar or lysosomal machinery and involved in nutrient recycling during starvation and normal developmental processes (Klionsky et al., 2007). An increasing body of evidence has implicated autophagy in the infection of plants by disease-causing fungi. In *M. oryzae*, it was shown that an autophagy mutant *ATG8*, failed to undergo death of the spore, and that programmed cell death is necessary for the generation of an appressorium with the capacity to infect the host plant (Veneault-Fourrey et al., 2006). Atg8 has been shown to be a reliable marker for autophagy so a *GFP:MoATG* strain was generated in order to

track autophagy in *M. oryzae* during a time course corresponding with plant infection (Kershaw and Talbot, 2009). A large burst of autophagic activity was observed in conidia prior to germination, and continued as the appressorium developed. Autophagosomes were abundant in conidia until the point where cells started to undergo cell death. However, autophagy also occurred in the appressorium as it developed (Kershaw and Talbot, 2009). To determine the relationship between autophagy and acetyl-CoA translocation, a *GFP:ATG8* construct was transformed into Guy11 and Δ*pth2* mutants. In both the wild type strain and the Δ*pth2* mutant autophagosomes were observed in conidia prior to germination and were seen to accumulate throughout germination, with numbers of autophagosomes decreasing steadily until a time corresponding to conidial cell death. Autophagy also occurred in the appressorium and increased steadily during early development of appressoria and as the appressorium matured. The numbers of autophagosomes in conidia and appressoria of the Δ*pth2* mutant throughout the timecourse of infection-related development, over a period of 24 h was similar to those seen in the wild type, suggesting that autophagic processes were not affected by loss of Pth2 (Figure 5.3).

Actin is an abundant, highly conserved protein polymer found in all eukaryotes and plays crucial roles in exocytosis, endocytosis, organelle movement and cytokinesis in fungi (Berepiki et al., 2011) and has been shown to be vital for fungal growth (Czymmek et al., 2005). During plant infection *M. oryzae* undergoes a switch back to polar growth at the point of penetration peg formation. Associated with this is the formation of an actin ring or toroidal network around the appressorium pore (Y. F. Dagdas, personal communication). To understand the role of Pth2 in actin accumulation and distribution, an actin-tagging construct, Lifeact:RFP (Lichius and Read, 2010) was obtained and transformed into Guy11 and Δ*pth2* mutants. Lifeact is a 17 amino acids

peptide derived from the actin-binding protein 140 (Abp140) of *S. cerevisiae* which specifically binds to filamentous actin (F-actin) (Riedl et al., 2008). Figure 5.4 shows distribution of actin in both the wild type, Guy11 and the Δ*pth2* mutant after inoculation on glass cover slip over a period of 48 h. Our observation revealed differences in actin distribution between Guy11 and Δ*pth2* mutants. In the Guy11 wild type strain after 24 h, an actin ring was clearly seen to form around the appressorium pore around the central vacuole at the base of the appressorium, corresponding to the point of penetration peg formation. However, in the Δ*pth2* mutant, F-actin localisation was observed as diffuse filaments throughout the appressorium. No clear ring or network was ever observed. This mislocalisation of actin was also observed after both 30 h and 48 h (Figure 5.4). This suggests that *PTH2* may have a role in the normal distribution of actin during appressorium maturation and may help to explain the infection deficient phenotype of the Δ*pth2* mutant.

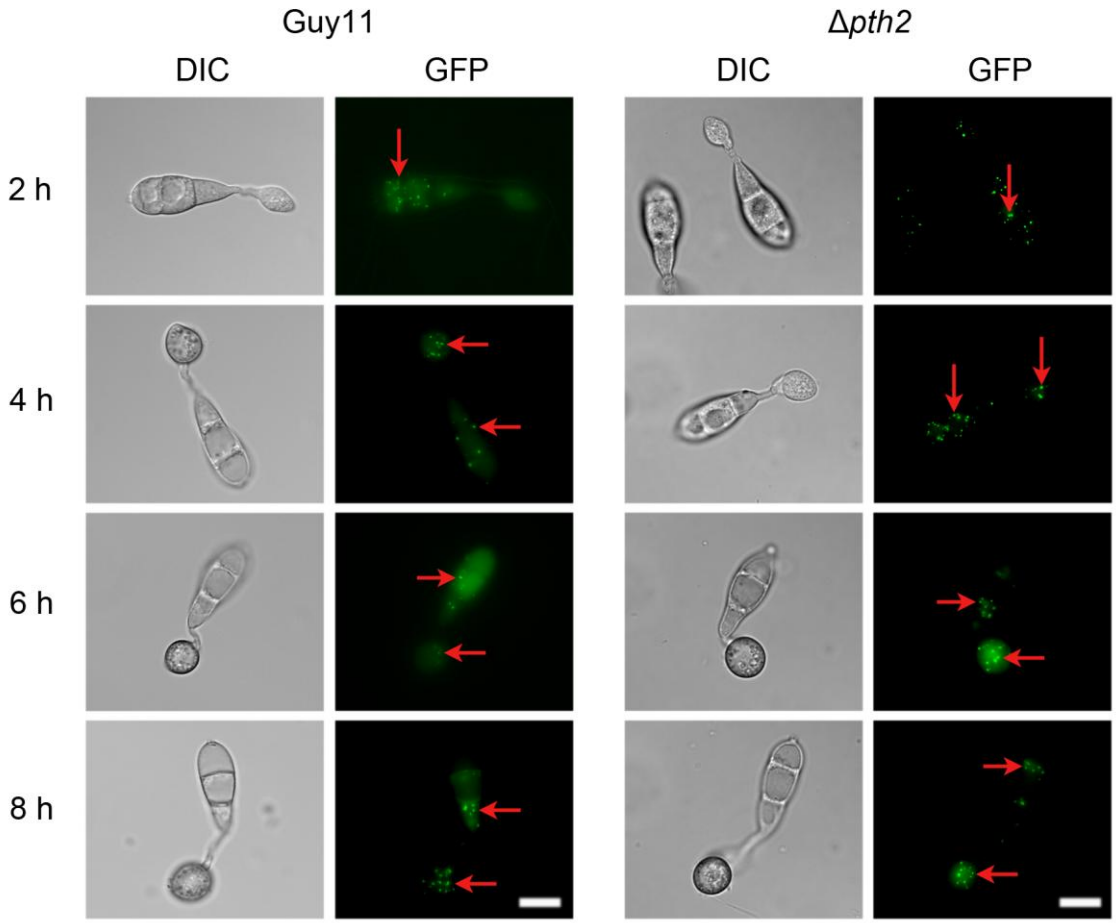

Figure 5.3 Cellular localisation of autophagosomes during infection-related development of *M. oryzae*.

Conidia were harvested from Guy11 and a Δ*pth2* transformant expressing a *GFP:ATG8* gene fusion (Kershaw and Talbot, 2009), inoculated onto glass coverslips and observed by epifluorescence microscopy at the times indicated. Autophagosomes are shown to have a similar localisation pattern in the Δ*pth2* mutants as compared to Guy11 (Scale bar = 10 µm).

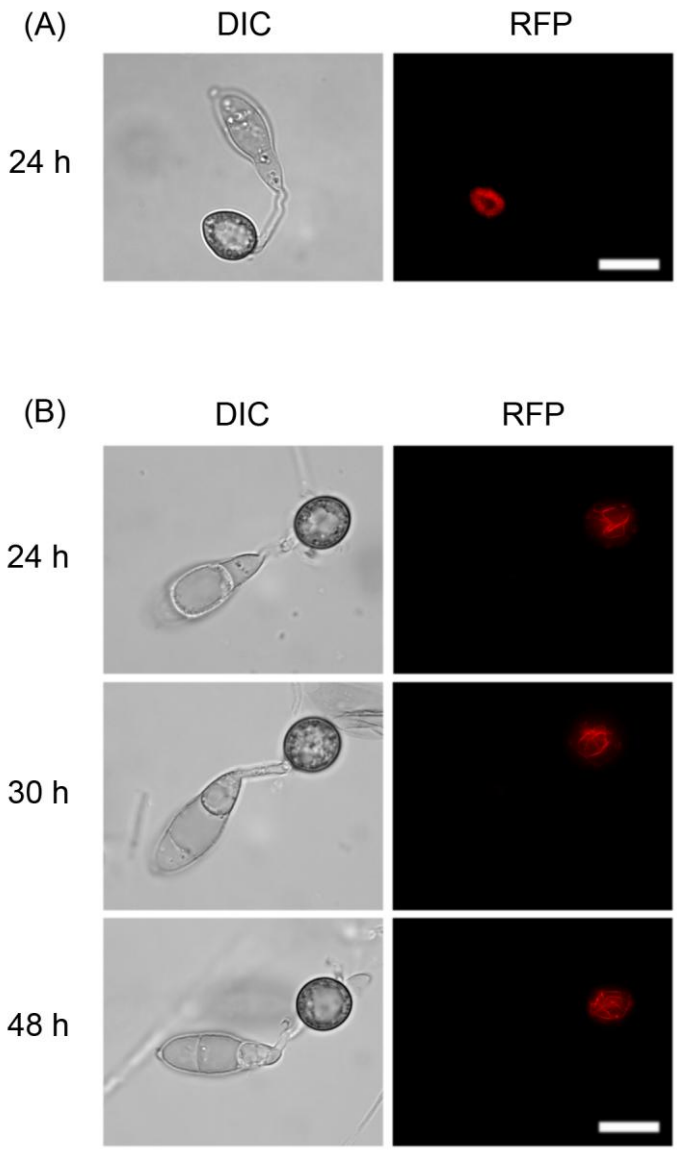

Figure 5.4 Live cell imaging to show cellular localisation of actin in Guy11 and Δ*pth2* mutants.

Conidia were harvested from Guy11 expressing a *Lifeact:RFP* fusion, inoculated onto glass coverslips and observed by epifluorescence microscopy. (A) Actin distribution in Guy11 after 24 h. (B) Actin distribution in a Δ*pth2* mutant at 24 h, 30 h and 48 h. Scale bar = 10 µm.

5.3.2 Carnitine biosynthesis and its importance in plant infection development.

5.3.2.1 Identification of genes involved in carntine biosynthesis in *M. oryzae*

Carnitine biosynthesis has recently been described in *Candida albicans* in a pathway involving 4 genes; *orf19.4316*, *orf19.6305*, *orf19.6306* and *orf19.7131* which encode trimethyllysine dioxygenase (*TMLD*), hydroxymethyllysine aldolase (*HTMLA*), trimethylaminobutyraldehyde dehydrogenase (*TMABADH*) and butyrobetaine dioxygenase (*BBD*) respectively (Strijbis et al., 2009) (Figure 5.2). Identification of genes involved in carnitine biosynthesis in *M. oryzae* was performed using the BLAST server at the Magnaporthe genome database (http://www.broadinstitute.org/). Amino acid sequences of *C. albicans TMLD*, *HTMLA*, *TMABADH* and *BBD* genes were used as queries. The top hits of each gene were then selected for further analysis; MGG_07454.6 (*TMLD*), MGG_11389.6 (*HTMLA*), MGG_05008.6 (*TMABADH*) and MGG_09250.6 (*BBD*).

The four genes were then re-named *CAR1* (*TMLD*), *CAR2* (*HTMLA*), *CAR3* (*TMABADH*) and *CAR4* (*BBD*). *CAR1* shares 37% amino acid identity to the *C. albicans TMLD* and possesses a taurine catabolism dioxygenase domain (TauD) (amino acids 93-367) (Figure 5.5). *CAR2* shares 46% amino acid identity to the *C. albicans HTMLA* and possesses a beta-eliminating lyase domain (amino acids 28-322) (Figure 5.6). *CAR3* shares 54% amino acid identity to the *C. albicans TMABADH* and possesses an aldehyde dehydrogenase family domain (amino acids 25-489) as shown in Figure 5.7. *CAR4* shares 33% amino acid identity to the *C. albicans BBD* and possesses an unknown protein domain (amino acids 135-214) and a TauD domain (amino acids 240-507) (Figure 5.8).

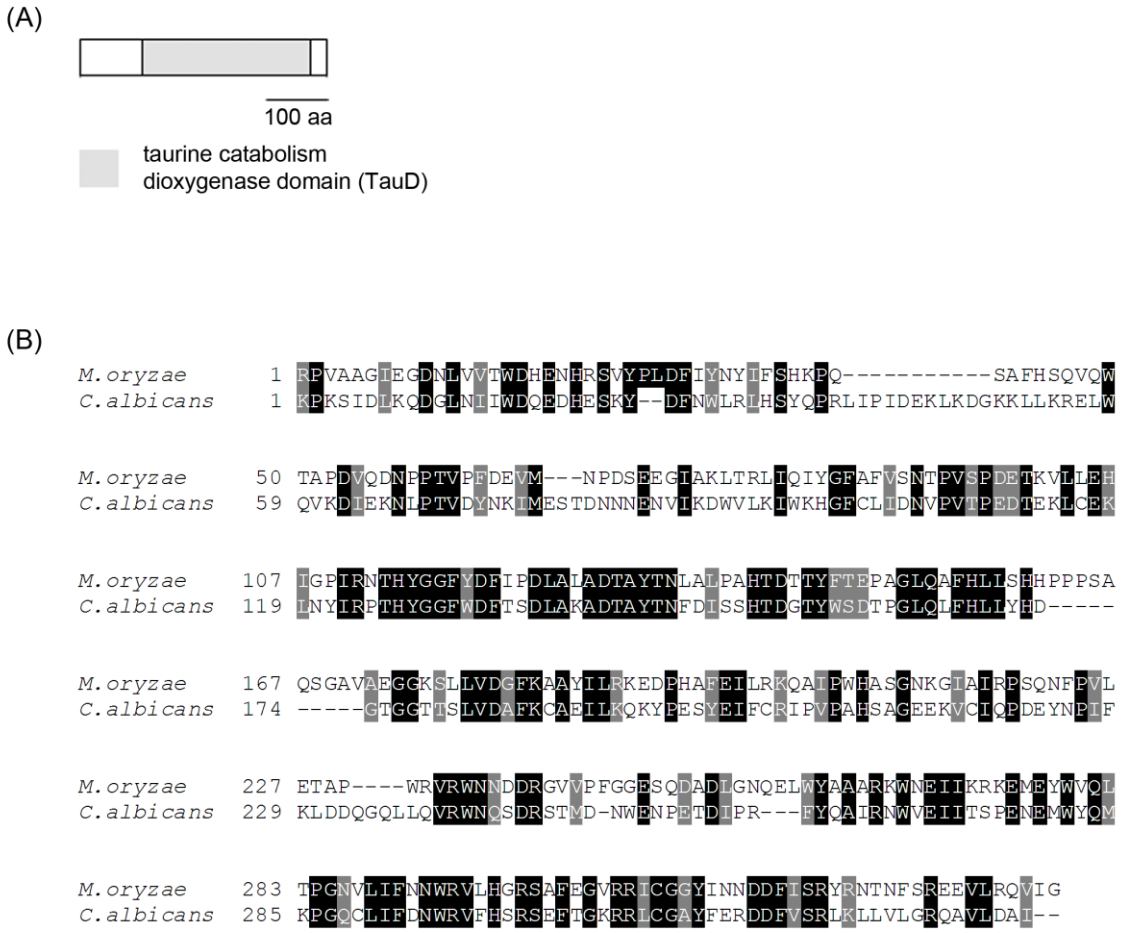

Figure 5.5 Alignment of the predicted amino acid sequence of *CAR1* with *C. albicans TMLD*-encoding genes and the structural motifs of the protein.

(A) Diagram showing protein domains of the *MoCAR1* gene product. MoCar1 has 393 amino acids and possesses a taurine catabolism dioxygenase domain (TauD) (Eichhorn et al., 1997). (B) Predicted amino acid sequence of the *M. oryzae CAR1* was aligned with *C. albicans* TMLD (orf19.4316) using the program CLUSTALW (Thompson et al., 1994). *CAR1* shows 37% amino acid identity to *C. albicans TMLD*. Identical amino acids are highlighted on a black background and similar amino acids on a grey background. Scale bar = 100 amino acid.

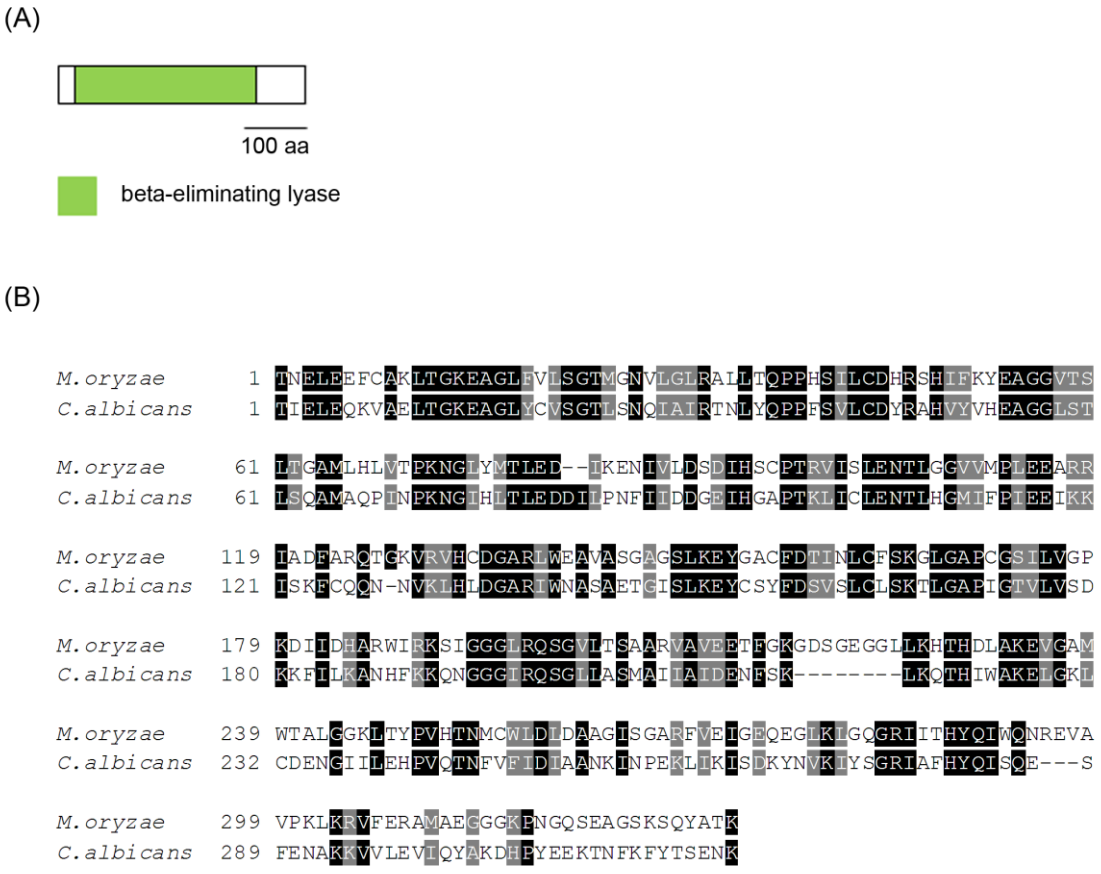

Figure 5.6 Alignment of the predicted amino acid sequence of *CAR2* with *C. albicans HTMLA*-encoding genes and the structural motifs of the protein.

(A) Diagram showing beta-eliminating lyase protein domain (Isupov et al., 1998) in *MoCAR2*. *MoCAR2* has 392 amino acids. (B) Predicted amino acid sequence of the *M. oryzae CAR2* was aligned with *C. albicans* HTMLA (orf19.6305) using the program CLUSTALW (Thompson et al., 1994). *CAR1* shows 46% amino acid identity to *C. albicans HTMLA*. Identical amino acids are highlighted on a black background and similar amino acids on a grey background. Scale bar = 100 amino acid.

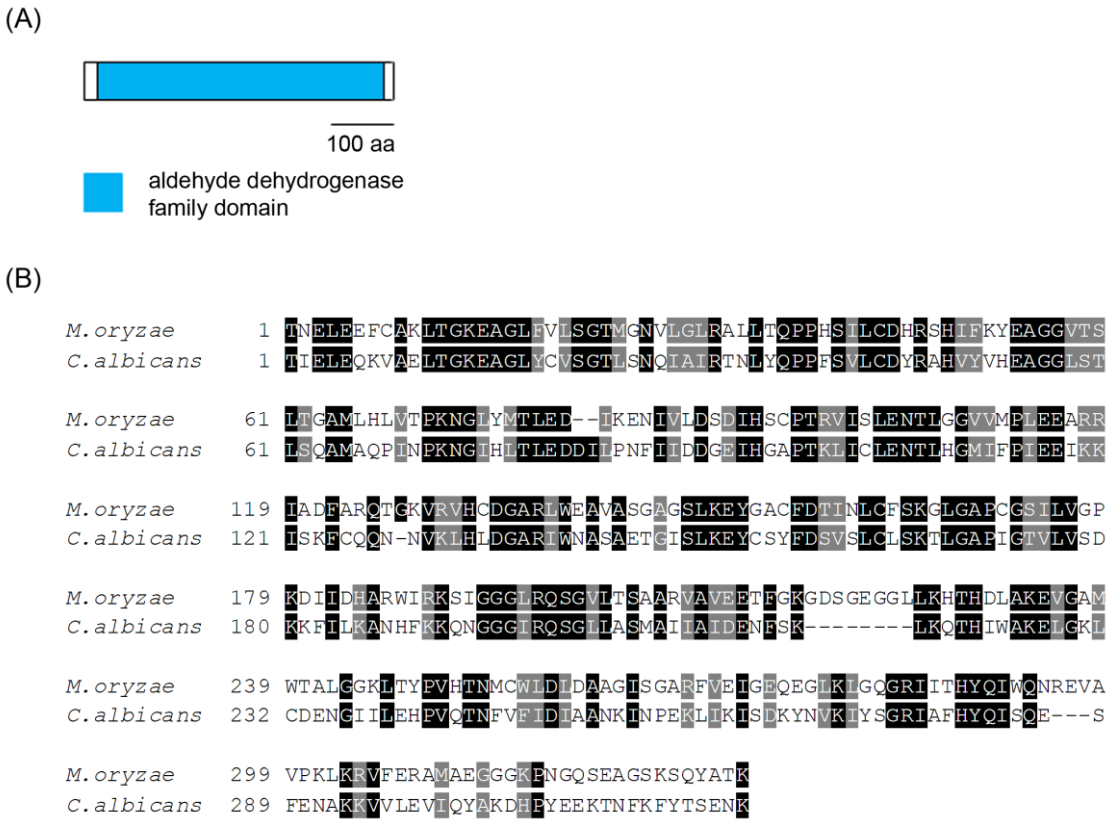

Figure 5.7 Alignment of the predicted amino acid sequence of *CAR3* with *C. albicans TMABADH*-encoding genes and the structural motifs of the protein.

(A) Diagram showing protein domain in *MoCAR3*. *MoCAR3* has 497 amino acids and possessed only an aldehyde dehydrogenase family domain (Steinmetz et al., 1997). (B) Predicted amino acid sequence of the *M. oryzae CAR3* was aligned with *C. albicans* TMABADH (orf19.6306) using the program CLUSTALW (Thompson et al., 1994). *CAR3* shows 54% amino acid identity to *C. albicans TMABADH*. Identical amino acids are highlighted on a black background and similar amino acids on a grey background. Scale bar = 100 amino acid.

(A)

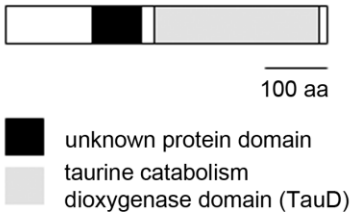

(B)

```
M.oryzae      1 LLRAQTRLPYARSRVAVVPPAPASRFITQRSATGNYGCNRSYSQPAAQTQAAAAGAAAAS
C.albicans    1 MLRQPLRQIRFHSKLAL-------------------------------------------

M.oryzae     61 GTPEHHHAAPGPLAAAWDSGSRTLAVRFNDGLETPLSKLWLRDSCRCSACVDSSSGQKNF
C.albicans   18 ------------AGYNSKEVTVTI---NGRTCTFNNVFLRDACQSPDSVDPISSQKLF

M.oryzae    121 ETCDVPSSLRVRKVGVAADGESVQVVWGDDFLTGGQQSHASVYPASFIQS-----ALDRP
C.albicans   61 TTADAATGLQINAPPVVEDS-SLKLQWSNN----GKLIN-SVYPVSFLENYSTNKRLGKF

M.oryzae    176 KPKDDVVRHTTWDKASFEKQVRFI--PYSPWIKGEGEVFWRGFLDLARLGLVFIKDVPES
C.albicans  115 FDKD----RKLWDKQELENNFASINMDYDDIITNDNS-FFQTLYNLNRYGLTFVNNIPTP

M.oryzae    234 ETA----------VEEMACAVGHAQTTFYGKTWDVVSKPQ-AENVAYTNVFLCLHQDLL
C.albicans  170 QISDMTEDNATQWPVYKIAEKFGYIKKTFYGTLFDVKNKKEKATNIAYTNTFLPLHMDLL

M.oryzae    282 YMQDPPRLQLLHCLANSCEGGESLFSDGIRAAEQVRSKNPKQFELLKNKPVYYHYDKNGH
C.albicans  230 YYESPPGLQLLHAIQNSTLGGENTFCDSYLAAEHVRKTDPRAYTALTQTPITFHYDNNNE

M.oryzae    342 WYEYNRPVVTLSK---DGSGAIDSIGWSPPFQDNFPAPQGLSASINSQDALEEWRAAARS
C.albicans  290 YYYYKRPLIVEDPEVGDGFPKIASINYAPPFQGPFEV----------DPHPDFIRGMQL

M.oryzae    399 FRDSSTAPESMFEYKMKPGECAIFDNMRILHGRRQF-QLTSGKRWLKGTYVGEQVLRSKL
C.albicans  339 FETFINDPANHFEIKMPEGTCVIFENRRALHSRNAFSDSNNGDRWLMGTYVDGDSFRSKL

M.oryzae    458 AQTPPHLRPE
C.albicans  399 RIGYRKVHT-
```

Figure 5.8 Alignment of the predicted amino acid sequence of *CAR4* with *C. albicans BBD*-encoding genes and the structural motifs of the protein.

(A) Diagram showing protein domains in *MoCAR4*. *MoCAR4* has 527 amino acids and possessed an unknown protein domain and a taurine catabolism dioxygenase (TauD) domain (Eichhorn et al., 1997). (B) Predicted amino acid sequence of the *M. oryzae CAR4* was aligned with *C. albicans* BBD (orf19.7131) using the program CLUSTALW (Thompson et al., 1994). *CAR4* shows 33% amino acid identity to *C. albicans BBD*. Identical amino acids are highlighted on a black background and similar amino acids on a grey background. Scale bar = 100 amino acid.

5.3.2.2 Targeted gene deletion of genes encoding carnitine biosynthesis enzymes.

In order to determine the role of carnitine in infection-related development in *M. oryzae*, targeted deletion of *CAR1, CAR2, CAR3* and *CAR4* was carried out to generate four mutants each lacking one of the genes required for carnitine synthesis. The targeted gene deletion constructs were generated by the split-marker strategy, as described in Section 2.11. These constructs were transformed into Guy11 and transformants selected based on their resistance to hygromycin B. Genomic DNA of putative transformants was extracted and digested with either *Sac*I (*CAR1* and *CAR3*) or *Xho*I (*CAR2* and *CAR4*) before being fractionated by gel electrophoresis. The fractionated genomic DNA was then transferred onto Hybond-N. In the case of *CAR1* and *CAR3* transformants, DNA was probed with fragments corresponding to the deleted open reading frame, in order to look for the presence or absence of the targeted sequence. *CAR1* putative transformants were probed with 1 kb of the open reading frame fragment generated by PCR using primers pTMLD.F1 and pTMLD.R1. After digestion with *Sac*I, a 10.8 kb hybridizing fragment was predicted to be present in the parental, Δ*ku70* strain (Kershaw and Talbot, 2009). No fragment was expected to be present in corresponding null mutants. The results of Southern blot analysis for *CAR1*, are shown in Figure 5.9. The results showed the 10.8 kb fragment was absent from all putative transformants of *CAR1*, confirming targeted deletion of *CAR1*, and Δ*car1* transformants were therefore selected for further analysis.

CAR3 putative transformants were probed with a 1 kb open reading frame fragment generated by PCR using primers pTMABADH.F1 and pTMABADH.R1. After digestion with *Sac*I an 8 kb fragment was predicted to be present in the wild type and no fragment was expected to be present in the corresponding null mutant. The results for Southern blot analysis for *CAR3* (Figure 5.10) show that the 8 kb fragment was absent

from all the putative transformants of *CAR3* and present only in recipient Δ*ku70* strain. This confirmed the targeted deletion of *CAR3* and positive Δ*car3* transformants were selected for further analysis.

For *CAR2* and *CAR4*, fragments upstream of the targeted genes locus were used to probe transformant DNA in order to screen for positive transformants based upon size difference, after digestion with *Xho*I.

CAR2 putative transformants were probed with a 1.5 kb fragment upstream of the targeted gene locus, previously generated for the gene deletion construct. Following replacement of the native coding sequence with the hygromycin resistance gene cassette, a size difference in the locus was generated. Figure 5.11 shows the size of the hybridizing restriction fragment observed in the wild type, Δ*ku70* (1.9 kb) and in the putative *CAR2* mutants (2.9 kb). The presence of the 2.9 kb fragments in lanes 1, 2 and 3 confirmed the targeted deletion of *CAR2* and the positive Δ*car2* transformants were selected for further analysis.

CAR4 putative transformants were probed with the 1.4 kb fragment upstream of the targeted gene locus, previously generated for the gene deletion construct. Figure 5.12 shows the size of the hybridizing restriction fragment observed in the wild type, Δ*ku70* (6.4 kb) and in the putative *CAR4* mutants (8.4 kb). The presence of the 8.4 kb fragment in lanes 1 and 3 confirmed the targeted deletion of *CAR4*. An unknown hybridizing restricted fragment was also observed in lane 2, suggesting the occurrence of ectopic insertion. The positive Δ*car4* transformants were selected for further analysis.

(A)

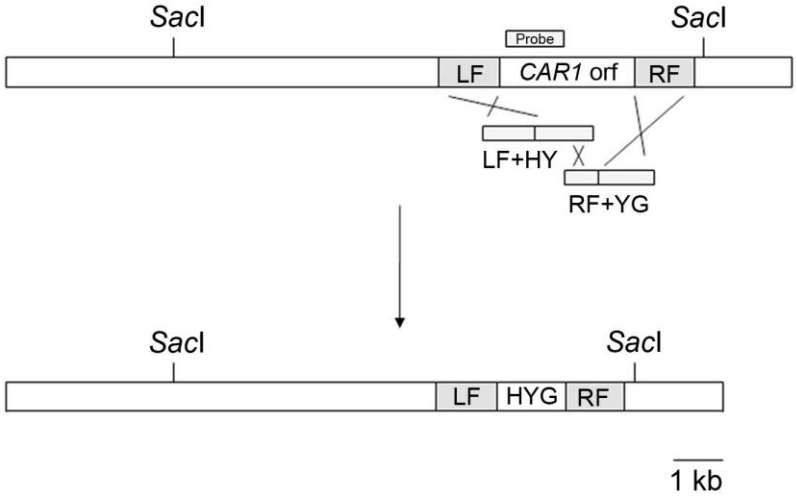

(B)

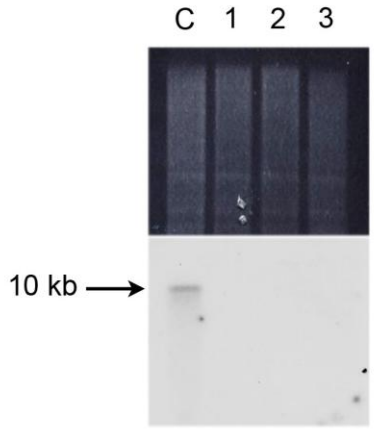

Figure 5.9 A schematic representation of the targeted deletion of *CAR1* by the split-marker deletion method.

(A) Diagram describing the targeted gene deletion of *CAR1*. (B) (B) Genomic DNA was restriction digested with *Sac*I, fractionated by gel electrophoresis and transferred to Hybond-N. The Southern blot was subsequently probed with a 1 kb fragment from the *CAR1* locus. The absence of the hybridising fragment reveals a correctly targeted deletion. The putative transformants in lanes 1, 2 and 3 are confirmed as Δ*car1* mutants. C: Wild type control, Δ*ku70*. Scale bar = 1 kb.

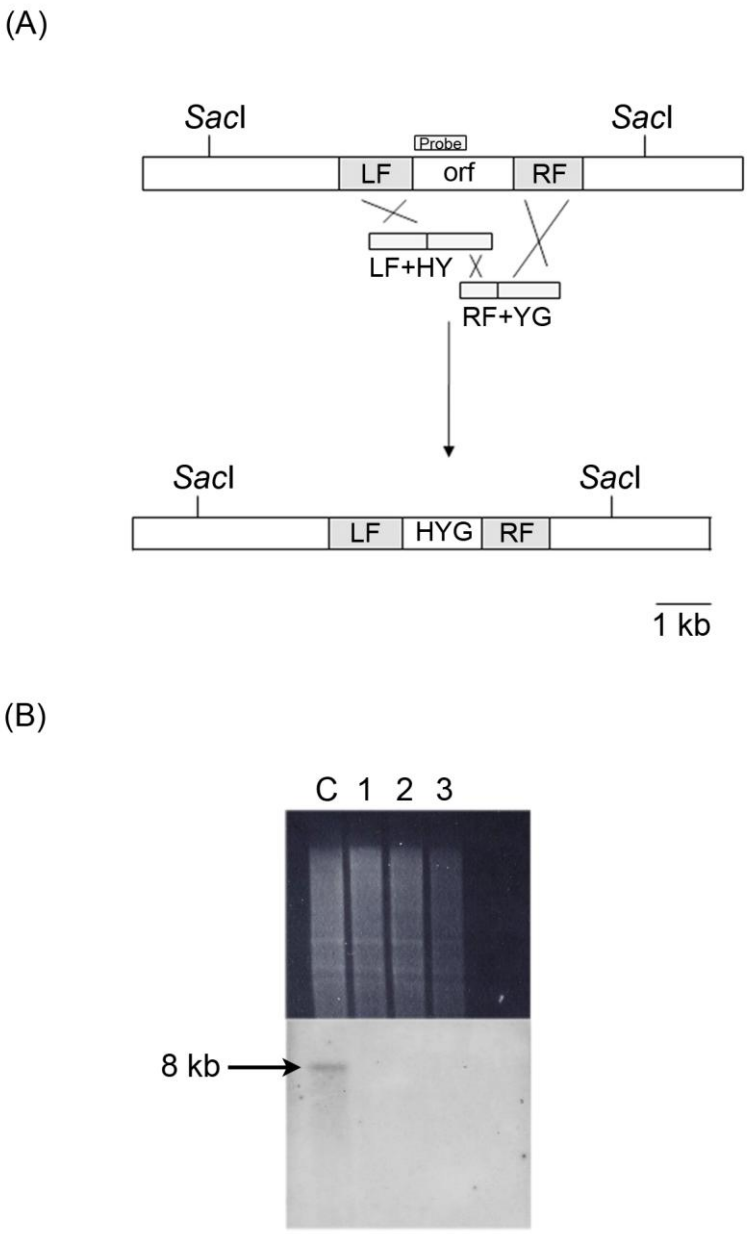

Figure 5.10 A schematic representation of the targeted deletion of *CAR3* by the split-marker deletion method.

(A) Diagram describing the targeted gene deletion of *CAR3*. (B) Genomic DNA was restriction digested with *Sac*I, fractionated by gel electrophoresis and transferred to Hybond-N. The Southern blot was subsequently probed with a 1 kb fragment from the *CAR3* locus. The absence of the hybridising fragment reveals a correctly targeted deletion. The putative transformants in lanes 1, 2 and 3 are confirmed as Δ*car3* mutants. C: Wild type control, Δ*ku70*. Scale bar = 1 kb.

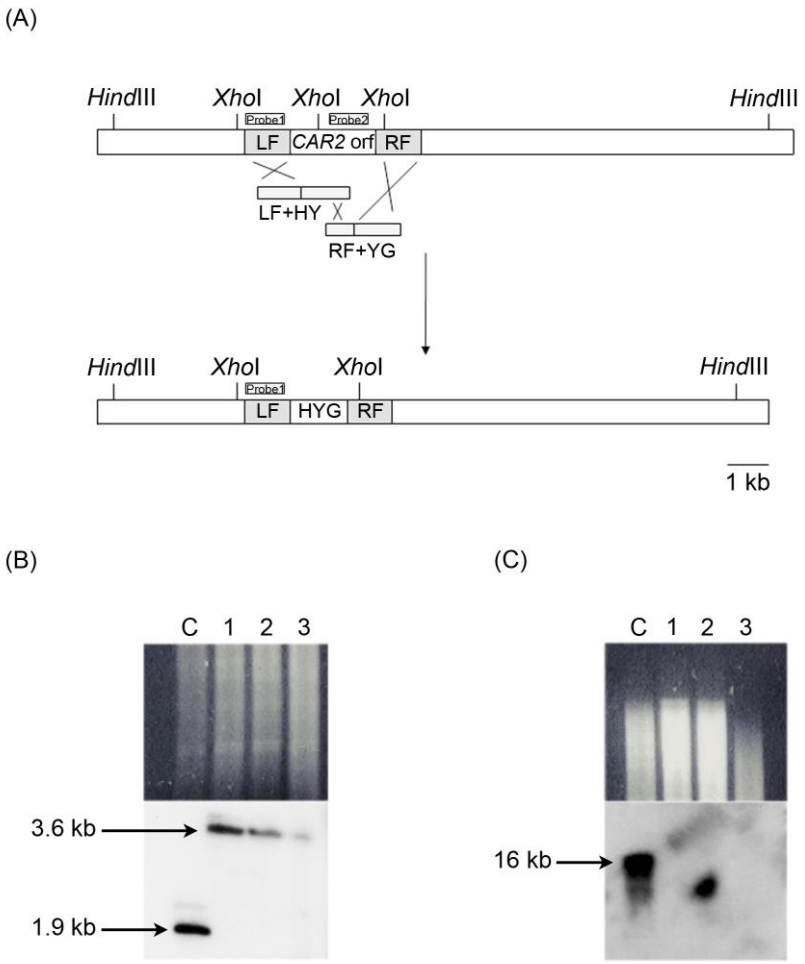

Figure 5.11 A schematic representation of the targeted deletion of *CAR2* by the split-marker deletion method.

(A) Diagram describing the targeted gene deletion of *CAR2*. (B) Genomic DNA was restriction digested with *Xho*I, and the Southern blot was probed with a 1.5 kb genomic fragment upstream of the *CAR2* coding region. The probe hybridised to a 1.9 kb fragment from *Xho*I digested Δ*ku70* and to a 3.6 kb fragment from Δ*car2* mutants. (C) Genomic DNA was restriction digested with *Hin*dIII, fractionated by gel electrophoresis and transferred to Hybond-N. The Southern blot was subsequently probed with a 1 kb fragment from the *CAR2* locus. The absence of the hybridising fragment reveals a correctly targeted deletion. The putative transformants in lanes 1, 2 and 3 are confirmed as Δ*car2* mutants. C: Wild type control, Δ*ku70*. Scale bar = 1 kb.

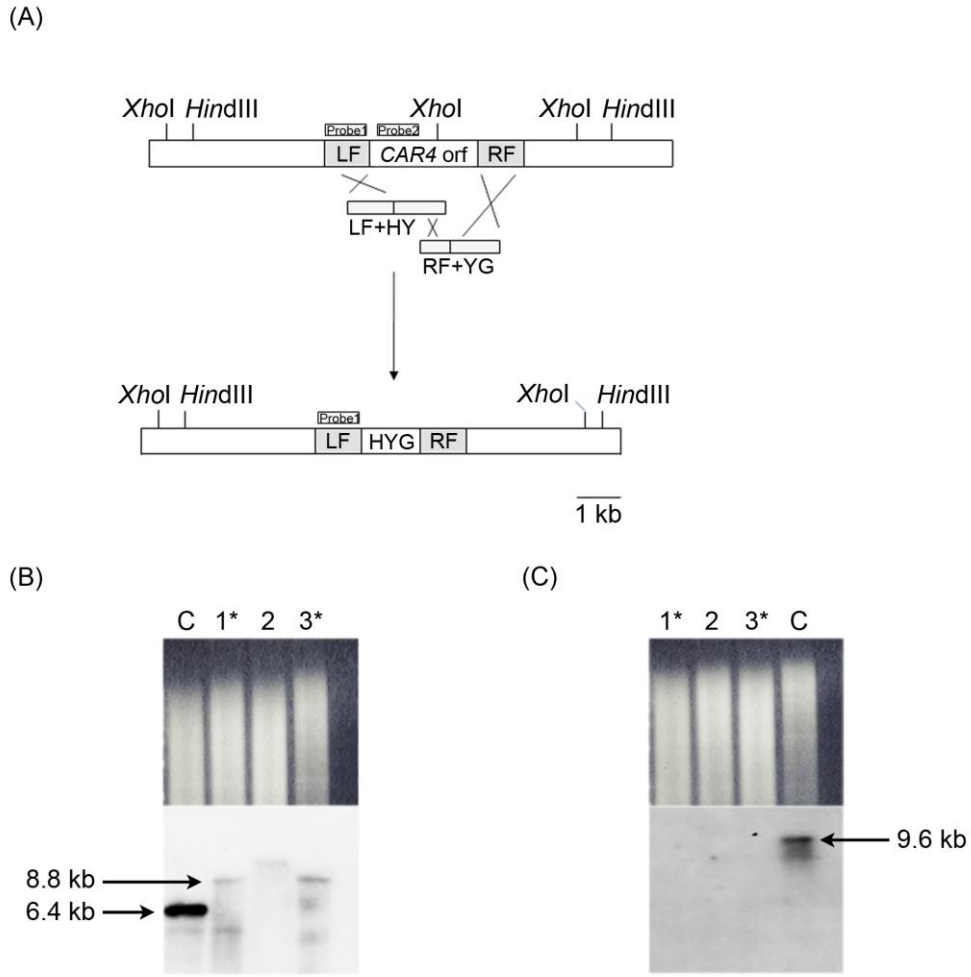

Figure 5.12 A schematic representation of the targeted deletion of *CAR4* by the split-marker deletion method.

(A) Diagram describing the targeted gene deletion of *CAR4*. (B) Genomic DNA was restriction digested with *Xho*I, and the Southern blot was probed with a 1.5 kb genomic fragment upstream of the *CAR4* coding region. The probe hybridised to a 6.4 kb fragment from *Xho*I digested Δ*ku70* and to a 8.8 kb fragment from Δ*car4* mutants. (C) Genomic DNA was restriction digested with *Hin*dIII, fractionated by gel electrophoresis and transferred to Hybond-N. The Southern blot was subsequently probed with a 1 kb fragment from the *CAR4* locus. The absence of the hybridising fragment reveals a correctly targeted deletion. The putative transformants in lanes 1 and 3 are confirmed as Δ*car4* mutants. C: Wild type control, Δ*ku70*. Scale bar = 1 kb.

5.3.2.3 Expression profile, carbon utilisation and pathogenicity of carnitine biosynthesis mutants.

The expression profile of *CAR1*, *CAR2*, and *CAR4* was examined throughout appressorium development by HT-SuperSAGE analysis (Figure 5.13) (Soanes et al., 2012). In this method, levels of transcript abundance for any gene are estimated by measuring the frequency of 26 base tags sequenced from mRNA extracted from different time points during appressorium maturation (Matsumura et al., 2010). Expression levels are compared to those obtained from mycelium grown in CM as a control. *CAR1* was expressed at a similar level to the mycelium grown on CM, while *CAR2* was expressed at a low level throughout appressorium development. By contrast, *CAR4* was highly expressed at the initial stages of appressorium development (4, 6 h) and reduced steadily in expression throughout appressorium maturation (14, 16 h). I was unable to include the expression profile of *CAR3* in the heatmap because we could not detect the expression of *CAR3* at the 4 h time point.

Because carnitine is involved in acetyl-CoA translocation, it was decided to test the ability of the carnitine biosynthesis mutants to utilise various carbon sources, Δ*car1*, Δ*car2*, Δ*car3* and Δ*car4* mutants were grown on minimal medium supplemented with different carbon sources (50 mM glucose, 50 mM acetate, 50 mM oleic acid or 50 mM triolein) and the growth of the mutants was observed after 14 days (Figure 5.14). The results show that Δ*car1* and Δ*car4* mutants were unable to grow on minimal medium with either acetate, oleic acid or triolein as the sole carbon source, suggesting that Δ*car1* and Δ*car4* mutants cannot utilise these alternative carbon sources. However, Δ*car2* and Δ*car3* mutants were still able to grow minimal medium with either acetate, oleic acid or triolein as the sole carbon source. This is surprising given that all four enzymes are part of the carnitine biosynthetic pathway and suggests that there might be alternative

enzymatic means of overcoming loss of *CAR2* and *CAR3* and therefore another pathway that contributes to production of 4-trimethyl-aminobutyraldehyde and γ-butyrobetaine in *M. oryzae*.

To investigate the role of the carnitine biosynthesis mutants in rice blast disease, conidia from Δ*car1*, Δ*car2*, Δ*car3* and Δ*car4* were spray-inoculated onto 3 week-old seedlings of the susceptible rice cultivar CO-39. Leaves inoculated with either Δ*car1*, Δ*car2*, Δ*car3* or Δ*car4* mutants all developed small necrotic lesions 3 days after inoculation and by 5 days symptom development was severe. The timing and level of infection was similar to that observed on leaves inoculated with the wild type strain, Guy11 (Figure 5.15).

The inability of Δ*car1* and Δ*car4* mutants to utilise alternative carbon sources was a phenotype similar to other observed in the Δ*pth2* mutant (Bhambra et al., 2006). However in contrast to Δ*pth2* which was unable to cause disease, Δ*car1* and Δ*car4* mutants were still fully pathogenic.

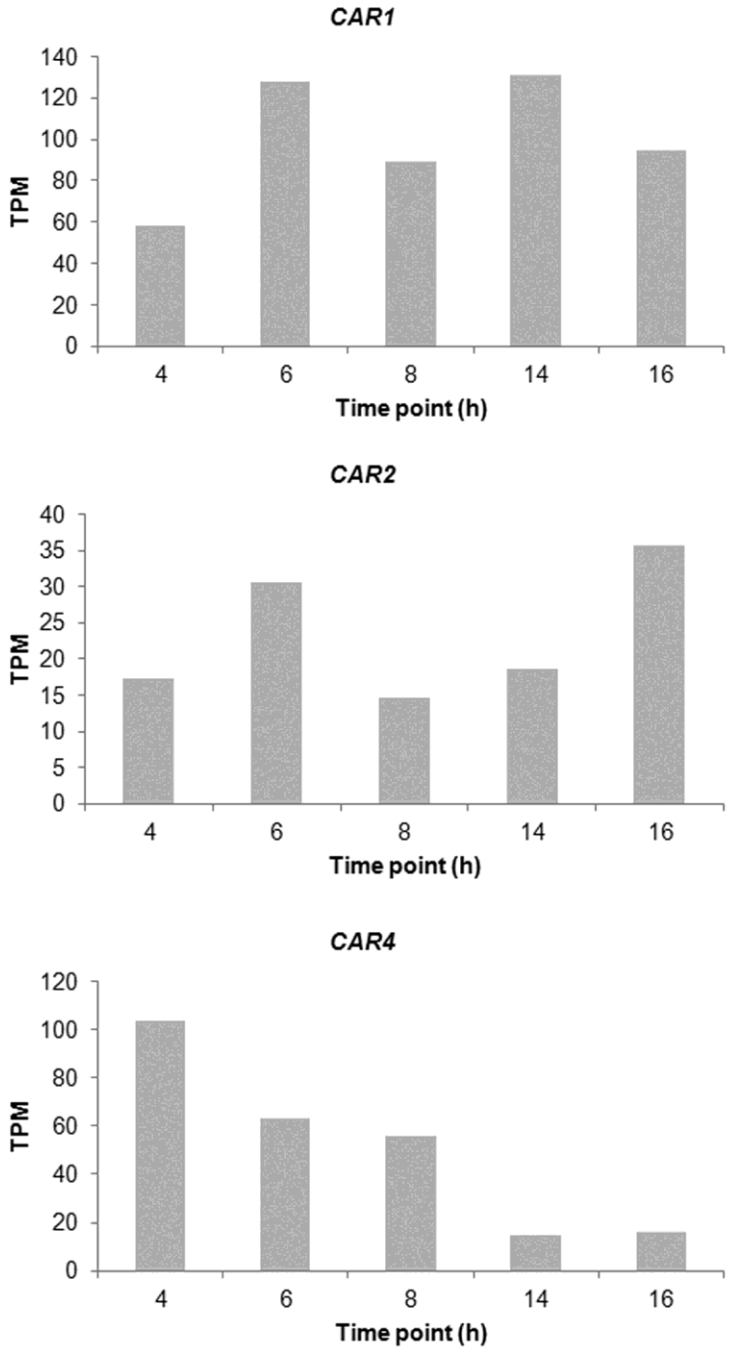

Figure 5.13 Expression profile produced from HT-SuperSAGE analysis of the wild type Guy11.

The heat map describes the relative expression profile of *CAR1*, *CAR2* and *CAR4* throughout appressorium development as compared to Guy11 mycelium grown in CM. The result is based on pool data from two biological replicates.

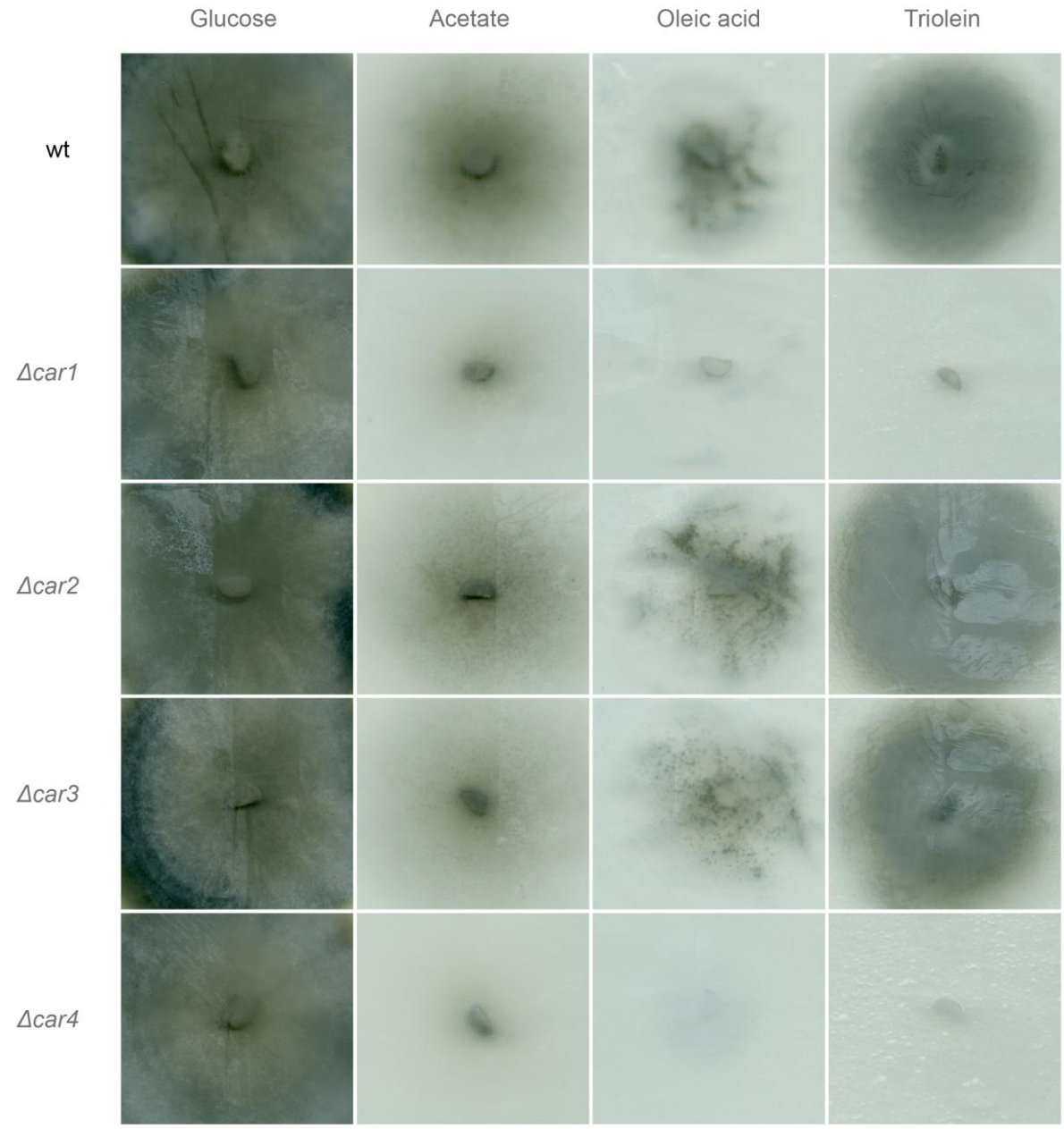

Figure 5.14 Vegetative growth of Guy11, Δ*car1*, Δ*car2*, Δ*car3* and Δ*car4* mutants on a range of different carbon sources.

The fungal strains were inoculated onto minimal medium supplemented with glucose, acetate, oleic acid or triolein and incubated at 24 °C for 14 days. Both Δ*car1* and Δ*car4* mutants were unable to utilise acetate and lipid as sole carbon source which is expected from the mutants. However, both Δ*car2* and Δ*car3* mutants were still able to grow on acetate and lipid.

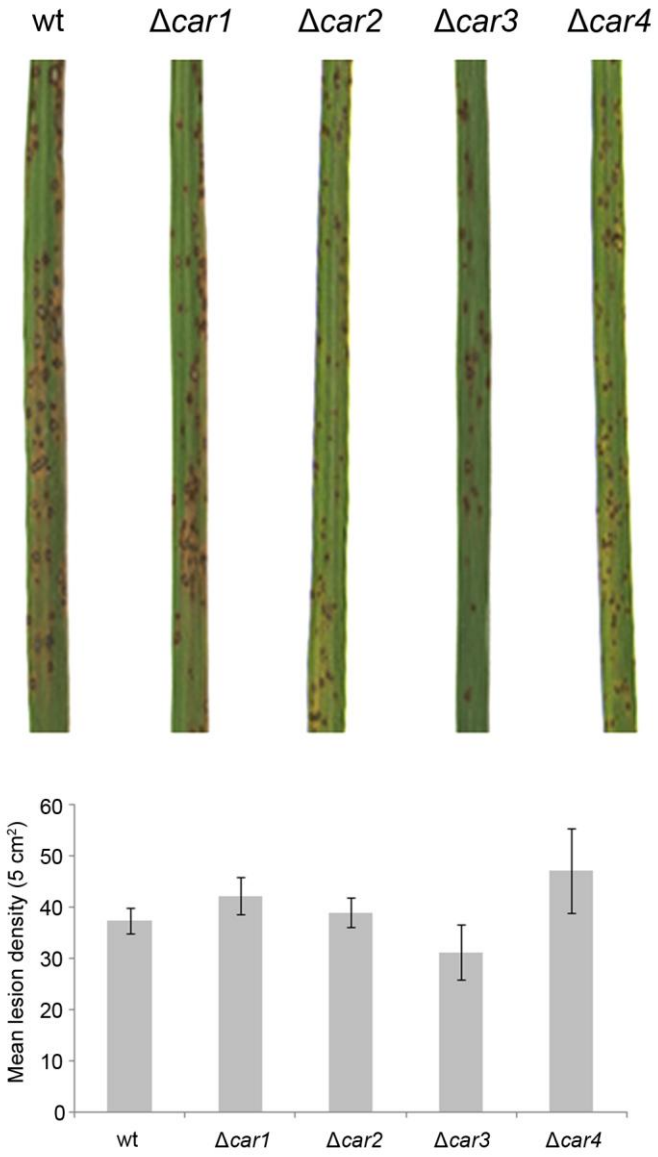

Figure 5.15 Plant pathogenicity assay on rice cultivar CO-39.

Conidial suspension from each fungal strain was spray inoculated onto 3 week old rice seedlings of rice cultivar CO-39. The plants were incubated at 24 °C with high light and 90% relative humidity for 5 days. There were no significant differences observed in disease lesion number between the wild type, Guy11, and the mutant strains (Student's t-test $P>0.05$).

5.3.3 Translocation of cytoplasmic acetyl-CoA

5.3.3.1 Identification of *ACS2, ACS3* and *CRC1*

To investigate other genes involved in acetyl-CoA translocation which may be important during infection-related development, I interrogated the *M. oryzae* database and generated a list of candidate genes, based upon BLAST analysis using the Genbank. I then analysed these genes using HT-superSAGE analysis, as previously described, to determine if any of these candidate genes showing differential expression, and in particular up-regulation during appressorium development. I identified 3 genes putatively involved in acetyl-CoA translocation that showed higher levels of expression during appressorium development and maturation compared to levels observed in mycelium; MGG_10492.6, MGG_00689.6 and MGG_04590.6. These genes were annotated in the Magnaporthe genome; MGG_10492.6 putatively codes for a mitochondrial carnitine carrier, MGG_00689.6 and MGG_04590.6 both potentially encode for acetyl-CoA synthetase. Whilst confirming the identity of these two acetyl-CoA synthetases by BLAST analysis using the Genbank database and reverse blast of the *S. cerevisiae* gene against the *M. oryzae* database I also identified a third gene which putatively encodes for acetyl-CoA synthetase, namely MGG_03201.6.

The results of the BLAST analysis was summarised in Table 5.2 and the alignment of each gene, MGG_10492.6 (*CRC1*), MGG_00689.6 (*ACS2*), MGG_04590.6 (*ACS1*) and MGG_03201.6 (*ACS3*) is shown in Figure 5.16, Figure 5.17, Figure 5.18 and Figure 5.19 respectively.

Table 5.2 Blast analysis results on MGG_10492.6, MGG_00689.6, MGG_04590.6 and MGG_03201.6.

Genes	Genes (Identity [%])			Protein
	C. albicans	*S. cerevisiae*	*A. nidulans*	
MGG_10492.6	orf19.2599 (51.8)	YOR100C (39)	ANID_05356.1 (70)	Mitochondrial carnitine carrier
MGG_00689.6	orf19.1743 (38.3)	YAL054C (37)	ANID_05833.1 (59)	Acetyl-CoA synthetase
MGG_04590.6	orf19.1064 (56.4)	YLR153C (55)	ANID_05626.1 (68)	Acetyl-CoA synthetase
MGG_03201.6	orf19.1064 (61.4)	YLR153C (61)	ANID_05626.1 (80)	Acetyl-CoA synthetase

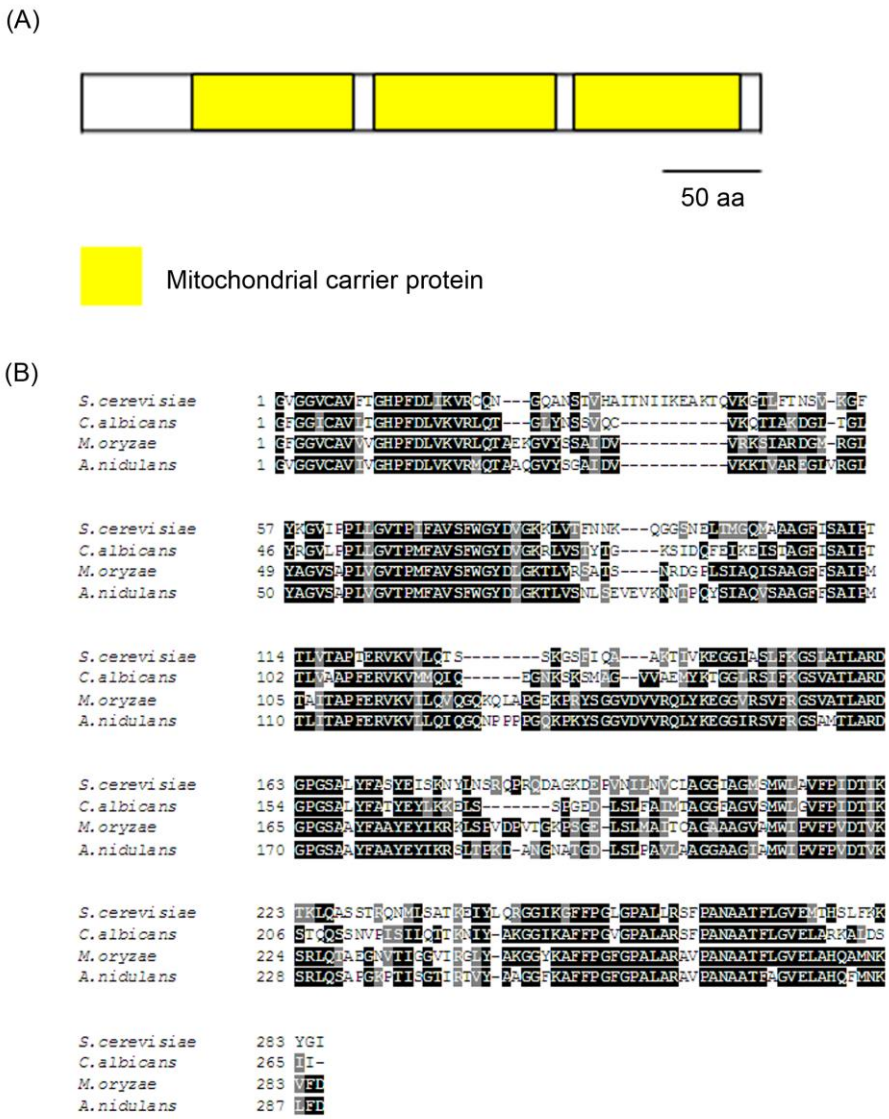

Figure 5.16 Alignment of the predicted amino acid sequence of *CRC1* with *C. albicans, S. cerevisiae* and *A. nidulans CRC1*-encoding genes and the structural motifs of the protein.

(A) Diagram showing protein domains in *MoCRC1*. *MoCRC1* has 345 amino acids and possesses 3 mitochondrial carnitine carrier domains (Falconi et al., 2006). (B) Amino acid alignment of *MoCRC1* with *C. albicans*, *S. cerevisiae* and *A. nidulans* mitochondrial carnitine carrier-encoding gene. Identical amino acids are highlighted on a black background and similar amino acids on a grey background.

(A)

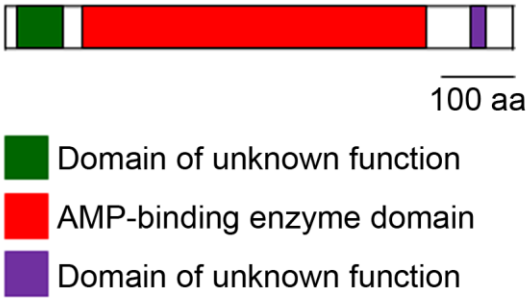
100 aa
Domain of unknown function
AMP-binding enzyme domain
Domain of unknown function

(B)


C.albicans
S.cerevisiae
M.oryzae
A.nidulans

Figure 5.17 Alignment of the predicted amino acid sequence of *ACS2* with *C. albicans, S. cerevisiae* and *A. nidulans* acetyl-CoA synthetase-encoding genes and the structural motifs of the protein.

(A) Diagram showing protein domains in *MoACS2*. *MoACS2* encodes a putative 700 amino acid protein possessing 2 domains of unknown functions and an AMP-binding enzyme domain (Conti et al., 1996). (B) Amino acid alignment of *MoACS2* with *C. albicans*, *S. cerevisiae* and *A. nidulans* acetyl-CoA synthetase. Identical amino acids are highlighted on a black background and similar amino acids on a grey background.

(A)

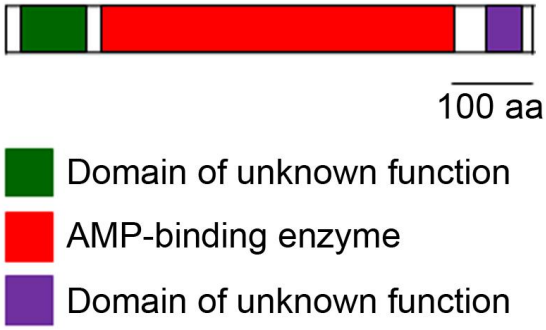
100 aa
Domain of unknown function
AMP-binding enzyme
Domain of unknown function

(B)

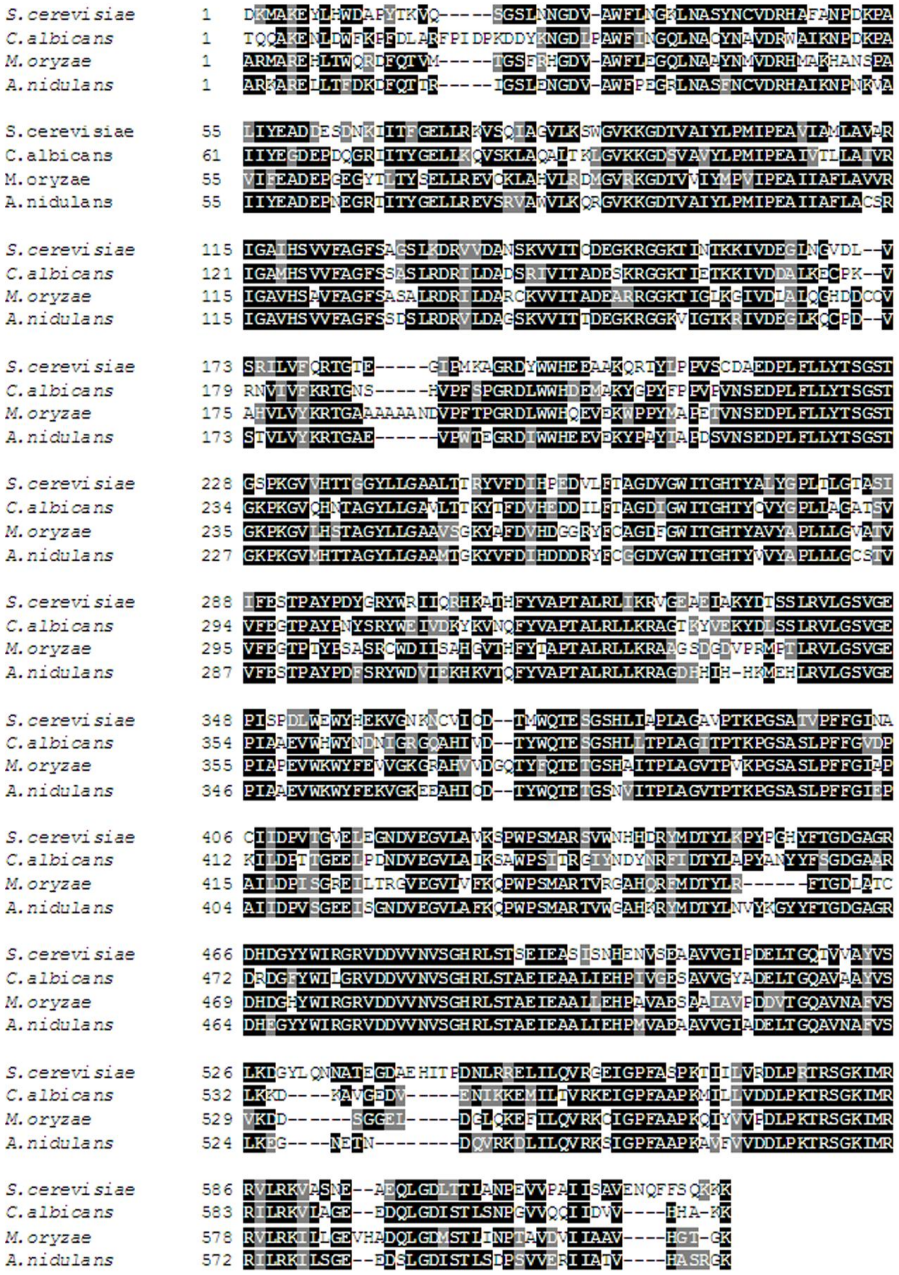
S.cerevisiae
C.albicans
M.oryzae
A.nidulans

Figure 5.18 Alignment of the predicted amino acid sequence of *ACS1* with *C. albicans, S. cerevisiae* and *A. nidulans* acetyl-CoA synthetase-encoding genes and the structural motifs of the protein.

(A) Diagram showing protein domains in *MoACS1*. *MoACS1* encodes a putative 661 amino acid protein possessing 2 domains of unknown function and an AMP-binding enzyme domain (Conti et al., 1996). (B) Amino acid alignment of *MoACS1* with *C. albicans*, *S. cerevisiae* and *A. nidulans* acetyl-CoA synthetase. Identical amino acids are highlighted on a black background and similar amino acids on a grey background.

(A)

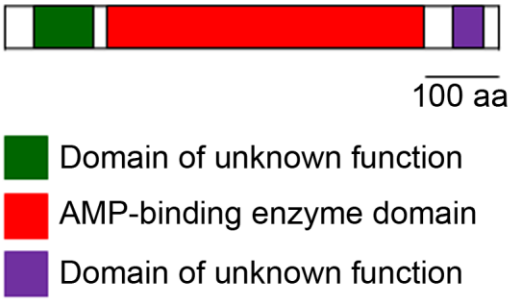

(B)

```
M.oryzae        1   WARMARELLTWSRDFETVYSGSLSAGDSAWFLEGELNASYNCIDRHALKDPNRVAIIYEA
A.nidulans      1   WARKARELLTFDKDFQTTRIGSLENGDVAWFPEGRLNASFNCVDRHAIKNPNKVAIIYEA
C.albicans      1   FGPLAKELLSWDHDFHTVKSGTLKNGDAAWFLGGELNASYNCVDRHAEANPDKPALICEA
S.cerevisiae     1   FDKMAKEYLHWDAPYTKVQSGSLNNGDVAWFINGKLNASYNCVDRHAEANPDKPAIIYEA

M.oryzae        61  DDPSSGRTLTYGELMREVCRTAHVLEQMGVRKGDTVAVYLPMIPEALIAFLAVTRIGAVH
A.nidulans      61  DEPNEGRTITYGELLREVSRVAWVLKQRGVKKGDTVAIYLPMIPEAIIAFLACSRIGAVH
C.albicans      61  DDEKDSHILTYGDLLREVSKVAGVLQSWGIKKGDTVAVYLPMNAQAIIAMLAIARIGAAH
S.cerevisiae     61  DDESDNKIITFGELLRKVSQIAGVLKSWGVKKGDTVAIYLPMIPEAVIAMLAVARIGAIH

M.oryzae        121 SVVFAGFSADSLRDRVVDGQSKVVITTDEGKRGGKLIGTKRIVDEALKNCPDVSHVLVYK
A.nidulans      121 SVVFAGFSSDSLRDRVLDAGSKVVITTDEGKRGGKVIGTKRIVDEGLKQCPDVSTVLVYK
C.albicans      121 SVIFAGFSAGSIKDRVNDASCKALITCDEGKRGGRTTNIKKLCDEALVDCPTVEKVLVYK
S.cerevisiae     121 SVVFAGFSAGSLKDRVVDANSKVVITCDEGKRGGKTINTKKIVDEGLNGVDLVSRILVFQ

M.oryzae        181 RTGA-DVPMMQGRDFWWHEEVEKWPNYIPPVPMNSEDPLFLLYTSGSTGKPKGVMHTTAG
A.nidulans      181 RTGA-EVPWTEGRDIWWHEEVEKYPAYIAPDSVNSEDPLFLLYTSGSTGKPKGVMHTTAG
C.albicans      181 RTNNPEIHLTEGRDYYWDVETAKFPGYLPPVSVNSEDPLFLLYTSGSTGTPKGVVHSTAG
S.cerevisiae     181 RTGTEGIPMKAGRDYWWHEEAAKQRTYLPPVSCDAEDPLFLLYTSGSTGSPKGVVHTTGG

M.oryzae        240 YLLGAAMTGKYVFDIHDGDRFFCGGDVGWITGHTYVVYAPLLLGVSTVVFEGTPAYPTFS
A.nidulans      240 YLLGAAMTGKYVFDIHDDDRYFCGGDVGWITGHTYVVYAPLLLGCSTVVFESTPAYPDFS
C.albicans      241 YLLGAALSTKYIFDIHPEDILFTAGDVGWITGHTYALYGPLLLGVPTIIFEGTPAYPDYG
S.cerevisiae     241 YLLGAALTTRYVFDIHPEDVLFTAGDVGWITGHTYALYGPLTLGTASIIFESTPAYPDYG

M.oryzae        300 RYWDIIDQHKITHFYVAPTALRLLKRAGDQWV-KHEMKHLRVLGSVGEPIAAEVWKWYFE
A.nidulans      300 RYWDVIEKHKVTQFYVAPTALRLLKRAGDHHI-HHKMEHLRVLGSVGEPIAAEVWKWYFE
C.albicans      301 RFWQIVEKHKATHFYVAPTALRLLRKAGEQEIAKYDLSSLRTLGSVGEPISPDIWEWYNE
S.cerevisiae     301 RYWRIIQRHKATHFYVAPTALRLIKRVGEAEIAKYDTSSLRVLGSVGEPISPDLWEWYHE

M.oryzae        359 IVGKEQAQIVDTYWQTETGSNVICPLAGVTPTKPGSASLPFFGIEPAIIDPVSGEEIHGN
A.nidulans      359 KVGKEEAHICDTYWQTETGSNVITPLAGVTPTKPGSASLPFFGIEPAIIDPVSGEEISGN
C.albicans      361 FVGKNQCHISDTYWQTESGSHLIAPLAGVVPNKPGSASYPFFGIDAAIIDPVTGVEIEGN
S.cerevisiae     361 KVGNKNCVICDTMWQTESGSHLIAPLAGAVPTKPGSATVPFFGINACIIDPVTGVELEGN

M.oryzae        419 DVEGVLGFKQAWPSMARTVWGAHKRYMETYMNVYNGFYFTGDGAARDHEGFYWIRGRVDD
A.nidulans      419 DVEGVLAFKQPWPSMARTVWGAHKRYMDTYLNVYKGYYFTGDGAGRDHEGYYWIRGRVDD
C.albicans      421 DAEGVLAIKDHWPSMARTVYKNHTKYMDTYMNPYPGYYFTGDGAARDHDGYYWIRGRVDD
S.cerevisiae     421 DVEGVLAVKSPWPSMARSVWNHHDRYMDTYLKPYPGHYFTGDGAGRDHDGYYWIRGRVDD

M.oryzae        479 VVNVSGHRLSTAEIEAALLEHHYVAEAAVVGIQDELTGQAVNAFVSLAEHVTTDND----
A.nidulans      479 VVNVSGHRLSTAEIEAALIEHPMVAEAAVVGIADELTGQAVNAFVSLKEGNETNDQ----
C.albicans      481 VVNVSGHRLSTAEIEAALIEDKKVSEAAVVGIHDDITGQAVIAYVALKEGNSDEDS----
S.cerevisiae     481 VVNVSGHRLSTSEIEASISNHENVSEAAVVGIPDELTGQTVVAYVSLKDGYLQNNATEGD

M.oryzae        535 ------ESLRKELITQVRRSIGPFAAPKAVFVVPDLPRTRSGKIMRRILRKILAGEEDQL
A.nidulans      535 --------VRKDLILQVRKSIGPFAAPKAVFVVDDLPKTRSGKIMRRILRKILSGEEDSL
C.albicans      537 ------EGLRKELVLQVRKTIGPFAAPKSVIIVQDLPKTRSGKIMRRILRKVSSNEADQL
S.cerevisiae     541 AEHITPDNLRRELILQVRGEIGPFASPKTIILVRDLPRTRSGKIMRRVLRKVASNEAEQL

M.oryzae        589 GDVSTLSDPTVVDRIITVHEY----KKK
A.nidulans      587 GDISTLSDPSVVERIIATVHAS----RGK
C.albicans      591 GDISTLSNPQSVEGIISAFGAQF---GKK
S.cerevisiae     601 GDLTTLANPEVVPAIISAVENQFFSQKKK
```

Figure 5.19 Alignment of the predicted amino acid sequence of *ACS3* with *C. albicans, S. cerevisiae* and *A. nidulans* acetyl-CoA synthetase-encoding genes and the structural motifs of the protein.

(A) Diagram showing protein domains in *MoACS3*. *MoACS3* encodes a putative 669 amino acid protein possessing 2 domains of unknown functions and an AMP-binding enzyme domain (Conti et al., 1996). (B) Amino acid alignment of *MoACS3* with *C. albicans*, *S. cerevisiae* and *A. nidulans* acetyl-CoA synthetase. Identical amino acids are highlighted on a black background and similar amino acids on a grey background.

5.3.3.2 Targeted deletion of *ACS1, ACS2, ACS3* and *CRC1* genes in *M. oryzae*

Targeted gene deletion of *M. oryzae ACS2, ACS3* and *CRC1* was carried out using the split marker technique as described in Section 2.11 (Catlett et al., 2003). These constructs were then transformed into Guy11 and transformants were selected based on their resistance to hygromycin B. Genomic DNA of putative transformants were extracted and digested with either *Spe*I (*ACS1*), *Xho*I (*ACS2*), *Hin*dIII (*ACS3*) or *Xmn*I (*CRC1*) before being fractionated by gel electrophoresis. The fractionated DNA was then transferred onto Hybond-N and probed with either the upstream flanking region of the targeted gene loci (*ACS1, ACS2* and *ACS3*) or the open reading frame fragment (*CRC1*). Southern blot analysis revealed deletion of *ACS2, ACS3* and *CRC1* genes. I was unable to generate an *ACS1* deletion mutant. A total of 30 putative transformants were screened and none contained the targeted deletion.

Putative transformants to delete *ACS2* were probed with a 1 kb open reading frame fragment generated by PCR using primers pACS2.F1 and pACS2.R1. After digestion with *Xho*I, a 6.4 kb fragment was predicted to be present in the wild type and no fragment was expected to be present in the corresponding null mutant. The results for Southern blot analysis for *ACS2* (Figure 5.20) show that the 6.4 kb fragment was absent in lanes 4, 6 and 7. Further confirmation was done by reprobing the membrane with the hygromycin cassette. For the null mutant, a single 6.4 kb fragment was expected to be present while no fragment should be detected in the wild type. Based on these results, transformants 6 and 7 were identified as Δ*acs2* mutants and selected for further analysis.

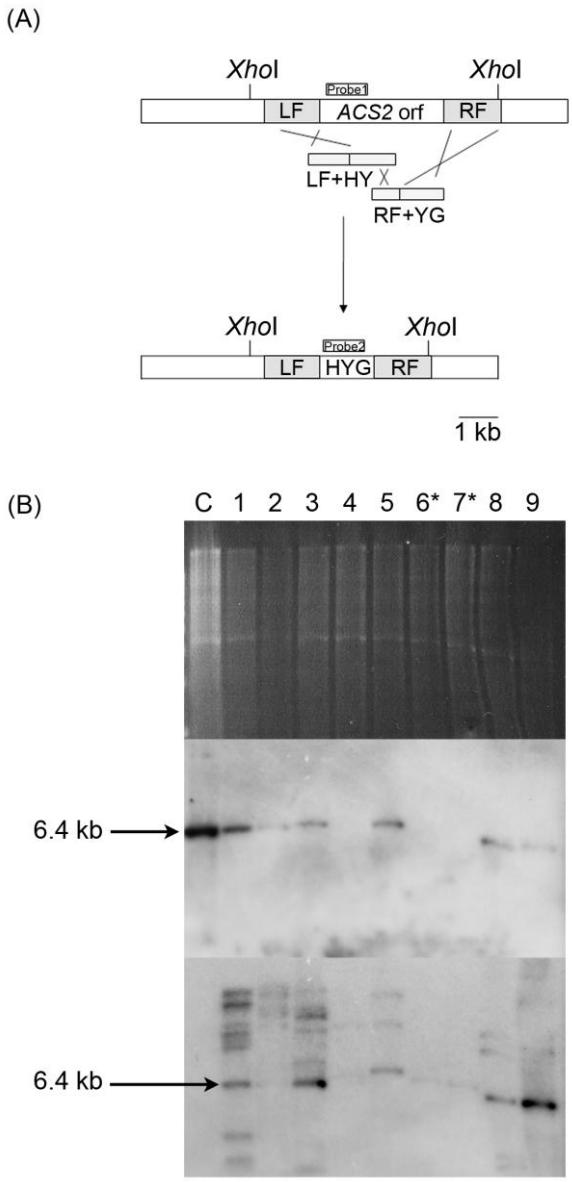

Figure 5.20 A schematic representation of the targeted deletion of *ACS2* by the split-marker deletion method.

Targeted gene deletion of the *ACS2* gene in *M. oryzae* Guy11. (A) Diagram describing the targeted locus of *ACS2*. (B) Genomic DNA was isolated and digested with *Xho*I before being fractionated in a 0.8% agarose gel. The gel was then processed by Southern blot analysis and probed with a 1 kb sequence of the open reading frame for presence and absence and further confirmed by probing with 0.8 kb of the hygromycin B phosphotransferase fragment. The putative transformants in lanes 6 and 7 are confirmed as Δ*acs2* mutants. C: Wild type control, Guy11.

ACS3 putative transformants were probed with a 1.5 kb fragment upstream of the targeted gene locus, previously generated for the gene deletion construct. Following replacement of the native coding sequence with the hygromycin resistance gene cassette, a size difference in the locus was generated. Figure 5.21 shows the size of the hybridizing restriction fragment observed in the wild type, Guy11 (2.2 kb) and in the putative *ACS3* mutants (3.7 kb). The presence of the 3.7 kb fragments in lanes 2, 3, 4, 5 and 8 confirmed the targeted deletion of *ACS3*. Further confirmation was done by reprobing the membrane with the hygromycin cassette. For the null mutant, a single 2.7 kb fragment was expected to be present while no fragment should be detected in the wild type. Based on these results, the positive Δ*acs3* transformants were selected for further analysis.

Putative transformants to delete *CRC1* were probed with a 1 kb open reading frame fragment generated by PCR using primers pCRC.F1 and pCRC.R1. After digestion with *Xmn*I, a 7.5 kb fragment was predicted to be present in the wild type and no fragment was expected to be present in the corresponding null mutant. The results for Southern blot analysis for *CRC1* (Figure 5.22) show that the 7.5 kb fragment was present in lanes 2, 3, 9 and 17. This confirmed the targeted deletion of *CRC1* and positive Δ*crc1* transformants were selected for further analysis.

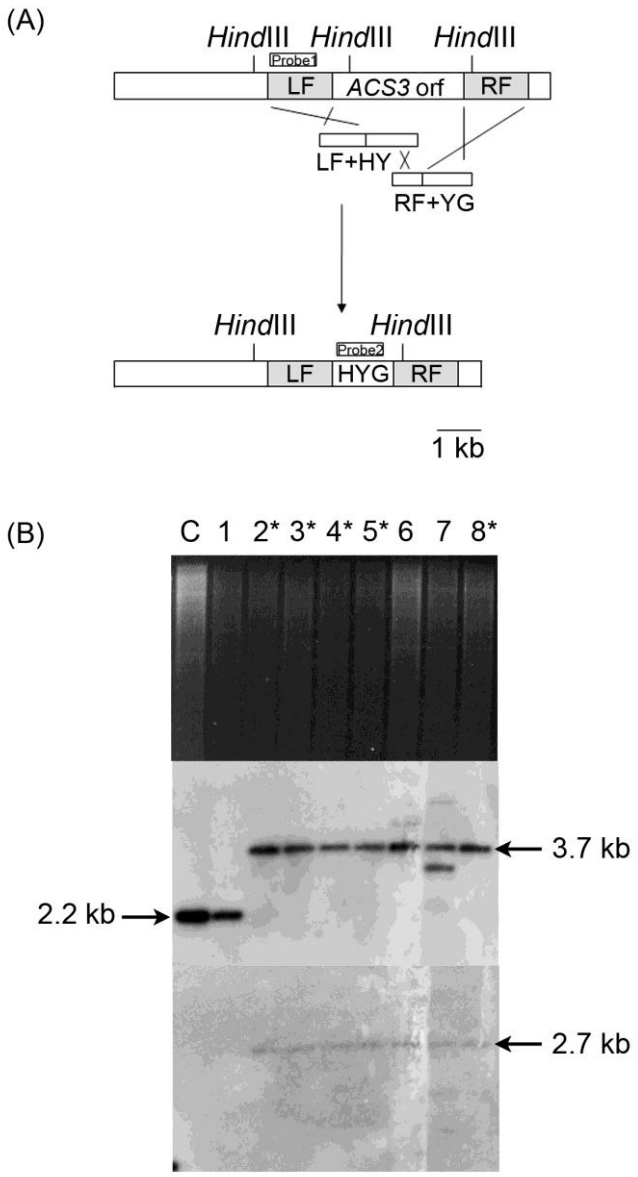

Figure 5.21 A schematic representation of the targeted deletion of *ACS3* by the split-marker deletion method.

Targeted gene deletion of the *ACS3* gene in *M. oryzae* Guy11. (A) Diagram describing the targeted locus of *ACS3*. (B) DNA was isolated and digested with *Hin*dIII before being fractionated in a 0.8% agarose gel. The gel was then processed by Southern blot analysis and probed with a 1 kb sequence of the upstream flanking region for size difference and further confirmed by probing with 0.8 kb of the hygromycin B phosphotransferase gene fragment. The putative transformants in lanes 2, 3, 4, 5 and 8 are confirmed as Δ*acs3* mutants. C: Wild type control, Guy11.

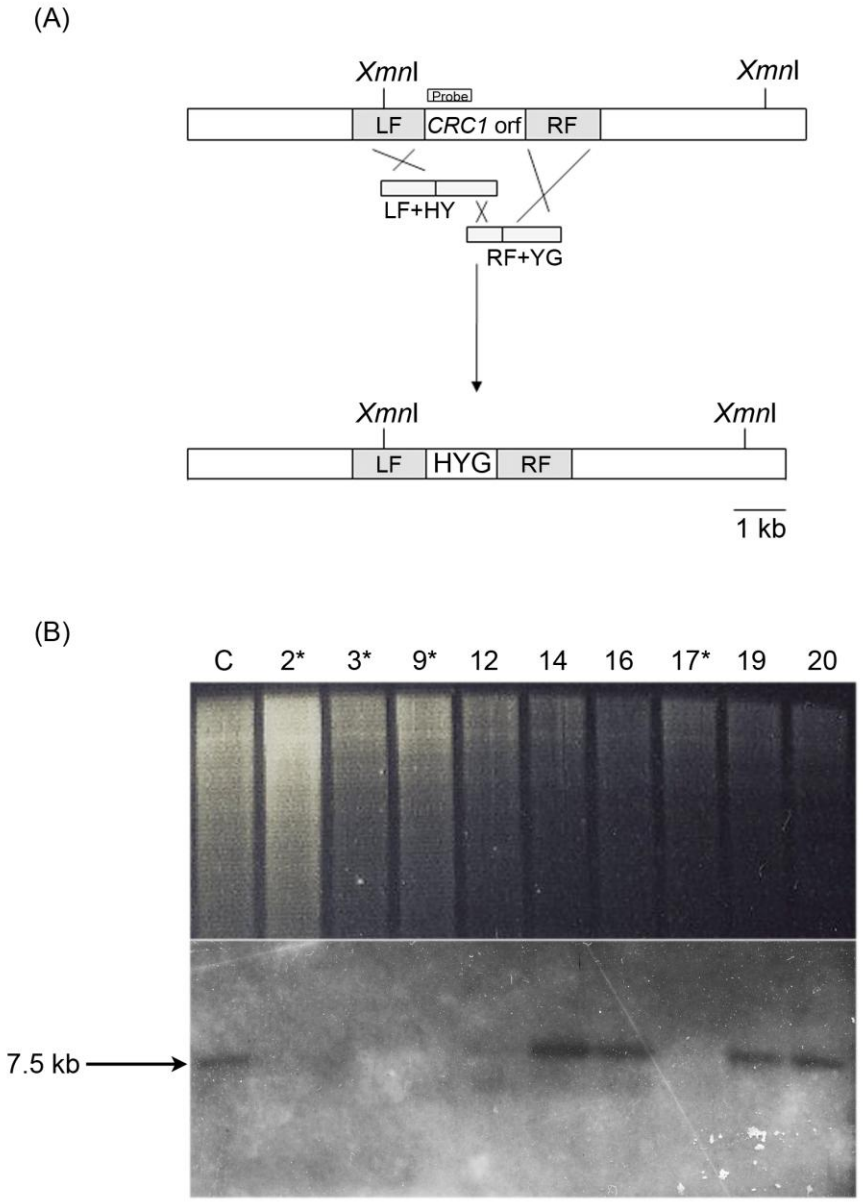

Figure 5.22 A schematic representation of the targeted deletion of *CRC1* by the split-marker deletion method.

Targeted gene deletion of the *CRC1* gene in *M. oryzae* Guy11. (A) Diagram describing the targeted locus of *CRC1*. (B) DNA was isolated and digested with *Xmn*I before being fractionated in a 0.8% agarose gel. The gel was then processed by Southern blot analysis and probed with a 1 kb sequence of the open reading frame for presence and absence. The putative transformants in lanes 2, 3, 9 and 17 are confirmed as Δ*crc1* mutants. C: Wild type control, Guy11.

5.3.3.3 Carbon source utilisation and pathogenicity of Δ*acs2*, Δ*acs3* and Δ*crc1* mutants

Mutants were grown on minimal medium supplemented with different carbon sources (50 mM glucose, 50 mM acetate, 50 mM oleic acid or 50 mM triolein) and the growth of the mutants was observed after 14 days (Figure 5.23). Our observations revealed that Δ*acs2*, Δ*acs3* and Δ*crc1* mutants were unable to grow on minimal medium supplemented with lipid (oleic acid or triolein). However, only Δ*crc1* mutants were unable to grow on minimal medium supplemented with acetate. Both Δ*acs2* and Δ*acs3* mutants were still able to utilise acetate as sole carbon source.

To investigate the role of each mutant in causing rice blast disease, plant infection assays were carried out using 3 week-old seedlings of susceptible rice cultivar CO-39, as described in Section 2.17. Both Δ*acs2* and Δ*acs3* mutants were still able to infect plants and produced necrotic lesions on the leaf surface following infection (Figure 5.24). However, Δ*crc1* mutants were severely reduced in their ability to cause plant infection as there were on average 1-2 lesions per 5 cm compared to the wild type strain, Guy11 which had on average 65 lesions per 5 cm (Figure 5.24). I conclude that *ACS2* and *ACS3* genes are required for lipid utilisation, but dispensable for fungal virulence. The mitochondrial carnitine carrier encoded by *CRC1* is required for growth on lipids and acetate but clearly has an important role in the ability of the fungus to infect its host, suggesting that the uptake of acteylcarnitine into mitochondria is essential for meeting the energy requirements for successful infection.

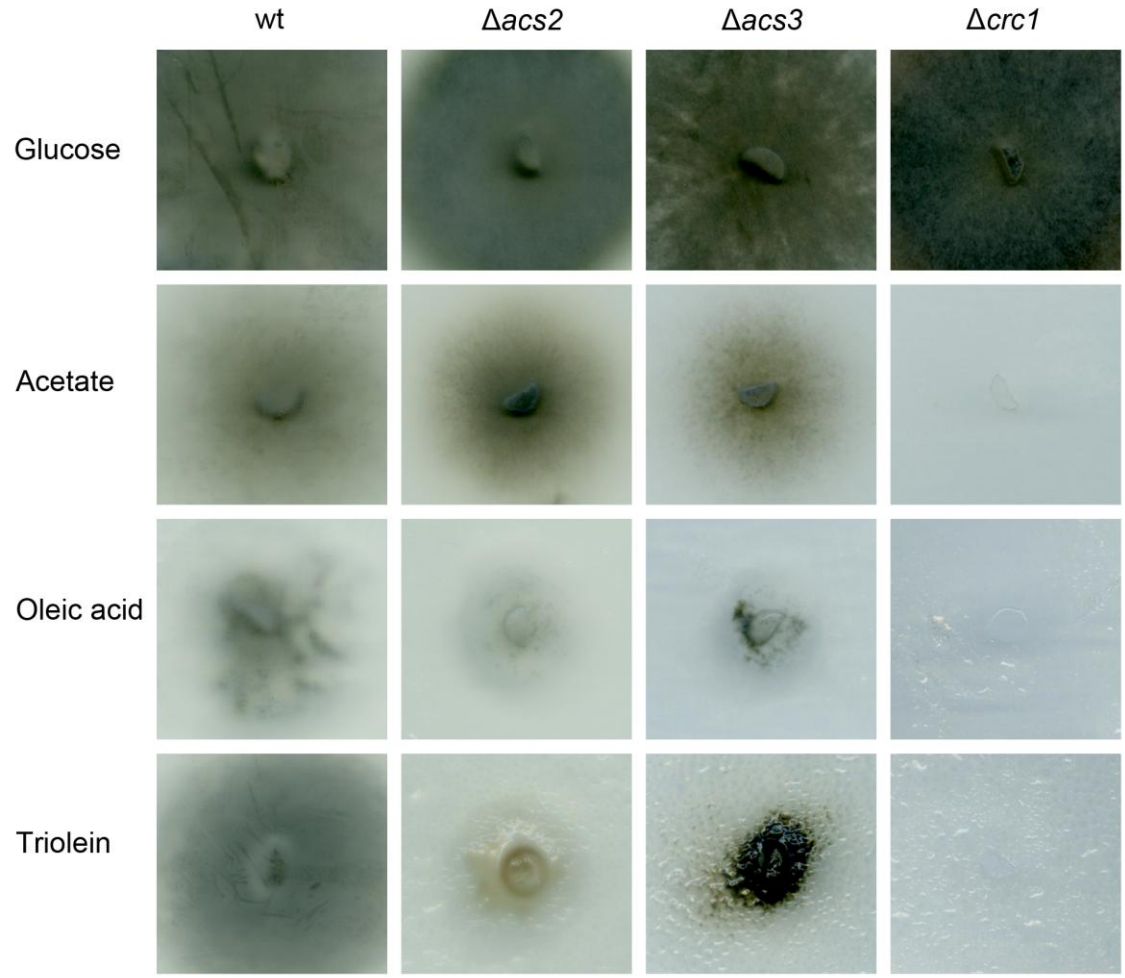

Figure 5.23 Vegetative growth of Guy11, Δ*acs2*, Δ*acs3* and Δ*crc1* mutants on a range of different carbon sources.

The fungal strains were grown on minimal medium supplemented with glucose, acetate, oleic acid or triolein. After 14 days of incubation at 24 °C, the results were recorded. All the mutants showed a growth defect on minimal medium containing lipid. Both Δ*acs2* and Δ*acs3* mutants were still able to grow on acetate, only the Δ*crc1* mutant was unable utilise acetate as sole carbon source.

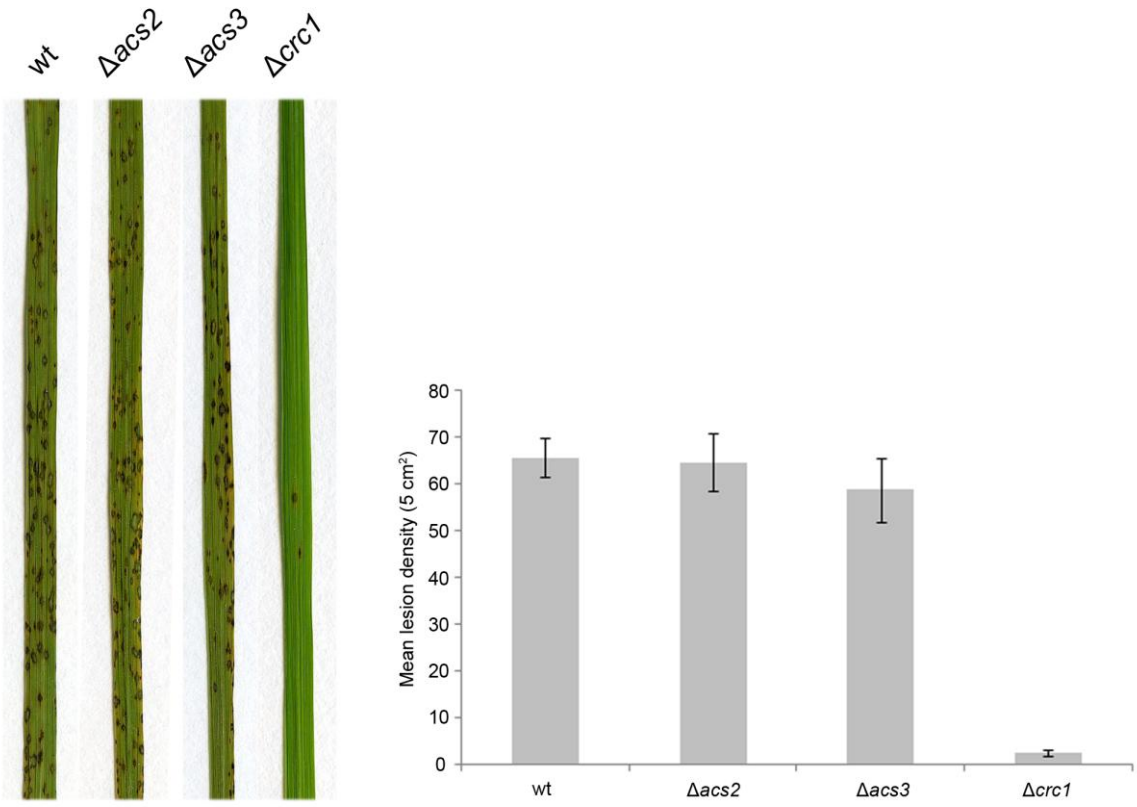

Figure 5.24 Pathogenicity assays on rice cultivar CO-39.

Conidia were harvested from a 12 day old culture of each fungal strain and 5×10^4 conidia/mL were sprayed onto 3 week-old rice seedlings. The plants were inoculated at 24 °C with high light and 90% humidity. After 5 days, disease symptoms were recorded. There was no significant difference observed between the wild type, Guy11, and Δ*acs2* and Δ*acs3* mutants (Student's t-test $P>0.05$). However, there was a large reduction in blast symptoms produced by the Δ*crc1* mutant (Student's t-test $P<0.05$).

5.3.3.4 Appressorium development and lipid mobilisation in Δ*acs2*, Δ*acs3* and Δ*crc1*

Appressorium development was observed in Δ*acs2*, Δ*acs3* and Δ*crc1* mutants (Figure 5.25 and Figure 5.26). Conidia were inoculated onto hydrophobic coverslips, allowed to germinate, and then observed at intervals. No significant difference can be seen in appressorium development between the wild type and the Δ*acs2*, Δ*acs3* and Δ*crc1* mutants. Germ tube emergence occurred within 1 h of inoculation and by 2 h the germ tube had hooked and begun to swell. An appressorium was observed by 4 h and appeared fully mature by 8 h. By 24 h conidia had collapsed in the wild type and all mutants. Therefore, in Δ*acs2*, Δ*acs3* and Δ*crc1* mutants no impairment or delay in appressorium development or programmed cell death of the spore was observed.

In order to observe lipid mobilisation in the Δ*acs2*, Δ*acs3* and Δ*crc1* mutants compared to Guy11, I visualised lipid droplets by staining with BODIPY. Conidia from the wild type Guy11 and the Δ*acs2*, Δ*acs3* and Δ*crc1* mutants were inoculated onto hydrophobic coverslips and the stain applied at time 0 h, and lipid droplets observed at intervals up to 24 h.

The mutants Δ*acs2*, Δ*car3* and Δ*crc1*, were all impaired in lipid mobilisation when compared to the wild type. In Guy11, lipid droplets were seen to move and accumulate at the tip of the germ tube within the first 2 h of infection (see Figure 5.25 and Figure 5.26). By 4 h, lipid droplets were observed in both conidia and appressoria (Figure 5.25 and Figure 5.26). By 6 h, a higher proportion of lipid droplets were seen to accumulate in the appressorium compared to the conidium, and by 8 h most lipid droplets had accumulated in the appressorium. In the case of Δ*acs2* and Δ*acs3* mutants, a delay in lipid mobilisation was observed (Figure 5.25). Lipid droplets were still apparent in conidia after 8 h ($P < 0.01$), and a number of lipid droplets were still present even after

24 h. In the Δ*crc1* mutant the observed delay in lipid mobilisation was most apparent (Figure 5.26). Lipid droplets were observed in the conidia after 8 h ($P < 0.01$) and even after 24 h were still present. Based on these observations, I conclude that although appressorium development itself was not impaired in Δ*acs2*, Δ*acs3* and Δ*crc1* mutants, lipid mobilisation from the conidia to the developing appressorium was delayed.

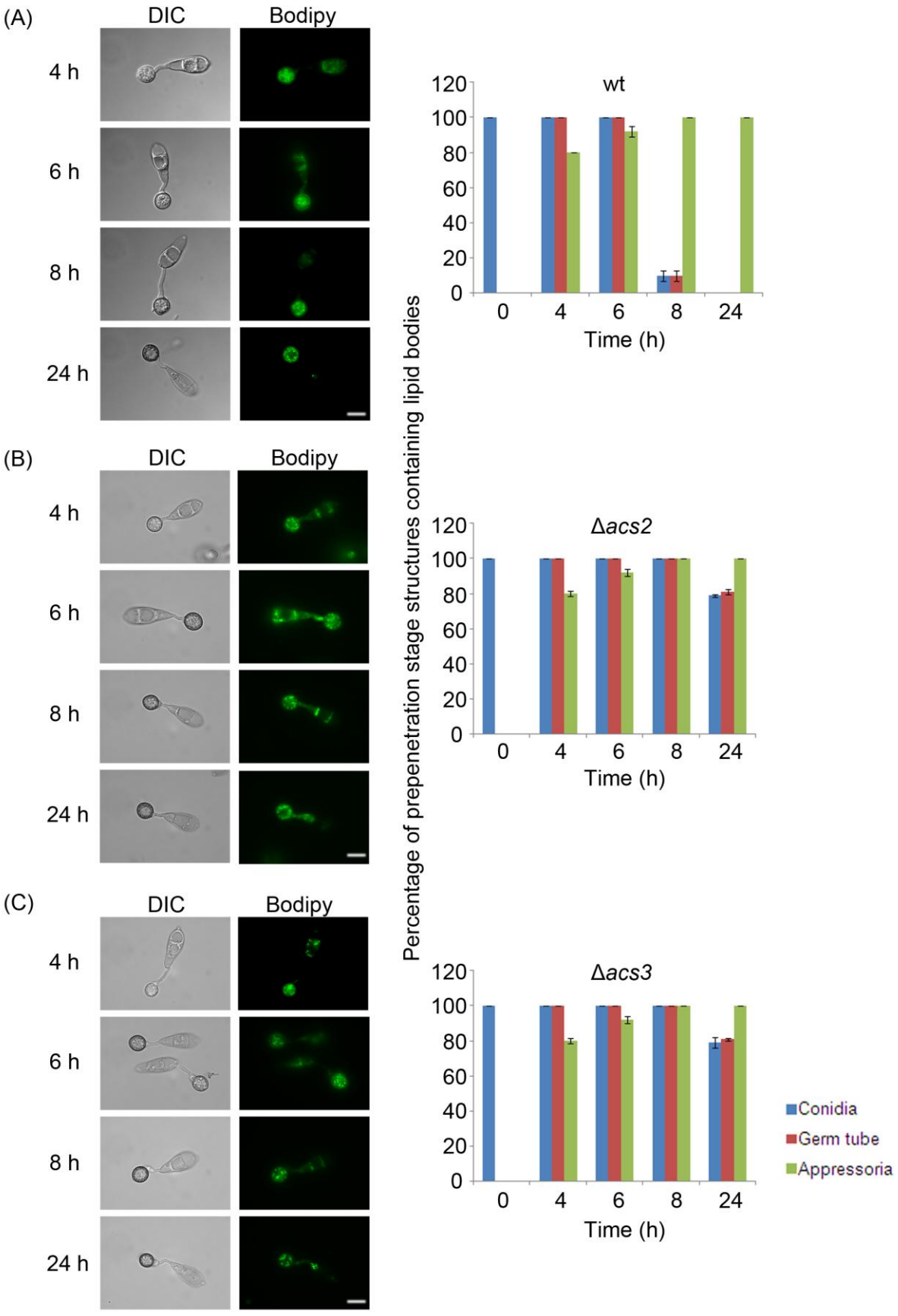
(A)
DIC
Bodipy
4 h
6 h
8 h
24 h
(B)
DIC
Bodipy
4 h
6 h
8 h
24 h
(C)
DIC
Bodipy
4 h
6 h
8 h
24 h
wt
Δacs2
Δacs3
Percentage of prepenetration stage structures containing lipid bodies
120
100
80
60
40
20
0
0
4
6
8
24
Time (h)
Conidia
Germ tube
Appressoria

Figure 5.25 Epifluorescence microscopy of lipid body distribution in the wild type, Guy11, and Δ*acs2*, Δ*acs3* mutants.

Lipid distribution in Guy11, Δ*acs2* and Δ*acs3* mutants are shown in (A), (B) and (C) respectively. The percentage of fungal structures that contained lipid bodies at a given time was recorded from a sample of 300 germinated conidia. In the wild type, Guy11, almost all lipid droplets mobilised and accumulated in appressoria by 8 h. In Δ*acs2* and Δ*acs3* mutants, the delay was observed at 8 h onwards in which lipid droplets were still apparent when compared to Guy11 ($P < 0.01$). Even after 24 h, the signal from lipid droplets was still detected in both conidia and appressoria. Scale bar = 10 µm.

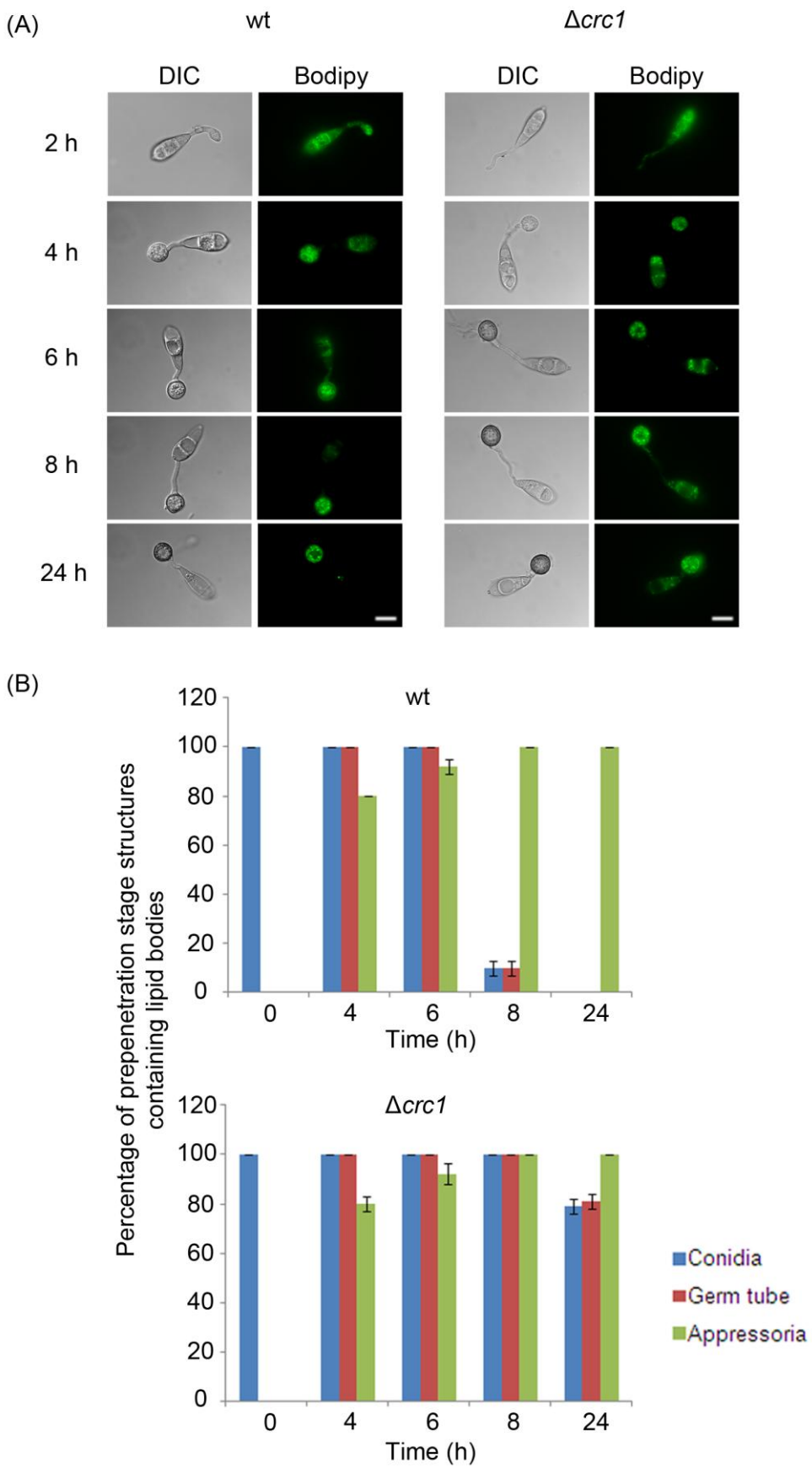
(A)
wt
Δcrc1
DIC
Bodipy
DIC
Bodipy
2 h
4 h
6 h
8 h
24 h
(B)
wt
Δcrc1
Percentage of prepenetration stage structures containing lipid bodies
120
100
80
60
40
20
0
0
4
6
8
24
Time (h)
Conidia
Germ tube
Appressoria

Figure 5.26 Epifluorescence microscopy of lipid body distribution in the wild type, Guy11, and Δ*crc1* mutant.

The percentage of fungal structures that contained lipid bodies at a given time was recorded from a sample of 300 germinated conidia is shown in (B). In the wild type, Guy11, almost all lipid droplets mobilised and accumulated in appressoria by 8 h. In Δ*crc1* mutant, the delay was observed as early as 8 h in which lipid droplets were still apparent when compared to Guy11 ($P < 0.01$). Even after 24 h, lipid droplets were still detected in both conidia and appressoria. Scale bar = 10 µm.

5.4 Discussion

In this chapter, I have shown the importance of maintaining the acetyl-CoA pool, acetyl-CoA translocation, and carnitine biosynthesis in *M. oryzae*. Acetyl-CoA is involved primarily in carbon and energy metabolism (Strijbis and Distel, 2010). It is, however, also involved in secondary metabolism pathways such as amino acid synthesis, chitin synthesis, and a number of other processes. I was primarily interested in the role of acetyl-CoA metabolism and its translocation during appressorium development in *M. oryzae*.

During plant infection, *M. oryzae* develops in nutrient-free conditions (Talbot, 2003). The fungus must therefore utilise nutrient sources present in the conidia in the form of trehalose, glycogen and lipid (Wang et al., 2005; Wilson and Talbot, 2009). Both trehalose and glycogen can be broken down into glucose which the fungus can then utilise for growth and energy production. Glucose metabolism via glycolysis produces pyruvate, which is transported into mitochondria where it will be converted into acetyl-CoA, which is required for the TCA cycle.

Lipid degradation is catalyzed by triacylglycerol lipases and will directly yield glycerol and fatty acids (Thines et al., 2000). During plant infection, glycerol has been shown to accumulate in the appressorium which may enable *M. oryzae* to generate turgor to penetrate the leaf cuticle (de Jong et al., 1997). Glycerol can also be used to synthesise glucose which is metabolised to produce acetyl-CoA (Salazar et al., 2009). Another source of acetyl-CoA is β-oxidation of fatty acids which has been shown to occur in peroxisomes (Wang et al., 2007) and probably also occurs in mitochondria. For further utilisation of acetyl-CoA, it needs to be transported across the peroxisomal membrane and this is achieved by formation of acetylcarnitine in a reaction catalysed by carnitine acetyltransferase (Figure 5.1).

In the yeast species *S. cerevisiae* and *C. albicans*, CAT is encoded by *CIT2* and *CTN2* respectively and both enzymes have been shown to be present in both peroxisomes and mitochondria (Elgersma et al., 1995). In *M. oryzae*, CAT is encoded by *PTH2* and has been shown to play a significant role in plant infection because deletion of *PTH2* enables the fungus to elaborate its invasive hyphae once it has penetrated the leaf cuticle (Bhambra et al., 2006). It has also been shown that *M. oryzae* Pth2 localises to peroxisomes (Bhambra et al., 2006), although it has also been shown recently that *PTH2* may have a mitochondrial localisation signal (MLS) suggesting that it might also have mitochondrial activity (Hynes et al., 2011), consistent with the localisation of *S. cerevisiae CIT2* and *C. albicans CTN2*. It was previously shown that Δ*pth2* mutants are non-pathogenic and this inability to infect rice plants was associated with a delay in lipid mobilisation resulting in impaired appressorium function. Although the *M. oryzae* Δ*pth2* mutant is able to penetrate rice leaves, growth of invasive hyphae is impaired, resulting in a failure to infect. An abnormal distribution of chitin in infection structures was also reported (Bhambra et al., 2006). Here, I have shown that F-actin is also mislocalised in the appressorium of a Δ*pth2* mutant at a time associated with infection. In the wild type it has been shown that an F-actin ring forms at the base of the appressorium, at the site of penetration peg formation and mislocalisation of this ring has been observed in a number of penetration deficient mutants including Δ*mst12* (Dagdas personal communication) and Δ*mps1* mutants (Xu et al., 1998). It would seem that the failure of Δ*pth2* mutant to proceed with invasive growth mat therefore be due to a failure in the generation of sufficient acetyl-CoA resulting in the abnormal distribution of both chitin and actin at the point of invasive growth, perhaps due to loss of metabolic activity. Alternatively the generation of an intracellular acetyl-CoA pool may be itself a metabolic checkpoint which then mediates or regulates cytoskeletal re-orientation.

Carnitine is also required for acetyl-CoA translocation. Unlike CAT which needs to be synthesised endogenously, in mammalian systems carnitine can be obtained from the diet (Vaz and Wanders, 2002). The carnitine biosynthesis pathway has been described in mammals (Vaz and Wanders, 2002), *N. crassa* (Kaufman and Broquist, 1977) and more recently *C. albicans* (Strijbis et al., 2009) and this involves four enzymatic steps catalysed by *TMLD, HTMLA, TMABADH* and *BBD*, respectively. I identified genes that putatively encode these four enzymes in the *M. oryzae* genome based on sequence homology with *C. albicans* (Strijbis et al., 2009) (*CAR1, CAR2, CAR3* and *CAR4* respectively) and targeted these genes for deletion.

I tested the ability of these mutants, which were each deficient in one of the enzymes putatively required for carnitine biosynthesis, to utilise alternative carbon sources. I found that only Δ*car1* and Δ*car4* mutants are unable to utilise acetate, oleic acid or triolein as sole carbon sources. This is consistent with results shown in the Δ*pth2* mutant (Bhambra et al., 2006). However both Δ*car2* and Δ*car4* mutants are able to utilise acetate, oleic acid or triolein as sole carbon source, suggesting that alternative components of the carnitine biosynthesis pathway may exist.

In the case of Δ*car2* and Δ*car3* mutants, both of the mutants can grow on acetate and lipid. BLAST analysis revealed that there are a number of genes that might encode TMABADH aside from the *CAR3* gene (MGG_05008.6). For example MGG_03900.6 and MGG_09456.6 which show 50% and 36% identity to TMABADH respectively. This may explains why the Δ*car3* mutant was still able to grow on acetate and lipid, as other genes might be able to carry out the function of *CAR3* in a Δ*car3* mutant. However, there was only one copy of *CAR2* which putatively encodes HTMLA in *M. oryzae*. There may therefore be other pathways that compensate for the loss of HTMLA and produce TMABA in *M. oryzae*. Recycling of nutrients during autophagy might, for

instance, provide the Δ*car2* mutant with an alternative source of TMABA or carnitine. In order to demonstrate this, TMABA or carnitine quantification would need to be carried out in the Δ*car2* mutant. Preliminary data, however, showed equivalent amount of carnitine in each mutant (Figure 5.27), although this analysis needs to be repeated.

To determine whether carnitine biosynthesis mutants are required for rice blast disease, plant infection assays were carried. Surprisingly Δ*car1*, Δ*car2*, Δ*car3* and Δ*car4* mutants were fully pathogenic. Since carnitine is necessary for the CAT dependent acetyl-CoA translocation one might expect that mutants with a possible deficiency in carnitine synthesis, would demonstrate a similar phenotype to Δ*pth2* mutants (Bhambra et al., 2006). The ability of these mutants to infect rice implies that the mutants are still able to retrieve or synthesise sufficient carnitine in order to maintain the acetyl-CoA pool and bring about infection. It would be necessary therefore to determine whether these mutants are unable to synthesise carnitine by direct measurement of carnitine in all four mutant backgrounds.

In order to determine more about the maintenance of the acetyl-CoA pool and its translocation, during infection in *M. oryzae*, I identified a number of genes which could be involved in acetyl-CoA translocation in *M. oryzae*, based upon homology to genes which have been functionally characterised in other fungi. I further analysed this gene set so as to identify genes up-regulated throughout appressorium development, based on HT-superSAGE analysis. Three genes were identified; MGG_10492.6 (*CRC1*), MGG_00689.6 (*ACS2*) and MGG_04590.6 (*ACS1*). Based on sequence homology with *S. cerevisiae*, *C. albicans* and *A. nidulans CRC1* putatively encodes for mitochondrial carnitine carrier, whilst *ACS1* and *ACS2* encode for acetyl-CoA synthetase. A third acetyl-CoA synthetase was also identified MGG_03201.6 (*ACS3*) which showed high

identity with *ACS1*. Targeted gene deletion for each gene was performed although only three mutants, namely Δ*acs2*, Δ*acs3* and Δ*crc1* were confirmed.

I have shown that the acetyl-CoA synthetase mutants, Δ*acs2* and Δ*acs3* were unable to grow on oleic acid and triolein. However both Δ*acs2* and Δ*acs3* mutants were able to grow on acetate. I reasoned that since there are three copies of the gene present in the genome, they might complement for the function of each other. However, the fact that Δ*acs2* and Δ*acs3* mutants are unable to grow on oleic acid and triolein is surprising given that these enzymes are not known to be involved in lipid utilisation, and is even more surprising given that they show some redundancy in function when grown on acetate as the sole carbon source.

To determine whether the acetyl-CoA synthetase mutants are required for disease formation, plant infection assays were carried out. The *M. oryzae* Δ*acs2* and Δ*acs3* mutants were still able to produce blast symptoms (Student's t-test with Guy11 $P > 0.05$). However, this does not preclude a role for acetyl-CoA synthetase in plant infection, as there are three genes in total that putatively encode acetyl-CoA synthetase. In order to determine role for acetyl-CoA synthetase in plant infection, I would therefore need to generate double or triple mutants.

The Δ*crc1* mutant was unable to utilise either oleic acid, triolein, or acetate as the sole carbon source, as reported for Δ*pth2* mutants (Bhambra et al., 2006). Significantly, the Δ*crc1* mutants, were severely reduced in rice blast disease, and symptom development was limited to 1-2 lesions on each leaf (Student's t-test $P < 0.005$). This strongly suggests that the uptake of acetylcarnitine into mitochondria is important for the ability of the fungus to utilise alternative carbon sources and for survival of the fungus, but more significantly it is also an essential requirement for successful plant infection.

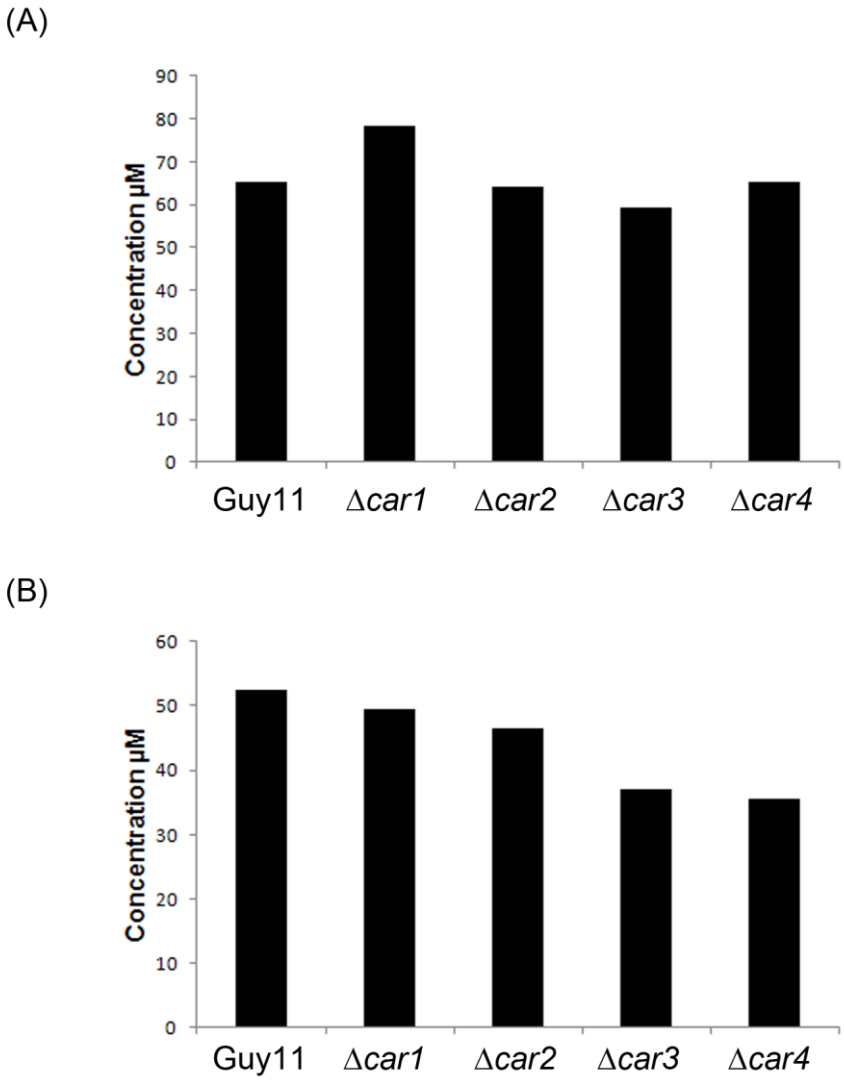

Figure 5.27 Comparison of carnitine concentration in the wild type, Guy11, *Δcar1*, *Δcar2*, *Δcar3* and *Δcar4* mutants.

(A) Carnitine was extracted from the fungal strains grown in CM and the concentration was measured using mass spectrometry. (B) Carnitine was extracted from the fungal strains grown in triolein and the concentration was measured using mass spectrometry. In both conditions, equivalent amount of carnitine was detected between the wild type, Guy11, and the mutant strains.

The requirement for translocation of acetyl-CoA into mitochondria during plant infection implies that a CAT with mitochondrial activity might also be required. I have yet to identify such a gene in *M. oryzae*, but as recent annotation of *PTH2* indicates, an additional 5' exon encoding an MTS (Hynes et al., 2011) it is therefore possible that *PTH2* also performs this function. This is consistent with what has been shown in *S. cerevisae* (Elgersma et al., 1995) and *C. albicans* (Strijbis et al., 2008). In *C. albicans*, it was shown for example that CAT activity in mitochondria is essential whilst its peroxisomal activity was dispensable (Strijbis et al., 2010). The authors also showed that acetyl-CoA can still be transported across the peroxisomal membrane even in the absence of peroxisomal CAT activity. The same mechanism of acetyl-CoA transport from the peroxisome may also occur in *M. oryzae*. It has also been suggested that transport of acetyl-CoA across the peroxisomal membrane, without the need of acetylcarnitine conversion, is possible in the presence of thioesterase (Strijbis et al., 2010) and this strategy has also been described in mammals (Leighton et al., 1989). Thioesterase is an enzyme that catalyzes the conversion of acetyl-CoA to acetate. The acetate produced might be able to cross the peroxisomal membrane by active transport or diffusion. It has been shown recently that the peroxisomal membrane contains pore-forming proteins that enable transfer of small molecules across the membrane (Grunau et al., 2009; Rokka et al., 2009). However, whether these channel- forming proteins also mediate the export of acetate from peroxisomes, is still not clear. It is possible therefore that the carnitine-dependent translocation from the peroxisomes is not essential for acetyl-CoA translocation, and that acetylcarnitine uptake into mitochondria via a Crc1-dependent and potentially Pth2-dependent mechanism is essential.

In order to demonstrate this in *M. oryzae*, *PTH2* localisation needs to be repeated using the recent annotation of *PTH2*. The MTS and PTS-deficient strains also need to be

constructed to determine whether CAT activity in mitochondria is more important than the CAT activity in peroxisomes in terms of plant infection development. The results obtained from these experiments will then explain the importance of maintaining the acetyl-CoA pool and translocation of acetyl-CoA, as well as its relationship to plant infection.

6.0 General Discussion

In this thesis, I have reported results that have provided further evidence of the importance of lipid metabolism and acetyl-CoA translocation to the development of rice blast disease by *Magnaporthe oryzae*. Previous studies in *M. oryzae* have demonstrated the importance of lipid droplet mobilisation from the conidium to the appressorium under control of the Pmk1 MAPK pathway (Thines et al., 2000), and subsequent cAMP-dependent degradation of lipid bodies by intracellular triacylglycerol lipases (Wang et al., 2007). The glyoxylate cycle has furthermore been shown to be required for temporal regulation of virulence (Wang et al., 2003), while carnitine acetyltransferase activity and fatty acid β-oxidation has previously been reported to be significant for plant infection (Bhambra et al., 2006; Ramos-Pamplona and Naqvi, 2006; Wang et al., 2007).

The current project set out to explore how lipid body mobilisation is regulated in *M. oryzae* and to identify novel genes involved in lipid metabolism that contribute significantly to virulence by the rice blast fungus. In this way, I hoped to be able to provide new insight into the physiology of appressorium function, the mechanism of appressorium turgor generation and how intracellular storage products within conidia of *M. oryzae* may be utilized to fuel the plant infection process, which occurs in the absence of exogenous nutrients. I first reported the characterisation of two potential transcriptional regulator genes, *FAR1* and *FAR2*, which are related to the *Aspergillus nidulans FarA* and *FarB* transcription factor-encoding genes, previously shown to be involved in regulating lipid utilization and acetyl-CoA translocation (Hynes *et al.*, 2006; Rocha *et al.*, 2008; Ramirez and Lorenz, 2009; Poopanitpan *et al.*, 2010). My findings revealed that in *M. oryzae*, *FAR1* and *FAR2* are expressed throughout infection-related development (Soanes et al., 2012) and Far1-GFP and Far2-GFP fusion proteins localise

to the nucleus when the fungus is grown in the presence of lipids, or during appressorium development. *FAR1* and *FAR2* regulate expression of genes involved in peroxisomal biogenesis, fatty acid β-oxidation, acetyl-CoA translocation and the glyoxylate cycle. Consistent with this, deletion mutants of *FAR1* and *FAR2* are unable to utilise lipids as sole carbon source, while Δ*far2* mutants are also unable to grow on acetate as sole carbon source. This observation suggests that *FAR2* has a distinct function compared to FarB in *A. nidulans* (Hynes et al., 2006). In *A. nidulans*, for example, acetate utilisation is regulated by *facB* (Todd et al., 1997) and deletion of *facB* leads to reduced levels of enzyme activities required for acetate utilisation, including acetyl-CoA synthase (encoded by *facA*), isocitrate lyase (encoded by *acuD*), malate synthase (encoded by *acuE*), phosphoenolpyruvate carboxykinase (encoded by *acuF*) and fructose-1,6-bisphosphatase (encoded by *acuG*) (Armitt et al., 1976). Interestingly, bioinformatic analysis of the *M. oryzae* genome database revealed the presence of a putative FacB encoding gene (MGG_04108.6) and it would therefore be valuable to determine whether it is *FAR2*, or the putative FacB gene, that regulates these genes in *M. oryzae*. In this way, it should prove possible to determine the exact nature of Far2-dependent regulation of acetate metabolism by *M. oryzae*. It was also reported in *A. nidulans,* that a consensus CCGAGG promoter sequence was the core binding motif for both *farA* and *farB* (Hynes et al., 2006). The authors predicted that this sequence would be present in the 5' upstream regions of genes induced by the presence of exogenous fatty acids which include those encoding proteins involved in peroxisomal biogenesis and fatty acid β-oxidation (Hynes et al., 2006). In *M. oryzae*, I have shown in this study that *FAR1* and *FAR2* are involved in regulating the expression of *PEX6*, *MFP1*, *PTH2* and *ICL1*, which play roles in peroxisomal biogenesis, fatty acid β-oxidation, acetyl-CoA translocation and glyoxylate cycle, respectively. Bioinformatic analysis of the

promoter for each of these genes revealed the presence of a CCGAGG motif (data not shown). To confirm whether *FAR1* and *FAR2* are transcriptional regulators and involved in regulating the expression of *PEX6*, *MFP1*, *PTH2* and *ICL1*, electrophoretic mobility shift assays (EMSA) should be carried out in future using radioactive labelled promoter fragments of *PEX6*, *MFP1*, *PTH2* and *ICL1* and nuclear protein extracts of Guy11, the Δ*far1* and Δ*far2* mutants, as well as using purified Far1 and Far2 protein. In this way, direct evidence could be obtained to define whether Far1 and Far2 act in a similar way in *M. oryzae*, which would also enable large-scale analysis of the range of genes regulated by these factor to be carried out using the RNa-seq or SuperSAGE methods recently developed for the fungus (Soanes et al., 2012).

I observed that both Δ*far1* and Δ*far2* mutants were able to form functional appressoria and cause disease. Therefore, *FAR1* and *FAR2* are dispensable for fungal virulence. Consistent with this observation, lipid droplet mobilisation was unaltered during appressorium development in both mutants. In *Fusarium oxysporum*, *CTF1*, a homologue of *FAR1,* was shown to regulate genes involved in fatty acid hydrolysis and is also involved in regulating expression of *Cut1* and *Lip1*, which encode cutinase and lipase, respectively (Rocha et al., 2008). We know that in *M. oryzae* triacylglycerol lipase activity is highly induced during appressorium maturation (Thines et al., 2000) and there are 28 genes that encode intracellular and extracellular lipases, as well as esterases found in *M. oryzae* genome (Wang et al., 2007). Following lipid degradation by triacylglycerol lipases, glycerol and fatty acid are generated and glycerol accumulation in the appressorium is important for turgor generation (de Jong et al., 1997) while fatty acids undergo β-oxidation to produce acetyl-CoA which needs to be transported across the peroxisomal and mitochondrial membrane to feed a significant number of biosynthetic pathways. My results have revealed that while acetyl-CoA

translocation is critical for pathogenesis (Bhambra et al., 2006), the other pathways involved in lipolysis and fatty acid metabolism are all individually dispensable for plant infection, or contribute in only a relatively minor way to virulence of *M. oryzae.* This indicates that either considerable redundancy exists in these pathways, or that there are numerous means of utilizing lipid droplets in order to fuel the initial stages of appressorium-mediated plant infection. This is consistent with earlier studies (Wang et al., 2007), which showed that any single triacylglycerol lipase-encoding gene was dispensable for pathogenesis. It still seems likely that lipid droplet mobilisation provides the predominant way in which glycerol is synthesized for turgor generation, although direct evidence by means of radio-labelling studies has still not been provided to support such an assertion. There is also the possibility that glycerol is synthesized from trehalose, glycogen or even intracellular mannitol through the alternative glycerol biosynthesis pathway which has been well characterised in *S. cerevisiae* and *A. nidulans* (Albertyn *et al.*, 1994; Ansell *et al.*, 1997; Pahlman *et al.*, 2001; de Vries *et al.*, 2003) and operates via glycerol-3-phosphate dehydrogenase providing glycerol-3-phosphate from dihydroxyacetone-3-phosphate during the initial steps in glycolysis (Thines et al., 2000).

It is clear from this study and earlier reports (Bhambra et al., 2006; Ramos-Pamplona and Naqvi, 2006) that carnitine-dependent acetyl-CoA translocation is critical for plant infection by *M. oryzae.* Two major pathways have been identified that are involved in acetyl-CoA translocation; the carnitine-dependent pathway and peroxisomal citrate synthase pathway (van Roermund et al., 1995). In the carnitine-dependent pathway, carnitine acetyltransferase (CAT) exchanges the CoA group of acetyl-CoA for carnitine to produce acetylcarnitine which can be transported between subcellular compartments. In the peroxisomal citrate synthase pathway, meanwhile, oxaloacetate and acetyl-CoA

undergo condensation to form citrate which can be transported across membranes. Carnitine acetyl-transferase activity (CAT) is required for carnitine-dependent acetyl-CoA translocation across the peroxisomal membrane. In *M. oryzae*, *PTH2* encodes the major CAT activity during appressorium development and is required for fungal virulence (Bhambra et al., 2006; Ramos-Pamplona and Naqvi, 2006). The biosynthesis pathway by which carnitine is made has recently been characterised in *C. albicans* (Strijbis et al., 2009) and I therefore identified the genes encoding enzymes putatively involved in carnitine biosynthesis in *M. oryzae.* My aim was to test the role of carnitine synthesis in pathogenesis by *M. oryzae* and I therefore generated Δ*car1*, Δ*car2*, Δ*car3* and Δ*car4* mutants to test the function of the corresponding genes. Based on the growth of these null mutants on medium supplemented with glucose, acetate, oleic acid or triolein, I concluded that both Δ*car1* and Δ*car4* mutants are unable to utilise acetate, oleic acid and triolein as carbon sources. However, all of the carnitine biosynthesis mutants (Δ*car1*, Δ*car2*, Δ*car3* and Δ*car4*) still retained their capacity to cause rice blast disease. This suggests that although carnitine is required for growth of *M. oryzae* on lipids and acetate, it is dispensable for plant infection. Unexpectedly, I found that both Δ*car2* and Δ*car3* mutants are able to utilise acetate, oleic acid and triolein. However, analysis of the *M. oryzae* genome revealed that as well as *CAR3*, which encodes trimethylaminobutyraldehyde dehydrogenase (TMABADH), there are also a number of alternative genes, which putatively encode for this enzyme including MGG_03900.6, MGG_09456.6, MGG_01230.6, MGG_03263.6, MGG_01991.6, MGG_00652.6, MGG_05814.6, MGG_01606.6, MGG_13331.6 and MGG_02766.6. It is therefore possible that there is redundancy at this step in carnitine biosynthesis, or that the *CAR3* homologue selected may not encode the major form of this enzyme. This would explain why the Δ*car3* mutant generated is still able to grow on minimal medium supplemented

with acetate, oleic acid or triolein. It will therefore be important to measure whether *CAR3* encodes the predicted enzymatic activity or to attempt to complement the existing Car3 mutant of *C. albicans* to directly test its function. It would also be valuable to delete each of the other potential TMABADH-encoding genes and see if their growth on lipid is affected. By contrast, *CAR2*, which putatively encodes hydroxytrimethyllysine aldolase (HTMLA) and is also dispensable for growth on acetate and lipid, only exists as a single copy gene in the *M. oryzae* genome. Therefore it is possible that there may be alternative pathways, which supply the Δ*car2* mutant with TMABA or carnitine, perhaps by means of recycling following acetyl-CoA translocation. In order to investigate this further, quantification of either TMABA or carnitine will need to be carried out and compared between the wild type, the Δ*car2* mutant and the autophagy-impaired Δ*atg8* mutant of *M. oryzae* (Veneault-Fourrey et al., 2006).

In humans, primary carnitine deficiency is caused by mutations in the sodium-dependent plasma membrane carnitine transporter *OCTN2*, which is responsible for maintaining the carnitine pool in the body (Wang *et al.*, 1999; Wang *et al.*, 2000). It is an autosomal recessive disorder, which presents with progressive cardiomyopathy and skeletal muscle weakness at ages 2-4 (Stanley *et al.*, 1991; Shoji *et al.*, 1998). This disorder can be caused by chronic administration of certain drugs such as pivalate and valproic acid (Lheureux and Hantson, 2009). In *C. albicans*, deficiency in carnitine results in loss of the ability of the fungus to grow lipid and acetate (Strijbis et al., 2009). However, the ability of carnitine-deficient *C. albicans* to cause infection has not been reported. Based on results reported here, it seems likely that carnitine recycling occurs in a very efficient manner during appressorium development by *M. oryzae* or that there are a number of redundant individual steps in the pathway, as originally characterized in *C. albicans.* It will therefore be necessary to carry out detailed biochemical analysis of

carnitine production in *M. oryzae* using the mutants generated in this project. I initiated this work by measuring carnitine levels in the fungus, but this proved inconclusive with unaltered levels of carnitine present in each mutant (data not shown).

To explore the precise role of acetyl-CoA utilization by *M. oryzae* during plant infection, I went on to search for genes directly involved in acetyl-CoA utilisation, based on DNA sequence homology and patterns of gene expression throughout appressorium development (Soanes et al., 2012). These results suggested that both acetyl-CoA synthetase and the mitochondrial carnitine carrier, are highly expressed during appressorium mediated plant infection. In the *M. oryzae* genome, there are three genes that encode for acetyl-CoA synthetase (*ACS1*, *ACS2* and *ACS3*) and the *CRC1* gene putatively encodes the mitochondrial carnitine carrier. I showed that Δ*acs2*, Δ*acs3* and Δ*crc1* mutants are unable to grow on lipids (oleic acid or triolein), consistent with the predicted functions of the corresponding genes. The Δ*crc1* mutant was also unable to utilise acetate as sole carbon source. Interestingly, I found that Δ*acs2*, Δ*acs3* and Δ*crc1* mutants exhibited a delay in lipid mobilisation from the conidium into the appressorium. Furthermore, the Δ*crc1* mutant is reduced in its ability to cause plant disease, while Δ*acs2* and Δ*acs3* mutants still retain their capability to infect plants.

The roles of acetyl-CoA synthetase have previously been characterised in *S. cerevisiae*, *C. albicans* and *A. nidulans* (Armitt *et al.*, 1976; De Virgilio *et al.*, 1992; Van Den Berg and Steensma, 1995; Carman *et al.*, 2008). In both *S. cerevisiae* and *C. albicans*, two copies of the gene encoding acetyl-CoA synthetase exist, *ACS1* and *ACS2*. The *ScACS1* gene is required for growth on acetate, but not on ethanol or glucose (De Virgilio et al., 1992), while *ScACS2* is required for growth on glucose, but not on ethanol and acetate (Van Den Berg and Steensma, 1995). Deletion mutants of both *ScACS1* and *ScACS2* were reported to be non-viable (Van Den Berg and Steensma, 1995). Mutants lacking

the *CaACS1* gene meanwhile were shown to be able to utilise glucose, acetate, ethanol and oleate as sole carbon source. By contrast, in *C. albicans* mutants lacking *CaACS2* were unable to grow on glucose and oleate but were able to grow on ethanol and acetate (Carman et al., 2008). *In vivo* analysis of *CaACS1* in mice also showed that it is not required for pathogenicity while the role of *CaACS2* in virulence is still unknown. It was suggested that because the growth defects of *ACS2*-depleted strain were so severe, it is extremely unlikely that it would retain virulence (Carman et al., 2008).

The mitochondrial carnitine carrier protein (Crc) was first identified in *S. cerevisiae* (*YOR100C*) (Palmieri et al., 1999) and shown to transport carnitine, acetylcarnitine, propionylcarnitine and, to a much lower extent, medium- and long- chain acylcarnitines (Palmieri et al., 1999). Mutants lacking the *YOR100C* gene were shown to be able to grow normally on glucose, glycerol and oleate, but deletion of *YOR100C* in a Δ*cit2* mutant (lacking carnitine acetyltransferase) resulted in a mutant that was unable to grow on oleate (van Roermund et al., 1999). Recently the role of the Crc protein was reported in *M. oryzae* (Yang et al., 2012). *CRC1* was shown to be involved in fungal virulence and its ability to grow on acetate and lipid were impaired, consistent with results reported in this thesis. Yang et al., (2012) also showed that deletion of Crc protein severely reduces appressorium turgor generation, appressorium penetration as well as development of infection hyphae. The sub-cellular localisation of *CRC1* in *M. oryzae* is still unknown, but would be expected to be mitochondrial. This is based on previous reports on *CRC1* homologues in other organisms including *A. nidulans* and *S. cerevisiae* (Palmieri *et al.*, 1999; De Lucas *et al.*, 2001). If this is the case, it suggests that utilisation of carnitine and acetylcarnitine in mitochondria is crucial for plant infection. *PTH2*, for instance, was previously shown to be localised in peroxisomes (Bhambra et al., 2006). However, recent annotation of *PTH2* in *M. oryzae* has revealed the presence

of a putative 5' mitochondrial targeting sequence in the *PTH2* gene. It is therefore possible that the importance of both *CRC1* and *PTH2* to virulence in *M. oryzae* is due to a requirement for mitochondrial β-oxidation during plant-infection development. In order to understand this process further, localisation of Pth2 using the most recent gene annotation should be carried out. If Pth2 is observed in both peroxisomes and mitochondria, as shown in *S. cerevisiae* (Elgersma et al., 1995) and *C. albicans* (Strijbis et al., 2008), a strain which lacks the mitochondrial Pth2 isoform needs to be constructed. If the hypothesis presented here is correct, then the *M. oryzae* strain which lacks only mitochondrial Pth2 activity will closely resemble the Δ*crc1* mutant (this thesis and Yang et al., 2012) and the Δ*pth2* mutant (Bhambra et al., 2006), whereas restriction of Crc1 from peroxisomes only, might show a less severe effect on pathogenesis.

Finally, I examined the mechanism of lipid storage in *M. oryzae* and the potential role of perilipin in lipid droplet organisation, movement and breakdown. Perilipin is a protein which forms a barrier at the phospholipid-rich periphery of lipid droplets, shielding them from being hydrolysed by cytosolic lipases (Brasaemle et al., 2000; Brasaemle, 2007) and potentially regulating lipase activity during lipid droplet utilisation. In *M. oryzae*, I identified a gene that putatively encodes for perilipin called *CAP20* (MGG_11916.6) and its gene product was found to localise specifically to the periphery of lipid droplets. I showed that only 60% of Δ*cap20* mutant conidia were able to form appressoria, which in turn affected pathogenicity of the mutant. The Δ*cap20* mutant of *M. oryzae* produced long germ tubes and, interestingly, multiple nuclei were observed in the germ tubes suggesting that deletion of *CAP20* also affects the pattern of nuclear division. *CAP20* is not, however, necessary for lipid utilisation since the Δ*cap20* mutant was still able to grow on minimal medium supplemented with lipid

(oleic acid and triolein). In mice, there are 4 types of perilipin; perilipin A, perilipin B, perilipin C and perilipin D encoded by a single gene (Lu et al., 2001). Perilipin A and B are expressed in adipocytes and steroidogenic cells while perilipin C and D expression is limited only in the steroidogenic cells (Lu et al., 2001). Perilipin A is the primary isoform of perilipin which is also the longest isoform compared to the other perilipins (Lu *et al.*, 2001; Brasaemle *et al.*, 2009). Mice lacking perilipin have been shown to have a greater lean body mass, increased metabolic rate, an increased tendency to develop glucose intolerance and peripheral insulin resistance (Tansey et al., 2001). In pathogenic fungi, the importance of perilipin in terms of virulence has been reported in *C. gloeosporioides* and in the entomopathogenic fungal species, *M. anisopliae* (Hwang et al., 1995; Wang and St. Leger, 2007). In both cases, mutants lacking perilipin were shown to have a reduction in virulence. Both Δ*Cgcap20* and Δ*Macap20* mutants were able to form appressoria, but these were non-functional and unable to penetrate the host (Hwang et al., 1995; Wang and St. Leger, 2007). It is clear from this study that further investigation needs to be carried out in order to understand the role of perilipin in pathogenic fungi. The most important part is to study the relationship between protein kinase A, perilipin and triacylglycerol lipases. It is predicted, for instance that Cap20 is phosphorylated by protein kinase A, based on a consensus phosphorylation site, as reported here. It would therefore be informative to express *CAP20*-mRFP and a cAMP-dependent protein kinase A mutant, Δ*cpkA*, and then examine *CAP20* activity and localisation throughout plant-infection development. Deletion of the protein kinase A binding site of *CAP20* would also be informative in order to understand the relationship between protein kinase A-mediated phosphorylation and the role of *CAP20* in pathogenesis. To determine the role of perilipin in regulating intracellular lipolysis, lipid

quantification and lipase assay also need to be performed and compared between the wild type, the Δ*cap20* mutant and the Δ*cpkA* mutant.

When considered together, the results reported in this thesis therefore provide further evidence that lipid mobilisation, fatty acid β-oxidation and acetyl-CoA metabolism in *M. oryzae* are all important for appressorium-mediated plant infection. It is clear, however, that there is considerable redundancy in acetyl-CoA utilization pathways, and the transport of acetyl-CoA across the mitochondrial membrane may well be as significant as peroxisomal translocation. It is also apparent from work reported here that transcriptional regulation of genes required for lipid droplet mobilisation during appressorium development in *M. oryzae* is distinct from the Far1 and Far2-depndent regulatory mechanism for lipid metabolism that appears to be utilized by a wide variety of filamentous fungi. In future it will be important to define the transcriptional regulators required for lipid body mobilisation and the genes they regulate. In this way, and coupled with more detailed biochemical analysis, it should prove easier to define the precise biochemical pathways necessary for intracellular lipolysis, the route of acetyl-CoA metabolism in appressoria and the function this fulfils during plant infection.

Bibliography

Adachi, K., and Hamer, J.E. (1998). Divergent cAMP signaling pathways regulate growth and pathogenesis in the rice blast fungus *Magnaporthe grisea* The Plant Cell *10*, 1361-1373.

Albertyn, J., Hohmann, S., Thevelein, J.M., and Prior, B.A. (1994). *GPD1*, which encodes glycerol-3-phosphate dehydrogenase, is essential for growth under osmotic stress in *Saccharomyces cerevisiae*, and its expression is regulated by the high-osmolarity glycerol response pathway. Molecular and Cellular Biology *14*, 4135-4144.

Ansell, R., Granath, K., Hohmann, S., Thevelein, J.M., and Adler, L. (1997). The two isoenzymes for yeast NAD^+-dependent glycerol 3-phosphate dehydrogenase encoded by *GPD1* and *GPD2* have distinct roles in osmoadaptation and redox regulation. The EMBO Journal *16*, 2179-2187.

Argüelles, J.C. (2000). Physiological roles of trehalose in bacteria and yeasts: a comparative analysis. Archives of Microbiology *174*, 217-224.

Armitt, S., McCullough, W., and Roberts, C.F. (1976). Analysis of acetate non-utilizing (*acu*) mutants in *Aspergillus nidulans*. Journal of General Microbiology *92*, 263-282.

Bentley, J., Boa, E., Danielsen, S., Franco, P., Antezana, O., Villarroel, B., Rodríguez, H., Ferrrufino, J., Franco, J., Pereira, R., Herbas, J., Díaz, O., Lino, V., Villarroel, J., Almendras, F., and Colque, S. (2009). Plant health clinics in Bolivia 2000—2009: operations and preliminary results. Food Security *1*, 371-386.

Berepiki, A., Lichius, A., and Read, N.D. (2011). Actin organization and dynamics in filamentous fungi. Nat Rev Micro *9*, 876-887.

Bhambra, G.K., Wang, Z.Y., Soanes, D.M., Wakley, G.E., and Talbot, N.J. (2006). Peroxisomal carnitine acetyl transferase is required for elaboration of penetration hyphae during plant infection by *Magnaporthe grisea*. Molecular Microbiology *61*, 46-60.

Black, P.N., and DiRusso, C.C. (2003). Transmembrane movement of exogenous long-chain fatty acids: proteins, enzymes, and vectorial esterification. Microbiology and Molecular Biology Reviews *67*, 454-472.

Blanchette-Mackie, E.J., Dwyer, N.K., Barber, T., Coxey, R.A., Takeda, T., Rondinone, C.M., Theodorakis, J.L., Greenberg, A.S., and Londos, C. (1995). Perilipin is located on the surface layer of intracellular lipid droplets in adipocytes. Journal of Lipid Research *36*, 1211-1226.

Bourett, T.M., and Howard, R.J. (1990). In vitro development of penetration structures in the rice blast fungus *Magnaporthe grisea*. Canadian Journal of Botany *68*, 329-342.

Bozza, P.T., Melo, R.C.N., and Bandeira-Melo, C. (2007). Leukocyte lipid bodies regulation and function: Contribution to allergy and host defense. Pharmacology & Therapeutics *113*, 30-49.

Brasaemle, D., Subramanian, V., Garcia, A., Marcinkiewicz, A., and Rothenberg, A. (2009). Perilipin A and the control of triacylglycerol metabolism. Molecular and Cellular Biochemistry *326*, 15-21.

Brasaemle, D.L. (2007). Thematic review series: Adipocyte Biology. The perilipin family of structural lipid droplet proteins: stabilization of lipid droplets and control of lipolysis. Journal of Lipid Research *48*, 2547-2559.

Brasaemle, D.L., Rubin, B., Harten, I.A., Gruia-Gray, J., Kimmel, A.R., and Londos, C. (2000). Perilipin A increases triacylglycerol storage by decreasing the rate of triacylglycerol hydrolysis. Journal of Biological Chemistry *275*, 38486-38493.

Breidenbach, R.W., and Beevers, H. (1967). Association of the glyoxylate cycle enzymes in a novel subcellular particle from castor bean endosperm. Biochemical and Biophysical Research Communications *27*, 462-469.

Bremer, J. (1962). Carnitine precursors in the rat. Biochimica et Biophysica Acta *57*, 327-335.

Bremer, J. (1983). Carnitine-metabolism and functions. Physiological Reviews *63*, 1420-1480.

Burney, J.A., Davis, S.J., and Lobell, D.B. (2010). Greenhouse gas mitigation by agricultural intensification. Proceedings of the National Academy of Sciences.

Cao, Y., Cheong, H., Song, H., and Klionsky, D.J. (2008). In vivo reconstitution of autophagy in *Saccharomyces cerevisiae*. The Journal of Cell Biology *182*, 703-713.

Carman, A.J., Vylkova, S., and Lorenz, M.C. (2008). Role of acetyl Coenzyme A synthesis and breakdown in alternative carbon source utilization in *Candida albicans*. Eukaryotic Cell *7*, 1733-1741.

Carter, A.L., Abney, T.O., and Lapp, D.F. (1995). Biosynthesis and metabolism of carnitine. Journal of Child Neurology *10*, 2S3-2S7.

Catlett, N.L., Lee, B.N., Yoder, O.C., and Turgeon, B.G. (2003). Split-marker recombination for efficient targeted deletion of fungal genes. Fungal Genetics Newsletter *50*, 9-11.

Cheng, C., Mu, J., Farkas, I., Huang, D., Goebl, M.G., and Roach, P.J. (1995). Requirement of the self-glucosylating initiator proteins Glg1p and Glg2p for glycogen accumulation in *Saccharomyces cerevisiae*. Molecular and Cellular Biology *15*, 6632-6640.

Choi, W., and Dean, R.A. (1997). The adenylate cyclase gene *MAC1* of *Magnaporthe grisea* controls appressorium formation and other aspects of growth and development. The Plant Cell *9*, 1973-1983.

Chumley, F.G., and Valent, B. (1990). Genetic analysis of melanin-deficient, nonpathogenic mutants of *Magnaporthe grisea*. Molecular Plant-Microbe Interactions *3*, 135-143.

Clifford, G.M., Kraemer, F.B., Yeaman, S.J., and Vernon, R.G. (2001). Translocation of hormone-sensitive lipase and perilipin upon lipolytic stimulation during the lactation cycle of the rat. Metabolism *50*, 1264-1269.

Conti, E., Franks, N.P., and Brick, P. (1996). Crystal structure of firefly luciferase throws light on a superfamily of adenylate-forming enzymes. Structure *4*, 287-298.

Couch, B.C., and Kohn, L.M. (2002). A multilocus gene genealogy concordant with host preference indicates segregation of a new species, *Magnaporthe oryzae*, from *M. grisea*. Mycologia *94*, 683-693.

Courtois-Verniquet, F., and Douce, R. (1993). Lack of aconitase in glyoxysomes and peroxisomes. Biochem. J. *294*, 103-107.

Czymmek, K.J., Bourett, T.M., Shao, Y., DeZwaan, T.M., Sweigard, J.A., and Howard, R.J. (2005). Live-cell imaging of tubulin in the filamentous fungus *Magnaporthe grisea* treated with anti-microtubule and anti-microfilament agents. Protoplasma *225*, 23-32.

de Jong, J.C., McCormack, B.J., Smirnoff, N., and Talbot, N.J. (1997). Glycerol generates turgor in rice blast. Nature *389*, 244-245.

De Lucas, J.R., Martínez, O., Pérez, P., Isabel López, M., Valenciano, S., and Laborda, F. (2001). The *Aspergillus nidulans* carnitine carrier encoded by the *acuH* gene is exclusively located in the mitochondria. FEMS Microbiology Letters *201*, 193-198.

De Virgilio, C., Bürckert, N., Barth, G., Neuhaus, J.-M., Boller, T., and Wiemken, A. (1992). Cloning and disruption of a gene required for growth on acetate but not on ethanol: The acetyl-coenzyme a synthetase gene of *Saccharmoyces cerevisiae*. Yeast *8*, 1043-1051.

de Vries, R.P., Flitter, S.J., Van De Vondervoort, P.J.I., Chaveroche, M.-K., Fontaine, T., Fillinger, S., Ruijter, G.J.G., D'Enfert, C., and Visser, J. (2003). Glycerol dehydrogenase, encoded by *gldB* is essential for osmotolerance in *Aspergillus nidulans*. Molecular Microbiology *49*, 131-141.

Dean, R.A. (1997). Signal pathways and appressorium morphogenesis. Annual Review of Phytopathology *35*, 211-234.

Dean, R.A., Talbot, N.J., Ebbole, D.J., Farman, M.L., Mitchell, T.K., Orbach, M.J., Thon, M., Kulkarni, R., Xu, J.R., Pan, H.Q., Read, N.D., Lee, Y.H., Carbone, I., Brown, D., Oh, Y.Y., Donofrio, N., Jeong, J.S., Soanes, D.M., Djonovic, S., Kolomiets, E., Rehmeyer, C., Li, W.X., Harding, M., Kim, S., Lebrun, M.H., Bohnert, H., Coughlan, S., Butler, J., Calvo, S., Ma, L.J., Nicol, R., Purcell, S., Nusbaum, C., Galagan, J.E., and Birren, B.W. (2005). The genome sequence of the rice blast fungus *Magnaporthe grisea*. Nature *434*, 980-986.

Deng, Y.Z., and Naqvi, N.I. (2010). A vacuolar glucoamylase, Sga1, participates in glycogen autophagy for proper asexual differentiation in *Magnaporthe oryzae*. Autophagy *6*, 455-461.

Deng, Y.Z., Ramos-Pamplona, M., and Naqvi, N.I. (2009). Autophagy-assisted glycogen catabolism regulates asexual differentiation in *Magnaporthe oryzae*. Autophagy *5*, 33-43.

Dirzo, R., and Raven, P.H. (2003). Global state of biodiversity and loss. Annual Review of Environment and Resources *28*, 137-167.

Dixon, K.P., Xu, J.R., Smirnoff, N., and Talbot, N.J. (1999). Independent signaling pathways regulate cellular turgor during hyperosmotic stress and appressorium-mediated plant infection by *Magnaporthe grisea*. The Plant Cell *11*, 2045-2058.

Duran, M., Loof, N.E., Ketting, D., and Dorland, L. (1990). Secondary carnitine deficiency. Journal of Clinical Chemistry and Clinical Biochemistry *28*, 359-363.

Eaton, S., Bartlett, K., and Pourfarzam, M. (1996). Mammalian mitochondrial β-oxidation. Biochemical Journal *1*, 345-357.

Ebbole, D.J. (2007). Magnaporthe as a model for understanding host-pathogen interactions. Annual Review of Phytopathology *45*, 437-456.

Eichhorn, E., van der Ploeg, J.R., Kertesz, M.A., and Leisinger, T. (1997). Characterization of α-ketoglutarate-dependent taurine dioxygenase from *Escherichia coli*. Journal of Biological Chemistry *272*, 23031-23036.

Elgersma, Y., van Roermund, C.W.T., Wanders, R.J.A., and Tabak, H.F. (1995). Peroxisomal and mitochondrial carnitine acetyltransferases of *Saccharomyces cerevisiae* are encoded by a single gene. EMBO J *14*, 3472-3479.

Fahy, E., Subramaniam, S., Brown, H.A., Glass, C.K., Merrill, A.H., Murphy, R.C., Raetz, C.R.H., Russell, D.W., Seyama, Y., Shaw, W., Shimizu, T., Spener, F., van Meer, G., VanNieuwenhze, M.S., White, S.H., Witztum, J.L., and Dennis, E.A. (2005). A comprehensive classification system for lipids. Journal of Lipid Research *46*, 839-862.

Falconi, M., Chillemi, G., Di Marino, D., D'Annessa, I., Morozzo della Rocca, B., Palmieri, L., and Desideri, A. (2006). Structural dynamics of the mitochondrial ADP/ATP carrier revealed by molecular dynamics simulation studies. Proteins: Structure, Function, and Bioinformatics *65*, 681-691.

Farkas, I., Hardy, T.A., Goebl, M.G., and Roach, P.J. (1991). Two glycogen synthase isoforms in *Saccharomyces cerevisiae* are coded by distinct genes that are differentially controlled. Journal of Biological Chemistry *266*, 15602-15607.

Feinberg, A.P., and Vogelstein, B. (1983). A technique for radiolabeling DNA restriction endonuclease fragments to high specific activity. Analytical Biochemistry *132*, 6-13.

Flood, J. (2010). The importance of plant health to food security. Food Security *2*, 215-231.

Foster, A.J., Jenkinson, J.M., and Talbot, N.J. (2003). Trehalose synthesis and metabolism are required at different stages of plant infection by *Magnaporthe grisea*. EMBO J *22*, 225-235.

Garcia, A., Sekowski, A., Subramanian, V., and Brasaemle, D.L. (2003). The central domain is required to target and anchor perilipin A to lipid droplets. Journal of Biological Chemistry *278*, 625-635.

Gilbert, R.D., Johnson, A.M., and Dean, R.A. (1996). Chemical signals responsible for appressorium formation in the rice blast fungus *Magnaporthe grisea*. Physiological and Molecular Plant Pathology *48*, 335-346.

Goff, S.A. (1999). Rice as a model for cereal genomics. Current Opinion in Plant Biology *2*, 86-89.

Goff, S.A., Ricke, D., Lan, T.-H., Presting, G., Wang, R., Dunn, M., Glazebrook, J., Sessions, A., Oeller, P., Varma, H., Hadley, D., Hutchison, D., Martin, C., Katagiri, F., Lange, B.M., Moughamer, T., Xia, Y., Budworth, P., Zhong, J., Miguel, T., Paszkowski, U., Zhang, S., Colbert, M., Sun, W.-l., Chen, L., Cooper, B., Park, S., Wood, T.C., Mao, L., Quail, P., Wing, R., Dean, R., Yu, Y., Zharkikh, A., Shen, R., Sahasrabudhe, S., Thomas, A., Cannings, R., Gutin, A., Pruss, D., Reid, J., Tavtigian, S., Mitchell, J., Eldredge, G., Scholl, T., Miller, R.M., Bhatnagar, S., Adey, N., Rubano, T., Tusneem, N., Robinson, R., Feldhaus, J., Macalma, T., Oliphant, A., and Briggs, S. (2002). A draft sequence of the rice genome (*Oryza sativa* L. ssp. *japonica*). Science *296*, 92-100.

Gregory, P.J., and Ingram, J.S.I. (2000). Global change and food and forest production: future scientific challenges. Agriculture, Ecosystems & Environment *82*, 3-14.

Grunau, S., Mindthoff, S., Rottensteiner, H., Sormunen, R.T., Hiltunen, J.K., Erdmann, R., and Antonenkov, V.D. (2009). Channel-forming activities of peroxisomal membrane proteins from the yeast *Saccharomyces cerevisiae*. FEBS Journal *276*, 1698-1708.

Hagen, J.H. (1961). Effect of glucagon on the metabolism of adipose tissue. Journal of Biological Chemistry *236*, 1023-1027.

Hamer, J.E., Howard, R.J., Chumley, F.G., and Valent, B. (1988). A mechanism for surface attachment in spores of a plant pathogenic fungus. Science *239*, 288-290.

Henson, J.M., Butler, M.J., and Day, A.W. (1999). The dark side of the mycelium: melanins of phytopathogenic fungi. Annual Review of Phytopathology *37*, 447-471.

Hiltunen, J.K., Mursula, A.M., Rottensteiner, H., Wierenga, R.K., Kastaniotis, A.J., and Gurvitz, A. (2003). The biochemistry of peroxisomal β-oxidation in the yeast *Saccharomyces cerevisiae*. FEMS Microbiology Reviews *27*, 35-64.

Holm, C., Belfrage, P., and Fredrikson, G. (1987). Immunological evidence for the presence of hormone-sensitive lipase in rat tissues other than adipose tissue. Biochemical and Biophysical Research Communications *148*, 99-105.

Holm, C., Kirchgessner, T.G., Svenson, K.L., Fredrikson, G., Nilsson, S., Miller, C.G., Shively, J.E., Heinzmann, C., Sparkes, R.S., and Mohandas, T. (1988). Hormone-sensitive lipase: sequence, expression, and chromosomal localization to 19 cent-q13.3. Science *241*, 1503-1506.

Howard, R.J., Ferrari, M.A., Roach, D.H., and Money, N.P. (1991). Penetration of hard substrates by a fungus employing enormous turgor pressures. Proceedings of the National Academy of Sciences *88*, 11281-11284.

Hwang, C.S., Flaishman, M.A., and Kolattukudy, P.E. (1995). Cloning of a gene expressed during appressorium formation by *Colletotrichum gloeosporioides* and a marked decrease in virulence by disruption of this gene. The Plant Cell *7*, 183-193.

Hwang, P.K., Tugendreich, S., and Fletterick, R.J. (1989). Molecular analysis of *GPH1*, the gene encoding glycogen phosphorylase in *Saccharomyces cerevisiae*. Molecular and Cellular Biology *9*, 1659-1666.

Hynes, M.J., Murray, S.L., Andrianopoulos, A., and Davis, M.A. (2011). Role of carnitine acetyltransferases in acetyl Coenzyme A metabolism in *Aspergillus nidulans*. Eukaryotic Cell *10*, 547-555.

Hynes, M.J., Murray, S.L., Duncan, A., Khew, G.S., and Davis, M.A. (2006). Regulatory genes controlling fatty acid catabolism and peroxisomal functions in the filamentous fungus *Aspergillus nidulans*. Eukaryotic Cell *5*, 794-805.

Idnurm, A., and Howlett, B.J. (2002). Isocitrate lyase is essential for pathogenicity of the fungus *Leptosphaeria maculans* to canola (*Brassica napus*). Eukaryotic Cell *1*, 719-724.

Igarashi, S., Utiamada, C.M., Igarashi, L.C., Kazuma, A.H., and Lopes, R.S. (1986). *Pyricularia* in wheat. 1. Occurrence of *Pyricularia* sp. in Paran state. Fitopatologia Brasileira *11*, 351-352.

Indiveri, C., Tonazzi, A., and Palmieri, F. (1990). Identification and purification of the carnitine carrier from rat liver mitochondria. Biochimica et Biophysica Acta (BBA) - Bioenergetics *1020*, 81-86.

Isupov, M.N., Antson, A.A., Dodson, E.J., Dodson, G.G., Dementieva, I.S., Zakomirdina, L.N., Wilson, K.S., Dauter, Z., Lebedev, A.A., and Harutyunyan, E.H. (1998). Crystal structure of tryptophanase. Journal of Molecular Biology *276*, 603-623.

Jaco, F., Sven, K., Jan, S., and Florian, B. (2008). Carnitine and carnitine acetyltransferases in the yeast *Saccharomyces cerevisiae*: A role for carnitine in stress protection. Current Genetics *53*, 347-360.

Jacome, L.H., and Schuh, W. (1992). Effects of leaf wetness duration and temperature on development of Black Sigatoka disease on banana infected by *Mycosphaerella fijiensis* var. *difformis*. Phytopathology *82*, 515-520.

Jenkins, C.M., Mancuso, D.J., Yan, W., Sims, H.F., Gibson, B., and Gross, R.W. (2004). Identification, cloning, expression, and purification of three novel human calcium-independent phospholipase A_2 family members possessing triacylglycerol lipase and acylglycerol transacylase activities. Journal of Biological Chemistry *279*, 48968-48975.

Jeon, J., Goh, J., Yoo, S., Chi, M.-H., Choi, J., Rho, H.-S., Park, J., Han, S.-S., Kim, B.R., Park, S.-Y., Kim, S., and Lee, Y.-H. (2008). A putative MAP kinase kinase kinase, *MCK1*, is required for cell wall integrity and pathogenicity of the rice blast fungus, *Magnaporthe oryzae*. Molecular Plant-Microbe Interactions *21*, 525-534.

Kamada, Y., Funakoshi, T., Shintani, T., Nagano, K., Ohsumi, M., and Ohsumi, Y. (2000). Tor-mediated induction of autophagy via an Apg1 protein kinase complex. The Journal of Cell Biology *150*, 1507-1513.

Karpichev, I.V., and Small, G.M. (1998). Global regulatory functions of Oaf1p and Pip2p (Oaf2p), transcription factors that regulate genes encoding peroxisomal proteins in *Saccharomyces cerevisiae*. Mol. Cell. Biol. *18*, 6560-6570.

Kaufman, R.A., and Broquist, H.P. (1977). Biosynthesis of carnitine in *Neurospora crassa*. Journal of Biological Chemistry *252*, 7437-7439.

Kawamura, M., Jensen, D.F., Wancewicz, E.V., Joy, L.L., Khoo, J.C., and Steinberg, D. (1981). Hormone-sensitive lipase in differentiated 3T3-L1 cells and its activation by cyclic AMP-dependent protein kinase. Proceedings of the National Academy of Sciences of the United States of America *78*, 732-736.

Kershaw, E.E., Hamm, J.K., Verhagen, L.A.W., Peroni, O., Katic, M., and Flier, J.S. (2006). Adipose triglyceride lipase: function, regulation by insulin, and comparison with adiponutrin. Diabetes *55*, 148-157.

Kershaw, M.J., and Talbot, N.J. (2009). Genome-wide functional analysis reveals that infection-associated fungal autophagy is necessary for rice blast disease. Proceedings of the National Academy of Sciences *106*, 15967-15972.

Kersten, S. (2001). Mechanisms of nutritional and hormonal regulation of lipogenesis. EMBO reports *2*, 282-286.

Klionsky, D.J. (2005). The molecular machinery of autophagy: unanswered questions. Journal of Cell Science *118*, 7-18.

Klionsky, D.J., Cuervo, A.M., and Seglen, P.O. (2007). Methods for monitoring autophagy from yeast to human. Autophagy *3*, 181-206.

Klionsky, D.J., and Emr, S.D. (2000). Autophagy as a regulated pathway of cellular degradation. Science *290*, 1717-1721.

Kohlhaw, G.B., and Tan-Wilson, A. (1977). Carnitine acetyltransferase: Candidate for the transfer of acetyl groups through the mitochondrial membrane of yeast. J. Bacteriol. *129*, 1159-1161.

Kornberg, H.L., and Madsen, N.B. (1958). The metabolism of C_2 compounds in microorganisms. 3. Synthesis of malate from acetate via the glyoxylate cycle. Biochem. J. *68*, 549-557.

Krattinger, A. (1998). The importance of ag-biotech to global prosperity. ISAAA Briefs *6*.

Kratzer, S., and Schüller, H.-J. (1995). Carbon source-dependent regulation of the acetyl-coenzyme A synthetase-encoding gene *ACSI* from *Saccharomyces cerevisiae*. Gene *161*, 75-79.

Kunze, M., Pracharoenwattana, I., Smith, S.M., and Hartig, A. (2006). A central role for the peroxisomal membrane in glyoxylate cycle function. Biochimica et Biophysica Acta (BBA) - Molecular Cell Research *1763*, 1441-1452.

Kurihara, T., Ueda, M., Okada, H., Kamasawa, N., Naito, N., Osumi, M., and Tanaka, A. (1992). Beta-oxidation of butyrate, the short chain length fatty acid, occurs in peroxisomes in the yeast *Candida tropicalis*. Journal of Biochemistry *111*, 783-787.

Lake, A.C., Sun, Y., Li, J.-L., Kim, J.E., Johnson, J.W., Li, D., Revett, T., Shih, H.H., Liu, W., Paulsen, J.E., and Gimeno, R.E. (2005). Expression, regulation, and triglyceride hydrolase activity of Adiponutrin family members. Journal of Lipid Research *46*, 2477-2487.

Leboeuf, B., Flinn, R.B., and Cahill, G.F. (1959). Effect of epinephrine on glucose uptake and glycerol release by adipose tissue in vitro. Proceedings of the Society for Experimental Biology and Medicine. Society for Experimental Biology and Medicine (New York, N.Y.) *102*, 527-529.

Lee, N., D'Souza, C.A., and Kronstad, J.W. (2003). Of smuts, blasts, mildews, and blights: cAMP signaling in phytopathogenic fungi. Annual Review of Phytopathology *41*, 399-427.

Lee, Y.H., and Dean, R.A. (1993). cAMP regulates infection structure formation in the plant pathogenic fungus *Magnaporthe grisea* The Plant Cell *5*, 693-700.

Leighton, F., Bergseth, S., Rørtveit, T., Christiansen, E.N., and Bremer, J. (1989). Free acetate production by rat hepatocytes during peroxisomal fatty acid and dicarboxylic acid oxidation. Journal of Biological Chemistry *264*, 10347-10350.

Leung, H., Borromeo, E.S., Bernardo, M.A., and Notteghem, J.L. (1988). Genetic analysis of virulence in the rice blast fungus *Magnaporthe grisea*. Phytopathology *78*, 1227-1233.

Leung, H., Lehtinen, U., Karjalainen, R., Skinner, D., Tooley, P., Leong, S., and Ellingboe, A. (1990). Transformation of the rice blast fungus *Magnaporthe grisea* to hygromycin B resistance. Current Genetics *17*, 409-411.

Lheureux, P.E.R., and Hantson, P. (2009). Carnitine in the treatment of valproic acid-induced toxicity. Clinical Toxicology *47*, 101-111.

Lichius, A., and Read, N.D. (2010). A versatile set of Lifeact-RFP expression plasmids for live-cell imaging of F-actin in filamentous fungi. Fungal Genetics Reports, 8-14.

Lillie, S.H., and Pringle, J.R. (1980). Reserve carbohydrate metabolism in *Saccharomyces cerevisiae*: responses to nutrient limitation. Journal of Bacteriology *143*, 1384-1394.

Liu, H., Suresh, A., Willard, F.S., Siderovski, D.P., Lu, S., and Naqvi, N.I. (2007). Rgs1 regulates multiple Gα subunits in Magnaporthe pathogenesis, asexual growth and thigmotropism. EMBO J *26*, 690-700.

Liu, S., and Dean, R.A. (1997). G protein α subunit genes control growth, development, and pathogenicity of *Magnaporthe grisea*. Molecular Plant-Microbe Interactions *10*, 1075-1086.

Londos, C., Brasaemle, D.L., Schultz, C.J., Adler-Wailes, D.C., Levin, D.M., Kimmel, A.R., and Rondinone, C.M. (1999). On the control of lipolysis in adipocytes. Annals of the New York Academy of Sciences *892*, 155-168.

Lorenz, M.C., Bender, J.A., and Fink, G.R. (2004). Transcriptional response of *Candida albicans* upon internalization by macrophages. Eukaryotic Cell *3*, 1076-1087.

Lorenz, M.C., and Fink, G.R. (2001). The glyoxylate cycle is required for fungal virulence. Nature *412*, 83-86.

Lu, X., Gruia-Gray, J., Copeland, N.G., Gilbert, D.J., Jenkins, N.A., Londos, C., and Kimmel, A.R. (2001). The murine perilipin gene: the lipid droplet-associated perilipins derive from tissue-specific, mRNA splice variants and define a gene family of ancient origin. Mammalian Genome *12*, 741-749.

Maggio-Hall, L.A., and Keller, N.P. (2004). Mitochondrial β-oxidation in *Aspergillus nidulans*. Molecular Microbiology *54*, 1173-1185.

Marcinkiewicz, A., Gauthier, D., Garcia, A., and Brasaemle, D.L. (2006). The phosphorylation of serine 492 of perilipin A directs lipid droplet fragmentation and dispersion. Journal of Biological Chemistry *281*, 11901-11909.

Marín, D.H., Romero, R.A., Guzmán, M., and Sutton, T.B. (2003). Black Sigatoka: An increasing threat to banana cultivation. Plant Disease *87*, 208-222.

Martinez-Botas, J., Anderson, J.B., Tessier, D., Lapillonne, A., Chang, B.H.-J., Quast, M.J., Gorenstein, D., Chen, K.-H., and Chan, L. (2000). Absence of perilipin results in leanness and reverses obesity in $Lepr^{db/db}$ mice. Nat Genet *26*, 474-479.

Matsumura, H., Yoshida, K., Luo, S., Kimura, E., Fujibe, T., Albertyn, Z., Barrero, R.A., Krüger, D.H., Kahl, G., Schroth, G.P., and Terauchi, R. (2010). High-throughput superSAGE for digital gene expression analysis of multiple samples using next generation sequencing. PLoS ONE *5*, 1-8.

McKinney, J.D., zu Bentrup, K.H., Munoz-Elias, E.J., Miczak, A., Chen, B., Chan, W.T., Swenson, D., Sacchettini, J.C., Jacobs, W.R., and Russell, D.G. (2000). Persistence of *Mycobacterium tuberculosis* in macrophages and mice requires the glyoxylate shunt enzyme isocitrate lyase. Nature *406*, 735-738.

Mead, D.A., Pey, N.K., Herrnstadt, C., Marcil, R.A., and Smith, L.M. (1991). A universal method for the direct cloning of PCR amplified nucleic acid. Nat Biotech *9*, 657-663.

Meijer, W.H., van der Klei, I.J., Veenhuis, M., and Kiel, J.A.K.W. (2007). *ATG* genes involved in non-selective autophagy are conserved from yeast to man, but the selective cvt and pexophagy pathways also require organism-specific genes. Autophagy *3*, 106-116.

Mitchell, T.K., and Dean, R.A. (1995). The cAMP-dependent protein kinase catalytic subunit is required for appressorium formation and pathogenesis by the rice blast pathogen *Magnaporthe grisea*. The Plant Cell Online *7*, 1869-1878.

Mittenbühler, K., and Holzer, H. (1988). Purification and characterization of acid trehalase from the yeast suc2 mutant. Journal of Biological Chemistry *263*, 8537-8543.

Murphy, D.J. (2001). The biogenesis and functions of lipid bodies in animals, plants and microorganisms. Progress in Lipid Research *40*, 325-438.

Nganje, W.E., Bangsund, D.A., Leistritz, F.L., Wilson, W.W., and Tiapo, N.M. (2004). Regional economic impacts of Fusarium head blight in wheat and barley. Applied Economic Perspectives and Policy *26*, 332-347.

Nishimura, M., Park, G., and Xu, J.-R. (2003). The G-beta subunit *MGB1* is involved in regulating multiple steps of infection-related morphogenesis in *Magnaporthe grisea*. Molecular Microbiology *50*, 231-243.

Nwaka, S., and Holzer, H. (1998). Molecular biology of trehalose and the trehalases in the yeast *Saccharomyces cerevisiae*. Progress in Nucleic Acid Research and Molecular Biology *58*, 197-237.

Oldenburg, K.R., Vo, K.T., Michaelis, S., and Paddon, C. (1997). Recombination-mediated PCR-directed plasmid construction in vivo in yeast. Nucleic Acids Research *25*, 451-452.

Pahlman, A.-K., Granath, K., Ansell, R., Hohmann, S., and Adler, L. (2001). The yeast glycerol 3-phosphatases Gpp1p and Gpp2p are required for glycerol biosynthesis and differentially involved in the cellular responses to osmotic, anaerobic, and oxidative stress. Journal of Biological Chemistry *276*, 3555-3563.

Paik, W.K., and Kim, S. (1971). Protein methylation. Science *174*, 114-119.

Palmieri, L., Lasorsa, F.M., Iacobazzi, V., Runswick, M.J., Palmieri, F., and Walker, J.E. (1999). Identification of the mitochondrial carnitine carrier in *Saccharomyces cerevisiae*. FEBS Letters *462*, 472-476.

Palmieri, L., Lasorsa, F.M., Vozza, A., Agrimi, G., Fiermonte, G., Runswick, M.J., Walker, J.E., and Palmieri, F. (2000). Identification and functions of new transporters in yeast mitochondria. Biochimica et Biophysica Acta (BBA) - Bioenergetics *1459*, 363-369.

Park, G., Xue, C., Zhao, X.H., Kim, Y., Orbach, M., and Xu, J.R. (2006). Multiple upstream signals converge on the adaptor protein Mst50 in *Magnaporthe grisea*. The Plant Cell *18*, 2822-2835.

Pennisi, E. (2010). Armed and Dangerous. Science *327*, 804-805.

Piekarska, K., Hardy, G., Mol, E., van den Burg, J., Strijbis, K., van Roermund, C., van den Berg, M., and Distel, B. (2008). The activity of the glyoxylate cycle in peroxisomes of *Candida albicans* depends on a functional β-oxidation pathway: evidence for reduced metabolite transport across the peroxisomal membrane. Microbiology *154*, 3061-3072.

Piekarska, K., Mol, E., Van den Berg, M., Hardy, G., van den Burg, J., Van Roermund, C., MacCallum, D., Odds, F., and Distel, B. (2006). Peroxisomal fatty acid β-oxidation is not essential for virulence of *Candida albicans*. Eukaryotic Cell *5*, 1847-1856.

Pinstrup-Anderson, P. (2000). The future world food situation and the role of plant disease. Canadian Journal of Plant Pathology *22*, 321-331.

Pollack, J.K., Harris, S.D., and Marten, M.R. (2009). Autophagy in filamentous fungi. Fungal Genetics and Biology *46*, 1-8.

Poopanitpan, N., Kobayashi, S., Fukuda, R., Horiuchi, H., and Ohta, A. (2010). An ortholog of *farA* of *Aspergillus nidulans* is implicated in the transcriptional activation of genes involved in fatty acid utilization in the yeast *Yarrowia lipolytica*. Biochemical and Biophysical Research Communications *402*, 731-735.

Pracharoenwattana, I., Cornah, J.E., and Smith, S.M. (2005). Arabidopsis peroxisomal citrate synthase is required for fatty acid respiration and seed germination. The Plant Cell Online *17*, 2037-2048.

Prigneau, O., Porta, A., and Maresca, B. (2004). *Candida albicans* CTN gene family is induced during macrophage infection: homology, disruption and phenotypic analysis of CTN3 gene. Fungal Genetics and Biology *41*, 783-793.

Pugh, T.A., Shah, J.C., Magee, P.T., and Clancy, M.J. (1989). Characterization and localization of the sporulation glucoamylase of *Saccharomyces cerevisiae*. Biochimica et Biophysica Acta (BBA) - Protein Structure and Molecular Enzymology *994*, 200-209.

Qi, L., Corella, D., Sorlí, J.V., Portolés, O., Shen, H., Coltell, O., Godoy, D., Greenberg, A.S., and Ordovas, J.M. (2004). Genetic variation at the perilipin (PLIN) locus is associated with obesity-related phenotypes in White women. Clinical Genetics *66*, 299-310.

Ramirez, M.A., and Lorenz, M.C. (2009). The transcription factor homolog CTF1 regulates β-oxidation in *Candida albicans*. Eukaryotic Cell *8*, 1604-1614.

Ramos-Pamplona, M., and Naqvi, N.I. (2006). Host invasion during rice-blast disease requires carnitine-dependent transport of peroxisomal acetyl-CoA. Molecular Microbiology *61*, 61-75.

Rebouche, C.J., and Engel, A.G. (1984). Kinetic compartmental analysis of carnitine metabolism in the human carnitine deficiency syndromes. Evidence for alterations in tissue carnitine transport. The Journal of Clinical Investigation *73*, 857-867.

Regev-Rudzki, N., Karniely, S., Ben-Haim, N.N., and Pines, O. (2005). Yeast aconitase in two locations and two metabolic pathways: seeing small amounts is believing. Molecular Biology of the Cell *16*, 4163-4171.

Riedl, J., Crevenna, A.H., Kessenbrock, K., Yu, J.H., Neukirchen, D., Bista, M., Bradke, F., Jenne, D., Holak, T.A., Werb, Z., Sixt, M., and Wedlich-Soldner, R. (2008). Lifeact: a versatile marker to visualize F-actin. Nat Meth *5*, 605-607.

Rispail, N., Soanes, D.M., Ant, C., Czajkowski, R., Grünler, A., Huguet, R., Perez-Nadales, E., Poli, A., Sartorel, E., Valiante, V., Yang, M., Beffa, R., Brakhage, A.A., Gow, N.A.R., Kahmann, R., Lebrun, M.H., Lenasi, H., Perez-Martin, J., Talbot, N.J., Wendland, J., and Di Pietro, A. (2009). Comparative genomics of MAP kinase and calcium-calcineurin signalling components in plant and human pathogenic fungi. Fungal Genetics and Biology *46*, 287-298.

Rocha, A.L.M., Di Pietro, A., Ruiz-Roldan, C., and Roncero, M.I.G. (2008). Ctf1, a transcriptional activator of cutinase and lipase genes in *Fusarium oxysporum* is dispensable for virulence. Molecular Plant Pathology *9*, 293-304.

Rokka, A., Antonenkov, V.D., Soininen, R., Immonen, H.L., Pirilä, P.L., Bergmann, U., Sormunen, R.T., Weckström, M., Benz, R., and Hiltunen, J.K. (2009). Pxmp2 is a channel-forming protein in mammalian peroxisomal membrane. PLoS ONE *4*, e5090.

Rottensteiner, H., and Theodoulou, F.L. (2006). The ins and outs of peroxisomes: Co-ordination of membrane transport and peroxisomal metabolism. Biochimica et Biophysica Acta (BBA) - Molecular Cell Research *1763*, 1527-1540.

Rowen, D.W., Meinke, M., and LaPorte, D.C. (1992). *GLC3* and *GHA1* of *Saccharomyces cerevisiae* are allelic and encode the glycogen branching enzyme. Molecular and Cellular Biology *12*, 22-29.

Salazar, M., Vongsangnak, W., Panagiotou, G., Andersen, M.R., and Nielsen, J. (2009). Uncovering transcriptional regulation of glycerol metabolism in Aspergilli through genome-wide gene expression data analysis. Molecular Genetics and Genomics *282*, 571-586.

Sambrook, J., Fritsch, E.F., and Maniatis, T. (1989). Molecular cloning: a laboratory manual. New York: Cold Spring Harbor Laboratory.

Sandeman, R.A., and Hynes, M.J. (1989). Isolation of the *facA* (acetyl-Coenzyme A synthetase) and *acuE* (malate synthase) genes of *Aspergillus nidulans*. Molecular and General Genetics MGG *218*, 87-92.

Saunders, D.G.O., Aves, S.J., and Talbot, N.J. (2010). Cell cycle-mediated regulation of plant infection by the rice blast fungus. Plant Cell, tpc.109.072447.

Schmalix, W., and Bandlow, W. (1993). The ethanol-inducible *YAT1* gene from yeast encodes a presumptive mitochondrial outer carnitine acetyltransferase. Journal of Biological Chemistry *268*, 27428-27439.

Schulz, H. (1991). Beta oxidation of fatty acids. Biochimica et Biophysica Acta (BBA) - Lipids and Lipid Metabolism *1081*, 109-120.

Secor, G.A., and Gudmestad, N.C. (1999). Managing fungal diseases of potato. Canadian Journal of Plant Pathology *21*, 213-221.

Shoji, Y., Koizumi, A., Kayo, T., Ohata, T., Takahashi, T., Harada, K., and Takada, G. (1998). Evidence for linkage of human primary systemic carnitine deficiency with *D5S436*: A novel gene locus on chromosome 5q. The American Journal of Human Genetics *63*, 101-108.

Singh, R., Kaushik, S., Wang, Y., Xiang, Y., Novak, I., Komatsu, M., Tanaka, K., Cuervo, A.M., and Czaja, M.J. (2009). Autophagy regulates lipid metabolism. Nature *458*, 1131-1135.

Skamnioti, P., and Gurr, S.J. (2009). Against the grain: safeguarding rice from rice blast disease. Trends in Biotechnology *27*, 141-150.

Smirnova, E., Goldberg, E.B., Makarova, K.S., Lin, L., Brown, W.J., and Jackson, C.L. (2006). ATGL has a key role in lipid droplet/adiposome degradation in mammalian cells. EMBO Rep *7*, 106-113.

Smith, J.J., Brown, T.W., Eitzen, G.A., and Rachubinski, R.A. (2000). Regulation of peroxisome size and number by fatty acid β-oxidation in the yeast *Yarrowia lipolytica*. Journal of Biological Chemistry *275*, 20168-20178.

Soanes, D.M., Chakrabarti, A., Paszkiewicz, K.H., Dawe, A.L., and Talbot, N.J. (2012). Genome-wide transcriptional profiling of appressorium development by the rice bast fungus *Magnaporthe oryzae*. PLoS Pathog *8*, e1002514.

Southern, E.M. (1975). Detection of specific sequences among DNA fragments separated by gel electrophoresis. Journal of Molecular Biology *98*, 503-517.

Stanley, C.A., DeLeeuw, S., Coates, P.M., Vianey-Liaud, C., Divry, P., Bonnefont, J.-P., Saudubray, J.-M., Haymond, M., Trefz, F.K., Breningstall, G.N., Wappner, R.S., Byrd, D.J., Sansaricq, C., Tein, I., Grover, W., Valle, D., Rutledge, S.L., and Treem,

W.R. (1991). Chronic cardiomyopathy and weakness or acute coma in children with a defect in carnitine uptake. Annals of Neurology *30*, 709-716.

Steinmetz, C.G., Xie, P., Weiner, H., and Hurley, T.D. (1997). Structure of mitochondrial aldehyde dehydrogenase: the genetic component of ethanol aversion. Structure *5*, 701-711.

Strange, R.N., and Scott, P.R. (2005). Plant disease: A threat to global food security. Annual Review of Phytopathology *43*, 83-116.

Strijbis, K., and Distel, B. (2010). Intracellular acetyl unit transport in fungal carbon metabolism. Eukaryotic Cell, EC.00172-00110.

Strijbis, K., van Roermund, C.W., van den Burg, J., van den Berg, M., Hardy, G.P.M., Wanders, R.J.A., and Distel, B. (2010). Contributions of carnitine acetyl-transferases to intracellular acetyl unit transport in *Candida albicans*. Journal of Biological Chemistry.

Strijbis, K., van Roermund, C.W.T., Hardy, G.P., van den Burg, J., Bloem, K., de Haan, J., van Vlies, N., Wanders, R.J.A., Vaz, F.d.r.M., and Distel, B. (2009). Identification and characterization of a complete carnitine biosynthesis pathway in *Candida albicans*. The FASEB Journal *23*, 2349-2359.

Strijbis, K., van Roermund, C.W.T., Visser, W.F., Mol, E.C., van den Burg, J., MacCallum, D.M., Odds, F.C., Paramonova, E., Krom, B.P., and Distel, B. (2008). Carnitine-dependent transport of acetyl Coenzyme A in *Candida albicans* is essential for growth on nonfermentable carbon sources and contributes to biofilm formation. Eukaryotic Cell *7*, 610-618.

Subramanian, V., Garcia, A., Sekowski, A., and Brasaemle, D.L. (2004). Hydrophobic sequences target and anchor perilipin A to lipid droplets. Journal of Lipid Research *45*, 1983-1991.

Sul, H.S., and Wang, D. (1998). Nutritional and hormonal regulation of enzymes in fat synthesis: studies of fatty acid synthase and mitochondrial glycerol-3-phosphate acyltransferase gene transcription. Annual Review of Nutrition *18*, 331-351.

Sweigard, J.A., Caroll, A.M., Farrall, L., and Valent, B. (1997). A series of vectors for fungal transformation. Fungal Genetics Newsletter *44*, 52-53.

Talbot, N.J. (1995). Having a blast: exploring the pathogenicity of *Magnaporthe grisea*. Trends in Microbiology *3*, 9-16.

Talbot, N.J. (2003). On the trail of a cereal killer: Exploring the biology of *Magnaporthe grisea*. Annual Review of Microbiology *57*, 177-202.

Talbot, N.J., Ebbole, D.J., and Hamer, J.E. (1993). Identification and characterization of *MPG1*, a gene involved in pathogenicity from the rice blast fungus *Magnaporthe grisea*. Plant Cell *5*, 1575-1590.

Tanphaichitr, V., and Broquist, H.P. (1973). Role of lysine and Є-*N*-Trimethyllysine in carnitine biosynthesis. Journal of Biological Chemistry *248*, 2176-2181.

Tanphaichitr, V., Horne, D.W., and Broquist, H.P. (1971). Lysine, a precursor of carnitine in the rat. Journal of Biological Chemistry *246*, 6364-6366.

Tansey, J., Sztalryd, C., Hlavin, E., Kimmel, A., and Londos, C. (2004). The central role of Perilipin A in lipid metabolism and adipocyte lipolysis. IUBMB Life *56*, 379-385.

Tansey, J.T., Sztalryd, C., Gruia-Gray, J., Roush, D.L., Zee, J.V., Gavrilova, O., Reitman, M.L., Deng, C.X., Li, C., Kimmel, A.R., and Londos, C. (2001). Perilipin ablation results in a lean mouse with aberrant adipocyte lipolysis, enhanced leptin production, and resistance to diet-induced obesity. Proceedings of the National Academy of Sciences *98*, 6494-6499.

Teixeira, L., Rabouille, C., Rørth, P., Ephrussi, A., and Vanzo, N.F. (2003). *Drosophila* Perilipin/ADRP homologue Lsd2 regulates lipid metabolism. Mechanisms of Development *120*, 1071-1081.

Teste, M.A., Enjalbert, B., Parrou, J.L., and François, J.M. (2000). The *Saccharomyces cerevisiae* YPR184w gene encodes the glycogen debranching enzyme. FEMS Microbiology Letters *193*, 105-110.

Thewes, S., Kretschmar, M., Park, H., Schaller, M., Filler, S.G., and Hube, B. (2007). In vivo and ex vivo comparative transcriptional profiling of invasive and non-invasive *Candida albicans* isolates identifies genes associated with tissue invasion. Molecular Microbiology *63*, 1606-1628.

Thines, E., Weber, R.W.S., and Talbot, N.J. (2000). MAP kinase and protein kinase A-dependent mobilization of triacylglycerol and glycogen during appressorium turgor generation by *Magnaporthe grisea*. Plant Cell *12*, 1703-1718.

Thompson, J.D., Higgins, D.G., and Gibson, T.J. (1994). CLUSTAL W: improving the sensitivity of progressive multiple sequence alignment through sequence weighting, position-specific gap penalties and weight matrix choice. Nucleic Acids Research *22*, 4673-4680.

Tilman, D., Balzer, C., Hill, J., and Befort, B.L. (2011). Global food demand and the sustainable intensification of agriculture. Proceedings of the National Academy of Sciences *108*, 20260-20264.

Todd, R.B., Murphy, R.L., Martin, H.M., Sharp, J.A., Davis, M.A., Katz, M.E., and Hynes, M.J. (1997). The acetate regulatory gene *facB* of *Aspergillus nidulans* encodes a Zn(II)2Cys6 transcriptional activator. Molecular and General Genetics MGG *254*, 495-504.

Tucker, S.L., and Talbot, N.J. (2001). Surface attachment and pre-penetration stage development by plant pathogenic fungi. Annual Review of Phytopathology *39*, 385-417.

Valent, B., Farrall, L., and Chumley, F.G. (1991). *Magnaporthe grisea* genes for pathogenicity and virulence identified through a series of backcrosses. Genetics *127*, 87-101.

Van Den Berg, M.A., and Steensma, H.Y. (1995). *ACS2*, a *Saccharomyces cerevisiae* gene encoding acetyl-Coenzyme A synthetase, essential for growth on glucose. European Journal of Biochemistry *231*, 704-713.

van Roermund, C.W.T., Elgersma, Y., Singh, N., Wanders, R.J.A., and Tabak, H.F. (1995). The membrane of peroxisomes in saccharomyces cerevisae is impermeable to NAD(H) and acetyl-CoA under in vivo conditions. EMBO J *14*, 3480-3486.

van Roermund, C.W.T., Hettema, E.H., van den Berg, M., Tabak, H.F., and Wanders, R.J.A. (1999). Molecular characterization of carnitine-dependent transport of acetyl-CoA from peroxisomes to mitochondria in *Saccharomyces cerevisiae* and identification of a plasma membrane carnitine transporter, Agp2p. EMBO J *18*, 5843-5852.

Vaz, F.M., and Wanders, R.J.A. (2002). Carnitine biosynthesis in mammals. Biochemical Journal *361*, 417-429.

Veneault-Fourrey, C., Barooah, M., Egan, M., Wakley, G., and Talbot, N.J. (2006). Autophagic fungal cell death is necessary for infection by the rice blast fungus. Science *312*, 580-583.

Vereecke, D., Cornelis, K., Temmerman, W., Jaziri, M., Van Montagu, M., Holsters, M., and Goethals, K. (2002). Chromosomal locus that affects pathogenicity of *Rhodococcus fascians*. Journal of Bacteriology *184*, 1112-1120.

Villena, J.A., Roy, S., Sarkadi-Nagy, E., Kim, K.-H., and Sul, H.S. (2004). Desnutrin, an adipocyte gene encoding a novel patatin domain-containing protein, is induced by fasting and glucocorticoids: Ectopic expression of desnutrin increases triglyceride hydrolysis. Journal of Biological Chemistry *279*, 47066-47075.

Vuorio, O.E., Kalkkinen, N., and Londesborough, J. (1993). Cloning of two related genes encoding the 56-kDa and 123-kDa subunits of trehalose synthase from the yeast *Saccharomyces cerevisiae*. European Journal of Biochemistry *216*, 849-861.

Wanders, R.J., Vreken, P., Ferdinandusse, S., Jansen, G.A., Waterham, H.R., van Roermund, C.W., and Grunsven, V. (2001). Peroxisomal fatty acid alpha- and beta-oxidation in humans: enzymology, peroxisomal metabolite transporters and peroxisomal diseases. Biochemical Society Transactions *29*, 250-267.

Wang, C., and St. Leger, R.J. (2007). The *Metarhizium anisopliae* perilipin homolog MPL1 regulates lipid metabolism, appressorial turgor pressure, and virulence. J. Biol. Chem. *282*, 21110-21115.

Wang, Y., Taroni, F., Garavaglia, B., and Longo, N. (2000). Functional analysis of mutations in the OCTN2 transporter causing primary carnitine deficiency: Lack of genotype–phenotype correlation. Human Mutation *16*, 401-407.

Wang, Y., Ye, J., Ganapathy, V., and Longo, N. (1999). Mutations in the organic cation/carnitine transporter OCTN2 in primary carnitine deficiency. Proceedings of the National Academy of Sciences of the United States of America *96*, 2356-2360.

Wang, Z.Y., Jenkinson, J.M., Holcombe, L.J., Soanes, D.M., Veneault-Fourrey, C., Bhambra, G.K., and Talbot, N.J. (2005). The molecular biology of appressorium turgor generation by the rice blast fungus *Magnaporthe grisea*. Biochemical Society Transactions *33*, 384-388.

Wang, Z.Y., Soanes, D.M., Kershaw, M.J., and Talbot, N.J. (2007). Functional analysis of lipid metabolism in *Magnaporthe grisea* reveals a requirement for peroxisomal fatty acid beta-oxidation during appressorium-mediated plant infection. Molecular Plant-Microbe Interactions *20*, 475-491.

Wang, Z.Y., Thornton, C.R., Kershaw, M.J., Li, D.B., and Talbot, N.J. (2003). The glyoxylate cycle is required for temporal regulation of virulence by the plant pathogenic fungus *Magnaporthe grisea*. Molecular Microbiology *47*, 1601-1612.

Weber, R.W.S., Wakley, G.E., Thines, E., and Talbot, N.J. (2001). The vacuole as central element of the lytic system and sink for lipid droplets in maturing appressoria of *Magnaporthe grisea*. Protoplasma *216*, 101-112.

Wilson, R.A., Jenkinson, J.M., Gibson, R.P., Littlechild, J.A., Wang, Z.-Y., and Talbot, N.J. (2007). Tps1 regulates the pentose phosphate pathway, nitrogen metabolism and fungal virulence. EMBO J *26*, 3673-3685.

Wilson, R.A., and Talbot, N.J. (2009). Under pressure: investigating the biology of plant infection by *Magnaporthe oryzae*. Nature Reviews Microbiology *7*, 185-195.

Wilson, W.A., Roach, P.J., Montero, M., Baroja-Fernández, E., Muñoz, F.J., Eydallin, G., Viale, A.M., and Pozueta-Romero, J. (2010). Regulation of glycogen metabolism in yeast and bacteria. FEMS Microbiology Reviews *34*, 952-985.

Xu, J.R., and Hamer, J.E. (1996). MAP kinase and cAMP signaling regulate infection structure formation and pathogenic growth in the rice blast fungus *Magnaporthe grisea*. Genes & Development *10*, 2696-2706.

Xu, J.R., Staiger, C.J., and Hamer, J.E. (1998). Inactivation of the mitogen-activated protein kinase *MPS1* from the rice blast fungus prevents penetration of host cells but allows activation of plant defense responses. Proceedings of the National Academy of Sciences *95*, 12713-12718.

Yang, J., Kong, L., Chen, X., Wang, D., Qi, L., Zhao, W., Zhang, Y., Liu, X., and Peng, Y.-L. (2012). A carnitine–acylcarnitine carrier protein, MoCrc1, is essential for pathogenicity in *Magnaporthe oryzae*. Current Genetics, 1-10.

Yu, J., Hu, S., Wang, J., Wong, G.K.-S., Li, S., Liu, B., Deng, Y., Dai, L., Zhou, Y., Zhang, X., Cao, M., Liu, J., Sun, J., Tang, J., Chen, Y., Huang, X., Lin, W., Ye, C., Tong, W., Cong, L., Geng, J., Han, Y., Li, L., Li, W., Hu, G., Huang, X., Li, W., Li, J., Liu, Z., Li, L., Liu, J., Qi, Q., Liu, J., Li, L., Li, T., Wang, X., Lu, H., Wu, T., Zhu, M., Ni, P., Han, H., Dong, W., Ren, X., Feng, X., Cui, P., Li, X., Wang, H., Xu, X., Zhai, W., Xu, Z., Zhang, J., He, S., Zhang, J., Xu, J., Zhang, K., Zheng, X., Dong, J., Zeng, W., Tao, L., Ye, J., Tan, J., Ren, X., Chen, X., He, J., Liu, D., Tian, W., Tian, C., Xia, H., Bao, Q., Li, G., Gao, H., Cao, T., Wang, J., Zhao, W., Li, P., Chen, W., Wang, X., Zhang, Y., Hu, J., Wang, J., Liu, S., Yang, J., Zhang, G., Xiong, Y., Li, Z., Mao, L., Zhou, C., Zhu, Z., Chen, R., Hao, B., Zheng, W., Chen, S., Guo, W., Li, G., Liu, S., Tao, M., Wang, J., Zhu, L., Yuan, L., and Yang, H. (2002). A draft sequence of the rice genome (*Oryza sativa* L. ssp. *indica*). Science *296*, 79-92.

Zhou, H., and Lorenz, M.C. (2008). Carnitine acetyltransferases are required for growth on non-fermentable carbon sources but not for pathogenesis in *Candida albicans*. Microbiology *154*, 500-509.

Zimmermann, R., Strauss, J.G., Haemmerle, G., Schoiswohl, G., Birner-Gruenberger, R., Riederer, M., Lass, A., Neuberger, G., Eisenhaber, F., Hermetter, A., and Zechner, R. (2004). Fat mobilization in adipose tissue is promoted by adipose triglyceride lipase. Science *306*, 1383-1386.